

Development of a Closed Loop Control System  
for Vibratory Milling

Wael Naji Alharbi

A thesis Submitted in Partial Fulfilment of the Requirement of  
Liverpool John Moores University for the Degree of Doctor of  
Philosophy

November 2017

---

## Acknowledgements

The author would like to express great thanks to many persons who contributed deeply in achieving the aim of this project.

Firstly, thanks to my Lord Allah for his guidance and blessings.

Many thanks to the government of Saudi Arabia (Ministry of Higher Education) for their generous support.

Special thanks go to my director of studies, Dr. Andre Batako for his appreciated advice, guidance, support, motivation and encouragement in carrying this research to the successful completion.

Thanks, are due to my research supervisions Dr. Barry Goom and Prof. Xun Chen for their valuable feedback, advice and help during all project stages.

Exceptional thanks to all technical staff and especially, Mr Peter Moran for their technical support during experimental works.

I am also grateful to Liverpool John Moores University represented by staff in general.

Finally, countless thanks to mother, wife, daughter, son and all my family for their help and good wishes.

## Abstract

Manufacturing makes ever-increasing demands for higher machining speeds. This is particularly true in car and aircraft production, but also for cutting tools. Vibration is used in various technological processes to improve the performance of the machines by intelligently exploiting the synergy of the oscillations. Vibration provides several benefits for various technologies, such as manufacturing, medical, communications, transport, industries, etc. Vibration assisted machining techniques have recently become an area of interest for many engineering applications. In machining processes, vibration can lead to improvements when applied in a controlled manner. Vibration assisted machining is a technique in which a certain frequency of vibration is applied to the cutting tool or the Workpiece to achieve better cutting performance

The aim of this project is to apply vibration to the work-piece during milling process in order to improve the machining performance. In this project, a theoretical modelling and experimental implementation of vibratory milling process are presented and explored in depth. The modelling focused on the control system which tracked and regulated the vibration amplitude in the cutting zone during machining. Here, hardware and software of advanced technology of LabVIEW applications were used to develop implement and optimise the control system.

The machine tool static, dynamic and compliance characteristics were investigated in terms of static analysis, natural frequencies and dynamic stiffness, using harmonic excitation, hammer impact test and the application of external forces.

Preliminary studies were undertaken, where, the effect of cutting parameters were evaluated and the optimal cutting conditions were determined. Series of machining tests were undertaken, with the aim of recording process performance data in terms of cutting forces that were used for the development of the control system.

A closed loop PID controller was developed using advanced Field-Programming-Gate-Array (FPGA) and Real-time Labview applications, using a non-interrupted real time target PC. An innovative and unique combination of FPGA and target PC allow the control system to have a very fast response in keeping the set amplitude of the vibration whilst recording simultaneously the machining data for further analysis. Aluminium and mild Steel were used in this investigation, along with a comparative study between conventional and vibratory milling and between open loop and closed loop control systems.

The results of this investigation show the benefits of the superimposed vibration. The outperformance of the vibratory machining over the conventional milling provides a very promising outlook for the application of subsonic vibration into machining as an alternative to ultrasonic process.

# Table of Contents

Acknowledgements.....	I
Abstract.....	II
Abbreviations.....	XVIII
Nomenclature.....	XX
1.1 Introduction.....	2
1.2 The Current Needs in Industry.....	3
1.3 Novel Approach to Milling.....	4
1.4 Possible Advantages .....	5
1.5 Project Aim and Objectives .....	5
1.5.1 Aim of the project.....	5
1.5.2 Objectives .....	6
1.6 Thesis Layout.....	7
2.1 Introduction.....	11
2.2 Vibration Assisted Machining .....	11
2.2.1 The History of Vibration Assisted Machining.....	12
2.2.2 Overview of Vibration Assisted Machining.....	12
2.2.3 Ultrasonic Assisted Machining .....	15
2.3 Cutting Mechanism in Vibration Assisted Machining.....	18
2.3.1 1-D Vibration Assisted Machining .....	18
2.3.2 2-D Vibration Assisted Machining .....	20
2.4 Milling Machine.....	22
2.4.1 Milling Machine Types.....	22
a) Peripheral Milling:.....	22
b) Face Milling.....	25
2.5 Cutting Force and Power .....	26

2.6 Remarks .....	29
3.1 Introduction.....	32
3.2 Control System Objectives .....	33
3.2.1 Transient System Response .....	33
3.2.2 Steady State Response .....	33
3.2.3 Stability control.....	33
3.3 The Design of the Control System.....	34
3.3.1 Continuous Controller.....	35
3.3.2 Discontinuous controller.....	35
3.4 Terminology.....	36
3.5 Control System Classification.....	38
There are two classifications of the control system an open loop control system and closed loop control system. In this section, each control system is clarified and explained in detail as follow.....	38
3.5.1 Open Loop Control System .....	38
3.5.2 Closed Loop Control System.....	39
3.6 PID Controller.....	41
3.6.1 Introduction.....	41
3.6.2 PID Control.....	44
Proportional Action:.....	46
Integral Action: .....	46
Derivative Action:.....	46
Summary: .....	47
3.6.3 Continuous PID Controller: .....	47
3.7 Time Domain Specification of controller performance .....	49
4.1 Introduction.....	52

4.2 CNC Machining Centre .....	52
4.3 Heidenhain CNC Controller .....	54
4.4 Work-piece Materials.....	56
4.5 Vibration System .....	56
4.6 Piezoelectric Actuator.....	58
4.7 Power Amplifier.....	59
4.8 Kistler Dynamometer.....	60
4.9 Function Generator .....	63
4.10 Programmes .....	65
4.10.1 Solid Works Software .....	65
4.10.2 Matlab and Simulink.....	65
4.10.3 LabVIEW Software .....	65
4.16 Data Acquisition Hardware.....	66
4.16.1 Module Input/Output Slots .....	70
5.1 Introduction.....	75
5.2 Forces Calibration.....	75
5.3 Forces calibration results .....	77
5.4 Amplitude Calibration .....	83
5.5 Identification of Optimum Driving Voltage and Frequency.....	86
5.6 Remarks .....	87
6.1 Introduction.....	89
6.2 Dynamics in machining applications .....	89
6.2.1 Resonance Vibration.....	92
6.3 Identification of the 5-axis spindle Unit response .....	94
6.3.1 Harmonic excitation test .....	94
6.3.2 Hammer Impact test.....	97

6.4 Spindle unit Static and dynamic stiffness .....	100
6. 5 Dynamic Stiffness of the Spindle Unit .....	105
7.1 Introduction.....	108
7.2 The System Identification Procedure.....	109
7.3 Mathematical Model .....	111
7.4 Mathematical Model for the Vibrating stage .....	113
7.5 Controller Design.....	115
7.5.1 Simulation and Analysis the Model with PID Controller.....	117
7.6 Experimental control system.....	120
7.7 LabVIEW programming for the control system .....	122
7.8 Basic Design Consideration .....	128
7.9 Implementation of the Experiment .....	128
7.10 Model Identification from Experimental Data.....	128
7.11 Process Transfer Function.....	130
7.11.1 Step Response .....	130
7.11.2 Pole and Zero Plot.....	131
7.11.3 Validation Result .....	132
7.12 PID Controller Design .....	133
7.12.1 Classical Tuning Method .....	134
7.12.2 Auto Tuning Method.....	135
8.1 Introduction.....	139
8.2 Experimental configuration .....	139
8.3 Experiment Setup.....	141
8.4 Machining trials .....	142
8.4.1 Machining Process Parameters .....	143
8.5 Results.....	146

8.5.1 Comparative Process Performance .....	146
Cutting Forces .....	147
Surface Roughness .....	150
Work-pieces imaging analysis .....	153
8.6 Remarks .....	155
9.1 Introduction.....	157
9.2 Cutting Forces in Milling process.....	159
9.2.1 Effect of depth of cut .....	159
9.2.2 Effect of vibratory milling .....	162
9.3 Milling Power and Torque .....	166
9.4 Milling Coefficient.....	169
9.5 Surface Roughness.....	171
9.6 Chips formation .....	177
9.7 Tool Wear .....	180
9.8 Effect of Machining Time.....	182
9.9 Remarks .....	184
10.1 Introduction.....	186
10.2 Experimental Approach .....	187
10.3 Performance of the closed loop PID Controller.....	189
10.4 Milling Forces .....	191
10.5 Milling Power and Torque .....	194
10.6 Surface Roughness.....	197
10.7 Remarks .....	204
11.1 Conclusions.....	206
11.2 Recommendations for future work .....	209
Reference .....	211

Appendix.....	216
A-1 Equipment.....	216
A-2 LabVIEW Code .....	227
A-3 SolidWorks design sheets .....	229
A-4 LabVIEW training certificates.....	233
A-5 G-code of CNC-Machining Center.....	235
A-6 Publishing Papers.....	237

## List of Figures

Figure 2. 1: Experimental setup for Ultrasonic Vibration Turning (Babitsky et al. 2004).....	16
Figure 2. 2: Applied Ultrasonic Vibration with Cutting Direction (Moriwaki et al. 1991).....	17
Figure 2. 3: 1-D Vibration assisted machining (Shamoto, 2004). .....	19
Figure 2. 4: 1-D Vibration Assisted cutting (Brehl, 2008). .....	20
Figure 2. 5: 1-D and 2-D Vibration Assisted Machining (Cerniway, 2001). .....	20
Figure 2. 6: Different types of Peripheral milling. (Knight and Boothroyd, 2005) & (Kalpakjian and Schmid, 2010). .....	24
Figure 2. 7: Both Rotational Directions of Cutter (Up and Down Milling). .....	24
Figure 2. 8: Different types of face milling. (Knight, Boothroyd, 2005) & (Kalpakjian and Schmid, 2010). .....	26
Figure 2. 9: a) Cutting forces. b) Force Circle. (Kalpakjian and Schmid, 2010).....	27
Figure 2. 10: The Cutting Force Compounds. ....	30
Figure 3. 1: The Control Design flow chart. ....	34
Figure 3. 2: Control System Block Diagram Components. ....	38
Figure 3. 3: Open Loop control system; a) Block Diagram. b) Experimental set up. ....	39
Figure 3. 4: Closed Loop Control System; a) Block Diagram. b) Experimental Configuration. .....	41
Figure 3. 5: Schematic of the PID Controller - Non-Interacting Form.....	44
Figure 3. 6: PID control of a plant. ....	45
Figure 3. 7: PID controller internal structure.....	45
Figure 3. 8: Block diagram of Continuous PID Controller.....	48
Figure 3. 9: Response of a typical PID closed loop system (www.ni.com). ....	50
Figure 3. 10: Response of a closed loop system with dead time (www.ni.com). ....	50

Figure 4. 1: 5- Axis CNC Machining Centre XR 610. ....	54
Figure 4. 2: The iTNC 530 Heidenhain CNC controller. ....	55
Figure 4. 3: Self Contained Vibration System. ....	57
Figure 4. 4: Piezoelectric Actuator P 212.8 ....	58
Figure 4. 5: Power Amplifier Type E-472.2 ....	60
Figure 4. 6: Measuring Forces Device. a) 3-axis Kistler 9257A Dynamometer. b) Kistler Charge Amplifier Type 5073. ....	62
Figure 4. 7: The GWINSTEK AFG-2225 function generator ....	64
Figure 4. 8: Two processing targets of the Compact Rio controllers (National Instruments UK 2017). ....	67
Figure 4. 9: The configuration of the NI-Compact RIO-9022. ....	68
Figure 4. 10: The analogue input module NI-9215. ....	71
Figure 4. 11: The analogue input module NI-9234. ....	72
Figure 4. 12: The Analogue Output NI-9234 Module Slot. ....	73
Figure 5. 1: Charge amplifier parameters setup. ....	76
Figure 5. 2: Experimental setup for calibration. ....	77
Figure 5. 3: Force Calibration in X-axis. ....	78
Figure 5. 4: Force Calibration in Y-axis. ....	78
Figure 5. 5: Force Calibration in Z-axis. ....	79
Figure 5. 6: Horizontal fixing of the Dynamometer. ....	80
Figure 5. 7: Experimental setup for horizontal calibration. ....	80
Figure 5. 8: The Angle between two force directions. ....	81
Figure 5. 9: Horizontal Calibration Graph in Z-axis. ....	83
Figure 5. 10: Eddy current sensor position. ....	84
Figure 5. 11: Experimental setting up for Amplitude calibration. ....	84

Figure 5. 12: Displacement Calibration Graph. ....	85
Figure 5. 13: Frequency Amplitude Graphs. ....	86
Figure 6. 1: Test setup and frequency responses of the sensory spindle unit (Denkena, B. et al., 2015).....	92
Figure 6. 2: Experimental set-up for Sweep-Sine Test for the spindle unit.....	95
Figure 6. 3: Set-up configuration for piezoelectric actuator and Eddy current sensor. ....	95
Figure 6. 4: Frequency Amplitude performance response for the spindle unit. ....	96
Figure 6. 5: Experimental Configuration for Hammer Impact Test. ....	97
Figure 6. 6: Impact Hammer tester and Eddy current sensor configuration. ....	98
Figure 6. 7: Spindle Unit system response.....	98
Figure 6. 8: Spindle unit deflection in $\mu\text{m}$ . ....	99
Figure 6. 9: Frequency spectrum analysing for the spindle unit response. ....	99
Figure 6. 10: the actual experimental set-up for the static stiffness and compliance investigation. ....	103
Figure 6. 11: the force-deflection response for Spindle unit. ....	104
Figure 6. 12: Dynamic stiffness of the spindle unit as frequencies function. ....	105
Figure 6. 13: The dynamic compliance of the spindle unit.....	106
Figure 7. 1: Modelling and system Identification process. ....	110
Figure 7. 2: Control Design Procedure ....	112
Figure 7. 3: Open Loop control Strategy: a) Simulink Model. b) Input-Output signals.....	116
Figure 7. 4: Closed Loop Control Strategy: a) Simulink Model. b) Step Response.....	118
Figure 7. 5: Results of applying Closed Loop control Strategy.....	119
Figure 7. 6: Experimental Configuration for Close Loop Control System.....	121
Figure 7. 7: The front-end panel of the LabVIEW Code.....	122

Figure 7. 8: Project Explorer for LabVIEW codes. ....	124
Figure 7. 9: LabVIEW code runs in PC (Block Diagram).....	125
Figure 7. 10: LabVIEW codes run in cRio divide: a) Real time code. b) Control code for signal Generator. ....	126
Figure 7. 11: code runs in FPGA device: a) FPGA Block diagram. b) FPGA Front Panel..	127
Figure 7. 12: Time Domain Representation.....	129
Figure 7. 13: Process performance in Step-Response effect.....	131
Figure 7. 14: Pole and Zero representation. ....	132
Figure 7. 15: Measured and Simulated model output representation. ....	133
Figure 7. 16: Blocks design in Simulink: a) Process Subsystem. b) PID Closed Loop control. .....	136
Figure 8. 1: Experimental Configuration for Vibration system. ....	139
Figure 8. 2: Experimental setup on 5-Axis Milling Machine. ....	140
Figure 8. 3: Experiment Configuration for Control and DAQ system. ....	140
Figure 8. 4: Actual setup For Vibratory Milling Experiment. ....	141
Figure 8. 5: Microscope Device Configuration setup.....	142
Figure 8. 6: Typical actual cutting force signal in Y-direction.....	145
Figure 8. 7: Cutting Forces Compounds. ....	147
Figure 8. 8: Cutting Forces in X Axis Direction.....	148
Figure 8. 9: Cutting Forces in Y Axis Direction.....	148
Figure 8. 10: Cutting Forces in Z Axis Direction. ....	149
Figure 8. 11: Resultant Cutting Forces of X and Y Axis Directions. ....	149
Figure 8. 12: the formula of Surface Roughness factors $R_a$ and $R_z$ (JIS B 0601, 1994).....	151
Figure 8. 13: Surface Roughness ( $R_a$ ). ....	151
Figure 8. 14: Surface roughness ( $R_z$ ). ....	152

Figure 8. 15: Work-piece surface finish imagine (a. Conventional milling and b. Vibratory milling) 60X.....	153
Figure 8. 16: Work-piece surface finish imagine (a. Conventional milling and b. Vibratory milling) 200X.....	153
Figure 8. 17: Work piece surface finish imagine (a. Conventional milling and b. Vibratory milling) 60X.....	154
Figure 8. 18: Work piece surface finish imagine (a. Conventional milling and b. Vibratory milling) 200X.....	154
Figure 9. 1: Milling Forces for Aluminium: a) Conventional milling. b) Vibratory Milling. ....	160
Figure 9. 2: Milling Forces for Steel: a) Conventional milling. b) Vibratory Milling. ....	161
Figure 9. 3: Normal Force for milling Aluminium: a) Varying feed rate. b) Varying depth of cut.....	163
Figure 9. 4: Normal Force for milling Steel. ....	164
Figure 9. 5: Resultant cutting Force for Aluminium: a) Varying feed rate. b) Varying depth of cut.....	165
Figure 9. 6: Resultant Cutting Force for Steel. ....	166
Figure 9. 7: Milling Power Consumption: a) Aluminium. b) Steel. ....	167
Figure 9. 8: Milling Torque: a) Aluminium. b) Steel. ....	168
Figure 9. 9: Milling Force Ratio: a) Aluminium. b) mild Steel.....	170
Figure 9. 10: Surface Finish Profile for Steel Work Piece: a) Conventional Milling. b) Vibratory Milling.....	172
Figure 9. 11: Effect of Feed Rate on Surface Roughness (Aluminium): a) Rz Value. b) Ra Value.....	173
Figure 9. 12: Effect of Depth of Cut on Surface Roughness (Aluminium): a) Rz Values. b) Ra Values. ....	174

Figure 9. 13: Effect of Depth of Cut on Surface Roughness (Steel): a) Rz Value. b) Ra Value. .....	175
Figure 9. 14: 3D surface finish profile: a) Conventional Milling. b) Vibratory Milling. ....	176
Figure 9. 15: Chips performs after machining Aluminium: a) Conventional Milling. b) Vibratory Milling.....	178
Figure 9. 16: Chips performs after machining steel: a) Conventional Milling. b) Vibratory Milling.....	178
Figure 9. 17: End mill cutter tool: a) Conventional Milling. b) Vibratory Milling. ....	181
Figure 9. 18: Sample signals of Actual Machining: a) Conventional Milling. b) Vibratory Milling.....	183
Figure 10. 1: Closed Loop Control System Configuration.....	187
Figure 10. 2: Actual $F_x$ Signals in Open Loop control mode.....	190
Figure 10. 3: Actual Input and Output Signals in Closed Loop Control Mode.....	190
Figure 10. 4: Machining Aluminium Cutting Forces; a) Normal Force. b) Resultant force. 192	
Figure 10. 5: Machining Mild Steel Cutting Forces; a) Normal Force. b) Resultant Force. .193	
Figure 10. 6: Milling Power Consumption in Closed Loop Control mode, a) Aluminium. b) Steel.....	195
Figure 10. 7: Milling Torque in Closed Loop Control Mode: a) Aluminium. b) Mild Steel.196	
Figure 10. 8: Surface Roughness for Machining Aluminium: a) Rz Value. b) Ra Value.....	198
Figure 10. 9: Surface Roughness for Machining Mild Steel: a) Rz Value. b) Ra Value. ....	199
Figure 10. 10: 3D surface finish a) Conventional Milling. b) Open Loop Control Vibratory Milling. c) Closed Loop Vibratory Milling. ....	201
Figure 10. 11: Surface Finish Profile for mild Steel Work Piece: a) Conventional Milling. b) Open Loop Control Vibratory Milling. c) Closed Loop Vibratory Milling. ....	203

## List of Tables

Table 2. 1: The Characteristics of both rotational directions of cutter. ....	24
Table 4. 1: Specifications of 5-Axis CNC Machining Centre. ....	53
Table 4. 2: The Specifications of the iTNC 530 Heidenhain CNC controller. ....	55
Table 4. 3: The dimensions of work-piece.....	56
Table 4. 4: The Specifications of Piezoelectric Actuator (P 212.8).....	59
Table 4. 5: The Specifications of Power Amplifier Type E-472.2 .....	59
Table 4. 6: Technical Data for Kistler Charge Amplifier Type 5073 (Kistler Instrument .....	61
Table 4. 7: Specification of the GWINSTEK AFG-2225 function generator. ....	64
Table 4. 8: The specifications of the NI-Compact RIO-9022.....	69
Table 4. 9: The specification of the NI-9215 Module Slot.....	70
Table 4. 10: The specification of the NI-9234 Module Slot.....	72
Table 4. 11: The Specification of the Analogue Output NI-9234 Module Slot.....	73
Table 5. 1: Horizontal Calibration Results. ....	82
Table 5. 2: Displacement calibration results.....	85
Table 7. 1: The physical parameters of the oscillation system (Ewad, 2015). ....	115
Table 7. 2: PID Controller's Parameters and Performance characteristics.....	119
Table 7. 3, Cohen-Coon tuning parameters. ....	134
Table 7. 4: The parameters of PID controller. ....	136
Table 8. 1: Experimental machining parameters. ....	144
Table 8. 2: Experimental Machining parameters.....	146

Table 9. 1: Experimental machining parameters. .... 158

Table 9. 2: Comparison in chip’s performance between conventional and vibratory milling.  
..... 179

Table 10. 1: Experimental parameters for Vibratory Milling. .... 188

## Abbreviations

PID	Proportional, Integral, Derivative controller
SISO	Single-Input, Single-Output
$E$	error signal
$U$	Input signal to the plant
FRF	Frequency Response Function
DBB	The Double Ball Bar
DAQ	Data Acquisition System
FPGA	Field Programmable Gate Array
CPU	Computer Processing Unit
PC	Personal Computer
$G(s)$	process transfer function
RMS	Root Mean Square
ARMAX	Auto Regressive Moving eXogenous
ARX	Auto Regressive eXogenous
AC	Alternating Current
$B(s)$	Primary Feedback Signal
$C(s)$	Control Output
DC	Direct Current
DDS	Dynamic Data System
DOE	Design Of Experimental
FEM	Finite Element Method
FRF	Frequency Response Function
$K_p$	Controller Proportional Gain

Kd	Controller Derivative Gain
Ki	Controller Integral Gain
MIMO	Multi Input, Multi Output
NI	National Instrument
PZT	Piezoelectric Lead Zirconate Titanate
R(s)	Reference Input
RPM	Revolution Per Minute
UAG	Ultrasonic Assisted Grinding
VAM	Vibration Assisted Machine
VI	Virtual Instruments
1D	One Dimensional
2D	Two Dimensional
Hz	Hertz
NI	National Instrument
FPE	Final Production Error

## Nomenclature

Symbol	Meaning	Units
$t_p$	Peak time	Sec
$t_s$	Setting time	Sec
$t_r$	Rise time	Sec
$T_{p1}$	Compensated system	-
$T_{p2}$	Uncompensated system	-
$T_i$	Integral time	Sec
$T_{p1}$	Compensated system	-
$T_d$	Derivative time	Sec
$X(t)$	Intermittent position	m
$X'(t)$	Intermittent velocity	m/s
$A$	Vibration amplitude	$\mu\text{m}$
$V$	Velocity	m/s
$f$	Frequency	Hz
$\omega$	Angular frequency	rad/s
$F_c$	Cutting force	N
$F_t$	Thrust force	N
$R$	Result force	N
$F$	Friction forces	N
$F_n$	Normal force	N
$\beta$	Friction angle	$^\circ$ Degree
$\phi$	Shear angle	$^\circ$ Degree
$F_s$	Shear force	N
$\alpha$	Rake angle	$^\circ$ Degree
$F_x$	Cutting force based on X-direction	N
$F_y$	Cutting force based on Y-direction	N
$F_z$	Cutting force based on Z-direction	N
$FR$	Resultant cutting force	N

$P$	Milling power	Watt
$M_c$	Milling torque	N/m
$K$	Stiffness	$N/\mu m$
$C_s$	Compliance	$\mu m/N$
$r$	Radius	$m$
<b>RPM</b>	Angular velocity	RPM (Rounds per Minute)
$V_f$	Feed rate	mm/min
$F_z$	Feed rate	mm/tooth
$\lambda_s$	Helix angle	$^\circ$ Degree
$R_a$	Arithmetical mean roughness	$\mu m$
$R_z$	Ten-point mean roughness	$\mu m$
$\mu$	Milling coefficient	-
Cos	Cosine	-
Sin	Sine	-
$m$	Mass	Kg

# Chapter 1

## Introduction

## 1.1 Introduction

Manufacturing makes ever-increasing demands for higher machining speeds. This is particularly true in car and aircraft production but also for cutting tools. Vibration is used in various technological processes to improve the performance of the machines by exploiting intelligently the synergy of the oscillations (Astashev & Babitsky 2007). Classic examples are vibration conveyers, ultrasonic assisted turning and drilling of aerospace materials, ultrasonic grinding and vibro-impact drilling in offshore technology.

Vibration provides several benefits for various technologies, such as manufacturing, medical, communications, transport, etc. Vibration assisted machining techniques have recently become an attraction for many engineering applications. In machining processes, vibration can lead to improvements when applied in a controlled manner. Vibration assisted machining is a technique in which a certain frequency of vibration is applied to the cutting tool or the work-piece (besides the original relative motion between these two) to achieve better cutting performance (Moriwaki et al. 1991). There is a number of different experiments set up to simplify the process, but the tendency is to give a wide range of machining processes to machine hard and brittle materials (Matsumura & Ono 2008).

However, machining technology does not generally exploit the positive aspects of superimposed vibration. The avoidance of vibration (chatter) is a main concern due to its effect on accuracy. However, chatter is a persisting problem regardless of the measures taken and a list of techniques is provided in (Altintas & Weck 2004) to reduce vibration. A self-excited vibration that leads to an undulation of the cutting force, with subsequent uneven wear or fracture of the tool, causes regenerative chatter. A possible solution to this type of chatter is to apply a periodic disengagement of the tool from the work-piece; and periodic variation of the work-speed, which has been reported to increase the productivity up to 300%, (Campa et al. 2011) (Gallemaers, 1986).

According to (Matsumura and Ono, 2008), they developed an application of vibratory machining using micro end mill. Here, they machined a glass work-piece in ductile mode. However, this type of vibratory machining is not suitable for mass production. Because of the design of the holder, cutting tool and milling resulted after cutting process affected the tool

wear and cutting angle, also led to limited profile. Moreover, the productivity in the area will be extremely affected if this problem has not been concerned.

Nowadays, many research projects are trying machine brittle and hard materials, such as ceramic, glass, steel alloys and stainless steel, to a mirror surface finish. These research projects are used in different types of machining applications.

Moreover, there are several machines prepared with vibration devices for the cutting process. However, these processes of vibration machining cannot be used efficiently for cutting hard and brittle materials. The reason behind this is that the excessive wear of diamond cutting tools is affected by high chemical activity with iron (Bonifacio & Diniz 1994). In addition, for this case, many research projects have explored different ways of using ultrasonic and vibration to improve the design, cutting tools, frequency and equipment devices. Also, these research projects were used for improving the cutting process efficiency with some basic experiments that were carried over from conventional machines.

Here, this thesis proposes to review many research projects that were carried out before this project involving the ultrasonic and vibration assisted machining process. Also, the vibratory machining is still an on ongoing investigation. The commonly established fundamentals based on both factors of vibration, amplitude and frequency, is presented together with applications. In this project, the capability of vibration assisted machining technology was identified and reviewed. In addition, this thesis discusses the future direction for the applications and researches of vibratory machining especially in the milling process.

## **1.2 The Current Needs in Industry**

In the United States, the industries usually spend around 150 billion dollars per year just for metal removing operations using conventional machining technology (King, R. I., Hahn 1986). However, at the current time these manufacturing costs are going to increase significantly, because of increasing development in novel technologies and further demands for higher quality products.

According to Liu and Cheng (2005), the development of metal removing technologies in recent years has not only been looking for better surface finishes, but also for improvements

of the applications sphere. In addition, the demand for technologies for high precision machining will be increased with the miniaturization and increasing complexity of audio/visual products.

In the manufacturing process, there are many conditions where some products or work-pieces cannot be manufactured by normal or conventional machining processes. The reason behind that is some parts need more dimensional accuracy and sometimes the materials used are too hard or too brittle to machine. Kalpakjian and Schmid (2010) presented one of the best known techniques called abrasive machining process for producing such a demanding product quality.

Some industrial companies related to components of aerospace or optical parts are considering diamond machining in order to achieve high quality and performance of the products. One of the most commonly known of these methods is called Vibration assisted diamond turning presented by Ikawa et al. (1991). Here, the process used a precision ground diamond cutter cable of nanometer positioning to produce nearly error free shapes (within micrometers of those desired) with great results in surface finish roughness for the products at nanometer scale. There are some benefits of using vibration assisted turning such as the modules and fracture toughness of cutting tools remained uniform with sharp edges over the extended cutting distance up to a numbers of kilometers (Ikawa et al, 1991).

### **1.3 Novel Approach to Milling**

In this project, the vibration is applied into the milling process in order to maintain process stability and accuracy. Here, the process needs to be checked and controlled to achieve an optimum level of the disengagement between the two parts which are the cutting tool and work-piece.

The required periodic disengagement of the tool from the work-piece and the variation of the work speed led to the subject of this current study.

In this current study, the subject is covered in two parts; the required periodic disengagement of the tool from the work-piece and work speed. Recently, most of the experimental or reported works are not using a controller or are not controlling the actual vibration amplitude and frequency of disengagement between the cutting tool and work-piece.

Here, the magnitude of the vibration is set at the actuator but some disturbances such as the cutting force actions, the compliance and the damping in the system can lead to making the vibration amplitude changeable with machining time.

Therefore, the intent of this project is to build a controller for intelligently controlling the superimposed oscillations to machining technology more generally. To achieve this point, the closed loop PID control system is built and used in vibration generators. Here, the set of feedback signals, that come from the interaction between the cutting process and structure dynamics, were used as controlling parameters during actual machining time or cutting process.

### **1.4 Possible Advantages**

- Improved finished surface quality.
- Pattern definition on finished surface.
- Reduced tool wear.
- Lateral oscillation induces chip breaking effect; therefore, less friction.
- Improved cutting efficiency with low cutting forces.
- Oscillation may reduce the load per tooth and reduce overall tool wear.
- Oscillation may keep the cutting tip sharp thus it may increase the tool life.

### **1.5 Project Aim and Objectives**

#### **1.5.1 Aim of the project**

The key aim of this project is to design, model, build and control a single-dimensional piezo actuator for milling machining operation. The control of the amplitude for the oscillation in the cutting process is the fulcrum of this investigation as it is the intrinsic parameter allowing controlled and prescribed motion to achieve efficiency and pattern generation on the

machined surface. This programme of work will proceed through several stages as illustrated in the objectives.

### 1.5.2 Objectives

To achieve the aim of this stage of work, the investigation will progress through a series of tasks and objectives designed to facilitate an effective delivery of the project. The key objectives of this study are as follows:

- To design the theory of control system (design of PID controller).
- To design Data or Signal acquisition and processing using:
  - ❖ Matlab / Simulink
  - ❖ LabVIEW, Filter design
- To develop a program or software using LabView Realtime and FPGA to control the piezo actuator inside vibration system including vibration amplitude and vibration frequency.
- To embed the “soft” controller in Target PC (Compact Rio) as autonomous controller (Closed Loop)
- To investigate the optimization and control the vibration amplitude of vibratory milling process for selected application case studies

## 1.6 Thesis Layout

The thesis contents are planned and structured based on the research findings. Also, the work of this project or dissertation is divided into eleven chapters as in the following illustrations:

Chapter 2 presents the critical review about related ideas for the preparation of research finding. Also, it presents an introduction, literature review of vibration assisted machining and machining process including one and two oscillation directions, types of milling and cutting forces in milling process.

In chapter 3, the background of control systems is explained in detail. Including the following topics; Objective and design of control system, control system classification, the implementation of the control system, some information about control strategy and time domain specifications in control system and in-depth explanation of Proportional Integral Derivative (PID) controller with its design and types.

Chapter 4 describes all equipment and software used during the experimental work. This includes the following equipment; CNC Machining centre, vibration system, milling cutting tools, some sensors such as accelerometer and Eddy current sensor, piezo-actuator, power amplifier, Kistler dynamometer, surface roughness measurement devices and data acquisition hardware. Also, required software such as Solid Works, Matlab-Simulink and LabVIEW are covered in this chapter.

In chapter 5, all configurations of the calibration process are presented in detail with their results. This includes Calibration setup and the forces calibration results for three directions X, Y and Z axis. It also covers the displacement response of the vibration system with different applied values of voltage amplitude and frequency.

Chapter 6 focuses on the machine tool characteristics such as static, natural frequencies and dynamic stiffness. Also, a number of experimental tests, such as harmonic excitation and hammer impact test, were conducted to identify the natural frequency of the spindle unit, as well as its stiffness response under varying loading conditions.

In chapter 7, the system identification procedure was described. This includes flowchart of the process and mathematical model. Also, this chapter focuses on controller design which includes simulation results, experimental control system, LabVIEW code, process transfer function and PID controller tuning methods.

Chapter 8 presents the results of preliminary experimental works of the vibratory milling process. This first set of results revealed the positive and negative aspects of the vibration system. In addition, this chapter shows the experimental configuration and setup, machining trials plan and process performance including cutting forces and finishing surface roughness.

In chapter 9, more investigations in experimental works of vibration effect on the milling process with open loop control system are carried out. This includes the effects on cutting forces, milling power, milling coefficient, surface roughness, chip performance and tool wear. Also, this chapter presents the effect of vibratory milling application on machining time.

Chapter 10 presents the experimental work dealing with a closed loop control system using the PID controller. Here, the PID controller impacts the machining process during vibratory milling. Also, this chapter describes the experimental configuration for the PID closed loop system and it shows the performance of this closed loop system on the vibratory milling based on milling forces, milling power and finishing surface roughness.

Chapter 11 presents the key conclusions drawn from this project including a detailed discussion of the experimental works. Also, this chapter gives a number of recommendations for further work.



# Chapter 2

## Literature Review

## 2.1 Introduction

As far as engineering research is concerned the literature review is the first and really crucial step in the whole process. It gives the researchers insight into their topics and can inform which kind of scientific work in specific areas have been done already. Despite the importance of machining processes and the wide use of milling machines, a range of main problems remain unsolved. In addition, many benefits can be achieved by using the applications of micro-vibration on the cutting tool, on the work-piece or on the tool bed during the machining process. The positive results can be in terms of reducing cutting forces, temperatures, better surface quality and so on.

In this chapter, an insight into the work of some key researchers in the field of vibration assisted machining was carried out as well as some explanations about the basics of the milling process.

## 2.2 Vibration Assisted Machining

The basic element of vibration assisted machining is the oscillation that can be generated using a series of methods; however, piezo-actuators are commonly used. Different designs of actuators have been developed for various applications such as vibration assisted turning, milling, drilling, grinding, and, recently, the combination of electric discharge micro-milling with vibration assisted machining has been reported (Brehl, 2008).

The fundamental feature of vibration assisted machining is that the tool face is separated from the workpiece repeatedly. This technique was first employed in the precision drilling of wood and low carbon steel (Cerniway, 2005).

There are a number of processes with vibration devices for cutting purposes using diamond tools. However, the existing vibration machining process does not effectively cut in hard and Brittle materials because of excessive wear of the diamond tool due to high chemical activity with iron (Bonifacio et al. 1994).

### **2.2.1 The History of Vibration Assisted Machining**

In the early 1960s, researchers were starting to work on vibration assisted machining when this technology achieved some good results in drilling wood. The first component of precision metal cutting which benefitted from the research push, was called the hydrostatic bearing with its sub-micrometre rotational accuracy. In addition, in the late 1970s and 1980s the development of linear motors and piezoelectric driven stages allowed for tool position and control on the nanometre scale which was along with the refinement of conventional machine components such as spindle, metrology, frames, etc. (Brehl & Dow 2008).

About forty years ago, the Vibration Assisted Machining technology was discovered and refined. Also, it has now found its way into the three primary machining processes which are milling, drilling, turning and planing. However, the turning process was established or classified as the relevant method because this machining process has a combination of relatively short machining time and good quality surface finish. In addition, an additional polishing step is sometimes required to meet the ever increasing demand of industry for high machining accuracy and better surface finish regardless of which machining process is used.

In applications of vibration assisted machining, the piezoelectric actuators became the basic components. In addition, several designs of the piezoelectric actuators have been developed into various application requirements. Some of these vibration assisted machining applications were applied into milling, grinding, turning and drilling (Endo et al. 2008).

### **2.2.2 Overview of Vibration Assisted Machining**

Brehl and Dow (2008) presented a review of vibration assisted machining. In their paper, the procedure of vibration assisted machining combined precision machining with small amplitude tool vibration for the fabrication process improvement. In addition, the periodic separation between the work-piece and the tool rake face can achieve the reduction of machining forces and chip thickness. Also, this process can improve the surface finish and extend the tool life. Moreover, the authors explained the effects of vibration assisted machining when the oscillation was applied in two ways:

- In one direction, when the tool tip was driven in small returning motion.
- In two directions, when the tool tip was driven in elliptical motion.

The frequency ranges from a few Hz to 40 kHz with amplitude values between 2  $\mu\text{m}$  and 100  $\mu\text{m}$  were used in the cutting process where vibration assisted machining was applied.

However, the operating frequency for the majority of experimental tests was 20 kHz and it was observed that there was a reduction in machining time as the machine time is inversely proportional to the rate of material removal.

In 2006, Chern and Chang have done some experiments using the method of vibration assisted machining. They found that this method can improve surface roughness and extend the cutting tool life. The technique was applying two directions of vibrations during micro-milling. Two piezoelectric actuators with linear guide ways were combined in order to oscillate the machine table with the work-piece. They have used one type of material which was Aluminium alloy. In experimental tests, the applied frequencies were between 500 Hz and 10 kHz and the amplitude sets were 0, 4, 7, and 10  $\mu\text{m}$ .

Moreover, the authors note that in the micro-milling process, the slot surface roughness was improved using mills of 1 mm diameter. In addition, there is an improvement in the tool life by 22 % with vibration assisted machining. This is because the oscillation can reduce the heat that is generated during end milling. On the other hand, there are no improvements in the tool life when the worktable oscillates at high frequencies (Chern & Chuang 2006).

In 2006 Xin-hong and others were investigating the problems caused by wheel loading and the rise of the temperature in the grinding zone. To prevent the loading phenomenon two techniques were used: high-speed grinding and vibration assisted grinding which tends to stop with loading and the formation of micro-welding phenomena, friction reduction allows a better coolant delivery to the grinding zone. In addition, they found that compared with the conventional grinding method, the ultrasonic vibration grinding method can produce a lower machined surface roughness and a higher material removal rate. Also it can extend the tool life. Therefore, this method is more suitable to machining hard and brittle materials. (Xin-hong et al. 2006).

Chern et al (2006) applied vibration in ultra-precision micro drilling at higher frequencies and observed a direct effect on tool life with the amplitude having the highest influence on the interaction between the cutting tool and work-piece.

In vibration assisted machining, the intermittent gap during cutting was identified as an important mechanism in vibrational cutting. Increasing the vibration amplitude means an enlargement of the gap that allows cutting fluid to extract the heat from the cutting process. This enhances the tool's life and reduces the production cost.

In vibration assisted machining, the following advantages were reported in processing hard-to-machine material. Considerable extended tool life was observed in diamond machining of CBN, cemented carbide tools and glass compared to conventional machining, (Shamoto and Moriwaki, 1999). Weber (1984) showed that 2D vibration provides longer tool life for the same machining configuration.

Using superimposed vibration it is possible to machine brittle materials as if they were ductile. This was reported by Xiao, Sato and Karube (2003), Zhou, et al. (2003) where in precision machining a small depth in the order of 1  $\mu\text{m}$  was used. Parts machined with vibration assistance are burr free.

In 2005, Taskesen and Ercan used separately one and two degrees of freedom systems to analyse the machining tool vibrations. They developed a software package analysing chatter vibrations. Their software uses input data from the process: geometry, tool, work-piece material cutting parameters. As a result one can obtain cutting forces, tool vibrations shear angle and chatter in turning, milling, drilling and grinding.

Surface roughness in vibratory machining is better than the quality achieved by conventional machining and can reach the nanometre range depending on process configuration. In large part machining, the superimposed vibration secures a degree of precision with limited tool wear and provides surface roughness about 10  $\mu\text{m}$  RMS with 1mm depth of cut (Shamoto, et al, 2005). In precision diamond turning, Rubenach (2003) achieved surface finishes in the range of 10-30 nm RMS, whereas Brehl et al. (2006) reported some economical machining distances of hundreds to several thousand metres in hardened steels.

When depth of cut is kept to a small value and the frequency carefully controlled, many brittle materials are machined as if they were ductile, producing chips by means of plastic deformation and with minimal sub surface cracking (Xiao, Sato, Karube, 2003). However, in practice ductile-regime machining frequency remains uneconomical since the critical depth of cut is very small.

Tsiakoumis, (2011) showed that the application of vibration to grinding improved the surface finish quality due to the lapping effect; a reduction of cutting force and reduction of grinding power; interrupted contact allowed for better coolant delivery over the entire contact zone with trapped coolant between successive oscillations which is impossible in continuous grinding and self-sharpening process because grains operate in two directions securing longer wheel life.

According to Ostasevicius, et al, (2013), a statistical analysis of the collected roughness data allowed us to establish that the dynamic characteristics (excitation frequency) of the tool and machining method (with or without the assistance of high-frequency vibrations) have the largest effect on surface quality. The reported research results demonstrate that it is crucial to dynamically tailor the excitation frequency of the vibration cutting tool in order to generate the required vibration mode in the mill cutter and thereby achieve the most pronounced improvement in surface finish in difficult-to-cut materials.

Ding et al, (2010) showed that on a three dimensional cutting force model of two dimensional (2D) vibration assisted micro end milling the maximum cutting force increases with an increase in the amplitude of the vibration, and the average cutting force increases when the amplitude is less than 2  $\mu\text{m}$  and remains almost constant after the amplitude exceeds 2  $\mu\text{m}$ .

### **2.2.3 Ultrasonic Assisted Machining**

In machining processes such as milling, grinding, drilling and turning, the ultrasonic assisted machining method is widely used. Babitsky and others (Babitsky et al. 2004) (Astashev & Babitsky 2007) have presented one of the most referable works. They successfully applied ultrasonic oscillations to the cutting tool during turning process. Here, their tests were on machining aviation materials. The oscillation was on the feed direction, not the same direction of the authors' previous works where the oscillations were applied on the tangential and radial directions. Figure 2.1 shows their experimental configuration of the ultrasonic transducer.

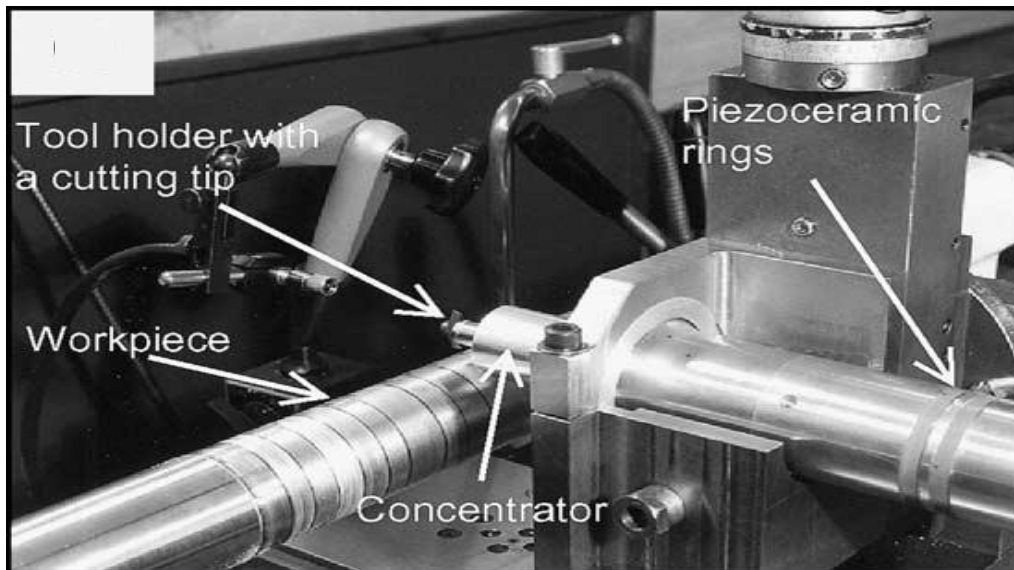


**Figure 2. 1: Experimental setup for Ultrasonic Vibration Turning** (Babitsky et al. 2004).

As the authors applied the vibration in their experimental tests on the feed direction, they had considered that the critical feed velocity should be more than the feed velocity. These parameters are determined by the vibration system parameters such as frequency and amplitude. Therefore, the authors have used the critical feed velocity equal to 25.64 m/min for vibration system. This is because they applied machining parameters equal to 0.05 mm/rev for feed rate, 20 m/min for cutting speed and 38 mm for the work-pike diameter, so with these machining parameters the feed velocity became 0.0084 m/min which is less than the critical feed velocity. The oscillation parameters were 17 kHz for frequency and 20  $\mu$ m for peak to peak tool displacement amplitude.

During turning of some materials such as Inconel-718 and mild steel, the authors found that there is a serious improvement up to 40 % in surface roughness of the work-piece compared to conventional turning.

In 2004 Mitrofanov and others presented in their paper a finite element model. They tried to apply in their work high values of frequency vibration up to 20 kHz with 10  $\mu$ m vibration amplitude in order to simulate ultrasonic vibration during the turning process. They worked to improve the machining process and reduce the heat, cutting force and noise radiation. In addition, the authors showed that the developed finite element model can provide the chip

formation and the cutting stresses along the surface of the work-piece in both machining modes: ultrasonic vibration and conventional (Mitrofanov et al. 2004).

According to the work of Moriwaki and others (Moriwaki et al. 1991) which was about applying ultrasonic vibration in diamond turning of stainless steel, in their application, there were three possible directions for applying vibration; thrust direction, feed direction and cutting direction. However, in the experimental work, the authors only used the ultrasonic vibration on the cutting direction.

Figure 2.2 shows the cutting direction and the applied vibration direction. In this work the ultrasonic vibration was used with different values of feed rate. Also, in this figure the symbols  $a$  and  $v$  stand for the vibration amplitude and the cutting speed respectively.

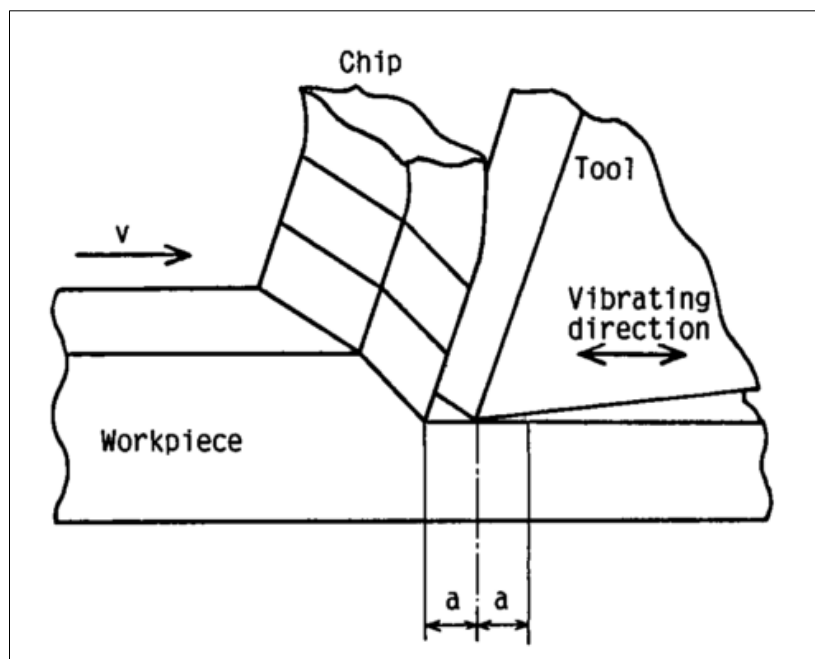


**Figure 2. 2: Applied Ultrasonic Vibration with Cutting Direction** (Moriwaki et al. 1991).

In the work of Moriwaki and others (Moriwaki et al. 1991), the vibration frequency of 40 kHz was applied into the diamond tool tip. This value of frequency is twice that of

conventional ultrasonic cutting. The reason why they used this high frequency is to reduce the vibration marks of the surface finish for work-piece. The authors used 3  $\mu\text{m}$  for the vibration amplitude and the speed value of 45 m/min as the maximum vibration speed. Here, they used the tool tip that was made of synthetic diamond and precisely ground.

These are some facts of the Moriwaki et al. experimental results:

- The tool wear was not significant throughout a number of tests and obtained with the same cutting tool.
- The best surface roughness was achieved with the smaller feed rate, where the surface roughness value was equal to 0.026  $\mu\text{m}$  which was reached at a feed rate of 3  $\mu\text{m}/\text{rev}$ .
- The regular vibration marks were still visible as well as the feed marks.

## 2.3 Cutting Mechanism in Vibration Assisted Machining

### 2.3.1 1-D Vibration Assisted Machining

In 1-D vibration assisted machining, the oscillation direction is moved in one plane to the work-piece surface as shown in figures 2.3 and 2.4.

The application of vibration assisted machining in figure 2.3 was designed by Shamoto (2004) and the oscillation in this approach is moved in one plane parallel to the surface of the work-piece, so inline to the principal cutting force.

However, there is another style of 1-D vibration assisted machining where the tool is driven in a linear path subjected to the vibration parameters such as frequency and amplitude as shown in figure 2.4. Moreover, this method has been used by some authors i.e. Shamoto, Isaev, Moriwaki, Skelton and Kumbabe, et al. in the early stages of their investigations of vibration assisted machining. The equations that explained the intermittent contact of tool rake face relative to the work-piece are given by:

$$X(t) = A \sin(\omega t) + Vt \quad (2.1)$$

$$X'(t) = \omega A \cos(\omega t) + V \quad (2.2)$$

Where:

- $X(t)$  and  $X'(t)$  are the intermittent position and velocity at time ( $t$ ).
- $A$  is vibration amplitude.
- $\omega$  is the angular frequency, so the vibration frequency is equals  $f = \frac{2\pi}{\omega}$
- $V$  is a velocity.

In addition, figure 2.4 shows the work-piece motions which are directed toward of the negative  $X$  direction. This phenomenon result is because  $V$  is the relative velocity between the tool and work piece.

In panel 1 of Figure 2.4 , the tool velocity  $X'(t)$  relative to the work is more than zero, so the tool rake face has just come into contact with the uncut material and is starting to cut. The time of initial contact with the uncut work material is selected as  $t_1$  in the same figure. In panel 2 the tool is at the limit of the linear vibration path with  $X'(t) = 0$ , and is about to reverse direction. The time the tool breaks contact with the work-piece material at the end of reverse direction. The time the tool breaks contact with the work-piece material at the end of its cutting motion is selected as  $t_2$ . In panel 3,  $X'(t)$  has reversed so that the tool withdraws from the work-piece. In panel 4, the tool velocity  $X'(t)$  is again positive, and the tool is shown advancing into contact with the work-piece as it starts a new cutting cycle (Brehl, 2008).

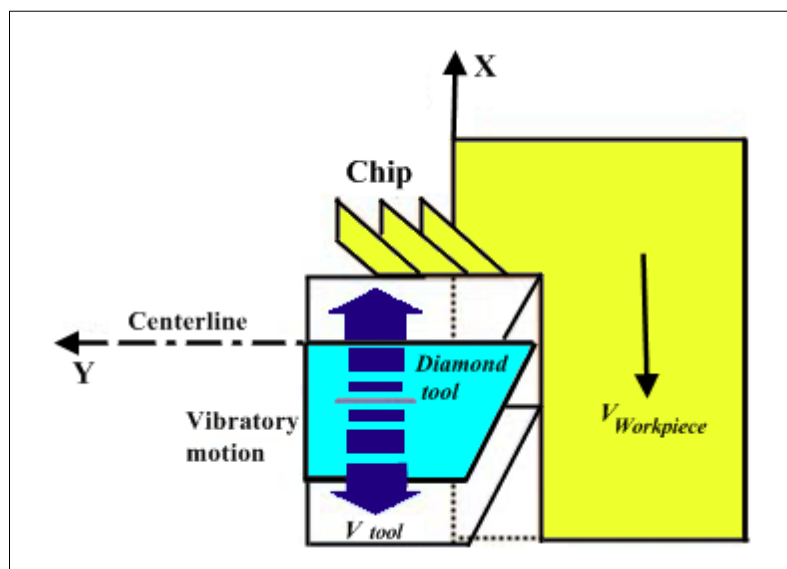


Figure 2. 3: 1-D Vibration assisted machining (Shamoto, 2004).

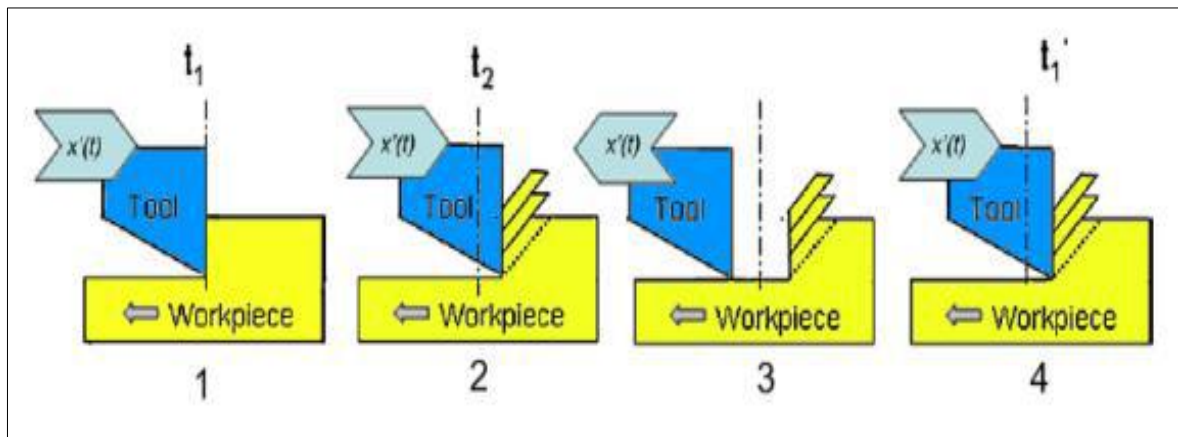


Figure 2. 4: 1-D Vibration Assisted cutting (Brehl, 2008).

### 2.3.2 2-D Vibration Assisted Machining

When the application of 1-D vibration assisted machining has one more motion, the 2-D vibration assisted machining system will be formed. Here, the vibration system will have elliptical tool or work-piece motion as seen in figure 2.5. In addition, this case can be achieved when the tool or work-piece is oscillated in both directions; cutting force  $X$  and thrust force  $Y$  as shown in figure 2.5.

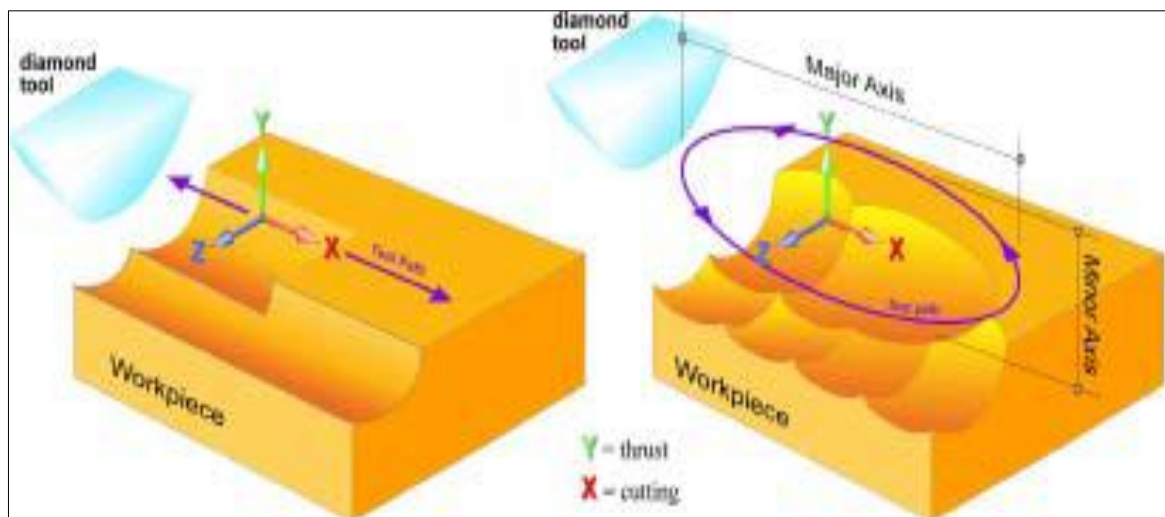


Figure 2. 5: 1-D and 2-D Vibration Assisted Machining (Cerniway, 2001).

Shamoto and Moriwaki (1999) have demonstrated experimentally the theory of reducing the cutting forces in the application of vibration assisted machining as seen in figure 2.5. Here, from their experimental works they observed that the values of both cutting forces, thrust force and instantaneous force (peak), are the same cutting forces values as in conventional cutting when they apply a low frequency on the oscillation system (from 0 to 6 Hz). However, they found that when the cutting tool does not have cutting forces at all, there is a zero time period. Thus, this case of no cutting force is coming from the kinematic disengagement (tool separation). Also, this happens when there is no contact between the cutting tool and the work-piece. The authors found that there is approximately 30% to 40% reduction of cutting forces in vibration assisted machining compared to conventional machining.

Another work was carried out by Ahmed et. al. (2007) in ultrasonic assisted turning. They observed that there was a decrease of up to 52% in the average cutting force when they increased the vibration amplitude. This happens again because by increasing the vibration amplitude, the part of a cycle for ultrasonic vibration machining with no contact between the cutting tool and work-piece will be increased.

In addition, the authors note that when the vibration frequency was increased from 10 kHz to 30 kHz, it could reduce the average cutting forces up to 47%, which also could increase the velocity of the cutting tool vibration. Therefore, the increasing value of vibration frequency or vibration amplitude leads to a reduction in cutting forces in the application of vibration assisted machining that is beneficial to increasing the accuracy of the cutting process and improving material removal rates.

## 2.4 Milling Machine

Milling machine is one of the important machining operations. In this operation the work-piece is fed against a rotating cylindrical tool. The rotating tool consists of multiple cutting edges (multipoint cutting tool), normally axis of rotation of feed given to the work-piece. The milling operation is distinguished from other machining operations on the basis of orientation between the tool axis and the feed direction. However, in other operations like drilling, turning, etc. the tool is fed in the direction parallel to the axis of rotation.

The cutting tool used in milling operation is called the milling cutter, which consists of multiple edges called teeth. The machine tool that performs the milling operations by producing the required relative motion between work-piece and tool is called the milling machine. It provides the required relative motion under very controlled conditions. These conditions will be discussed later in this project as milling speed, feed rate and depth of cut.

Normally, the milling operation creates plane surfaces. Other geometries can also be created by the milling machine. The milling operation is considered an interrupted cutting operation in which the teeth of the milling cutter enter and exit the work-piece during each revolution. This interrupted cutting action subjects the teeth to a cycle of impact force and thermal shock on every rotation. The tool material and cutter geometry must be designed to bear the above stated conditions. Depending upon the positioning of the tool and work-piece, the milling operation can be classified into different types.

### 2.4.1 Milling Machine Types

Milling operation is broadly classified as peripheral milling and face milling.

#### a) **Peripheral Milling:**

This operation is also called plain milling operation. In this operation the axis of the rotating tool is always kept parallel to the surface being machined as seen in figure 2.6. This operation is done by the cutting edges on the outside periphery of the milling cutter. Different types of peripheral milling operations are possible as described below.

#### Slab Milling:

In this milling operation the cutter width extends beyond the work-piece on both sides.

### Slotting:

This is another type of milling operation, also called a slot milling operation. In this case width of the cutter is less than the width of work-piece. It is used to make a slot in the work-piece. Thin slots can be made by using very thin milling cutters. The work-piece can be cut into two pieces by making a very thin slot throughout the depth of the work-piece. Cutting the work-piece this way by slot milling is called saw milling.

### Side Milling:

The cutter is used for milling the sides of a work-piece.

### Straddle Milling:

It is just like side milling with the difference that the cutting (milling operation) takes place simultaneously on both the sides of the work-piece.

Peripheral milling is also classified on the basis of the rotational direction of the cutter, as up milling and down milling.

### Up Milling:

It is also called conventional milling; in this case the movement of the cutter teeth is opposite to the direction of feed motion as seen in figure 2.7. The advantages over conventional milling are (Kalpakjian and Schmid, 2010):

- 1- Tooth engagement is not a function of work-piece surface characteristics.
- 2- Contamination or scale (oxide layer) on the surface does not adversely affect tool life.

### Down Milling:

It is also called climb milling. In this case the direction of the cutter motion is the same as that of the direction of feed motion as displayed in figure 2.7. The advantage is that the downward component of the cutting force holds the work-piece in place, particularly for slender parts. However, because of the resulting impact forces when the teeth engage the work-piece, this operation must have a rigid work-holding setup, and gear backlash must be eliminated in the table feed mechanism.

Table 2.1 presents the comparisons between both rotational directions of cutter:

**Table 2. 1: The Characteristics of both rotational directions of cutter.**

Up Milling	Down Milling
<ul style="list-style-type: none"> <li>• Tool rotation opposite to the feed</li> <li>• The chip starts as thin and increases in thickness</li> <li>• The length of the chip is longer</li> <li>• Tool life is relatively short</li> <li>• Need more clamping force to hold the work-piece.</li> </ul>	<ul style="list-style-type: none"> <li>• Tool rotation is parallel to the feed</li> <li>• The chip starts at max thickness leaves out thin.</li> <li>• The chip length is short</li> <li>• Tool life is relatively long</li> <li>• Need less force to hold work-piece.</li> </ul>

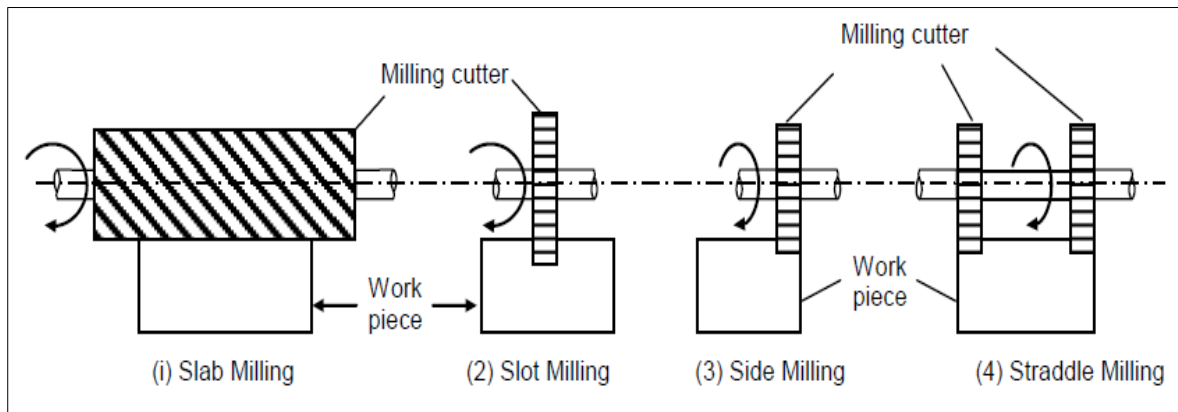


**Figure 2. 6: Different types of Peripheral milling. (Knight and Boothroyd, 2005) & (Kalpakjian and Schmid, 2010).**

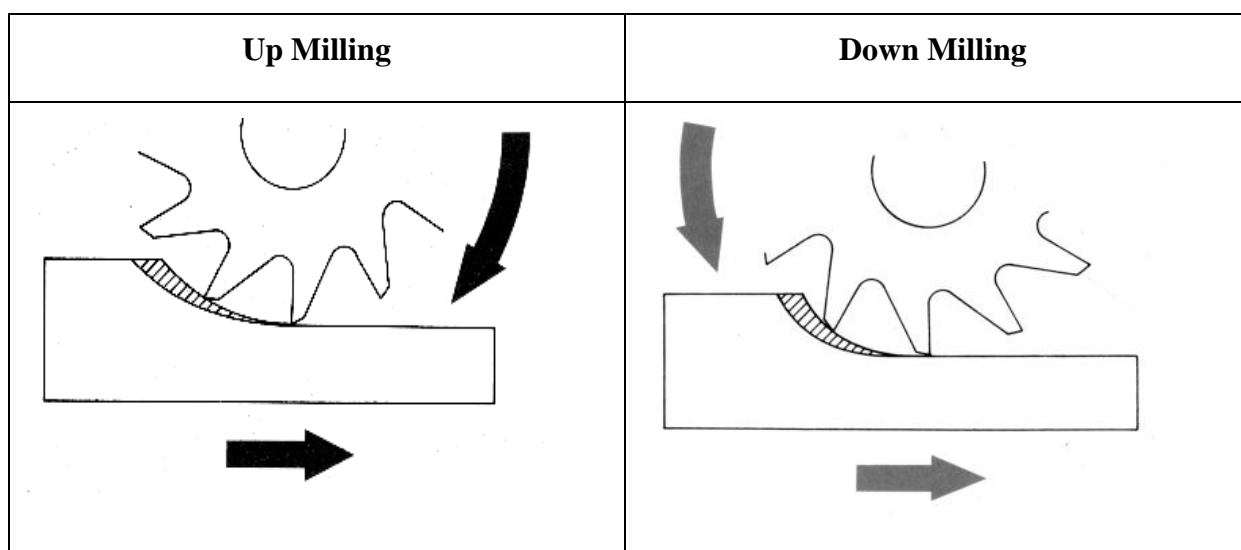


**Figure 2. 7: Both Rotational Directions of Cutter (Up and Down Milling).**

**b) Face Milling**

In the operation of face milling, axis of the milling cutter remains perpendicular to the surface being milled. In this case cutting action is done by cutting edges of both sides (end and outside) periphery of the milling cutter. Depending upon the relative geometry of the work-piece and milling cutter face, milling can be classified in different types as described below.

Conventional Face Milling:

In this case the diameter of the milling cutter is greater than the width of the work-piece. The milling cutter remains overhanging on both sides of the work-piece.

Partial Face Milling:

In this case the milling cutter overhangs the work-piece on one side only.

End Milling:

In case of end milling, a thin (low diameter) cutter is used as compared to the work-piece width. It is used to make a slot in the work-piece.

Profile Milling:

This is just like end milling in which the outer side periphery of a flat part is machined (milled).

Pocket Milling:

This is a selective portion milling on the flat surface of a work-piece used to make shallow pockets there.

Surface Contouring:

In this operation a ball nose cutter is fed back and forth across the work-piece along a curvilinear path at short intervals. This creates the required contours on the surface of the work-piece. This operation is used to make contours of moulds and dies and this time the operation is named as die sinking.

Figure 2.7 shows the types of face milling.

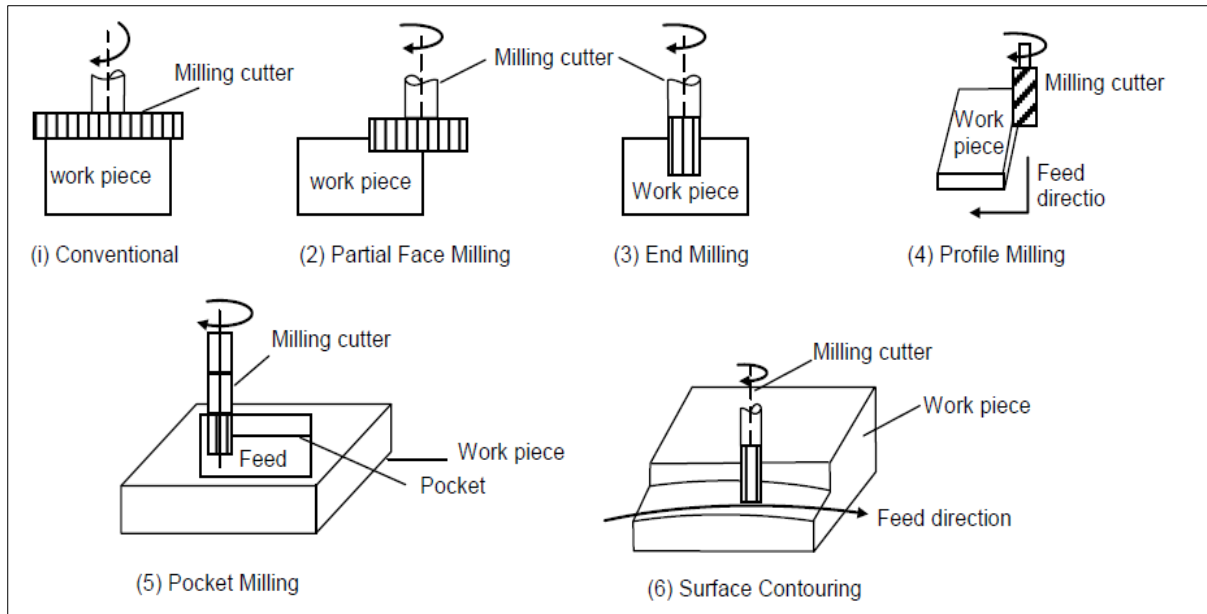


**Figure 2. 8: Different types of face milling. (Knight, Boothroyd, 2005) & (Kalpakjian and Schmid, 2010).**

## 2.5 Cutting Force and Power

Knowledge of the cutting forces and power involved in machining operations is important for the following reasons:

1- Data on cutting forces is essential so that:

- Machine tools can be properly designed to minimize distortion of the machine components, maintain the desired dimensional accuracy of the machined part, and help select appropriate tool holders and work holding devices.
- The work-piece is capable of withstanding these forces without excessive distortion.

2- Power requirements must be known in order to enable the selection of a machine tool with adequate electric power.

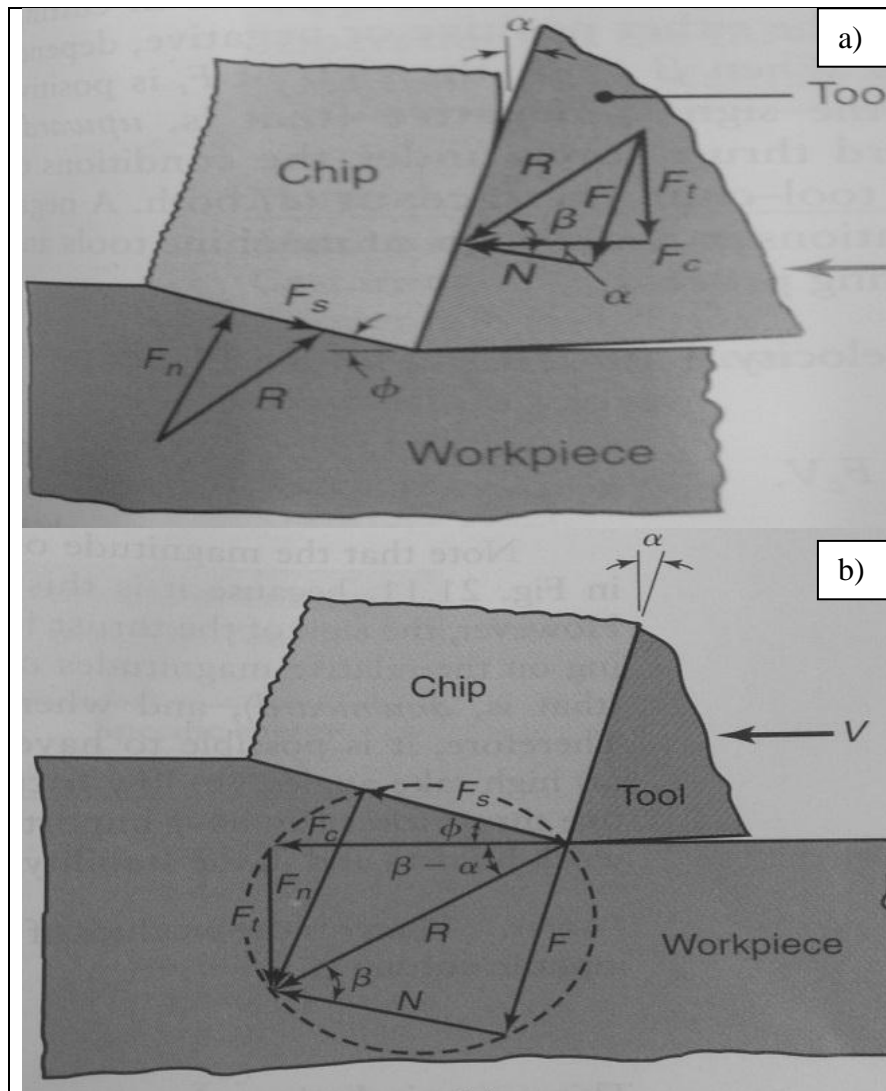


Figure 2. 9: a) Cutting forces. b) Force Circle. (Kalpakjian and Schmid, 2010).

The forces acting in orthogonal cutting are shown in Figure 2.9.a. The cutting force ( $F_c$ ) acts in a direction to the cutting speed ( $V$ ) and supplies the energy required for cutting.

The thrust force ( $F_t$ ), acts in a direction normal to the cutting force. These two forces produce the result force ( $R$ ) as can be seen from the forces circle shown in Figure 2.8.b. In addition, the result force can be resolved into two components on the tool face: firstly, a friction force ( $F$ ) that is along the tool chip interface. Secondly, a normal force ( $N$ ) which is vertical to the tool-chip interface (Kalpakjian and Schmid, 2010). The equations for the friction force and normal force are shown below:

$$F = R \sin \beta \quad (2.3)$$

$$N = R \cos \beta \quad (2.4)$$

Where  $\beta$  is the friction angle.

Moreover, the resultant force is balanced by an equal and opposite force along the shear plane and is resolved into a shear force ( $F_s$ ) and normal force ( $F_n$ ). Therefore, these forces can be derived as:

$$F_s = F_c \cos \phi - F_t \sin \phi \quad (2.5)$$

$$F_n = F_c \sin \phi + F_t \cos \phi \quad (2.6)$$

Where  $\phi$  is a shear angle.

The direction of thrust force ( $F_t$ ) can be affected by rake angle and friction angle as shown in equations below:

$$F_t = R \sin(\beta - \alpha) \quad (2.7)$$

$$F_t = F_c \tan(\beta - \alpha) \quad (2.8)$$

Where  $\alpha$  is a rake angle.

In addition, the value of the cutting force ( $F_c$ ) is always positive, because it is the force which is required for the cutting process. On the other hand, the thrust force can be either positive or negative value; it is dependant on the relative value of friction angle ( $\beta$ ) and rake angle ( $\alpha$ ). When the friction angle is greater than the rake angle the sign of the thrust force is positive (downward), and when the friction angle is smaller than the rake angle the thrust force will get a negative sign (upward).

Power is the product of force and velocity. Thus, from figure 2.9b, the power input in cutting can be shown as (Kalpakjian and Schmid, 2010):

$$\mathbf{power = F_c V} \quad (2.9)$$

## 2.6 Remarks

In this present work the cutting forces are important as they are affecting the quality of the work-piece. In addition, the magnitude of cutting forces can be affected by many factors such as tool geometry, feed rate, cutting speed, material properties and depth of cut.

In the milling process, the cutting forces are made of three cutting forces based on their directions  $F_x$ ,  $F_y$  and  $F_z$  as shown in figure 2.10.

These three cutting forces are measured during machining time using dynamometer sensor as explained deeply in chapter 4.

Therefore, the resultant cutting force ( $FR$ ) can be defined by equation 2.12:

$$FR(x, y \& z) = \sqrt{Fx^2 + Fy^2 + Fz^2} \quad (2.10)$$

Now, milling power and milling torque can be calculated as;

$$Power (W) = \frac{Cutting\ Force\ (FR) * Feed\ Rate\ \left(\frac{mm}{min}\right)}{60 * 1000} \quad (2.11)$$

$$Mc (Nm) = \frac{30 * power(w)}{\pi * RPM} \quad (2.12)$$

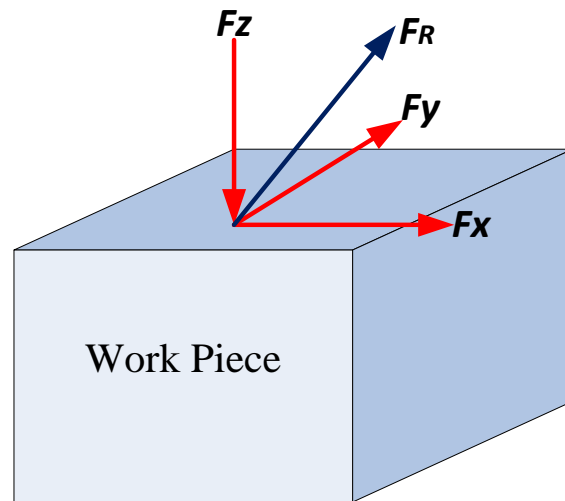


**Figure 2. 10: The Cutting Force Compounds.**

# **Chapter 3**

## **Control Background**

### 3.1 Introduction

Nowadays control engineering systems play a significant role in the modern civilization developments. The self-operation systems have become widely used and have a massive impact on our life. Simple domestic applications like air conditioning or complicated applications like rocket science are all classified as automation devices that need to use the control system knowledge. Therefore, topics like mechanical, hydraulic, pneumatic, electric, thermal and sometimes computer programs become nowadays a part of control system applications. The key point for designing a control system is observing and regulating the system operation to reach a desired specification of the system outputs or performance. In addition, the elements of any automatic controlled systems are actuators, plant, sensors and control unit. In sensitive cases, some control system applications use mathematical models for designing the systems to allow adjusting the controller performance for them.

The classification of any control system can be according to the system equations and characteristics. For example, some mechanical systems are commonly classified as motion control system such as velocity control, position control and torque control. In addition, a self-control system can be defined as a process of the interconnection between the system devices or components. Therefore, the outputs of the system should follow the desired signals as closely as possible. All the following systems can be part of the objects of designing control systems; the automatic control like controlling room temperature, the power amplification like automobiles' power assisted steering system and remote control like antenna position control.

In this chapter, the objectives, design, terminology, parameters of control systems and PID controllers are explained in detail (B. Wayne Bequette 2003).

## **3.2 Control System Objectives**

There are three objectives for the control system; they are transient response, steady state response and system stability (B. Wayne Bequette 2003).

### **3.2.1 Transient System Response**

In control systems, the transient response is important. It can be the primary reaction of the system output from the input signal. Therefore, the components of the system are appropriated with transient response of the process plant in controlled systems. Moreover, the key point of designing the control system is achieving a desired transient response by adjusting various design components or design parameters.

### **3.2.2 Steady State Response**

Steady state response of control systems is a function of input signal and it is also called forced response. When the transient response is decayed to zero, the steady state response is similar to the input signals and what should remain.

The steady state errors should be considered by the control system designers and they need to produce a corrective action to minimise the value of the steady state error.

### **3.2.3 Stability control**

The natural and force response are known as the total system response. In the natural response, the system can be dissipated or acquired energy dependent on the parameters of the system such as geometry and mass not on the input signals. On another hand, the force response is dependent on the input signals excitation.

Here, the natural response should be approaching zero or vibrating slightly leaving only the force response for getting a useful and stable control system. However, some systems note that the natural response is growing without limit or bounds rather than in the force responses. In these cases, if the limit stops are not considered on the control system design, the system becomes unstable and may lead to physical destruction.

### 3.3 The Design of the Control System

The following points should be considered in order to reach a good design and implementation for the control system:

- The desired specification of the system outputs.
- The system output signal such as feedback sensor with its resolution and dynamic response.
- The kind of the control device.
- The process plant.
- The kind of actuating devices.

Figure 3.1 presents the design flow chart for the control system design.

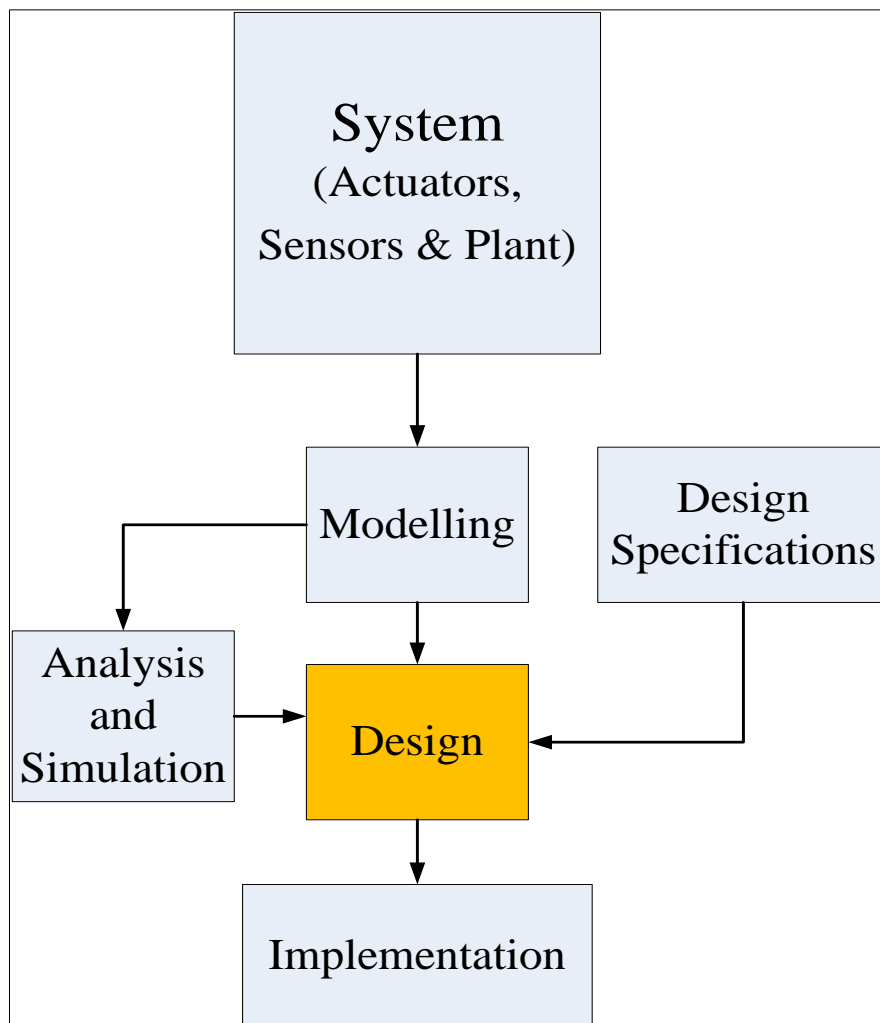


Figure 3. 1: The Control Design flow chart.

For designing any control systems, there are many different ways. However, using one of the following ways, the operated variables can be generated from the error.

- By analogue or digital signals.
- Mechanically or electrically.
- Secondary energy (with or without)

On the control response, these three ways are not effective. Thus, they significantly influence the controller selection and the main principal value for determining the control response is the operated variables. So, the control system design is classified according to the response of control signals. Also, there are two classifications for the control signals; continuous and discontinuous signals (D'Azzo, J. and Houpis 1966).

### **3.3.1 Continuous Controller**

The operated variable of the controller outputs can be changeable to any values within the range of controller outputs in case of the continuous controller.

In addition, the action of the continuous controllers can be the sum of all or some of proportional, integral or differential, and can become individually of these action elements.

### **3.3.2 Discontinuous controller**

In this case, of control system design, the operated variable of the discontinuous controller can only have discrete or separate values.

In discontinuous controller, the distinction or the different state of the operated variable is made between two or more positions controller compared to continuous controllers which use a continuous signal.

## 3.4 Terminology

In this section, the terminology of control system process that simulated in Matlab software is discussed and explained step by step as seen in figure 3.2. Each step of the control system process is described in a numbered sequence.

### 1. Reference Point or Input $R(s)$ :

It is also called Set point. Reference input is the external signal that is applied to a closed loop control system in order to serve as the reference and standard of comparison for the directly controlled variable or to clarify the specified action of the plant process.

### 2. Summing point:

Any point in a control system block or components at which signals are added or subtracted or it is probably the point at which various control signals are added and then given out for further calculation. It has a symbol of a circle with cross as seen in figure 3.2.

### 3. Error Signal:

It is the value of the subtraction between the reference (set) point and the primary feedback signals. It also can be called a control action or actuating signal.

### 4. Control Element:

It is known as the controller and is the component that sends the control signals to the plant of the process.

### 5. Control signals:

Also called Manipulated variable. The control signals are the conditions or orders which the controller applies to the process plant.

### 6. Plant model:

The plant is described as a physical object that needs to be controlled. Also, it is the combination of the process and actuators. It is often referred to as a transfer function which describes the relationship between the inputs and the outputs of the system.

**7. Disturbance:**

The disturbance is not considering input signals that apply to controlled system or any process system. These disturbance signals can affect the controlled system outputs.

**8. Process outputs:**

Also called Controlled outputs. The process outputs is the quantity or conditions of the process plant that have been controlled.

**9. Feedback element:**

The feedback elements are feedback loop that take the output signals back to the system for establishing the function relationship between the primary feedback signal and the system controlled outputs.

**10. Feedback Signals:**

These signals are coming from the controlled outputs or the process outputs. They also are algebraically calculated with the reference input point for obtaining the controller signals.

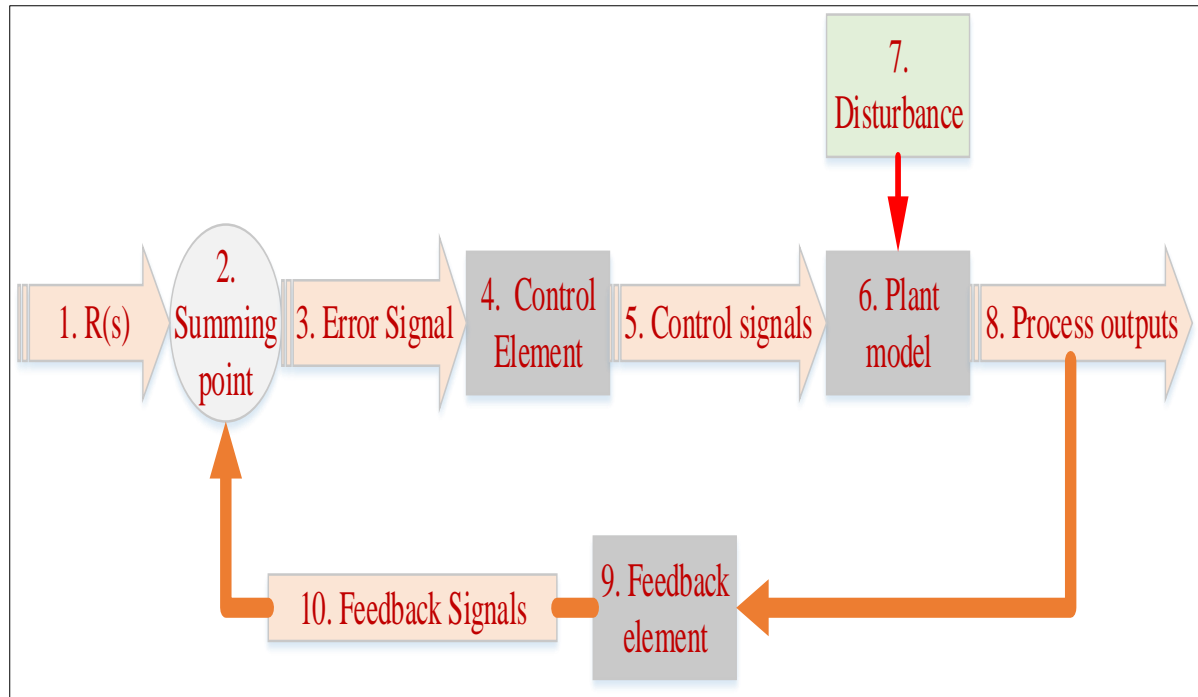


**Figure 3. 2: Control System Block Diagram Components.**

### 3.5 Control System Classification

There are two classifications of the control system an open loop control system and closed loop control system. In this section, each control system is clarified and explained in detail as follow.

#### 3.5.1 Open Loop Control System

Open loop control system is usually used with some simple processes where the inputs are known in advance. In addition, the controller outputs have no significant disturbance, so the changing of disturbance inputs makes the process outputs sensitive to these changes. The disturbance inputs can be known as inconsideration inputs, which affect the process outputs to be variable of desired process outputs.

The control actions in open loop control systems are not dependent on the process outputs. However, the open loop controller should be calibrated and adjusted at steady intervals to ensure a proper operation. There are two main features for using the open loop control system:

- It can be able to perform accurately but it is dependent on its calibration.
- This control system is not generally troubled with instability issues.

The block diagram and experimental set-up of open loop control systems are presented in figure 3.3

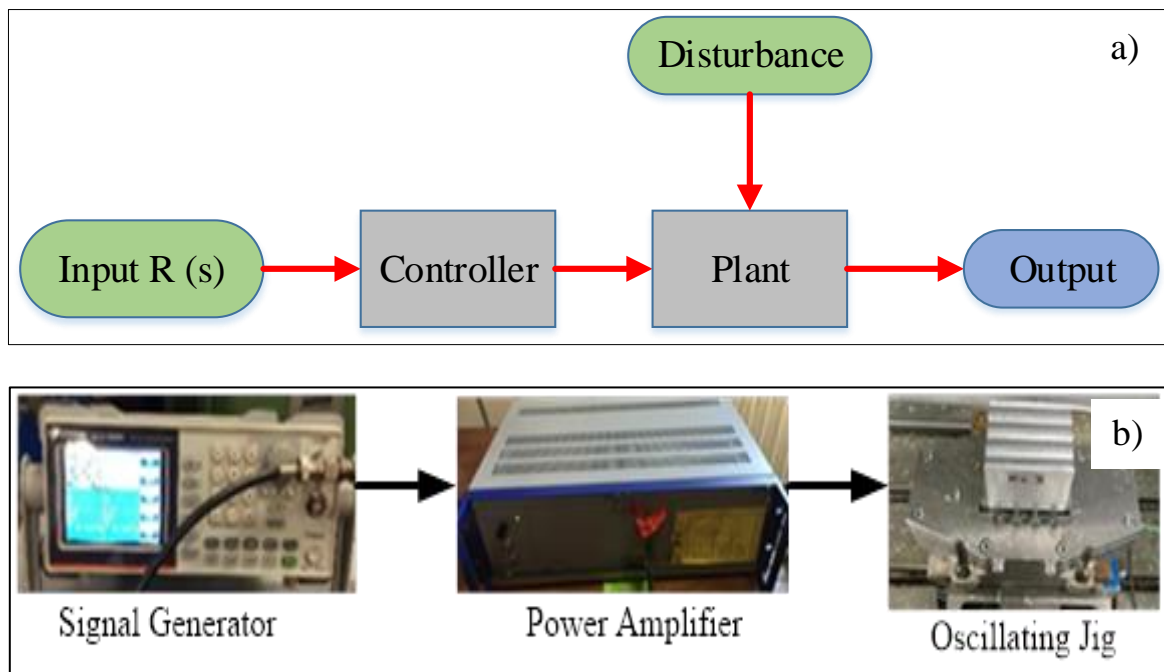


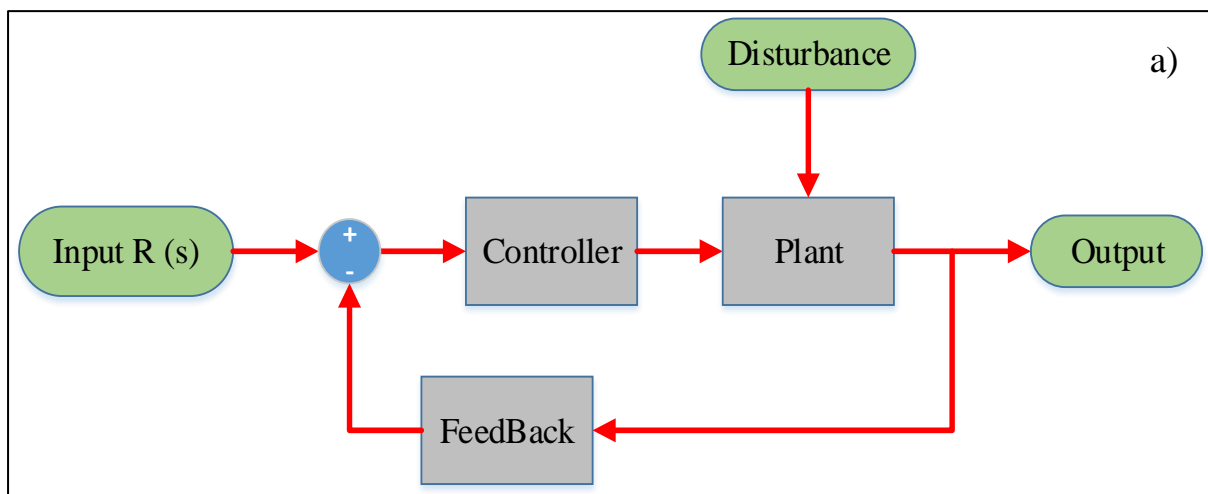
Figure 3. 3: Open Loop control system; a) Block Diagram. b) Experimental set up.

### 3.5.2 Closed Loop Control System

In the closed loop control system, the control actions are often dependent on the process outputs. The system with a closed loop controller is also called feedback control system. Here, the feedback signals are the key elements of the closed loop control system (Phillips C. L. 2000).

In addition, the feedback signals are the process output variables that be returned to the process for the controlling procedure. Therefore, these feedback signals can let the appropriate control action be formed as some function of the input and output. Moreover, the feedback control actions are classified as continuous and discontinuous as was mentioned in section 3.3.

Figure 3.4 shows a block diagram and experimental setup of the closed loop control system. Also, this figure notes that there is a feedback path on the closed loop system. The reference input (set point) and the process output are subtracted from each other after delivering the process outputs to the first summing junction via feedback path. Then, the actuating signals are generated from the difference value between the reference input and process output. After that, the controller system drives the actuating signal to the plant. However, if the system has no difference and the process outputs have matched the reference input (set point) then the controller or the control system is not going to send any actuating signals to the process plant.



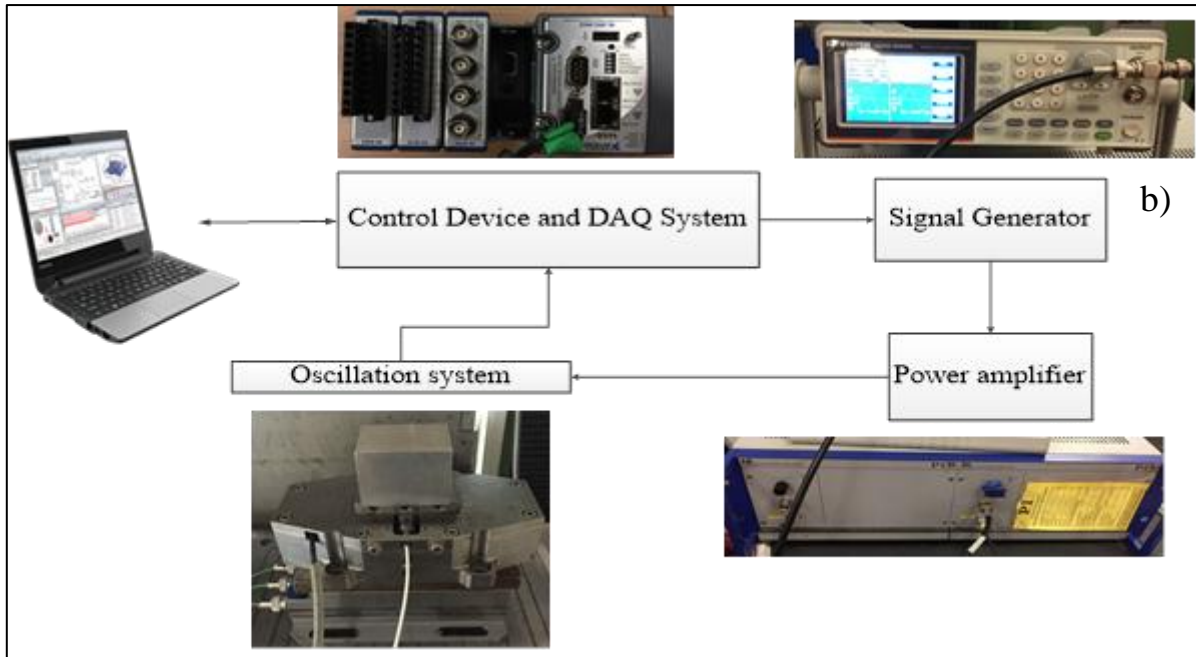


Figure 3. 4: Closed Loop Control System; a) Block Diagram. b) Experimental Configuration.

## 3.6 PID Controller

### 3.6.1 Introduction

The Proportional-Integral-Derivative (PID) controller will be introduced in this section. The basic algorithm will be explained in detail as will be the case in its various representations. In addition, this chapter will give the properties description of the controller in a closed loop. It will discuss the reset windup concept that happens when the connection of an integral action for the controller is applied into a process with a saturating actuator, and several methods to avoid it will be discussed too.

There are several key functions of the Proportional-Integral-Derivative (PID) controller. For example, it can provide feedback, it is able to remove the offsets of steady state by integral action and it can have expectations of the future by derivative action. The Proportional-

Integral-Derivative controllers are well suited to various control problems, mainly when dynamics of the process are benign and the requirements of the performance are unassuming. In several industries, the PID controllers can be used. Therefore, there are many different forms of the controllers. Hundreds of thousands from standalone systems designed for one or a few loops are produced every year. PID control is an integral part of a dispersed control process. Generally, Controllers are integral to several control systems of the special-purpose type. A lot of the control loops in process control are of the PID control type. Many useful features of PID control are considered trade secrets so have not been widely disseminated. Mode switches and anti-windup techniques are examples (B. Wayne Bequette 2003)..

The PID control can be combined with other processes to make the complex systems of automation which can be used for transportation, energy production, and manufacturing. Also, these can logically include selectors, sequential machines and blocks of simple function. Many sophisticated control strategies are also organized hierarchically, such as model predictive control. At lowest level the PID control can be used, the set-point is given to the controllers at the lower level by the multivariable controller. In the control engineering, the PID controllers are often considered to be the bread and butter, and they become the main part of the control engineer's toolbox.

The Proportional-Integral-Derivative controllers have been observed in several technology developments, such as integrated circuits and transistors. The most dramatic influence of the Proportional-Integral-Derivative controller was on the microprocessor development as practically, factories currently are manufacturing all PID controllers based on microprocessors. This can be developed with additional features, such as, gain scheduling, automatic tuning and continuous adaptation. Because these are fairly new development areas, their terminology is not yet well-established. For the purposes of this study, auto-tuning can be defined as the automatic tuning of the controller parameters on order from an external signal or an operator; also adaptation can be described as the controller's parameters are always updated. Some degree of automatic tuning is considered standard in PID controllers today. There are various methods and approaches to tuning and adaptation but the simple controller is still considered to be a benchmark for any new ideas.

Another important development is the emergence of the field-bus, it has the potential to drastically influence the design and structure of future distributed control systems. The most important ingredient of the field-bus concept is the PID controller. It could help to standardize the field as a whole.

The PID controller became familiar to many applications and process engineers and there is a well-established practice of installing, tuning, and the controllers' applications in society and industry. However, there is still vast potential for the improvement of PID control. Moreover, most controllers in the control rooms of any industry are operated in a manual mode, and among these controllers which are in automatic mode, the derivative action of PID controller is often stopped because it is difficult to be tuned correctly. The poor tuning practice and the limitations of equipment such as sensors and valves are the main reasons for poor performance. The valve problems can include hysteresis, striation and wrong sizing. The limitations of measurement can include excessive filtering in "smart" sensors, no anti-aliasing or poor filters, improper calibration and excessive noise. There is substantial room for improvement across this list of problems. The demands for improving quality is the reason for this improvement of the controller, which is manifested by applying standards such as ISO 9000. The main basics for improving performance of the control loop are knowledge and understanding of the control system. Knowledge of specific process is required for specific areas as well as understanding PID control generally (Astrom, Karl J. and Hagglund 1994).

The popular controller that has been used in processing industries for over 70 years is the Proportional, Integral, Derivative (PID) controller, despite significant developments in the theory of advanced control. The PID controller is usually used in applications of Single-Input, Single-Output (SISO) with acceptable results for simple processes. However, the presence of increasingly complex process interactions causes the obstruction for the extension of the single loop design procedure for the PID controllers to multivariable processes.

A control algorithm is usually applied to The PID controller and today this algorithm can control many feedback loops. These controllers are used by thousands of instrument and control engineers worldwide on a daily basis. There are many different directions that the PID algorithm can be approached from. The PID algorithm can be shown as a tool which we can operate using some basic rules, but we can also approach more analytically (Astrom and Hagglund 1994).

Proportional Action, Integral Action and Derivative Action are the components of the PID controller. They are usually referred to as the Ziegler-Nichols PID tuning parameters. Nowadays, it has become the most popular control algorithm used in industry (Astrom, Karl J. and Hagglund 1994). This chapter will explain the basic concept of the PID controls. The algorithms of the PID controllers are mainly used in feedback loops. In addition, the PID controllers can be applied in different types like a stand-alone controller or as part of Distributed Control System (DCS) or Direct Digital Control (DDC) package.

Nowadays, a lot of the industrial controllers use PID or modified the schemes of PID control. Figure 3.5 below shows a simple diagram of a PID controller, and it is illustrated in its parallel or non-interacting form.

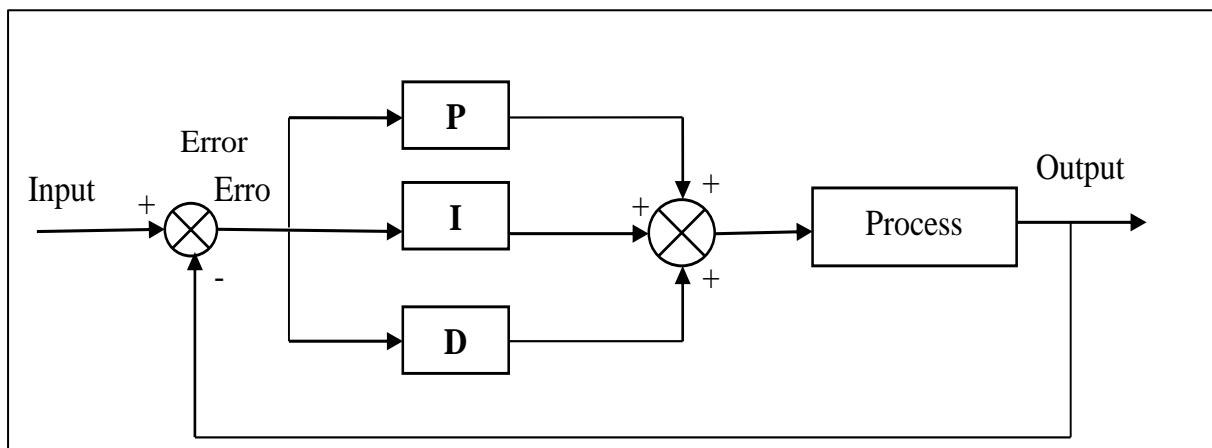


**Figure 3. 5: Schematic of the PID Controller - Non-Interacting Form.**

### 3.6.2 PID Control

The block diagram that shown in figure 3.6, illustrates a closed-loop system with a PID controller in the direct path, which is the most common configuration. The system's output should follow as closely as possible the reference signal (set-point). The PID controller is characterized by three gains, as shown in figure 3.7.

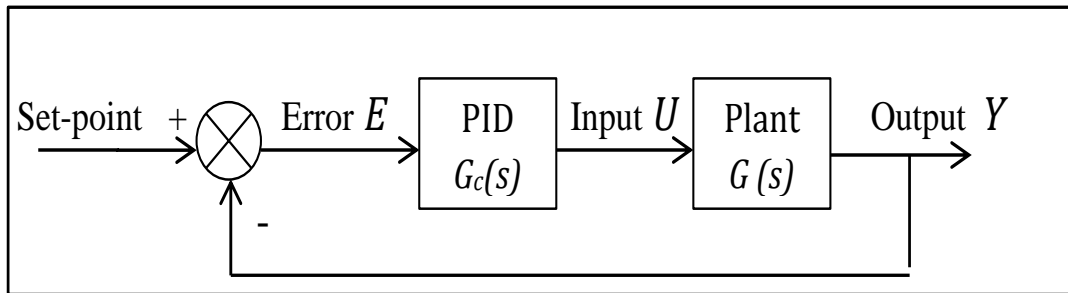


Figure 3. 6: PID control of a plant.

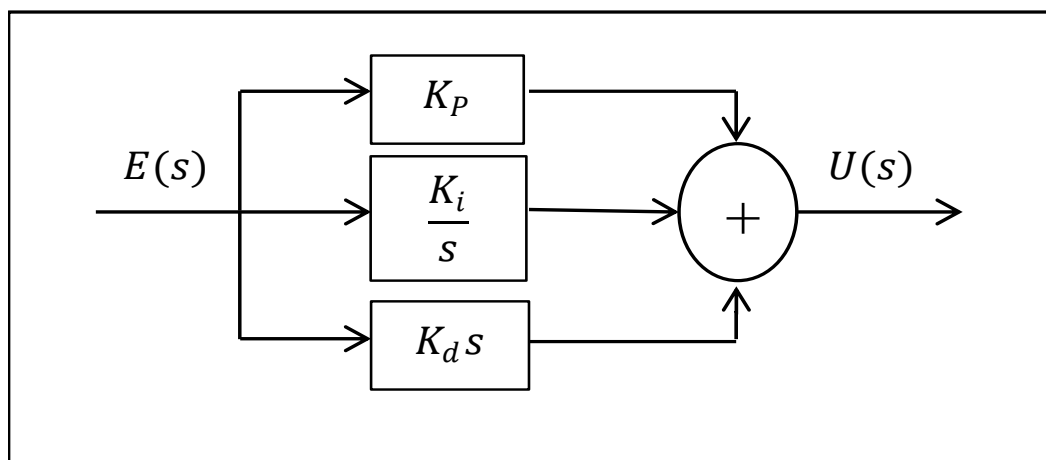


Figure 3. 7: PID controller internal structure.

In the frequency domain, the relation between the PID controller input  $E$  (error signal) and output  $U$  (input to the plant) can be expressed by the following transfer function:

$$G_C(s) = \frac{U(s)}{E(s)} = K_P + \frac{K_i}{s} + K_d s \quad (3.1)$$

$$G_g(s) = \frac{Y(s)}{R(s)} = \frac{G_C(s)G(s)}{1+G_C(s)G(s)} \quad (3.2)$$

In the PID controller tuning, the gains  $K_p$ ,  $K_i$  and  $K_d$  are selected so that the given performance specifications are satisfied. By employing the Ziegler-Nichols method for PID tuning those gains can be obtained through experiments with the process under controlled conditions (Ogata K. 2010). The step response and the value of  $K_p$  that results in marginal stability are used as starting points for obtaining gain values that guarantee a satisfactory behaviour. Finer adjustments to the gains can then be carried out if necessary.

### **Proportional Action:**

The proportional to the control error is control action. The output of the proportional controller is used as a part of the system error to control the process, but there will be offset error in the process system.

$$P_{term} = K_p \times Error \quad (3.3)$$

### **Integral Action:**

The influence of the integral action is to let the process output equal or nearly equal the set-point in the steady state. There is a control error in the steady state in proportional action, but the integral action can lead to a small positive error to increase control signal or a negative error to decrease control signal.

The integral controller output, and therefore its signal strength, is relative to the time amount for an error present in the system. The integral controller can remove the offset which was occurred by the proportional controller, but it will occur a phase lag into the process.

$$I_{term} = K_I \times \int Error dt \quad (3.4)$$

### **Derivative Action:**

The derivative action's purpose is to improve the stability of the closed-loop system. The instability of the system can be explained as follows. In the process dynamics, there is a delay

in the time taken before the control variable changing is shown in the process output. Therefore, the control system during this time will be late to correct the error. In proportional and derivative action, the controller action can be taken as if the control is made proportional to the output predicted of the process. This is true where the prediction is made by extrapolating the error by the tangent for curve of the error.

The output of the derivative controller is proportional to the change rate of the error. Derivative control can be applied to remove or decrease any overshoot of the system. Also, it provides a phase lead action which can change the phase lag that is introduced by the integral controller.

$$D_{term} = K_D \times \frac{d(Error)}{dt} \quad (3.5)$$

### Summary:

The PID controller has three terms. The proportional term  $P$  corresponds to proportional control. The integral term  $I$  gives a control action that corresponds proportionally to the time of the integral error. This can make the steady state error equal zero. The term of derivative  $D$  is relative to the time derivative of the control error. This term can predict the process system from any future error.

### 3.6.3 Continuous PID Controller:

The following transfer function shows the three controllers when they are combined together.

$$G_c(s) = K \left( 1 + \frac{1}{sT_i} + sT_d \right) \quad (3.6)$$

This can be illustrated as block diagram shown in figure 3.8.

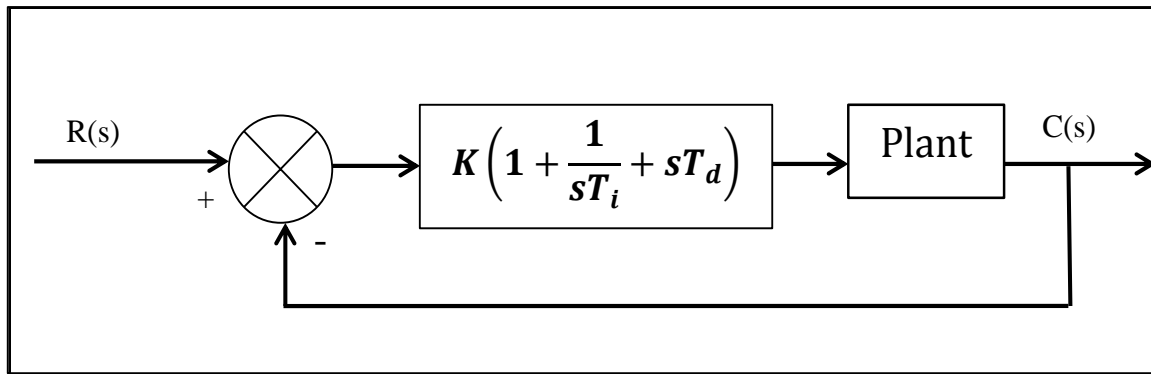


**Figure 3. 8: Block diagram of Continuous PID Controller.**

The PID controller can be defined basically as acting on the variable to control it using a correct mixture of the three control actions which are the P control action; I control action and D control action.

The control action that is proportional to the actuating error signal, can be called the *P* action. The signal actuating error is defined as the difference between the input and the feedback signal. The control action, which is proportional to the integral of the actuating error signal, can be called the *I* action. Finally, the control action which is proportional to the derivative of the actuating error signal can be called the *D* action. The continuous PID controller can be achieved by the integration of all these three actions.

Nowadays, this controller is commonly used in industries, also many research studies and applications have been completed in recent years.

### 3.7 Time Domain Specification of controller performance

Figures 3.9 and 3.10 show an example of the analysis parameters that are used to analyse the performance of controller on the controlled system or process. In addition, these parameters are described as follow:

- **Rise Time:**  
It is the time value (usually in seconds) that the system output response needs to move from 10% to 90 % of the final value.
- **Time Delay:**  
It can be called dead time. Time delay is the time value (usually in seconds) which is required for the system output response to just start rising as seen in figure 3.10.
- **Overshoot:**  
It is the maximum peak of the process output which can be calculated from the following formula:  
$$\text{Overshoot} = \text{Maximum peak} - \text{Final Value} \quad (3.7)$$
- **Peak Time:**  
It is the time that the system response needs to reach the first peak of the overshoot.
- **Settling Time:**  
It is the time taken by the controller to let the response curve reach and stay within the range of the final value which could be normally about  $\pm 5\%$  of the set point.
- **Steady State Error:**  
Steady state error is defined as the difference between the set point or the reference input and the process output (final value). Moreover, in closed loop control systems the PID controller tries to minimise the value of steady state error for the process output.

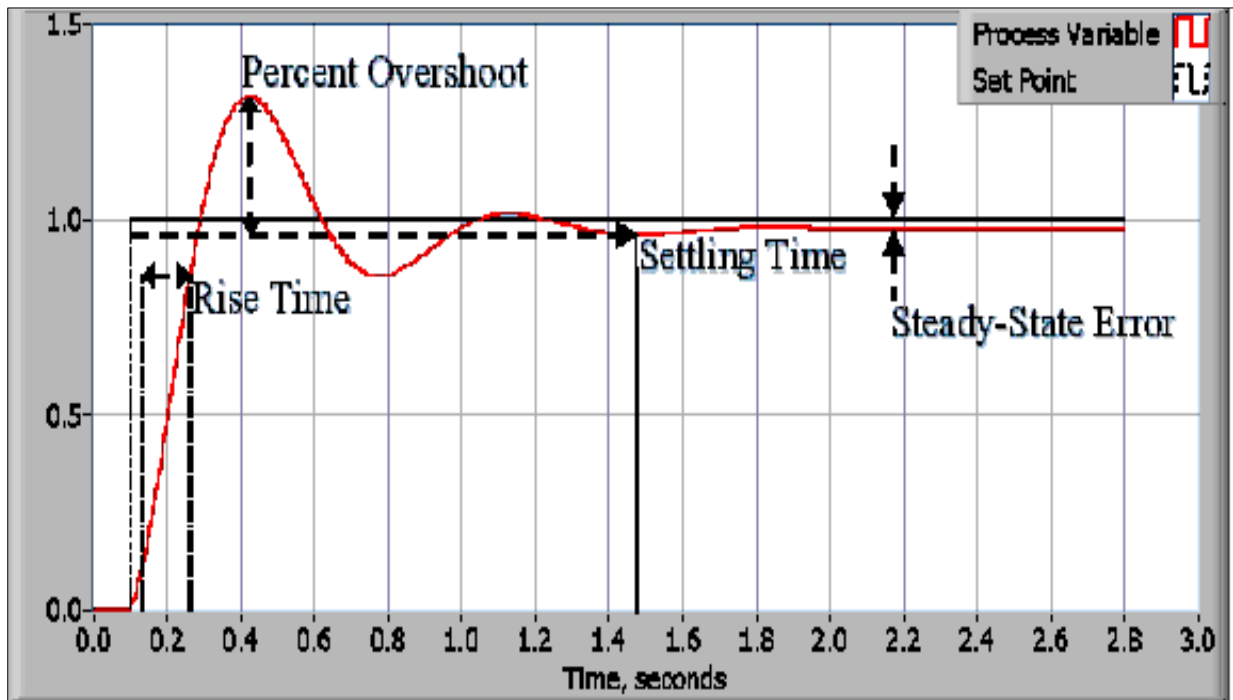


Figure 3. 9: Response of a typical PID closed loop system ([www.ni.com](http://www.ni.com)).

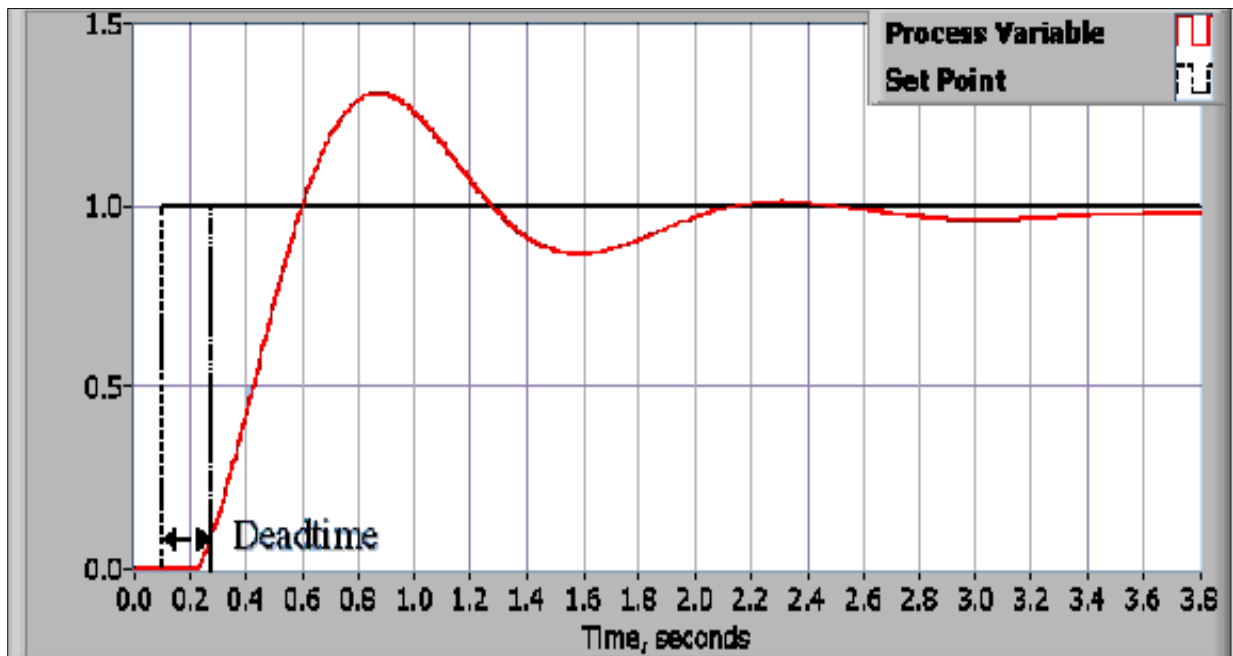


Figure 3. 10: Response of a closed loop system with dead time ([www.ni.com](http://www.ni.com)).

# **Chapter 4**

# **Equipment**

## 4.1 Introduction

In this project, many pieces of equipment were developed and used for the experimental works. These pieces of equipment included: 5-axes CNC Milling Machine, Oscillation system with Piezoelectric Actuator, Data Acquisition system including NI cRio, LabView software package (Real Time and FPGA), Power Amplifier, Signal Generator, range of sensors applications and more. In addition, this chapter describes in detail the feature of each part for the project equipment.

## 4.2 CNC Machining Centre

In this project, the Bridge port XR 610 VMC-5 Axis CNC Milling machine was used for the experimental works. It has Heidenhain iTNC CNC controller which can simulate and run cutting code in the Milling machine. This CNC Milling machine has a motor power which can reach 21 kilo Watt. The machine has its own cooling system pressure air and liquid. Its motor can work with torque up to 132 Nm. The range of spindle speed is between 600 and 12000 RPM. The work table side is 900 mm Length and 600mm Width. The traverse speed can reach 43 m/min for the directions of X-axis and Y-axis, however 36 m/min in Z-axis direction. The travels range of the Worktable are 760 mm, 610 mm and 610 mm for X-axis, Y-axis and Z-axis directions respectively. This worktable can carry loads up to 500 Kg. the coolant unit can operate at maximum pressure 20 psi with 60 L/min, also for Air coolant the air pressure can run up to 80 psi.

Table 4.1 shows the CNC Milling machine specifications, and figure 4.1 illustrates the actual photo of this Milling machine.

**Table 4. 1: Specifications of 5-Axis CNC Machining Centre.**

<b>Parameters</b>	<b>Value</b>
CNC- Controller	Heidenhain iTNC 530 Control
X-Axis Table Travel	610 mm
Y-Axis Saddle Travel	510 mm
Z-Axis Head Travel	610 mm
Feed Rate in X, Y and Z directions	20000 mm/min (20 m/min)
Spindle Motor Power	21 kW
Spindle Torque	134 Nm
Spindle Retention Force	12010 N
Spindle Speed	600 to 12000 RPM
Worktable size	900*500 mm
Table load	500 kg
Automatic Tool Changer	Up to 24 tools
Max. Tool Diameter	125 mm
Max. Tool Length	300 mm
Motion Accuracy	0.010 mm



**Figure 4. 1: 5- Axis CNC Machining Centre XR 610.**

### **4.3 Heidenhain CNC Controller**

The Bridge port XR 610 VMC-5 Axis CNC Milling machine has CNC control called the iTNC 530 from Heidenhain as seen in figure 4.2. This controller is a versatile, workshop-oriented contouring control for milling, drilling and boring machines.

The iTNC 530 has some advantages such as control motion optimization, short block times and special control strategies. The iTNC 530 controller allows the user to generate G-codes for machining process and to simulate the cutting strategies via installed simulation software before running the G-codes into the CNC machine center.

## Chapter 4 Equipment

Some G-codes that are designed and run by the certified candidate user for this project are presented in appendix A-4 with a training certificate.

Table 4.2 shows some features and specifications of the iTNC 530 Heidenhain controller.



**Figure 4. 2: The iTNC 530 Heidenhain CNC controller.**

**Table 4. 2: The Specifications of the iTNC 530 Heidenhain CNC controller.**

<b>Features</b>	<b>Values</b>
Operating system	HEROS real-time operating system for machine control
NC program memory	RAM memory: $\geq 2$ GB Hard Disk: Approx. 144 GB
Input resolution and display step	Linear axes: up to $0.1 \mu\text{m}$ Angular axes: to $0.0001^\circ$
Input Range	Maximum 100 cm
Range of traverse	100 cm
Spindle Speed	60 000 RPM
Operation Temperature	0 to $50^\circ\text{C}$

## 4.4 Work-piece Materials

In this project, the experimental works were carried out with two types of work-piece material. These are Aluminium and mild Steel. For investigating the new cutting method at the initial stage, the Aluminium work-piece was chosen due to its property. Also, Aluminium is commonly used in the industry for constructing lightweight components.

The experiments were done for milling tests in two modes - conventional and single axis vibratory milling; the dimensions of the work-piece are listed in table 4.3.

**Table 4. 3: The dimensions of work-piece.**

Work-piece Dimensions	Value
The length	60 mm
The width	50 mm
The width of Cutting tool contact with work-piece	10 mm
The height	50 mm

## 4.5 Vibration System

The oscillation system shown in figure 4.3 is used as a vibration device in the experiment setup to vibrate the work-piece holder. Here, the vibration system is mounted to the table of the milling machine. It is also linked to a power amplifier that receives a sine wave signal from the function generator. Moreover, the oscillation system contains a piezoelectric actuator fix with displacement bridge amplifier, the holder of the work-piece and the casing that covers all these elements.

The operation steps of the vibration system are as follows:

1. The function generator sends the signals with selected sine wave's parameters such as amplitude and frequency to the power amplifier.

2. Then these waves are magnified by a factor of 100 times and sent to the piezo actuator.
3. The crystals inside the piezo actuator are expanded and contracted alternately, and this process produces the oscillation movements.
4. The amplitude of oscillation depends on the voltage magnitude that is applied to the piezo actuator.

The full figure for the vibration system is illustrated in figure 4.3. An accelerometer is mounted on the free moving holder of the work-piece for measuring the actual acceleration signals during machining time. In addition, a 3-axes dynamometer was fixed under the vibration system to measure the cutting forces, also one of these forces signals is used for controlling the system which will be described in chapter 7.

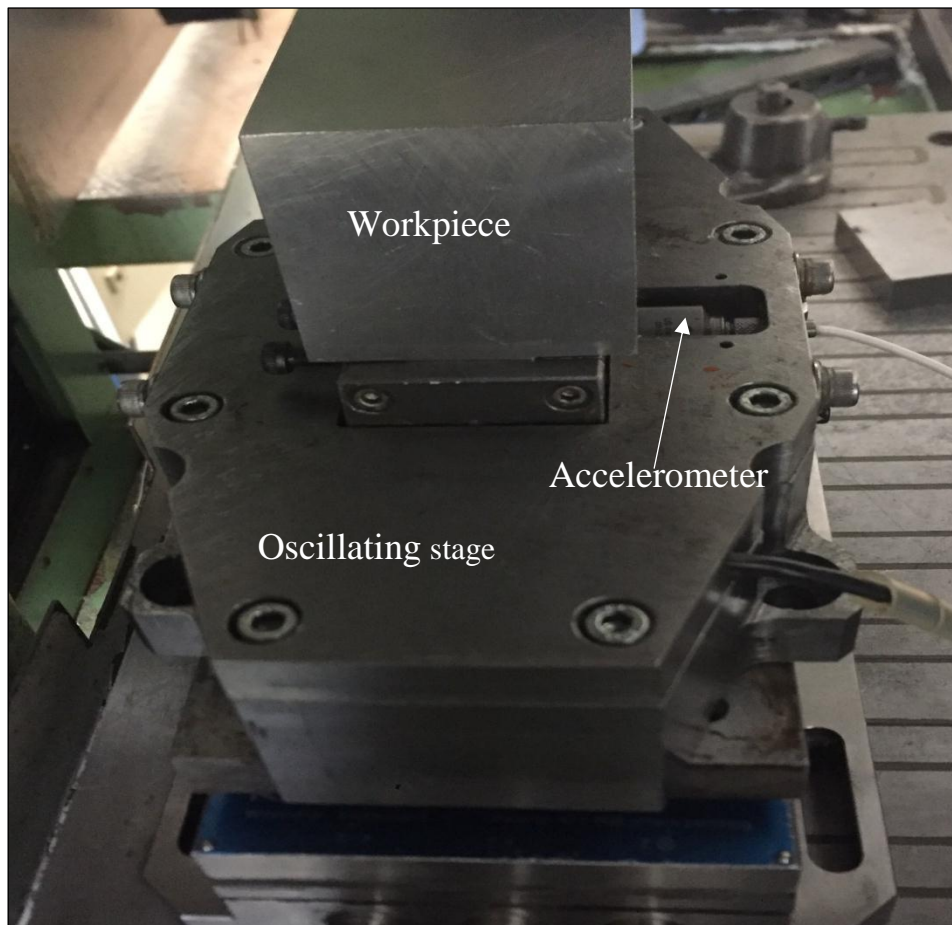


**Figure 4. 3: Self Contained Vibration System.**

## 4.6 Piezoelectric Actuator

The piezoelectric actuator can work at high frequencies and produce a small displacement with high force depending on applied voltage. The piezo has ceramic elements that can produce vibration by expansion and contraction process.

Here are some advantages and features of the piezoelectric actuator:

- Has low power consumption, high energy conversion, high efficiency.
- Can produce large generated force up to 2000N with stable displacement up to 120  $\mu\text{m}$ .
- Can reduce shift and creep phenomena.
- Has high response speed and easy to handle and use.
- No maintenance required and subject to no wear because there are no moving parts.

A full view of the piezoelectric actuator is illustrated in figure 4.4

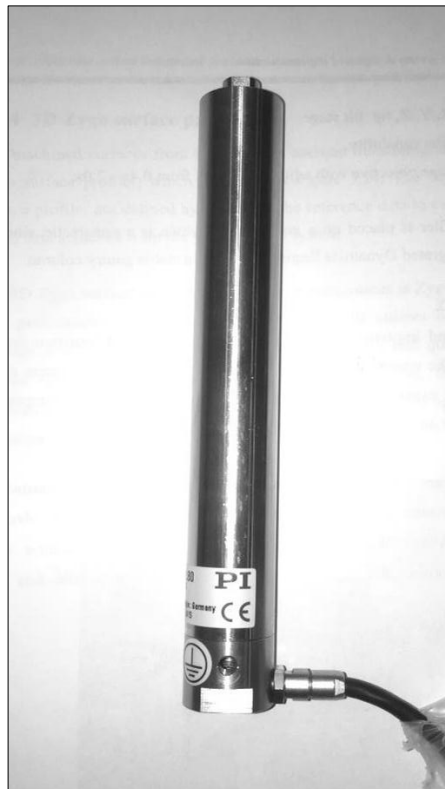


**Figure 4. 4: Piezoelectric Actuator P 212.8**

Table 4.4 shows the full specifications of the piezoelectric actuator that was used in this study (Physik Instrumente (PI) GmbH & Co. KG 2017).

**Table 4. 4: The Specifications of Piezoelectric Actuator (P 212.8)**

<b>Technical Data</b>	<b>Value</b>
Diameter	18 mm
Length	139 mm
Translator Diameter	8 mm
Pulling Force Capacity	300 N
Pushing Force Capacity	2000 N
The Weight	0.21 Kg
Open Loop Travel	120 $\mu$ m

## 4.7 Power Amplifier

The power amplifier is generally used to increase the size of any signals. In this project, the amplifier E 472.2 Physic Instrument is used for experimental works. It has two channels and is specially designed to drive high capacitance piezoelectric actuators. In addition, the range of output voltage is between 0 and 1100 Volts with average output power up to 110 Watts that is used for dynamic open loop operation.

The full specifications of the power amplifier are listed in table 4.5 and figure 4.5 illustrates the device's image.

**Table 4. 5: The Specifications of Power Amplifier Type E-472.2**

<b>Technical Data</b>	<b>Value</b>
Number of Channel	2
Maximum Output Voltage	1100 Volts
Average Output Power	110 Watts

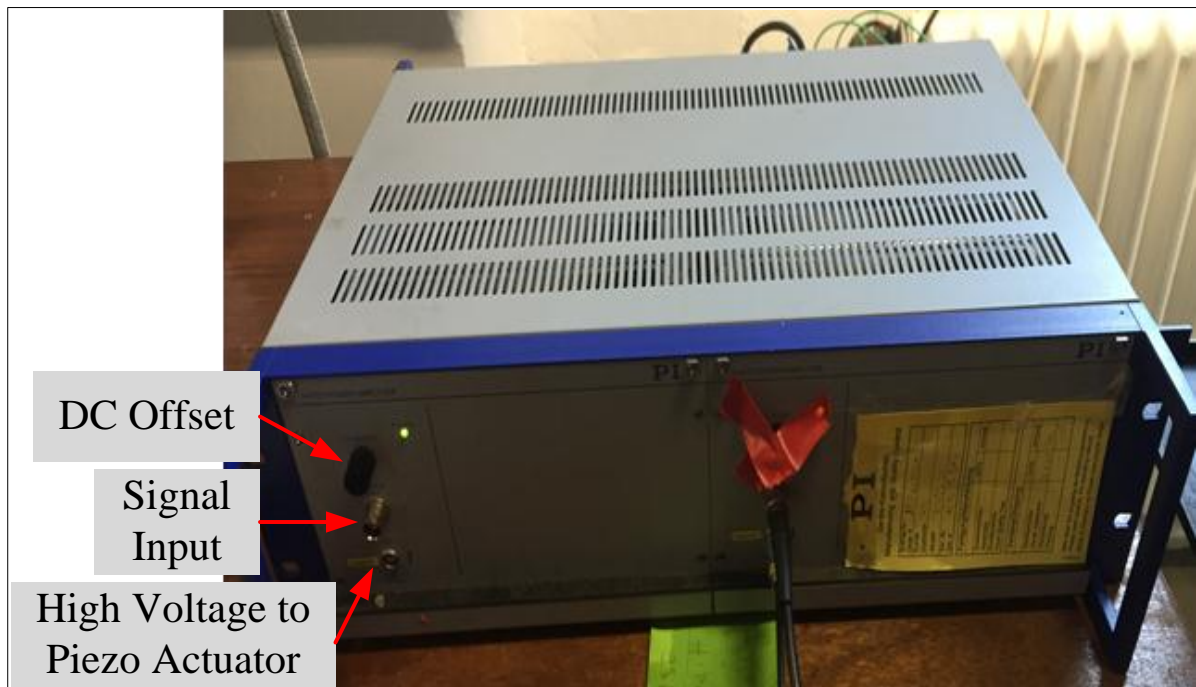


Figure 4. 5: Power Amplifier Type E-472.2

## 4.8 Kistler Dynamometer

Milling forces were measured using a 3-axis Kistler dynamometer type 9257 A as seen in figure 4.6.a. it can measure Normal force  $F_z$  and two directions of tangential force  $F_x$  and  $F_y$ . This dynamometer can measure loads up to 5000 N in each direction with a resolution less than 0.01 % of full scale. It also has a high natural frequency, great rigidity and insensate to temperature influence.

In addition, the forces' measurements were obtained by mounting the vibration system with the work-piece on the load cell of dynamometer. Here, the loads were simultaneously transferred to the computer and the different 3-directions X, Y and Z are perpendicular to each other.

The dynamometer was connected to a charge amplifier (figure 4.6.b), and a Data acquisition system was used to record the data from the dynamometer. This charge amplifier that is seen in figure 4.6.b is suitable for applications with almost all piezo actuator sensors. Moreover, the output signals of the charge amplifier are suitable for monitoring, closed loop control and optimisation for industrial measuring procedures.

The Technical data and specifications of the Kistler charge amplifier type 5073 are illustrated in table 4.6.

**Table 4. 6: Technical Data for Kistler Charge Amplifier Type 5073** (Kistler Instrument Group 2017) .

<b>Parameters</b>	<b>Value</b>
Output Voltage Range	$\pm 10$ Volts
Maximum Output Current	5 mA
Output Impedance	10 $\Omega$
Output Voltage Limit	$\pm 11$ Volts
Minimum Operation Temperature	-40° C
Maximum Operation Temperature	+80° C
Error (Transfer Facture)	0.5 %

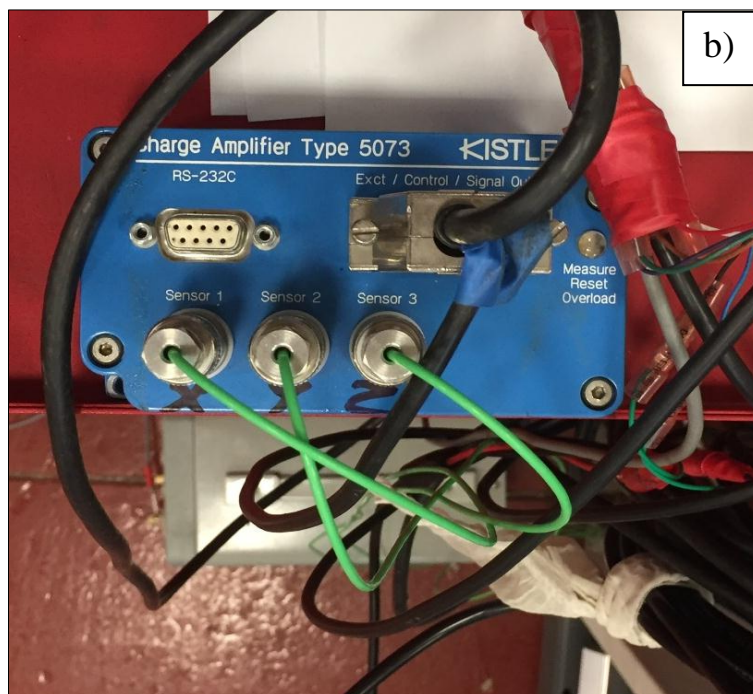


**Figure 4. 6: Measuring Forces Device. a) 3-axis Kistler 9257A Dynamometer. b) Kistler Charge Amplifier Type 5073.**

## 4.9 Function Generator

The function generator can be used to provide various patterns signals (Sine Wave, Square Wave, Ramp Wave, Triangle Wave, Noise) with selected frequency and amplitude. In addition, the GWINSTEK function generator under model No. AFG-2225 was used in this current study to produce sine wave signals that feed to oscillation system.

Here are some of the main features of the GWINSTEK AFG-2225 function generator:

- Two output channels
- True waveform output to display
- User defined output section
- USB interface
- Waveforms editing via PC
- Waveforms characteristics can be controlled via LabVIEW software.

For closed loop control procedure, NI cRio hardware and newly designed LabVIEW code was connected to the function generator via USB Port. The controller can make any required change on waveforms' characteristics directly inside the function generator.

Table 4.7 illustrates the specifications of the GWINSTEK AFG-2225 function generator and its image is shown in figure 4.7.

**Table 4. 7: Specification of the GWINSTEK AFG-2225 function generator.**

Parameters	Value
Output wave function	Sine, Square, Ramp, Pulse, Noise, standard waveforms
Frequency Range	1 $\mu$ Hz to 25 MHz
Resolution (at High frequency)	1 $\mu$ Hz
Point wave length	4k points
Amplitude Range	10 volts p-p
Amplitude accuracy	$\pm 2$ % (Max. Position)
Impedance	50 $\Omega$
Amplitude Resolution	1 mV
Number of output channel	2

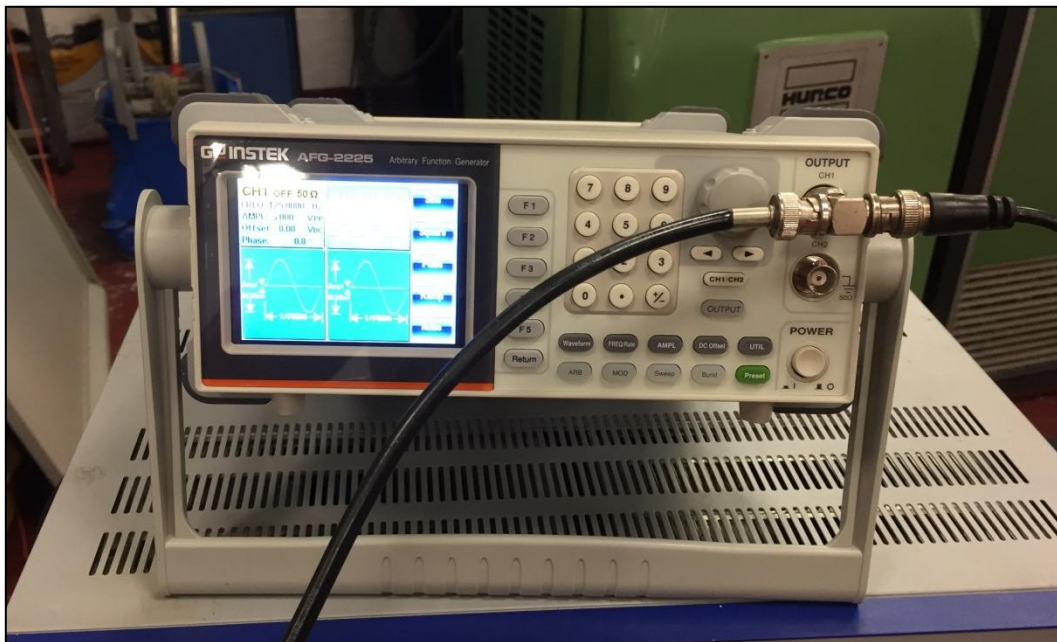


**Figure 4. 7: The GWINSTEK AFG-2225 function generator**

## **4.10 Programmes**

In this study, three programs were used for designing, simulations, investigations and system control. The programs are Solid-works, Matlab with Simulink and LabVIEW.

### **4.10.1 Solid Works Software**

The SolidWorks software is an application of mechanical design automation which has an advantage over some graphical user interface software such as Microsoft Windows. Moreover, the SolidWorks software can allow the designer or user to quickly sketch out ideas, experiment with features and dimensions, and produce models and detailed drawings.

In this project, the SolidWorks software was used to design an initial vibration plate and the work-piece samples. Then, all these parts were manufactured based on the design sheet. Moreover, some SolidWorks design sheets are shown in appendix A-2

### **4.10.2 Matlab and Simulink**

Matlab software and graphical Matlab Simulink were used in this project. They were used to load all experimental data for analysing and investigation procedures. In addition, Matlab was used to analyse experimental data to design and develop the initial phase of the control system. Here, the system identification tool box in Matlab was used to identify the initial transfer function for the vibration system as well as filtering, analysing and plotting loaded experimental data. Matlab Simulink and control tool box was also used to simulate and build PID controller to the vibration system in both control cases, closed loop and open loop. Further development and investigations were carried out in chapter 7 of system identification and control.

### **4.10.3 LabVIEW Software**

In this project, both Real Time LabVIEW and FPGA LabVIEW software were used during real time of the machining process with vibratory milling. Here are some advantages of using Rael time and FPGA LabVIEW Software (National Instruments UK 2011):

### **Real Time LabVIEW**

- Deterministic.
- Hard real-time performance.
- Many real-time drivers and analysis functions available.

### **FPGA LabVIEW has:**

- True parallelism, it can provide parallel tasks and pipelining.
- High reliability, its designs can become a custom circuit.
- High determinism, it can run algorithms at deterministic rates down to 25 ns (faster in many cases).
- Reconfigurable, the user can create new code or adjust existing code.

In addition, to reach the high level of speed response for the closed loop control system as this project required, both software packages, Real Time and FPGA were used. Real time software allows Digital communication protocols such as communicating between PC, signal generator and NI-cRio devices. However, FPGA was used for faster algorithms response for PID control system and Data Acquisition system and hardware.

Further discussions in real time and FPGA LabVIEW software are described in Chapter 7.

## **4.16 Data Acquisition Hardware**

A Data acquisition system was used in order to record the acquired data from the accelerometer and forces sensors (Dynamometer) as well as controlling the feedback signals. A laptop based LabVIEW software and NI-compact RIO-9022 uses a combination of application software, some modular hardware to record the output sensors' signals and transfer them to digital signals for transferring them to the hard disc drive for further analysis. In addition, the controller has been built by LabVIEW code that was installed in NI -Compact RIO.

The platform of NI-Compact RIO-9022 features a range of embedded controllers with two processing target(National Instruments UK 2017) as seen in figure 4.8 :

1. A real-time processor that is used for signals processing and communications.

2. FPGA programme that is user-programmable to implement high-speed control and custom timing and triggering directly in hardware.

The NI-Compact RIO-9022 contained the following parts:

1. Integrated Processor I/O:
  - a) Gigabit Ethernet.
  - b) USB.
  - c) Serial
  - d) SD card
  - e) Mini Display Port.
2. Processor: intel Atom
3. FPGA: Xilinx Zynq-7000
4. Modular I/O:
  - a) Analogue Input
  - b) Analogue Output

The configuration of the NI-Compact RIO-9022 with the I/O Modular is illustrated in figure 4.9.

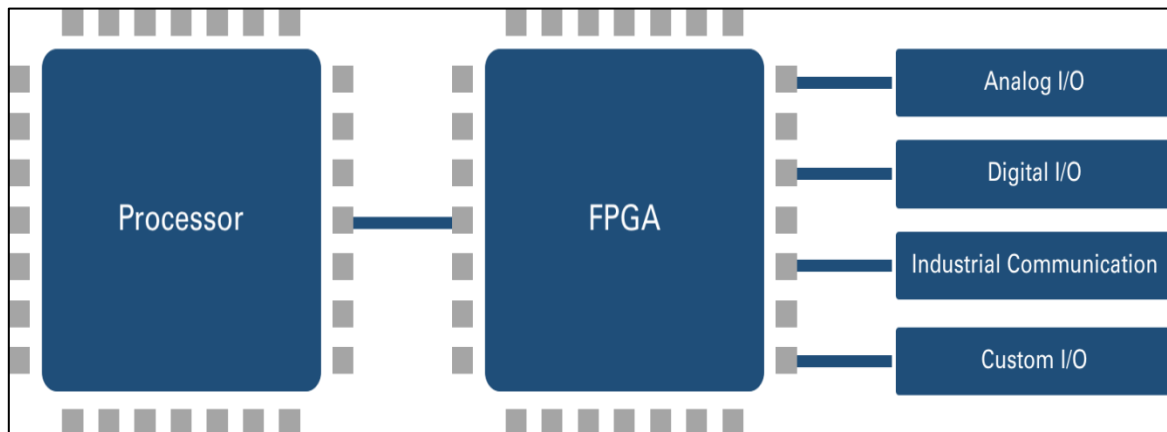


**Figure 4. 8: Two processing targets of the Compact Rio controllers** (National Instruments UK 2017).

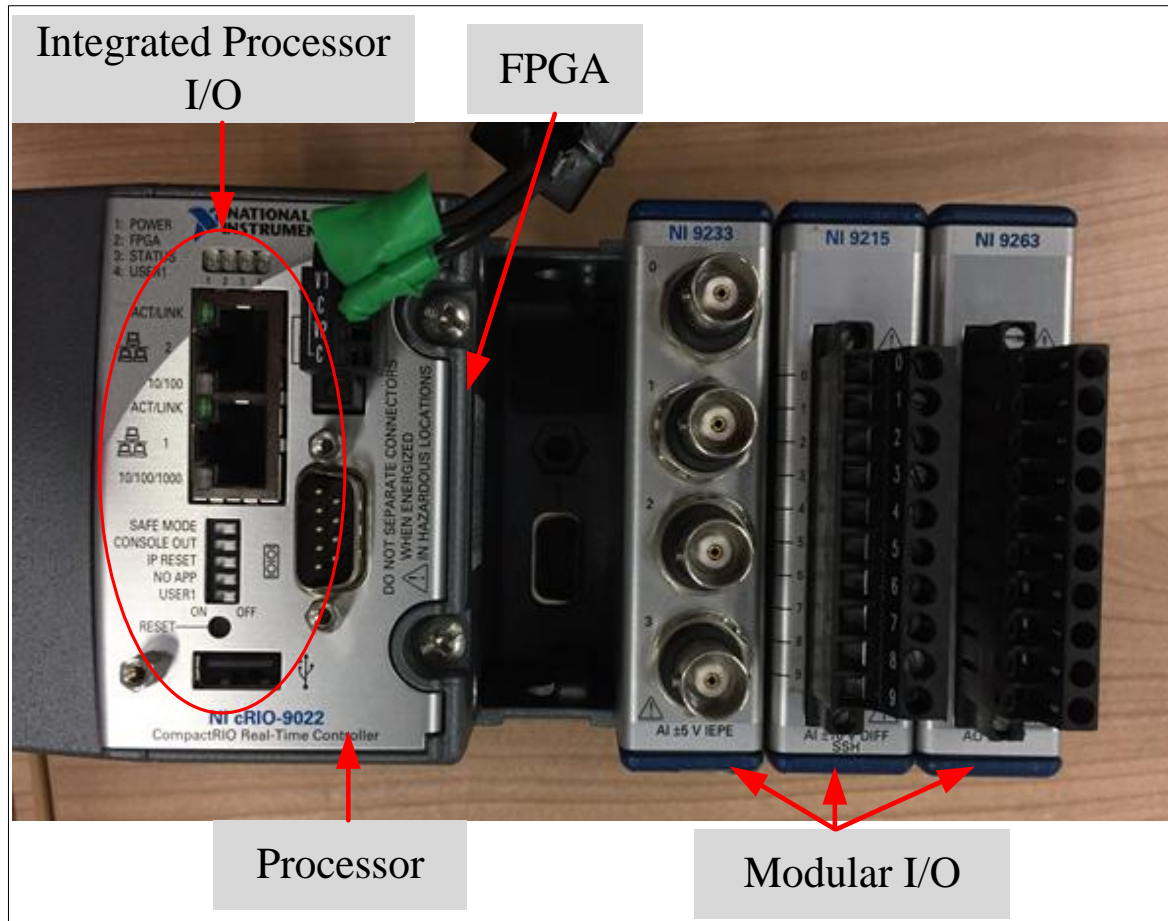


Figure 4. 9: The configuration of the NI-Compact RIO-9022.

Table 4.8 displays some specifications and technical data for the NI-Compact RIO-9022 DAQ Hardware.

**Table 4. 8: The specifications of the NI-Compact RIO-9022.**

Features	Values
Processor	1.33 GHz Dual-Core Intel Atom
Operating system	NI Linux Real Time
On-board Storage	2 GB
FPGA	Xilinx Zynq-7000
Number of I/O module slots	4
Other I/O	Gigabit Ethernet, USB, RS232, Mini Display port and SD card port.
Power	17 Watts , 9 Volts
Operating Environment Temperature	-20 to 55 °C
Weight	600 Grams

### 4.16.1 Module Input/Output Slots

In this project, three modules slots were used to act as the interface between the NI-Compact RIO-9022 and the experiment environment via sensors. The Typical DAQ functions of these modules are Analogue input, Vibration input and Analogue output.

#### Analogue input:

The NI-9215 (see figure 4.10) is an analogue input module which is used in this project to collect signals from dynamometer sensors and function generator. The NI 9215 includes four simultaneously sampled analogue input channels and successive approximation register (SAR) 16-bit analogue-to-digital converters (ADCs). For safety and noise protection, the NI 9215 module contains a channel-to-earth ground double isolation barrier. Also, it has a high common-mode voltage range.

The module specifications and technical data are shown in table 4.9.

**Table 4. 9: The specification of the NI-9215 Module Slot.**

Technical Data	Value
Input Voltage Level	$\pm 10$ volts
Number of Channels	4
Sampling rate	100 kS/s/ch
Simultaneous	Yes
Resolution	16 bits



**Figure 4. 10: The analogue input module NI-9215.**

**Vibration input:**

The NI-9234 Slot Module was used in this project to measure signals from the accelerometer sensor. It has 4 channels with input voltage between  $\pm 5$  volt. In addition, the input channels simultaneously measure signals. Each channel also has built-in anti-aliasing filters that automatically adjust to your sample rate. When used with NI software, this module provides processing functionality for condition monitoring such as frequency analysis and order tracking (National Instruments UK 2017).

Table 4.10 displays some important specifications of the NI-9234 Module with its photo in figure 4.11.

**Table 4. 10: The specification of the NI-9234 Module Slot.**

Feature	Value
Input Voltage Range	$\pm 5$ Volts
Resolution	24 Bits
Antialiasing filter	Yes
Number of input channels	4
Maximum Sampling Rate	50 kS/s



**Figure 4. 11: The analogue input module NI-9234**

**Analogue output:**

The analogue output slot module NI-9263 is a High-performance analogue output module. It is used to send output signals from LabVIEW code via NI Compact RIO to the vibration system during machining time. The module slot is shown in figure 4.12 and the important characteristics or specifications are found in table 4.11.

**Table 4. 11: The Specification of the Analogue Output NI-9234 Module Slot.**

Features	Value
Output Voltage Range	$\pm 10$ volts
Number of channels	4
Sampling Rate	100 kS/s/ch
Resolution	16 Bits



**Figure 4. 12: The Analogue Output NI-9234 Module Slot**

# **Chapter 5**

## **Calibration**

## 5.1 Introduction

Calibration is defined as an association between measurements as well as the validation of specific measurement techniques and equipment. Simply, it can be known as a comparison between measurement X of known correctness made or set with one device and another measurement Y made in as similar a way as possible with a second device.

In this chapter, the calibration process will take two stages. First, the measurement forces device is calibrated and investigated. Second, the Oscillation Jig with fitting work-piece will be calibrated to obtain Displacement Amplitude for a range of applied frequencies and voltages. The sensors' output will be calibrated using respective nominal certified scales as shown in manufacture's manual or data sheets.

## 5.2 Forces Calibration

For this investigation, the force measurement device named as 3-axis Kistler dynamometer type 9257 A has been used, it also has been calibrated for measuring forces in machining time. Here, this Kistler Dynamometer can measure loads up to five Kilo Newton (kN). When the cutting tool mills the work-piece there are three forces, first one is in Z-direction which called Normal force. The other two forces are major cutting forces which are in X and Y direction. Therefore, the calibration process was taken for three forces in X, Y and Z directions for the Kistler dynamometer. This calibration process has reached up to 200 N of load. As recommended by the manufacture, the calibration was done in two modes, loading and unloading, with environment temperature about 20°C.

For setup configuration for connection of the dynamometer and charge amplifier, the following parameters were set up:

- Measurement force in X-direction used a sensitivity of 8.004 pC/N with 499 MU/voltage for scale setting up.
- Measurement force in Y-direction used a sensitivity of 8.015 pC/N with 499 MU/voltage for scale setting up.
- Measurement force in Z-direction used a sensitivity of 3.755 pC/N with 1000 MU/voltage for scale setting up.

Figure 5.1 below shows these parameters inside the charge amplifier's software:

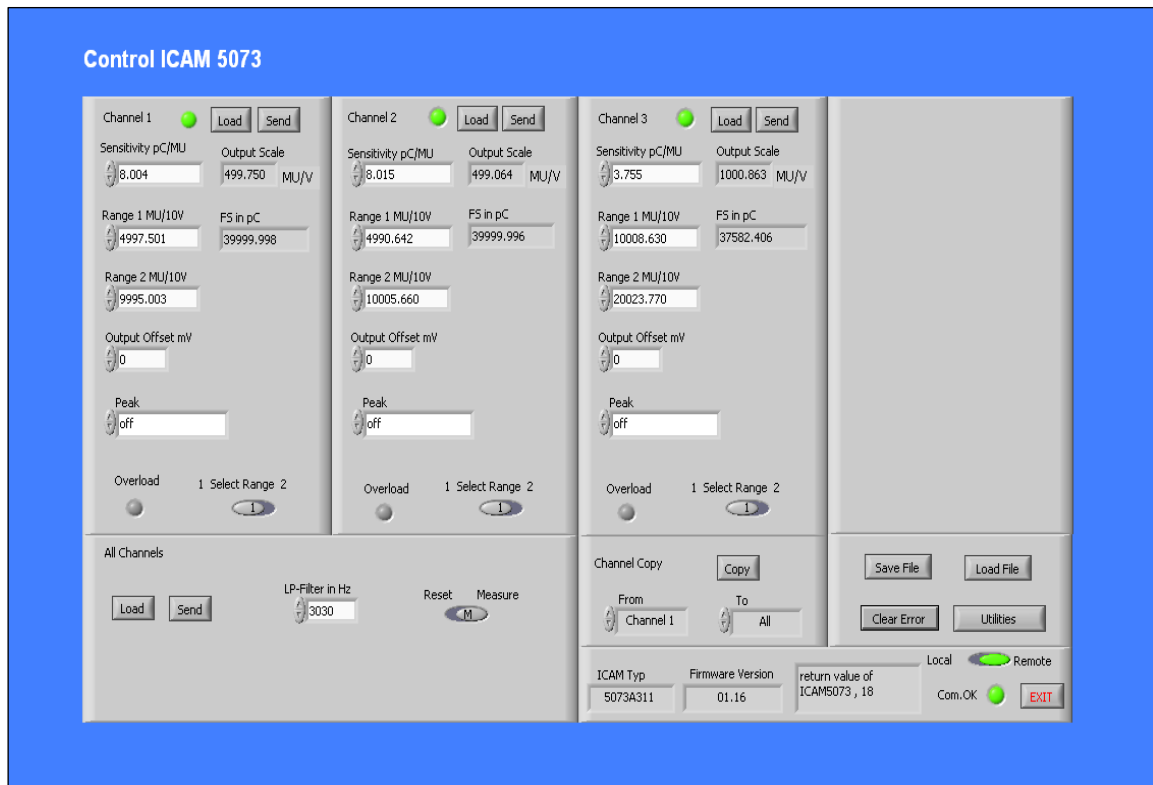


**Figure 5. 1: Charge amplifier parameters setup.**

For reaching the same configuration as well as the actual milling trials, the work-piece was mounted in the oscillation system during the calibration process.

The following figure shows the configuration of the calibration process.

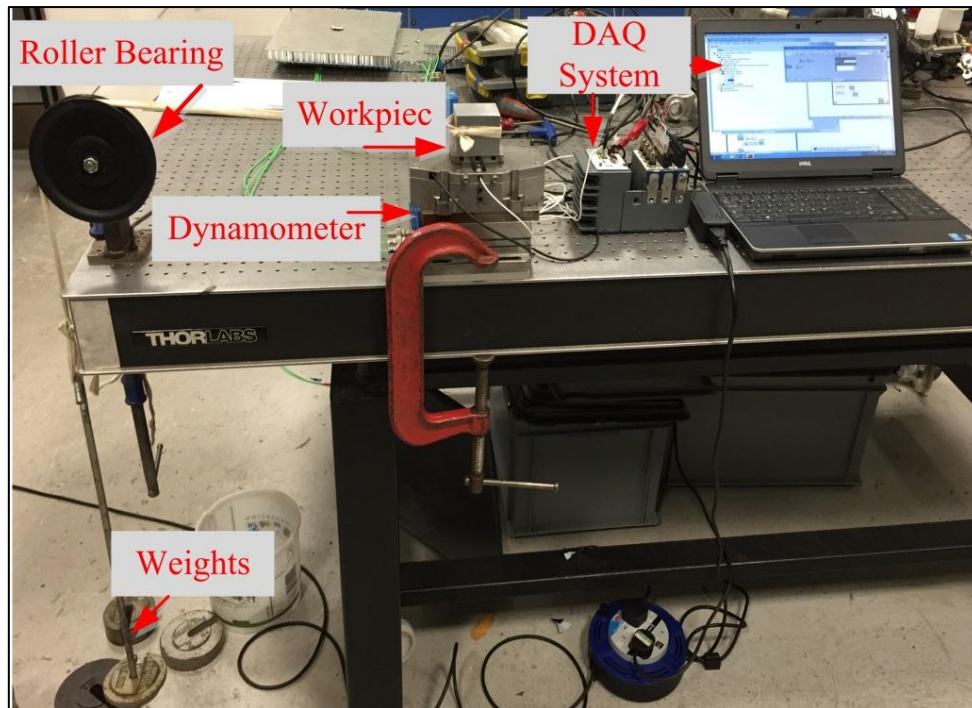


Figure 5. 2: Experimental setup for calibration.

### 5.3 Forces calibration results

For recording all signals coming from the dynamometer sensors, the LabVIEW real time software with data acquisition system was used as illustrated in figure 5.2. The average of reading data for three tests was taking place in order to have more accuracy and minimise errors. As shown in the following figures, the average of twenty loading and unloading calibration results were obtained.

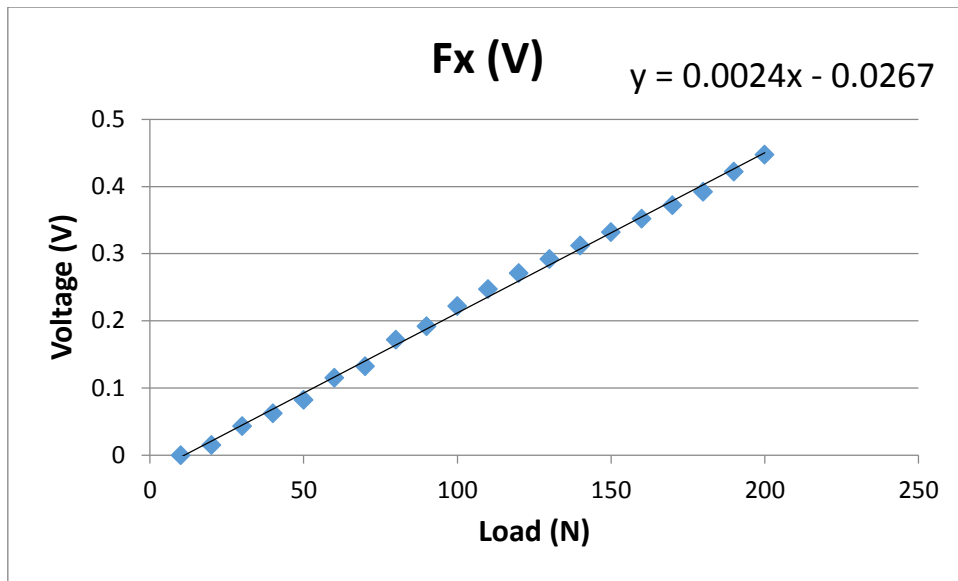


Figure 5. 3: Force Calibration in X-axis.

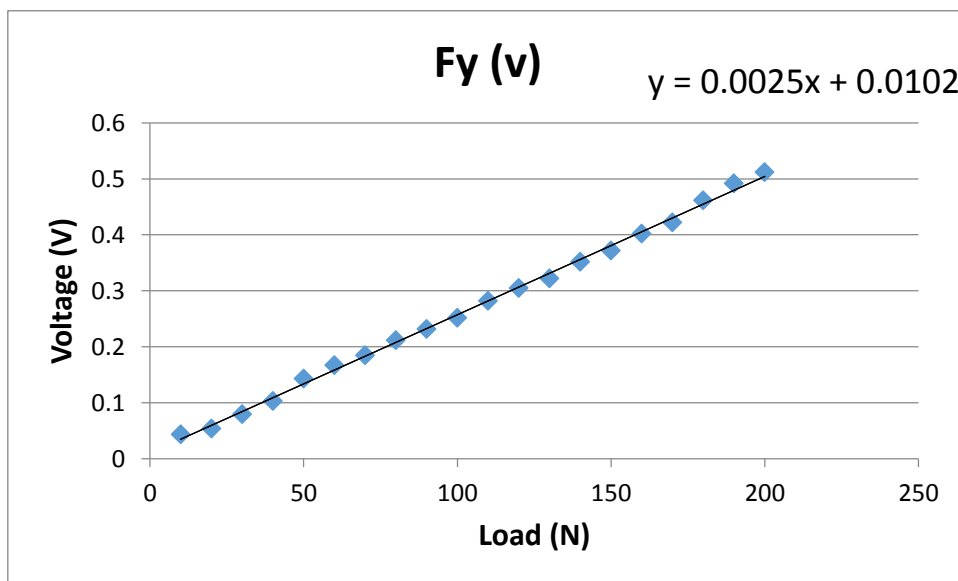
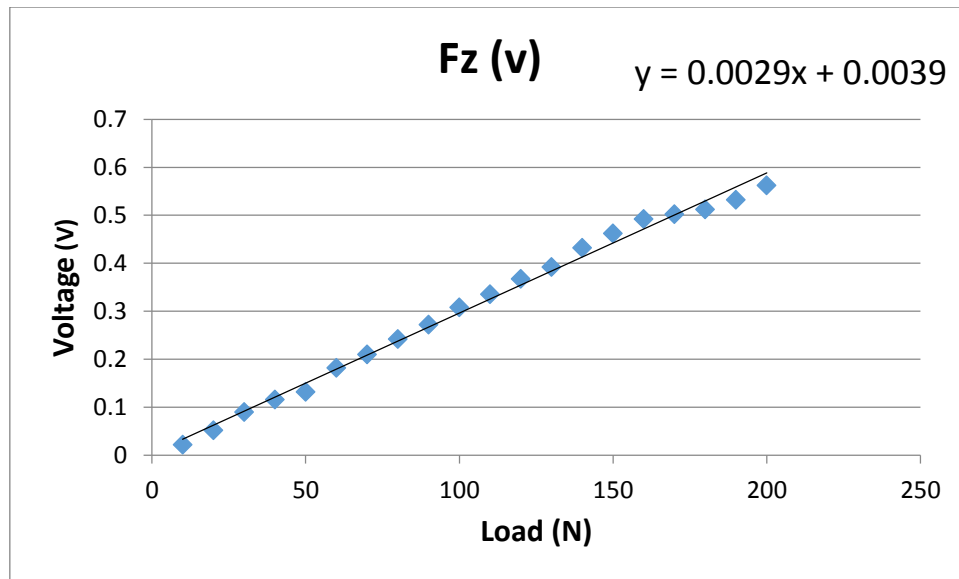


Figure 5. 4: Force Calibration in Y-axis.



**Figure 5. 5: Force Calibration in Z-axis.**

Figures 5.3, 5.4 and 5.5 represent the calibration results for three forces components X, Y and Z, as well as their curves. These graphs show the first order regressions (equations). They observe the linearity of the Dynamometer's reading data, also it is still linear over the calibration range without any hysteresis. In addition, these linear equations which are obtained from graphs will be used to convert the forces unit from Volt to Newton.

For experiment of spindle deflection, the Kistler dynamometer was fixed horizontally on the machine tool (CNC milling machine) as shown in figure 5.6. Due to the manufacturer's setting of the dynamometer, the Calibration test need to be done horizontally in only one direction as the deflection test needs it. Therefore, the dynamometer is calibrated in Z-axis from the direction shown in the Kistler device.



**Figure 5. 6: Horizontal fixing of the Dynamometer.**

Figure 5.7 below presents the actual setting of horizontal calibration of force in Z-axis. A LabVIEW code was used to show and record all output voltages coming from the Dynamometer sensor. Charge amplifier and compact cRio devices were used as required for the DAQ acquisition system. Some weights are used as a load applied into the Dynamometer which will be considered as forces in Newton units.

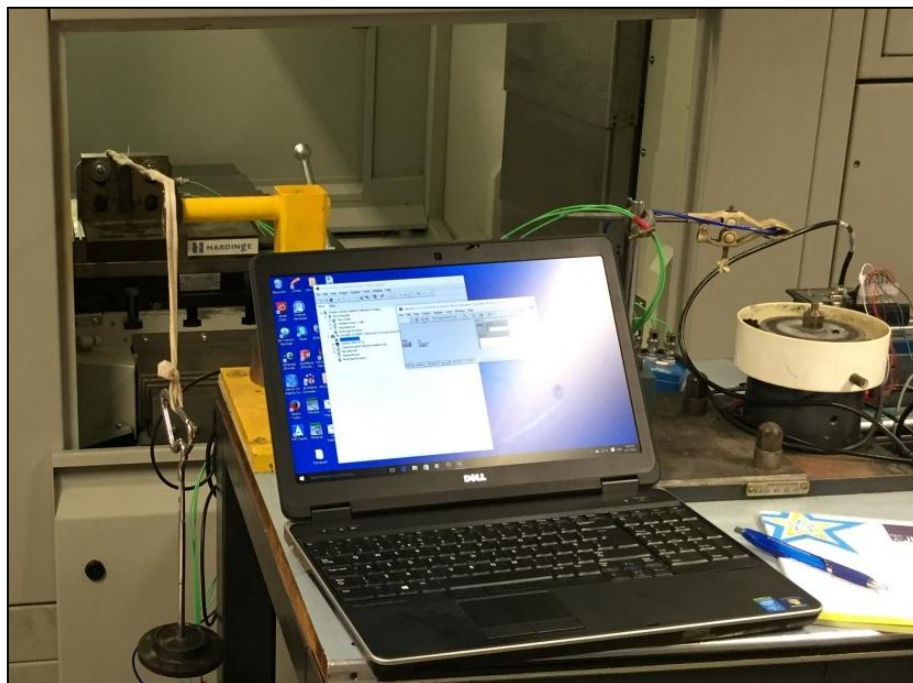


**Figure 5. 7: Experimental setup for horizontal calibration.**

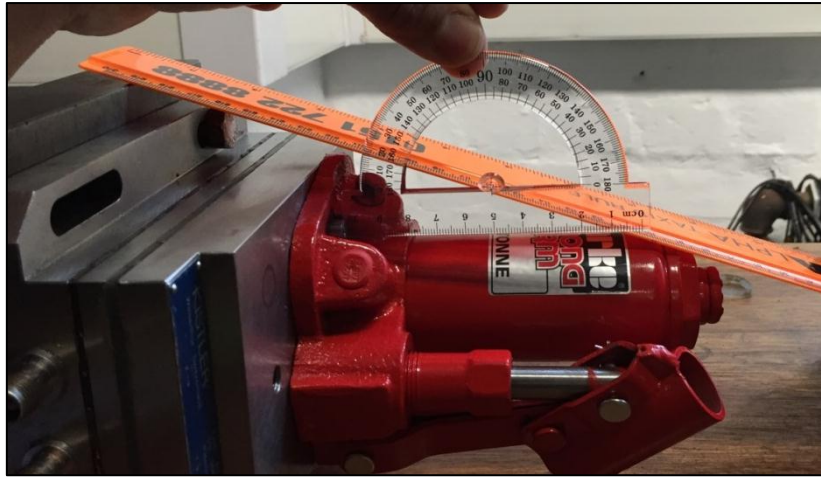


**Figure 5. 8: The Angle between two force directions.**

To set up this horizontal calibration in lab, it requires that the calibration process should be done in the same condition and environment of real or actual deflection experiment. Here, the dynamometer was calibrated with a jack fixed on the top of its surface as shown in Figure 5.8. However, it notes that there is an angle value between the horizontal position and the system holder. This angle was measured as shown above figure 5.8 above, also it was nearly equal to 20 degrees. Here, the angle value has been used to calculate the force in the horizontal direction, which is similar to the forces of the deflection test.

$$F_z = F_{zx} \cos 20 + F_{zy} \sin 20 \quad \text{But} \quad F_{zy} = 0 \quad (5.1)$$

$$\text{Then } F_{zx} = \frac{F_z}{\cos 20} \quad (5.2)$$

This formula obtains the relationship between two different directions of force.

The initial calibration has been done up to 80 Newton with 8 readings of data. This was done in two ways of load; loading and unloading but the average of them was considered. The table below presents all measured and calculated forces data for the calibration process in Z-axis.

**Table 5. 1: Horizontal Calibration Results.**

F (Kg)	Fz (N)	Fzx (N)	V_out (v)	V_out (mv)
1.65	16.17	17.21361	0.039	39
2.65	25.97	27.64611	0.069	69
3.65	35.77	38.0786	0.095	95
4.65	45.57	48.5111	0.119	119
5.65	55.37	58.94359	0.155	155
6.65	65.17	69.37608	0.185	185
7.65	74.97	79.80858	0.215	215
8.15	79.87	85.02482	0.225	225

The figure 5.9 represents the calibration curve between force measured in mV and load force measured in N; also it notes that the relationship between output of the dynamometer and the applied load is linear. Moreover, the linear regression or equation that is shown in figure 5.9 will be used in order to convert forces unit from voltage (mV) to Newton (N).

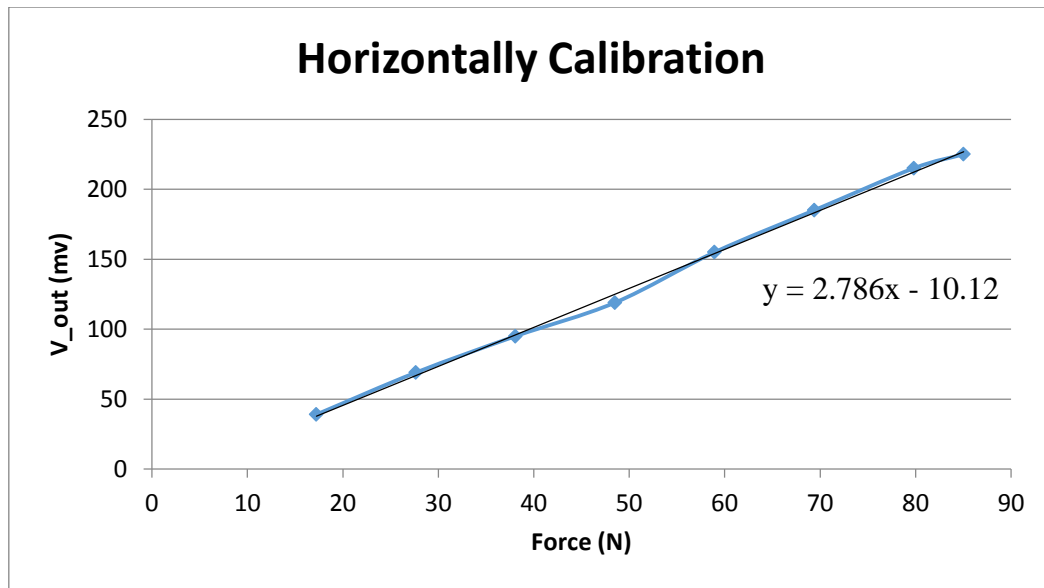


Figure 5. 9: Horizontal Calibration Graph in Z-axis.

## 5.4 Amplitude Calibration

The main propose for this calibration is to obtain the relationship between the output voltages with frequencies that are applied into the vibration system and displacement.

For calibration criteria, the Eddy current sensor and its software were used. This sensor was held by a steel support mounted to the table bed of the machine as shown in figure 5.10. In addition, figure 5.11 shows the experimental setup and data acquisition system to obtain all the voltage output values. The range of displacement measurement was  $\pm 1$  mm with accuracy of  $0.1\mu\text{m}$ . In order to obtain more accurate output measurement output, this experiment was carried out several times.

The piezo actuator can be driven by applied voltage up to 1000 volts with support from the power amplifier. This power amplifier can take up to 10 volts as a maximum input.

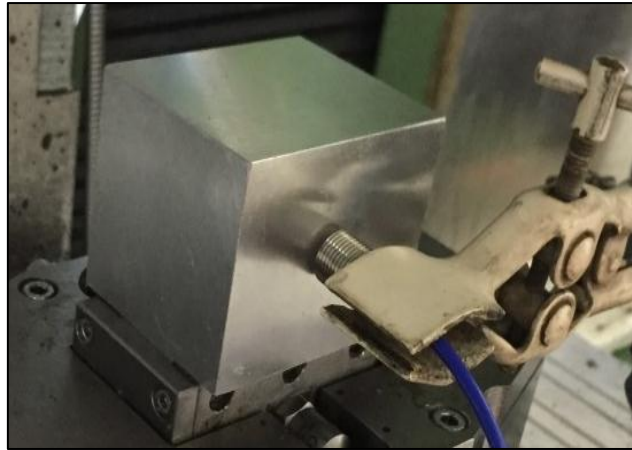


**Figure 5. 10: Eddy current sensor position.**



**Figure 5. 11: Experimental setting up for Amplitude calibration.**

The calibration graph in figure 5.12 describes the relationship between the output voltages with frequencies that are applied into the vibration system and displacement. Moreover, it notes that by increasing the input voltage with a selected frequency the vibration amplitude or displacement will increase.

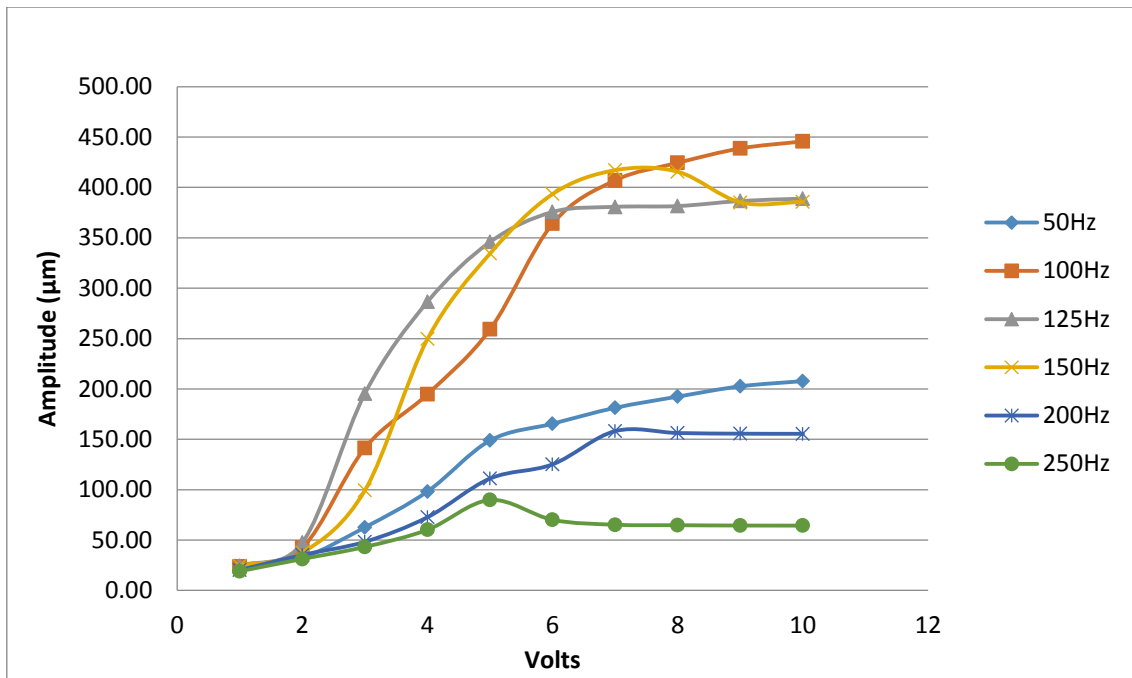


Figure 5. 12: Displacement Calibration Graph.

Table 5. 2: Displacement calibration results.

Amplitude (µm)	1v	2v	3v	4v	5v	6v	7v	8v	9v	10v
<b>50Hz</b>	23.1	32.6	62.7	98.3	148.9	165.5	181.3	192.4	202.6	207.8
<b>100Hz</b>	23.7	42.6	141.4	194.8	259.1	364.1	407.1	424.4	438.7	445.7
<b>125Hz</b>	24.4	47.5	195.5	286.5	345.8	375.7	380.7	381.5	386.5	388.8
<b>150Hz</b>	24.6	37.6	99.4	249.6	334.4	393.5	417.1	415.5	385.2	385.6
<b>200Hz</b>	20.3	35.3	48.3	72.7	111.1	125.2	158.2	156.3	155.6	155.5
<b>250Hz</b>	19.1	31.3	43.2	60.3	89.8	70.1	65.3	64.7	64.4	64.4

## 5.5 Identification of Optimum Driving Voltage and Frequency

The main propose for this investigation is to achieve a displacement amplitude value of 200  $\mu\text{m}$  for oscillating the work-piece as it is an average value of all displacement amplitudes that can be reached by the oscillation system. However, the oscillation system should not meet or reach the resonate frequency of both the spindle unit and the oscillation system bulks.

As seen in table 5.2 there is a range of frequency with voltage that can be applied to the oscillation jig to achieve displacement amplitude around 200  $\mu\text{m}$  as highlighted in red color.

In Chapter 6 of dynamics of the machine tool, the machine spindle has been investigated in two ways harmonic excitation and hammer impact test. It notes that the resonant frequency of the spindle can be reached by applying frequency around 100 Hz. At this value of frequency the spindle may start light shaking during machining time. So, the oscillation jig should avoid this frequency value.

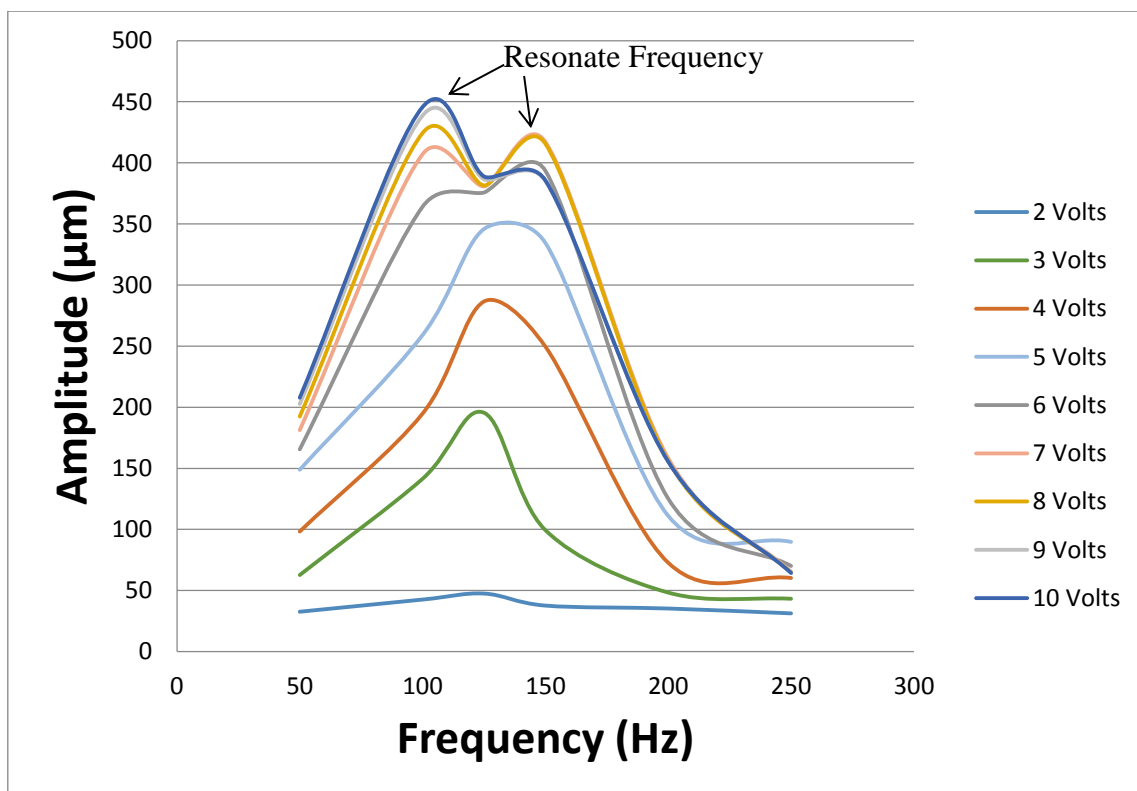


Figure 5. 13: Frequency Amplitude Graphs.

Figure 5.13 above shows the relationship between frequency and amplitude. It notes that the high displacement amplitude of oscillating the work-piece can reach frequency values between 100 and 150 Hz, but this notes that the oscillation system meets its resonant frequencies which are 100 and 150 Hz as observed from graphs in figure 5.13. In addition, it was observed that at higher frequency and voltage the oscillation system starts ringing at high pitch which is harmful to the equipment and operators, so high excitation voltage is not recommended for this type of oscillation jig.

Here it also notes that a frequency value of 125 Hz secured the target of oscillation displacement with lowest excitation to avoid resonant frequencies. Therefore, the oscillation jig is run at excitation of 3 volts with applied frequency value of 125 Hz.

### **5.6 Remarks**

First, the Key measurement parameters of dynamometer calibration have been clearly identified in two stages or conditions, normal position and horizontal position for the dynamometer device. It also observes that the calibration outputs were linear for both conditions.

Second, in displacement amplitude calibration, the oscillation jig or system was investigated and shows the relationship between vibration amplitude and applied Voltage with frequency. In addition, from identifying the optimum driving voltage and frequency, it notes that the optimum point is to avoid the resonant frequencies of the oscillation system and machine spindle. Moreover, the oscillation jig was ringing at high pitch when the frequency values higher than 150 Hz are applied to the piezoelectric actuator oscillation.

## **Chapter 6**

# **Investigation into machine tool Dynamic Response**

## 6.1 Introduction

The aim of this chapter is to understand and identify the characteristics of the static and dynamic response of the milling machine tool. The investigation of static and dynamic behaviour for the oscillation jig is equally important. A proper and controlled application process of vibration needs a fundamental understanding of machine tool response to external excitation. It is prudent to discover how the machine tool and the oscillation system performed under the conditions of external dynamic loading.

In this chapter, stiffness and natural frequencies of the milling machine's spindle are studied and obtained by experimental works. These experimental works include an impact hammer test and a continuous harmonic excitation force using a piezoelectric actuator.

## 6.2 Dynamics in machining applications

A high level of accuracy is always required when machining a work-piece. To achieve this level of accuracy, the characteristics and dynamics of the machine should be studied and analysed, the machine responds to excitations and inputs. Many papers have been published explaining and identifying the machine's dynamic characteristics such as milling and grinding.

In part of computational modelling and simulation, Xiao et al, (1992) have used intelligent plunge control to develop Optimisation Strategies for a grinding cycle. Also, in 1980, Garcia-Gardea et al. developed a Dynamic Data System (DDS) approach which was used for estimating the dynamic characteristics of machining process. This approach work by analysing the cutting force signals, is also based on the statement that, the cutting forces signals should have all features of machine dynamics. Due to the fact that the modelling was based on real experiment data which was collected from machining operations, the DDS method can give better accuracy on dynamic characteristics estimation for the machine tool.

Cheng et al, (2007) worked on a milling machine, they tried to explain and identify the frequency response of a spindle for the tool holder. The impact test has been used with a low-mass accelerometer in order to determinate the Frequency Response Function (FRF) of the system unit. Non- rotating mode for the spindle was used for this approach. In addition, this method can provide acceptable results and reliable predictions of the response. On the other hand, some spindles' responses vary with their spindle rotating speed and the predictions of Frequency Response Functions (FRF) based on the non-rotating mode for spindle may not be sufficient when the spindle is rotating at a speed of about 10,000 RPM. However, another measuring method called Reacceptance Coupling Substructure Analysis was used for the system response predictions, it also was shown that the response was quite different (Movahhedy and Mosaddeh, 2006; Schmitz et al., 2004; Xiong, G.L. et al., 2003; Tian and Hutton, 2001).

The dynamics of the cylindrical grinding machine have been studied using model experimental data by Jiang et al. (2007). During the grinding process, they were trying to collect and avoid typical values of the machine-produced vibration. In this work, non-contact displacement sensors and accelerometers were used to collect readings of 25 measuring points which were set on the grinding machine. In the first experiment, the machine's natural frequency was identified in the condition of static mode, where the impact load was used to produce the input excitation force. The critical frequencies have been identified for the wheel that was rotating with speeds of 70-700 RPM in a second experiment. The same test was performed but in a real grinding process. Also, the critical vibration frequencies during the grinding process were revealed and also analysis of the relationship between the work-piece spindle speed and surface coarseness was obtained. In addition, it concludes that when they were increasing the spindle speed, the surface roughness of the work-piece was improved. As the result of that, the work-piece should be ground at high spindle speed in order to improve the surface roughness.

In 2005 Zhang et al. studied some ways in dynamic analysis of machining process, to improve the surface roughness of the work-piece. In order to achieve that, they worked to determine the characteristics of frequency amplitude for the machining process. The following conditions of machining process have been considered:

- The grinding wheel type is Synthetic Aluminium Oxide (250 mm).
- Cutting speed was between 30 to 35 m/s.
- Depth of Cut 0.005 to 0.03 mm.
- Grain size was about 0.4 and 0.5 mm.
- The range of vibration frequency was from 0 to 120 Hz.
- The range of vibration amplitude was from 0.001 to 0.002 mm.

They concluded that the developed model was only giving good results with the considered range of vibration frequency, also the machine quality behaviour was changed with the changing of frequency.

The Finite Element Method (FEM) has been used by Kang et al., (2001) for modelling a harmonic response of the milling machine. In order to identify the stability margins, analysing of modal, static and stability have been conducted. They identified the natural frequencies of their system, these frequencies and model shapes of the jigs allowed them to obtain the instability speed threshold. However, for the design of spindle bearing systems, the Computation Aided Engineering (CAE) strategies cannot present a complete solution.

Denkena et al. (2016) have done an experiment to investigate the dynamic behaviour of the integrated z-slide (the spindle unit) in a CNC-milling machine. They used an electro dynamic shaker to provide the excitation force. This shaker was fixed in vertical direction to the spindle unit. They also used a force sensor fixed to the tool side, so the applied force could be measured. The spindle was excited with a linear frequency sweep. The maximum excitation frequency they reached was 200 Hz. Moreover, their results show that the sensitivity of the strain gauges is quite stable in the range of frequency values under 100 Hz. Then, the natural frequency of the spindle unit was appearing from 100 Hz to 150Hz as shown in figure 6.1.

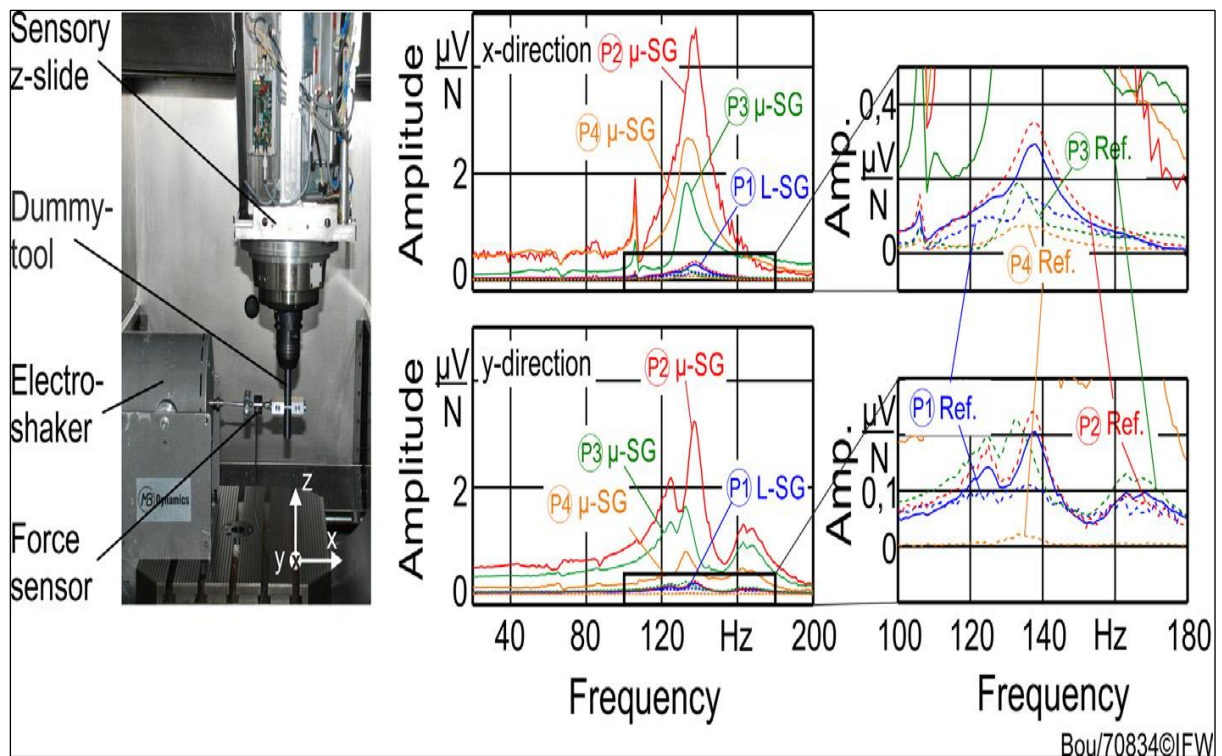


**Figure 6. 1: Test setup and frequency responses of the sensory spindle unit (Denkena, B. et al., 2015).**

Prakosa and others (Prakosa et al. 2013) were dealing with an activity in machine tools' performance that can improve spindle static and dynamic stiffness. They were identifying mathematical models for static stiffness, dynamic stiffness and temperature rise in the milling machine tool. Their models conformed well to the results from real experiments. To validate the dynamic model for their spindle unit, they used the Frequency Response Function (FRF) experiment using a Hammer impact and spectrum analyser. However, they validated the static stiffness model experimentally. A pneumatic actuator was used to actuate static load at the machine spindle head. Also, a dial indicator was used to measure the corresponding deflection.

### 6.2.1 Resonance Vibration

Modes are used as a simple and efficient means of characterizing resonance in vibration. The majority of structures can be made to resonate. Under the best experimental conditions, a structure can be made to vibrate with excessive, sustained, oscillatory motion. Resonant

vibration is caused by an interaction between the inertial and elastic properties of the materials within a structure. Resonant vibration is often the cause of, or at least a contributing factor to, many of the vibration related problems that occur in structures and operating machinery. To better understand any structural vibration problem, the resonances of a structure need to be identified and quantified. A common way of doing this is to define the structure's modal parameters (Guillaume, 2006).

Forced vibration can come from:

- External loads.
- Ambient excitation.
- Imbalances.
- Internally generated forces.

Resonant vibration occurs when one or more of the resonances or natural modes of vibration of a machine or structure is excited. Resonant vibration typically amplifies the vibration response far beyond the levels of deflection, stress, and strain caused by static loading (Boisson et al. 2014).

Modes and resonances are intrinsic properties of a structure and shape. Resonances are determined by the material properties (mass, stiffness, and damping properties) and boundary conditions of the structure. Each mode is defined by a natural (modal or resonant) frequency, modal damping, and a mode shape. If the material properties or the boundary condition of a structure change, its modes will definitely change. For example, if mass is added to a beam structure, it will in a different way because its modes have changed.

At or near the natural frequency of a mode, the overall vibration shape (operating deflection shape) of a machine or structure will tend to be dominated by the mode shape of the resonance.

From the works that have been done on this issue of machine system response, it is to be noted that it is not simple to identify the system's dynamic characteristics. Also, there are no fully accurate results that come from computation methods and simulation analysis because other external factors are not considered, which can affect performance and stability of the system. However, this work gives a clear view of the system's response.

### **6.3 Identification of the 5-axis spindle Unit response**

Investigation of the natural frequency of the milling machine's spindle should be done before any vibration experiment. Therefore, to determine and identify the response and natural frequency of the spindle system, the spindle unit was stationary and tested in the two following static tests:

- 1- Harmonic excitation test.
- 2- Hammer impact test.

#### **6.3.1 Harmonic excitation test**

In this investigation test, the piezoelectric actuator produces a continuous harmonic excitation force that was applied to the spindle system of 5-Axis Milling machine. The value of this force was defined as 44 N. This piezo actuator was run at specific force with a sweep sine wave. Different values of frequency was used, and the deflection of the spindle unit was measured at each frequency; a high resolution eddy current displacement sensor was fixed next to the spindle. A full experiment configuration set-up is shown in figure 6.2 below.

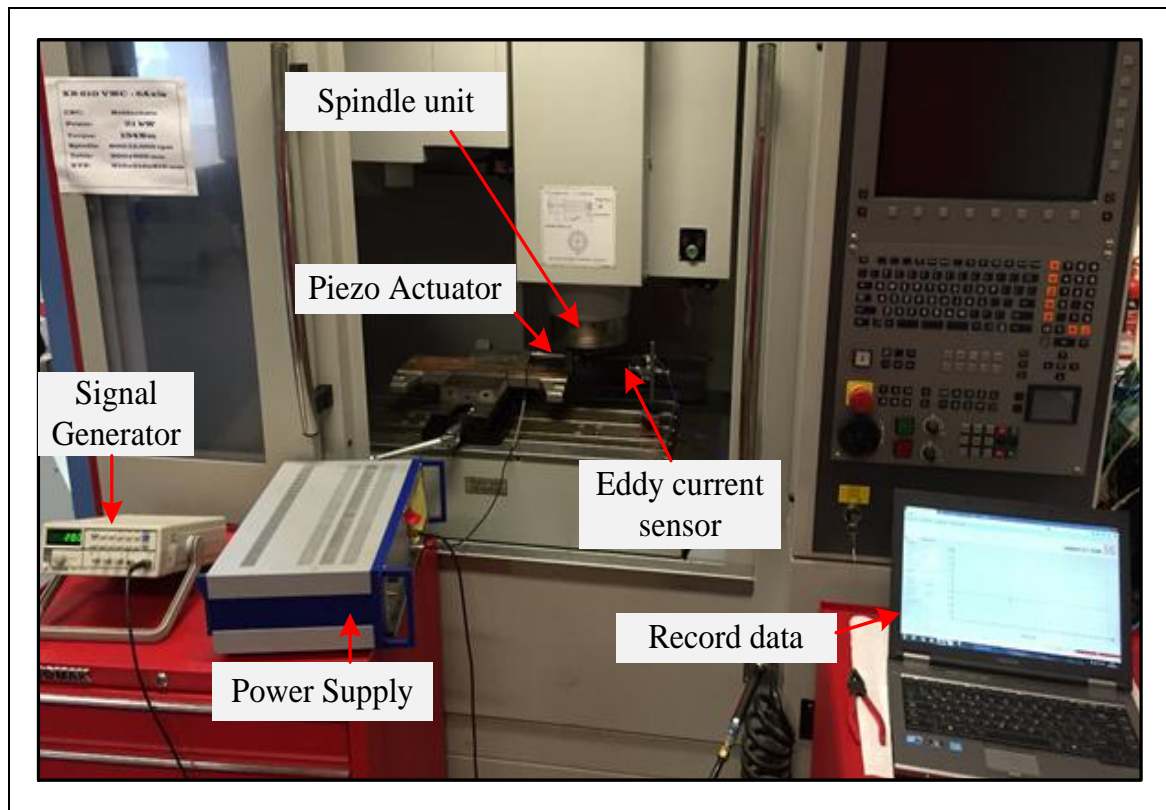


Figure 6. 2: Experimental set-up for Sweep-Sine Test for the spindle unit.

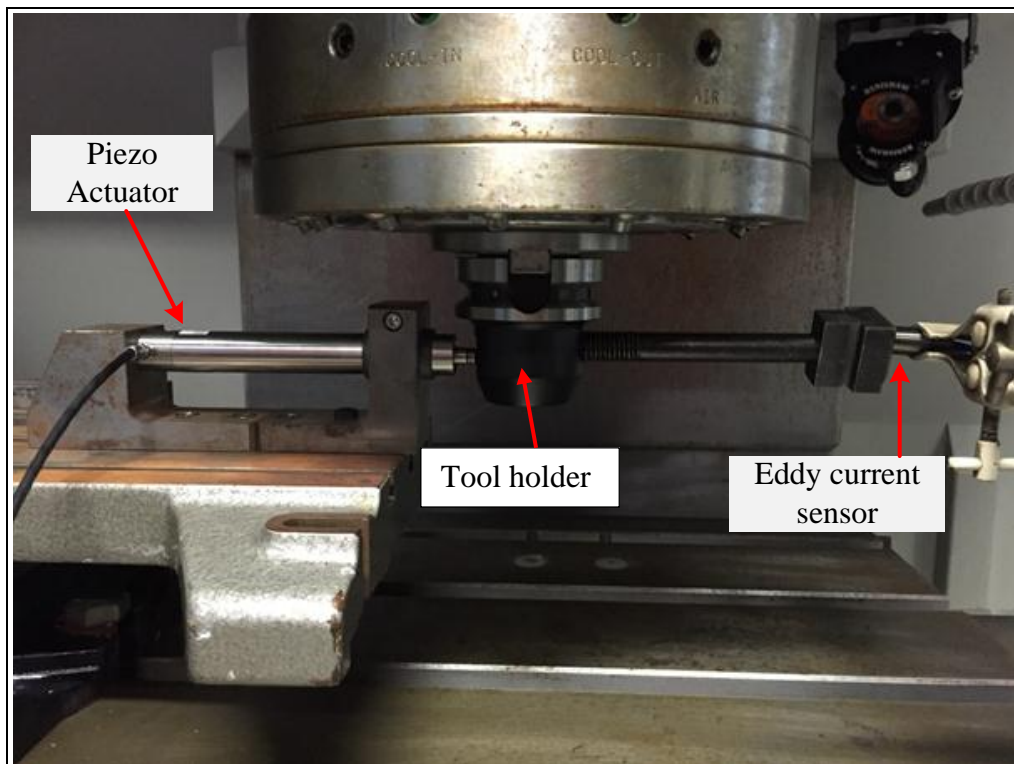
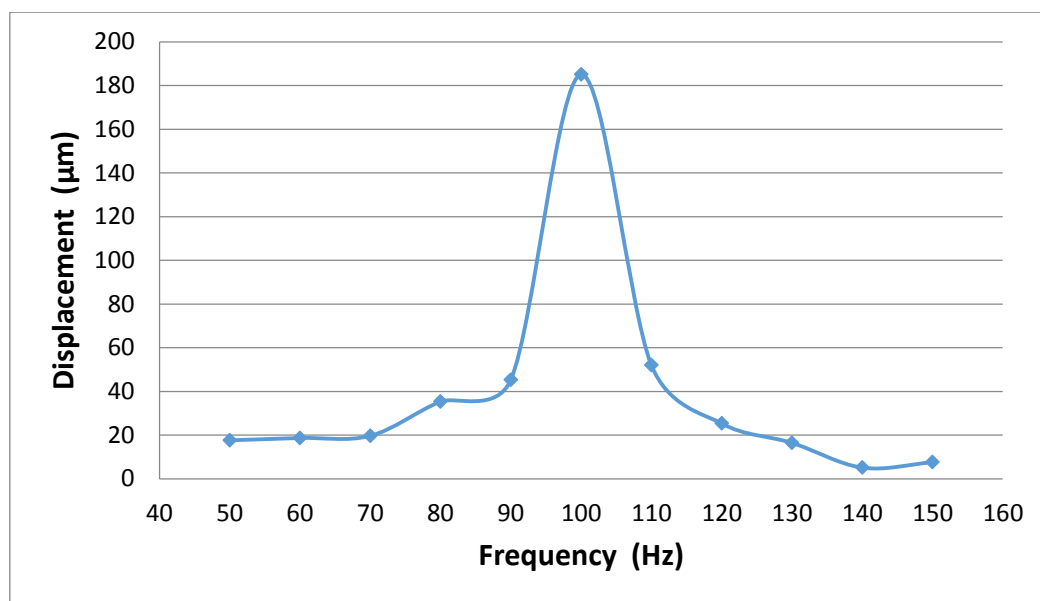


Figure 6. 3: Set-up configuration for piezoelectric actuator and Eddy current sensor.

The piezoelectric actuator was fixed vertically next to the machine's spindle. Here, the actuator applies vibration in the vertical direction of the spindle so only vertical movement was recorded. The piezoelectric actuator was mounted on a steel holder that was fixed to the milling machine table. The sine wave signals were generated from a function generator and amplified for moving the piezo actuator. This function generator allowed modifying and controlling the system's characteristics such as the amplitude and frequency. An Eddy current displacement sensor was used and held by a steel stand next to the machine spindle in line with the piezoelectric actuator. This displacement sensor allowed measurement of the spindle deflection as shown in figure 6.3. The signal from the sensor was recorded using a software provided by the manufacturers. The applied force was kept constant without any change by fixing the sine waves amplitude on the signal generator. The frequency value was increased step by step over a range of frequency values. Figure 6.4 shows the graph of the amplitude frequency characteristic for the milling machine spindle unit.



**Figure 6. 4: Frequency Amplitude performance response for the spindle unit.**

The piezoelectric actuator was run with the sweep sine wave to apply an excitation force into the spindle of the CNC-Milling machine. The results of this sweep-sine test are shown in figure 6.4, indicating the natural frequency of the spindle unit as 100 Hz with high displacement or deflection of about 180 µm.

### 6.3.2 Hammer Impact test

In vibration testing, the impulse input or impact hammer is widely used for natural frequency obtaining and mode shaping. The reason behind why it is widely used is down to its simplicity and convenience for the experiment (Mao et al. 2010).

The experimental equipment of the hammer impact test consists of an impact hammer, high resolution Eddy current sensor, charger amplifier and Data acquisition software installed in a PC. Figure 6.5 below depicts the full configuration of the experimental set up.

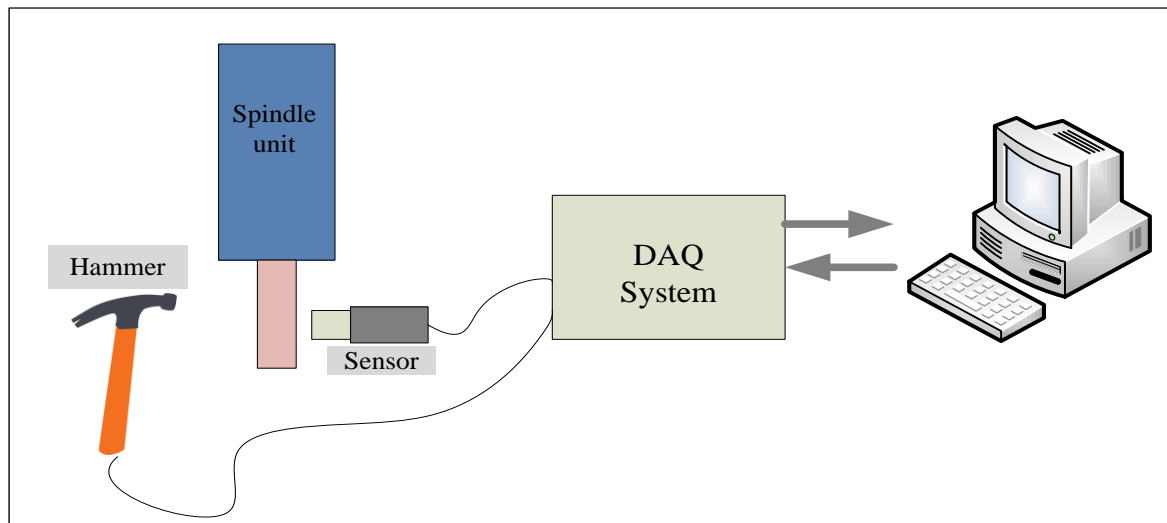


**Figure 6. 5: Experimental Configuration for Hammer Impact Test.**

The hammer impact was applied to the spindle unit of the CNC machine in the horizontal direction. As shown in figure 6.6 below the Eddy current sensor or displacement sensor was held by a steel stand fixed to the machine's table. The sensor position was on the other face of the spindle opposite the hammer impact direction. So, the sensor can take measurements of the spindle deflection when the hammer hits the spindle.

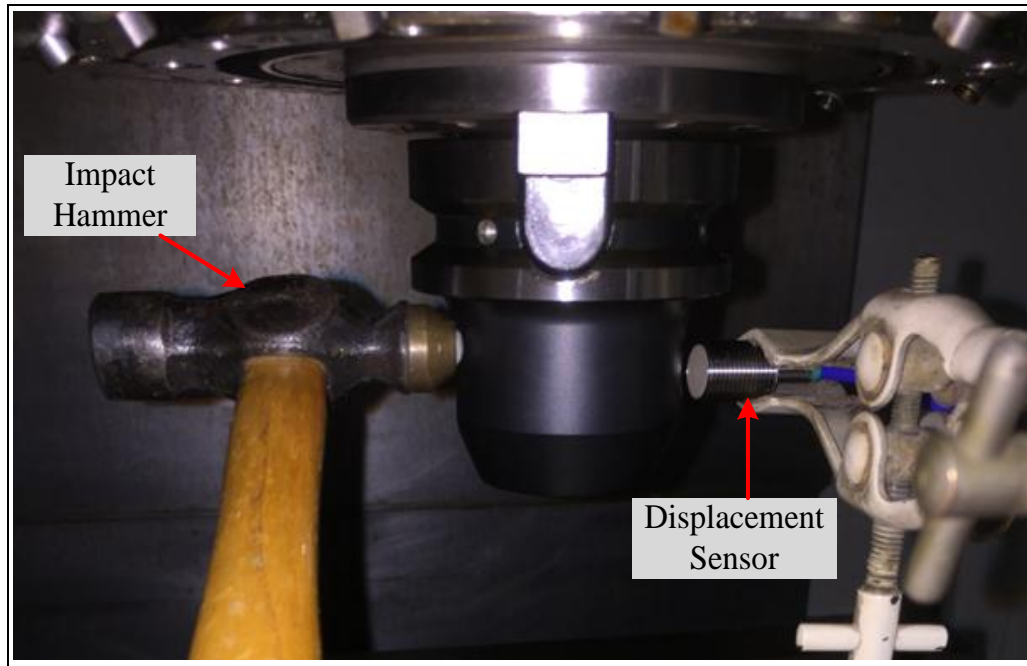


**Figure 6. 6: Impact Hammer tester and Eddy current sensor configuration.**

For modal analysis of transient force excitation, the impact force was applied on the tool holder of the spindle unit for the CNC 5-axis milling machine as displayed in figure 6.6. The corresponding signals that come from the Eddy current sensor were recorded on a laptop using the specific programme the manufacturer provided.

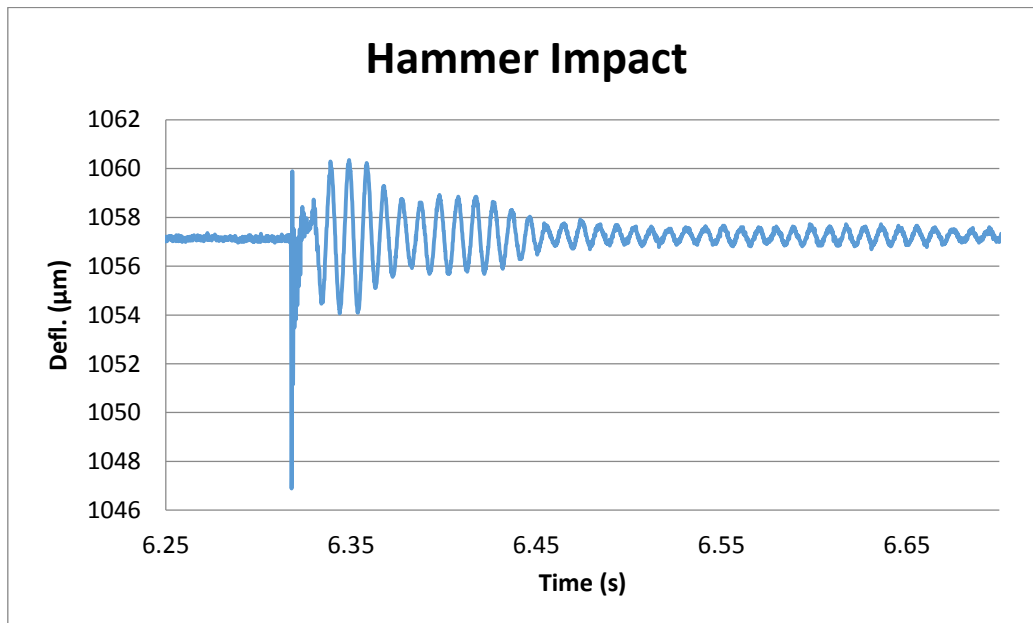


**Figure 6. 7: Spindle Unit system response.**

Figure 6.7 above presents the system dynamic response after the impulse force was applied. Here, the eddy current sensor measured varying values of the deflection for the milling machine's spindle unit during time.

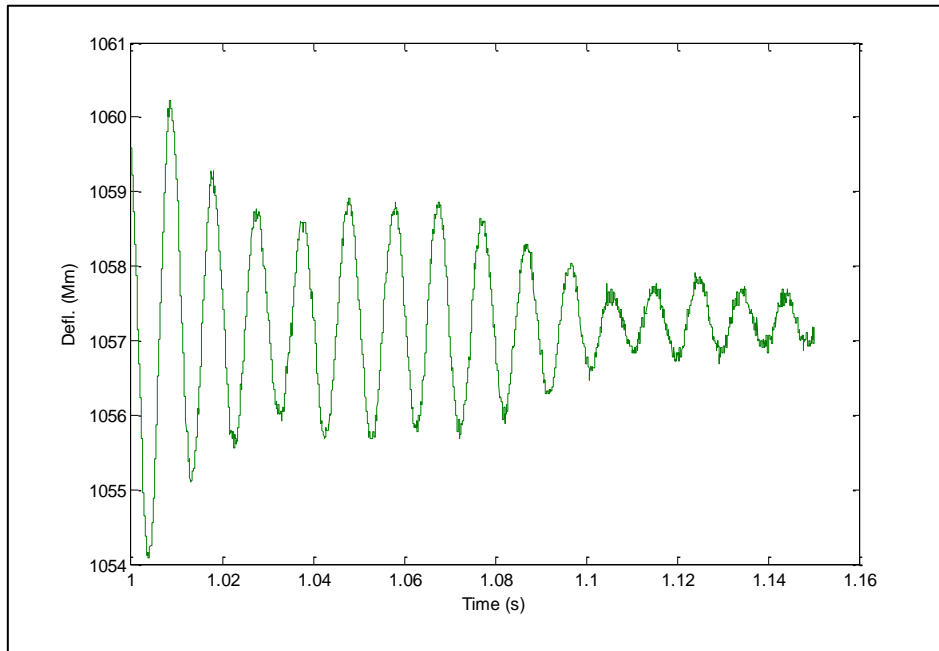


Figure 6. 8: Spindle unit deflection in  $\mu\text{m}$ .

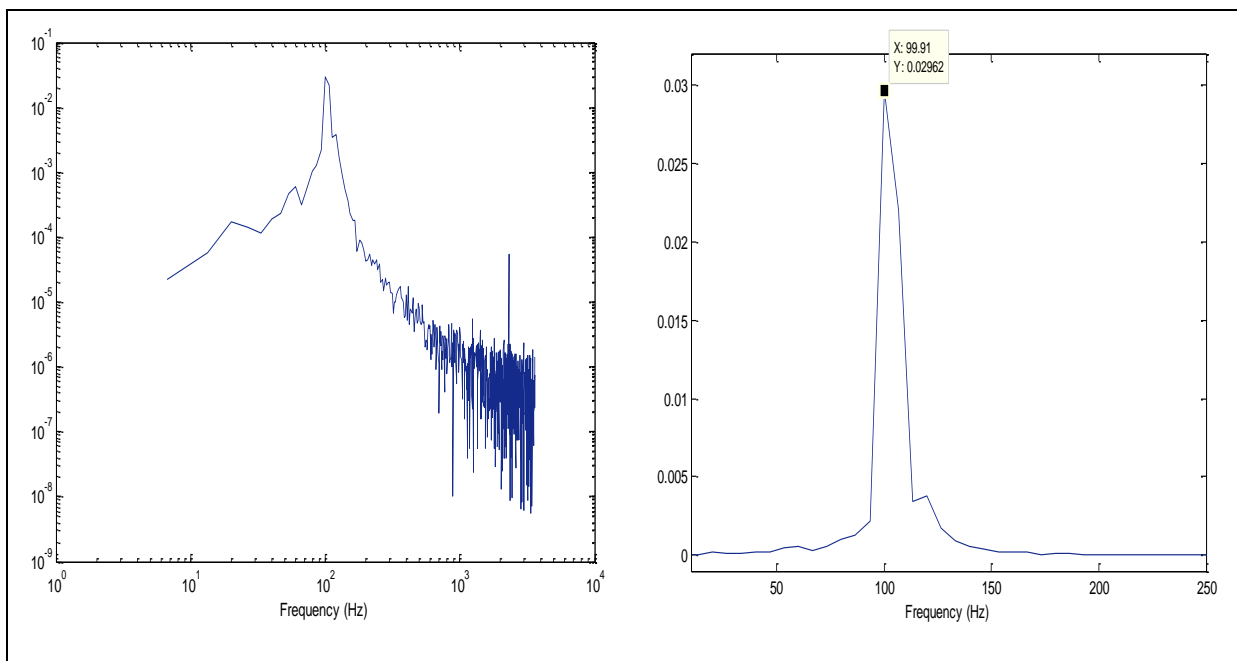


Figure 6. 9: Frequency spectrum analysing for the spindle unit response.

For this Frequency Response Function (FRF) experiment, Matlab software provides the spectrum analysis tool box which was used to define the natural frequency of the spindle unit.

Figures 6.8 and 6.9 present graphs of spindle unit deflection and dynamic response after analysing the signals from the eddy current sensor. In addition, a spectral data analysis is displayed in figure 6.9, it also notes that the natural frequency of the spindle unit for the CNC 5-axis Milling machine is nearly equal to 100 Hz as it is the peak point in the data spectra's graph (figure 6.9).

The natural frequency of the spindle unit for the CNC Milling machine was identified and validated using two static experiments, harmonic excitation test and hammer impact test. These two static tests have proved that a value of 100 Hz is defined as the natural frequency of the CNC Milling machine's spindle unit.

This value of frequency or the area with the highest amplitude peak should not be applied into the piezoelectric actuator during vibration assisted milling. On the other hand, during the conduction of the vibratory milling machine, the area of low displacement amplitude is the most appropriate frequency values to drive the piezoelectric actuator.

### **6.4 Spindle unit Static and dynamic stiffness**

Abuthakeer et al. (2011) were attempting to define static and dynamic stiffness for cast iron bed of the milling machine. Their objective of this static behaviour analysis is to determine the strain of lathe bed. They used hydraulic jack to support and load the cast bed. For measuring the load readings, the strain gauges were fitted on right and left side on the bed near the area where load was applied. The strain readings were recorded while the loads were increased in steps.

Another work in describing the dynamics was by Pawlowski and Orynski in 2002, they described the static and dynamics of cylindrical machining using a physical model. The key elements of their project were that measuring successfully the static of three structures for grinding machine; the wheel headstock, the wheel itself and work-piece.

Also, in cylindrical grinding, Zaruba (2005) determined the static stiffness and compliance for his machine. Frist, in the condition of static forces, the forces were linked to slow changes in relative position for the wheel and work-piece as the value of frequency is zero. Second, the dynamic forces condition was related to that determining the static stiffness while the working frequency of the rotating wheel is running.

Koura et al. (2014) have used an integrated simulation system to evaluate the static and dynamic response of a milling machine. They have discussed the design consideration of the evaluation system based on finite element technique (FET). Also, they obtained a reliable model could replace many experiments test which can be carried out when changing is subjected in the parameters that affect cutting condition. In their work, they were modelling and meshing several elements of the milling machine includes mechanical structure. In addition, the behaviour of milling machine was identified in following terms:

- Static Loop stiffness in both directions X and Y.
- Mode shapes.
- Frequency responses function at tool canter point.

In machine tools, there are various test methods (ISO 230-1, 2012). Some of these test can be done as a regular test (fast test) but other test methods can be too long and take time to be performed (a few hours) (Archenti et al. 2012). Knapp (1983) has run the fast test methods based on circular test as a circle path and all deviations from the base circle are recorded. In this circular test, the changes in the distance between the spindle unit nose and the centre of circle were measured. The movement accuracy was calculated from the errors of the motion traces that can be identified from analysing the traces (Kakino, Y., et al., 1993).

In the early 1980s, the double ball bar (DBB), based on the circular test, was developed as a device that can be used for quick experiments and it was used ISO 230-4 and ANSI B5.54-2005 as an instrument for their circular test (Archenti, et al., 2012), (Bryan, 1982), and (ISO 230-4, 2005). In addition, in this ball bar measurements, the test will be ensured united practice and make it possible to reliably find many machine tool deviation types from this simple measurement.

In machine tool design, Dynamic stiffness is the key parameter which can improve the quality of the work-piece and increase life of the machine tool. Essentially, the spindle unit of CNC 5- axis milling machine is subjected to some kind of dynamic tests to determinate the spindle unit stiffness and compliance as they are the main characteristics for any machine configurations.

The 5-axis CNC milling machine is used in this part of work, and only the static stiffness and compliance of its spindle unit are investigated. These tests were done using the following procedure. An external force has been applied to the centre of the tool holder for spindle unit. This force was applied using a hydraulic jack that was placed horizontally in spindle direction (in X-axis direction) in order to measure the static stiffness. The hydraulic jack was applying arrange of force and the dynamometer (Kistler 9257A) was used to measure the applied forces and has been calibrated horizontally in Chapter 5 in order to convert the dynamometer output values from volts to Newton. As the spindle direction in milling machine is in Z-axis, all devices of this work were fitted in X-axis, starting by hydraulic jack then the dynamometer sensor as shown in figure 6.10. In addition, the eddy current sensor was used for measuring the spindle unit deflection. This displacement sensor was positioned on line of the applied force direction (the hydraulic jack) and it was held by a steel holder based on machine table. A Real-time LabVIEW Data Acquisition system was used to record readings of the load. Figure 6.10 below shows the actual experimental set.

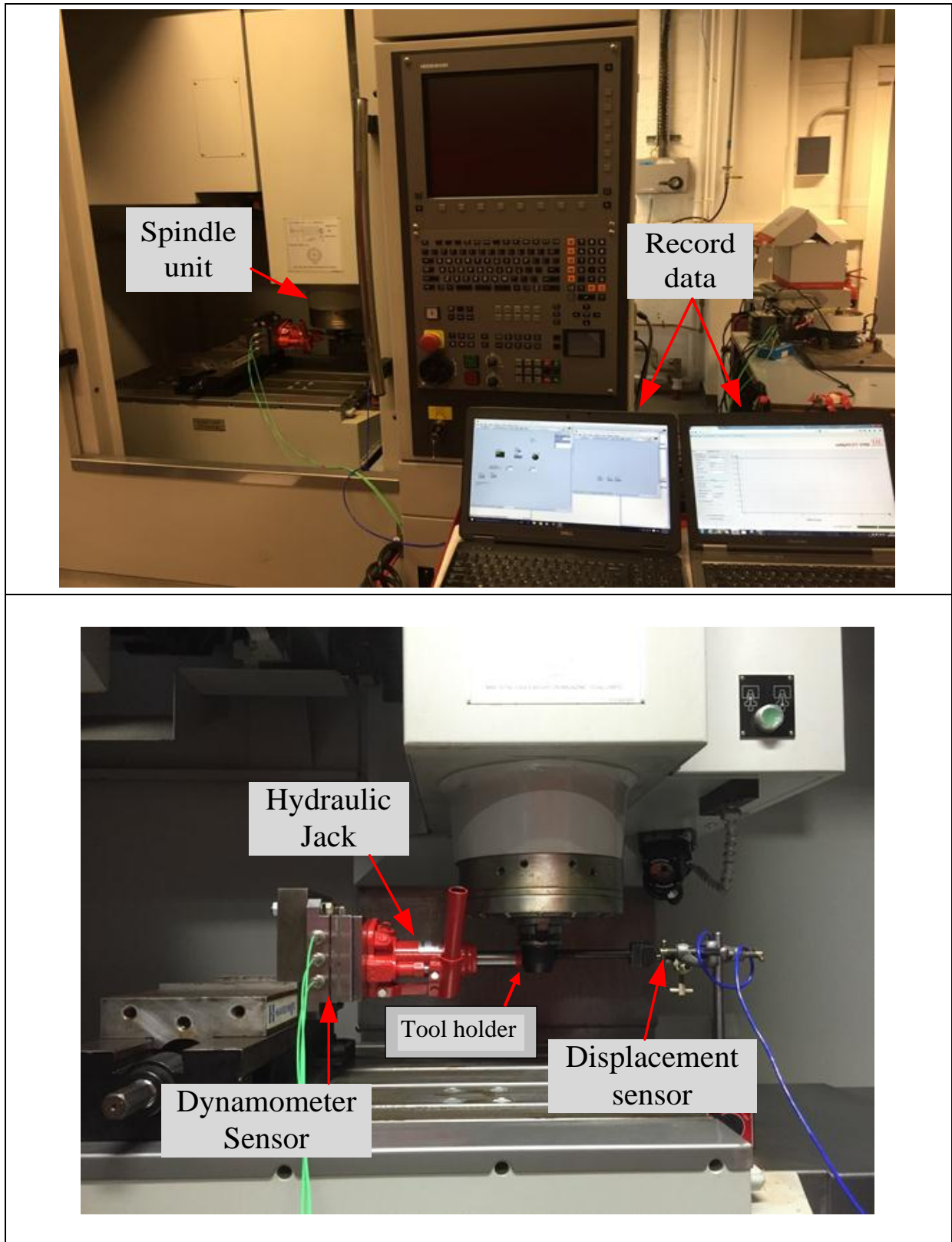
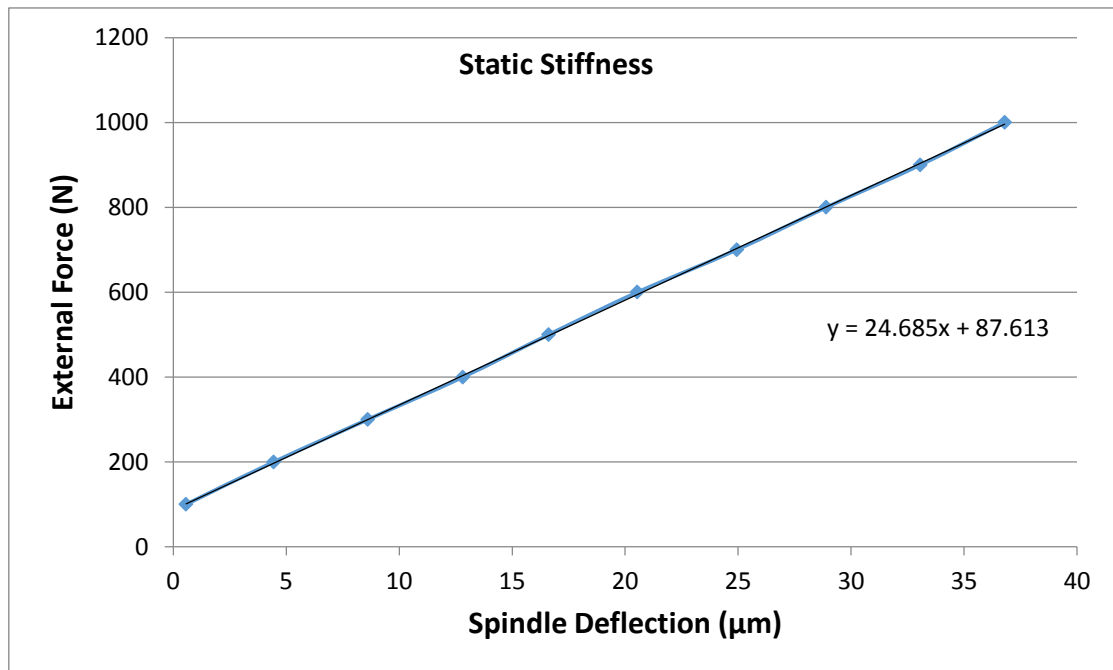


Figure 6. 10: the actual experimental set-up for the static stiffness and compliance investigation.

Figure 6.11 shows the force-deflection graph that was recorded by taking the average of three repeated tests and ten loads were applied into the spindle unit of the milling machine.



**Figure 6. 11: the force-deflection response for Spindle unit.**

From the above graph of the force-deflection relationship, it is noted that the relationship between the external forces and deflection of the milling machine’s spindle unit is linear. The average value of the stiffness for this spindle was defined by linear approximation as:

$$K = 24.68 \text{ N}/\mu\text{m}.$$

The compliance  $C_s$  of the spindle unit for the CNC milling machine can be calculated by the inverse of the stiffness as:

$$C_s = 1/k = 1/24.68 = 0.04\mu\text{m}/\text{N}. \quad (6.1)$$

## 6.5 Dynamic Stiffness of the Spindle Unit

Based on the theory of vibration, the spindle's dynamic stiffness is depending on the frequency value that drives the excitation force. Therefore, a sweep sine wave test was used to excite the spindle unit; the value of driven frequency was varied from 50 Hz to 150 Hz with a constant magnitude value. It is noted that the frequency value of 100 Hz was the resonant frequency of the spindle unit.

Figure 6.12 below shows the dynamic stiffness as a frequency function for the spindle unit. These values of dynamic stiffness (K) were defined as:

$$K_d(S) = \frac{F(s)}{X(s)} \quad (6.2)$$

Where:

$F(s)$  is applied force and  $X(s)$  is the displacement deflection.

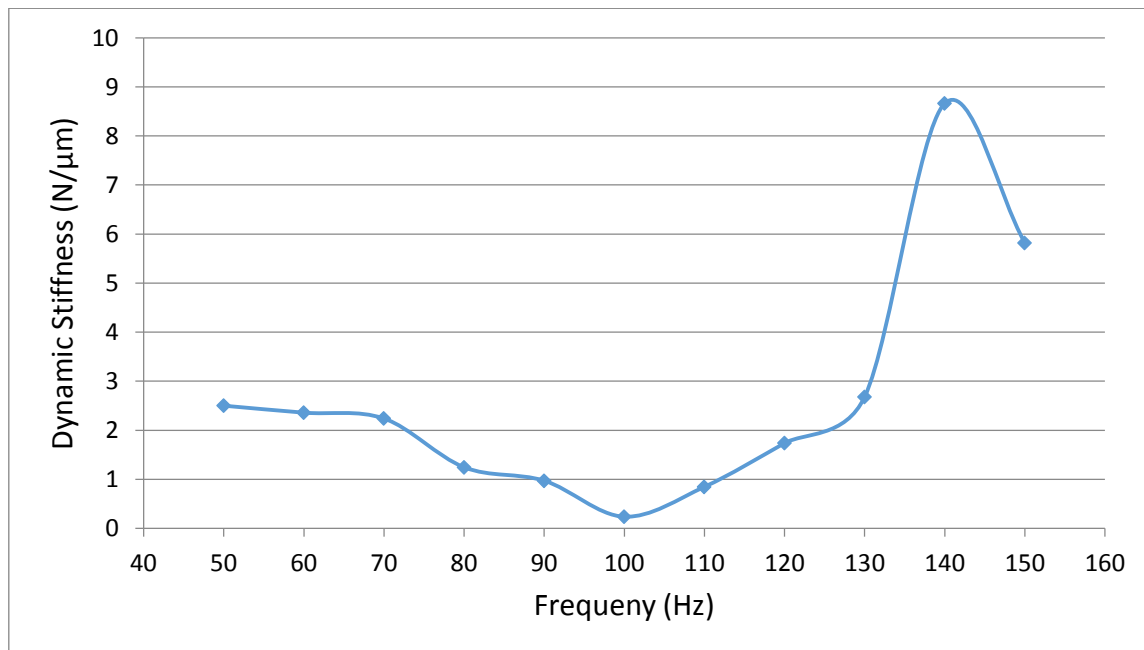
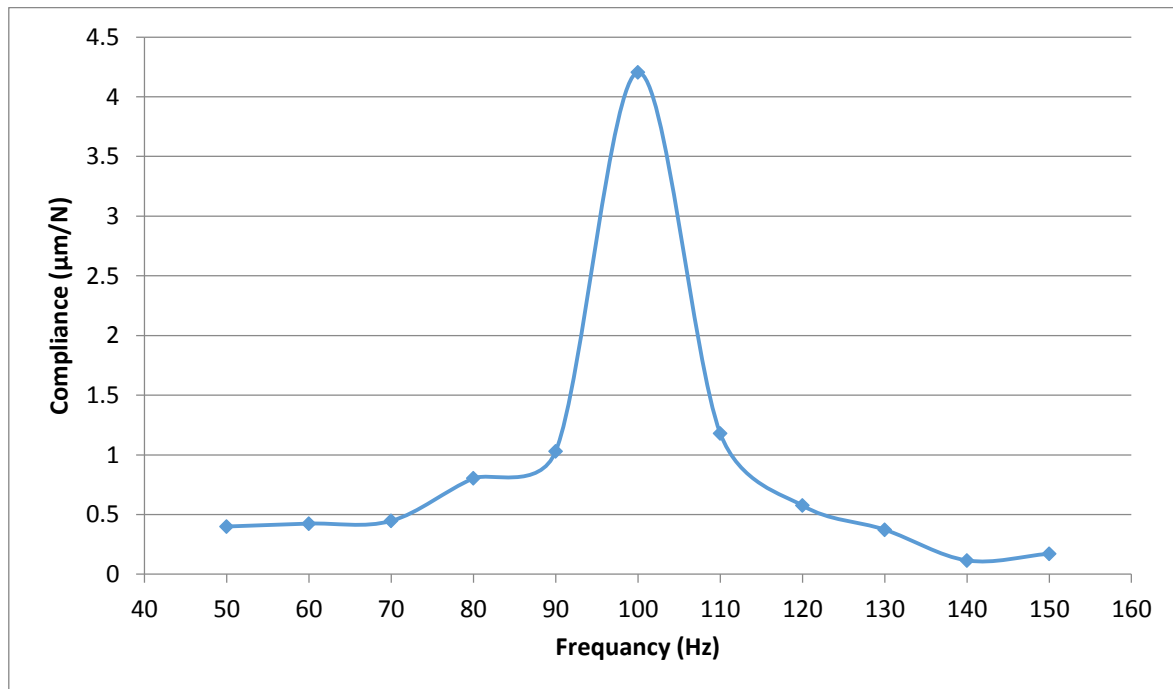


Figure 6. 12: Dynamic stiffness of the spindle unit as frequencies function.

According to the graph in figure 6.12 above, it is seen that during excitation at the resonant frequency of the spindle unit (100 Hz), the spindle unit has the lowest stiffness. Moreover, at this point of resonance, the compliance value of the milling machine's spindle was the highest (figure 6.13). After this point of resonance peak, the dynamic stiffness of the spindle unit increased. The advantage of these experiments was to gain the knowledge of dynamic stiffness for the system, so the resonant modes can be identified and then avoided during the machining process.



**Figure 6. 13: The dynamic compliance of the spindle unit.**

In figure 6.13 above, the dynamic compliance values of the spindle unit for the CNC- milling machine were calculated and illustrated using the equation 6.1 which is the inverse of the stiffness. Moreover, this graph shows that the compliance of the spindle system is nearly 4.2 µm/N at the resonant frequency point.

# **Chapter 7**

## **Closed Loop Controller Development**

## 7.1 Introduction

For building a mathematical model of any dynamic system, the system identification methods are widely used on the input and output data that are observed and measured from the system or experiments. The system identification is a determination of any system specific parameters which are based on inputs and outputs of the system.

The most important consideration in controller design for the system is defining a clear and good model for the process plant that needs to be controlled, because the controller design will be based on this mathematical model. This model can be only obtained via a numerical process called system identification. In this process, the acquiring of data from a plant will be involved and then analysed numerically. Then, the data response will be tested to estimate the plant's parameters.

The design of a control system requires a mathematical model of the dynamics of the process. Here, the process dynamics can be difficult to obtain due to the complexity of this process, also dynamics may be completely or partially unknown. Sometimes in some case (nonlinearities, large state dimensions, etc.) it will be too complex to base controller design on the system, even if the mathematical model is known (B. Wayne Bequette 2003).

There are three different types of system Identification:

1. White box models: model structure based on first principles, such as Newton's law, model parameters estimated from measured data.
2. Black box models: model structure and its parameters completely unknown, they are reconstructed from data.
3. Grey box models: model structure partially known from first principles, the rest is only estimated from Input/Output data.

## 7.2 The System Identification Procedure

In system identification, the main object is determination of a mathematical model of the dynamic and physical system using observed data. The following steps are involved in system identification:

1. Description of the task, the purpose of the model and the final goal of the model.
2. Study initial data, the challenges present in the task at hand and useful graphs displaying the data.
3. Design the experiment. At first, enumerate the main challenges for identification, and formalize where to focus on during the experiment. Then design an experiment so as to maximize the information which can be extracted from observations made during the experiment.
4. Identify model system; find a good model structure and parameters which explain the behaviour of the system during the experiment.
5. Update or refine the analytical model based on identification results.
6. Verify model system; the model should be adequate for the purpose of extracting or explaining the important effects.

A flowchart of the typical system identification experiment is shown in Figure 7.1.

Similarly, system identification tries to determine out the dynamics of a system by relating input signal to corresponding output, i.e. from observed input-output behaviour.

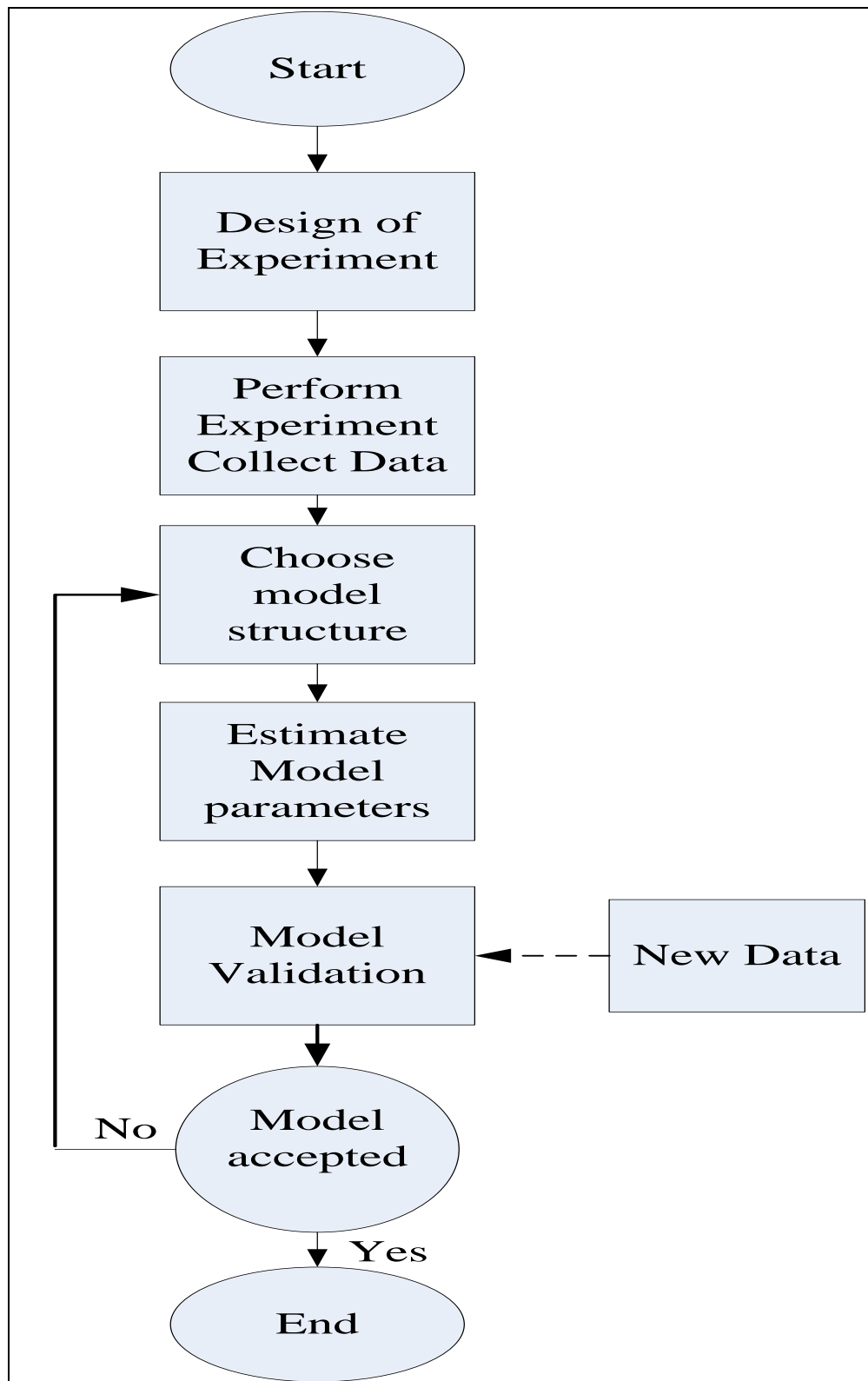


Figure 7. 1: Modelling and system Identification process.

## 7.3 Mathematical Model

In this chapter, some Mathematical models for the physical oscillation device are used to design and test the performance of the controller that will be based in the vibration system. The ordinary different equations are used to describe these Mathematical models. In order to design and implement a control system, a number of elements are required. These required elements are illustrated bellow:

1. The knowledge of process outputs.
2. The knowledge of controlling devices.
3. The knowledge of actuating devices.
4. The knowledge of the main plant.

The flowchart in figure7.2 below describes the steps of controller design system:

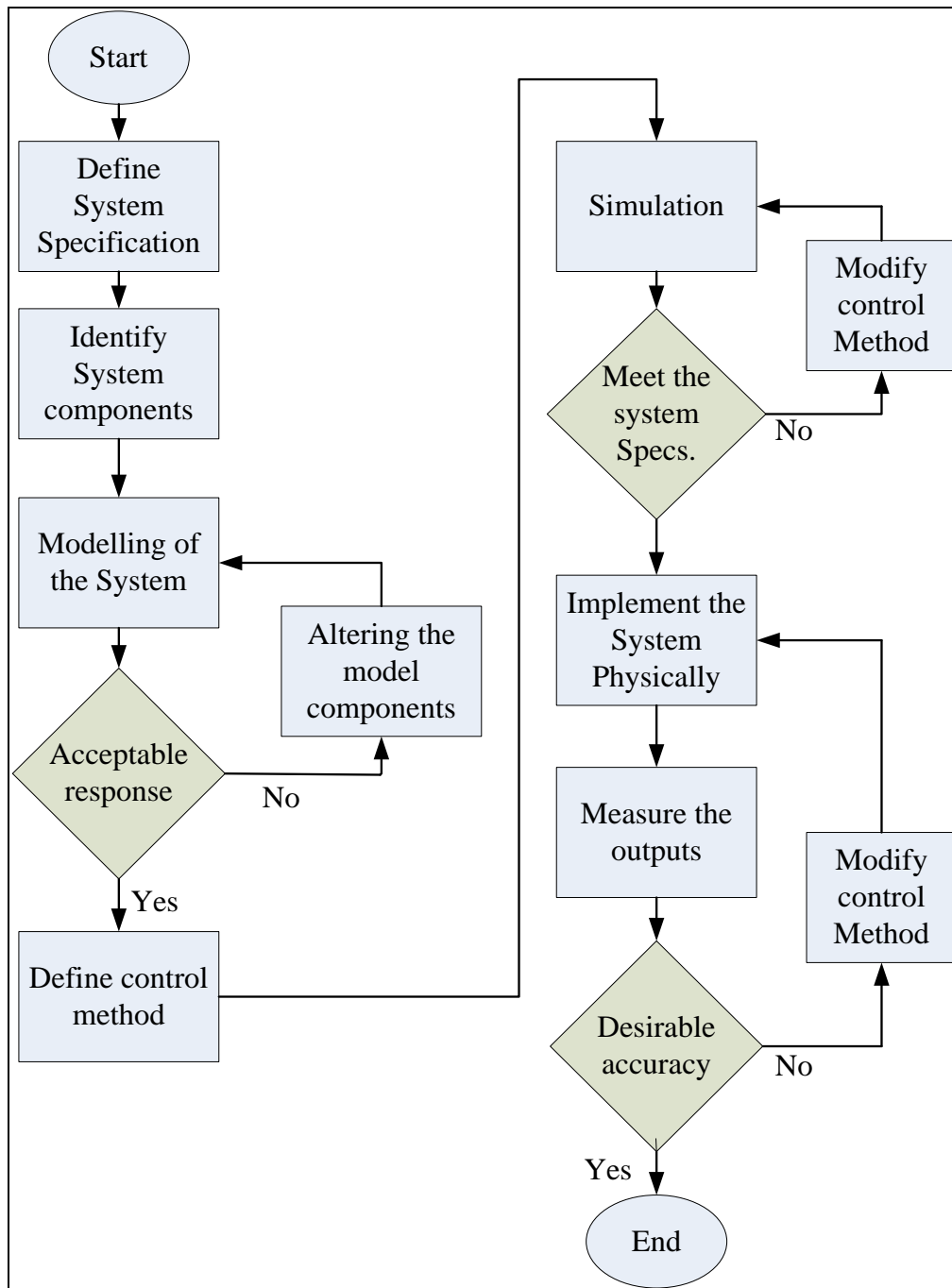


Figure 7. 2: Control Design Procedure

## 7.4 Mathematical Model for the Vibrating stage

The controlled system had an input variable (reference input) and an output variable (controlled value). The system response was described in terms of dependence of the output variable on the input variable. These responses between one or several variables can be described using mathematical equations based on physical laws. Such physical relationships can be determined by experimentation.

A mathematical model was derived from the actual oscillating jig designed for the preliminary investigation to design a closed loop control system. Below are key points for the use of mathematical modelling:

- Develop a better understanding of the design system
- Allow to design a controller and test it without any risk
- Low cost production

Most of the work done on the topic of vibratory machining mainly state the amplitude and frequency generated by the oscillator. However, the actual magnitude to the oscillatory displacement achieved in the cutting zone is rarely reported. Therefore, this project sets up to actually control the amplitude of the vibration in the cutting area. A typical mathematical model derived from the actual oscillating rig designed by Ewad, (2015) will be used as preliminary investigation into the design of a closed loop control system. Below are the equations of motion of the initial rig to be controlled.

$$(m_{pz} + m_r) \frac{d^2y}{dt^2} + (C_{pz} + C_r) \frac{dy}{dt} + (K_{pz} + K_r) y = F_{pz}(t) + F_t(t) \quad (7.1)$$

$$\frac{d^2y}{dt^2} = \frac{F_{pz}(t) - F_t(t) - (C_{pz} + C_r) \frac{dy}{dt} - (K_{pz} + K_r) y}{(m_{pz} + m_r)} \quad (7.2)$$

Where:

$m_{pz}$  : Equivalent mass of the piezoelectric translator.

$m_r$  : Mass of the moving part in the workspace table.

$C_{pz}$  : Equivalent damping coefficient of the piezoelectric translator.

$C_r$  : Equivalent damping coefficient of the springs.

$K_{pz}$  : Stiffness of the piezoelectric translator.

$K_r$  : Stiffness of the springs for preload.

$F_{pz}$  : Force generated by the piezo electronic translator.

$F_t$  : Tangential cutting force.

In order to apply vibration to machining, an in-depth understanding of milling machine Process technology is required. A sound knowledge of dynamics and control is a pre-requisite for successful design modelling and implementation of two-dimensional oscillation and to control and synchronise the vibration so that prescribed elliptic motion of the work-piece is achieved.

## 7.5 Controller Design

A PID controller was designed and simulated for controlling the amplitude of the oscillation system-and to stabilise the displacement amplitude of the oscillation jig. A proper model for the system was built using a mathematical model. This model was used to find analytical solutions for the problem and to enable the prediction of the system behaviour from a set of parameters and initial conditions.

### Modelling and Simulation

A second order model has been used to design and control the first mode of the vibration system, as the set point of the controller is the recommended value of displacement amplitude equal to 200  $\mu\text{m}$ , because it is an average value of all displacement amplitudes that can be reached by the oscillation system. The controller output can only send signals to the signal generator when this value is changed.

Figure 7.3 shows Simulink code designed in MATLAB software and the open loop control signals. Here, the physical parameters that are displayed in table 7.1 were used for simulation proposes according to Ewad, (2015). A second order filter was used to cut off frequencies over 200 Hz to clear output signals from noise. In addition, this Simulink code was designed using equation 7.2.

**Table 7. 1: The physical parameters of the oscillation system** (Ewad, 2015).

Physical Parameters	Value
$m_{pz}$	0.5 Kg
$m_r$	1.5 Kg
$C_{pz}$	0.94
$C_r$	
$K_{pz}$	5902825 N/m
$K_r$	

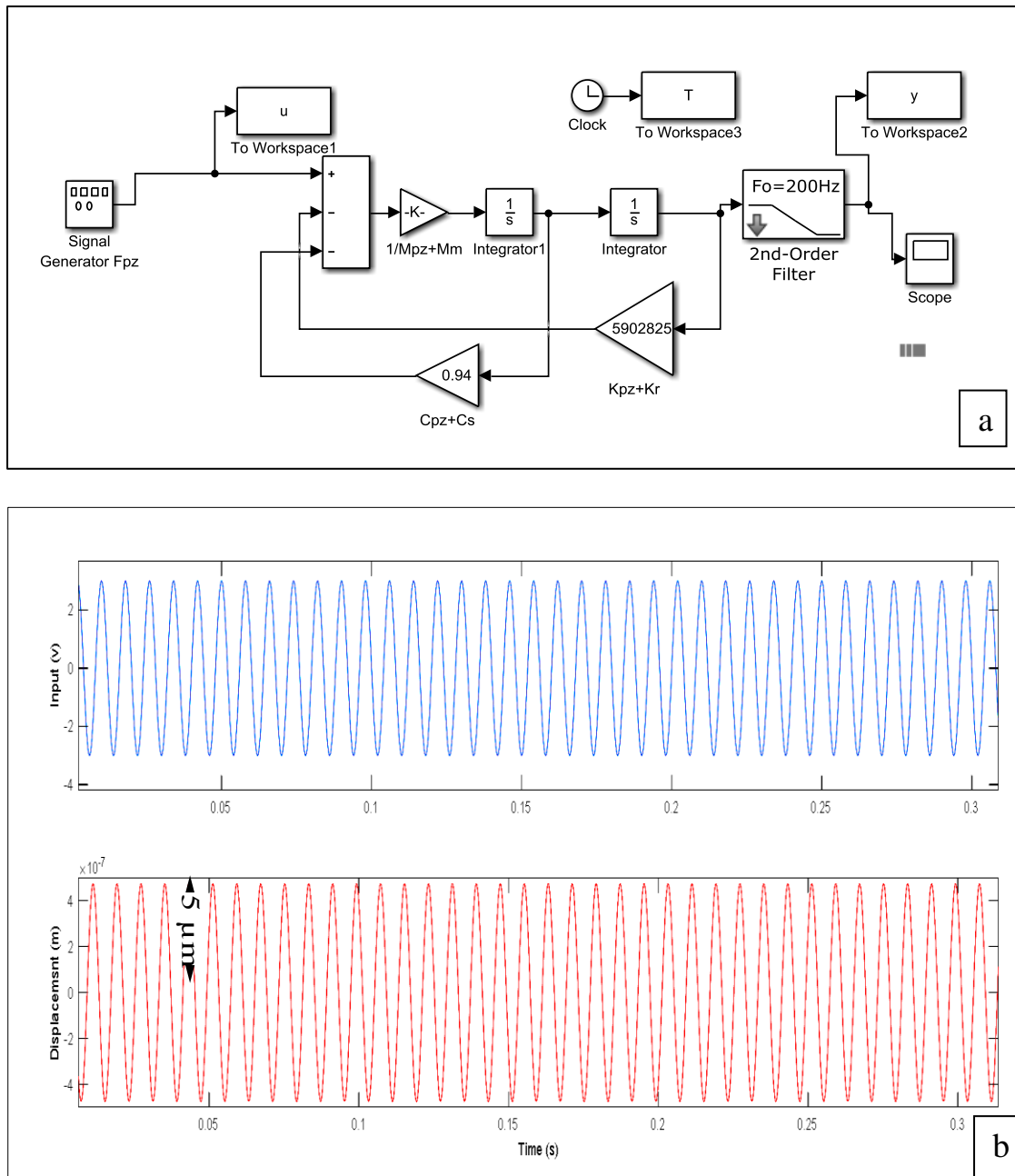


**Figure 7.3: Open Loop control Strategy: a) Simulink Model. b) Input-Output signals.**

The simulation results of the open loop control system observed that:

1. The output signals had rough amplitude especially in the case of disturbances because this system does not have feedback unity signal, so can tracking the errors in the amplitude.
2. The response of the system does not satisfy the required amplitude of 200 μm.
3. The system shows the stability of the oscillation frequency with time.

### 7.5.1 Simulation and Analysis the Model with PID Controller

MATLAB Simulink software was used to simulate the unity feedback system response. Here, the parameters of the PID controller can be tuned.

Figure 7.4 shows Simulink design of the unit step input response for the modelling system. It also displays a good performance of the PID controller. Moreover, the results in table 7.1 display the characteristics of PID step response performance such as rise time, peak time, settling time and maximum overshoot. Here, the PID closed loop control with feedback unit is shown in figure 7.4.a. The components of the PID controller were mentioned in chapter 3, section 3.6.2. The system step response in figure 7.4.b was developed using a self-tuning system, where the response speed has increased and minimised the steady state error to around zero. An example of this tuning method is presented in section 7.12.2.

In Figure 7.5, the output signals were displayed after a successful tuning for the PID controller parameters, also it shows the system response satisfies the requirements, which is displacement amplitude of 200  $\mu\text{m}$ .

Therefore, it can conclude that for controlling the vibration system in the milling process, it is possible to use this newly designed PID Closed Loop controller.

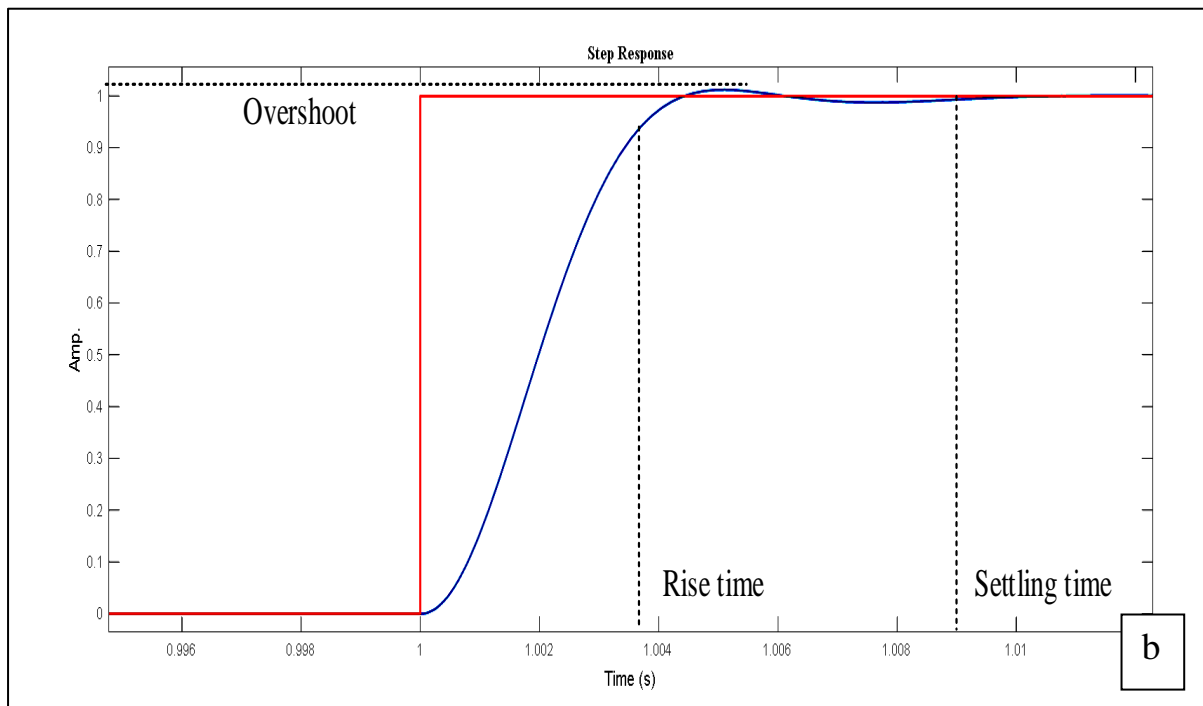
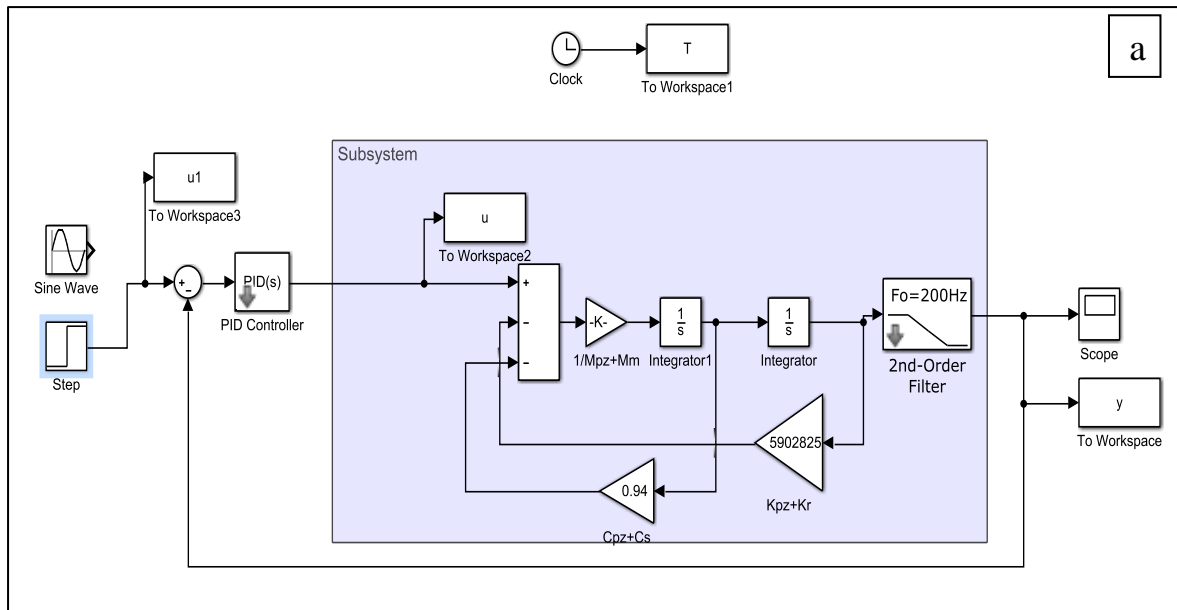
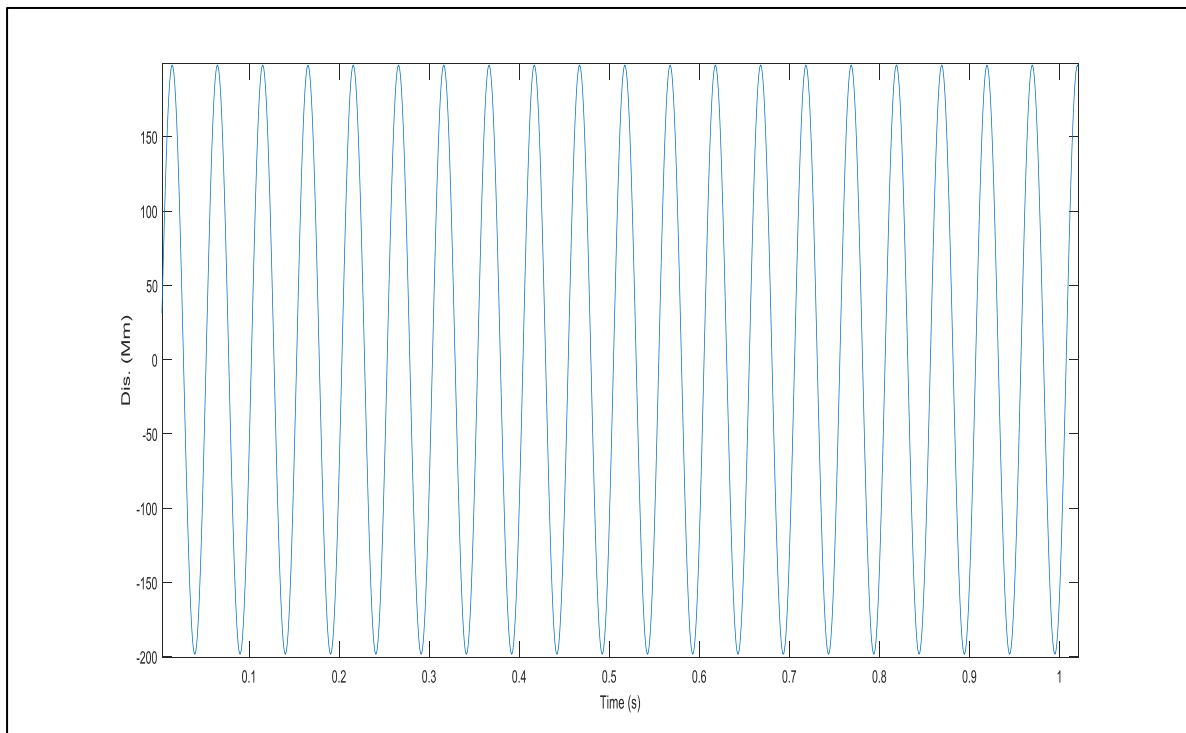


Figure 7. 4: Closed Loop Control Strategy: a) Simulink Model. b) Step Response.

**Table 7. 2: PID Controller’s Parameters and Performance characteristics.**

Controller Parameters	
P	36257.57
I	22682064
D	8.44
Performance of PID controller	
Rise time	0.008 Sec
Settling time	0.0098 Sec
Overshoot	0.027 %
Closed-loop stability	Stable
Peak	1



**Figure 7. 5: Results of applying Closed Loop control Strategy.**

## 7.6 Experimental control system

The National Instrument NI cRIO-9022 was used with Real time and FPGA applications in order to have a faster data acquisition system and controller response. The cRIO-9022 device had analogue input and output signals (I/O) via the NI 9233 unit and USB port, which allowed the PID controller to control the output signals from the signals generator that produced the oscillation during the milling process. This fast real-time response system was used to set up a data acquisition system (DAQ) in order to verify the effective strategies for the vibration control system. The DAQ system has FPGA (The Field Programmable Gate Array) and Real time LabVIEW applications that allowed embedding the PID controller inside the FPGA and Real time LabVIEW Code as shown in figures 7.8 and 7.9.

The main parts of the system set-up contained: the LabVIEW software interface, the PID controller algorithm and the visual front-end panel for running and measuring signals and issuing control signals from the PID controller. The cutting force in X- axis was used as feedback to sense the system response. Some LabVIEW Codes were developed especially for this investigation, as they are the key tool for these experimental works. The main codes are displayed in figures 7.8, 7.9 and 7.10 and other codes are available in Appendix A-1.

The LabVIEW code allows collecting data and signals from several sensors such as cutting forces and acceleration. In addition, The PID control algorithm was designed to make the required adjustment and send feedback signals to the Signal Generator based on a numerical value of the error signal.

Figure 7.6 shows the experimental set-up of the closed loop control system. Also, this figure notes that there is a feedback link in the closed loop system. The reference input (set point) and the process output are subtracted from each other after delivering the process outputs to the first summing junction via the feedback path. Then, the actuating signals are generated from the differences value between the reference input and process output. After that, the controller system drives the actuating signal and sends it to the plant. However, if the system has no difference and the process outputs have matched the reference input (set point) then the controller does not send any actuating signals to the process plant.

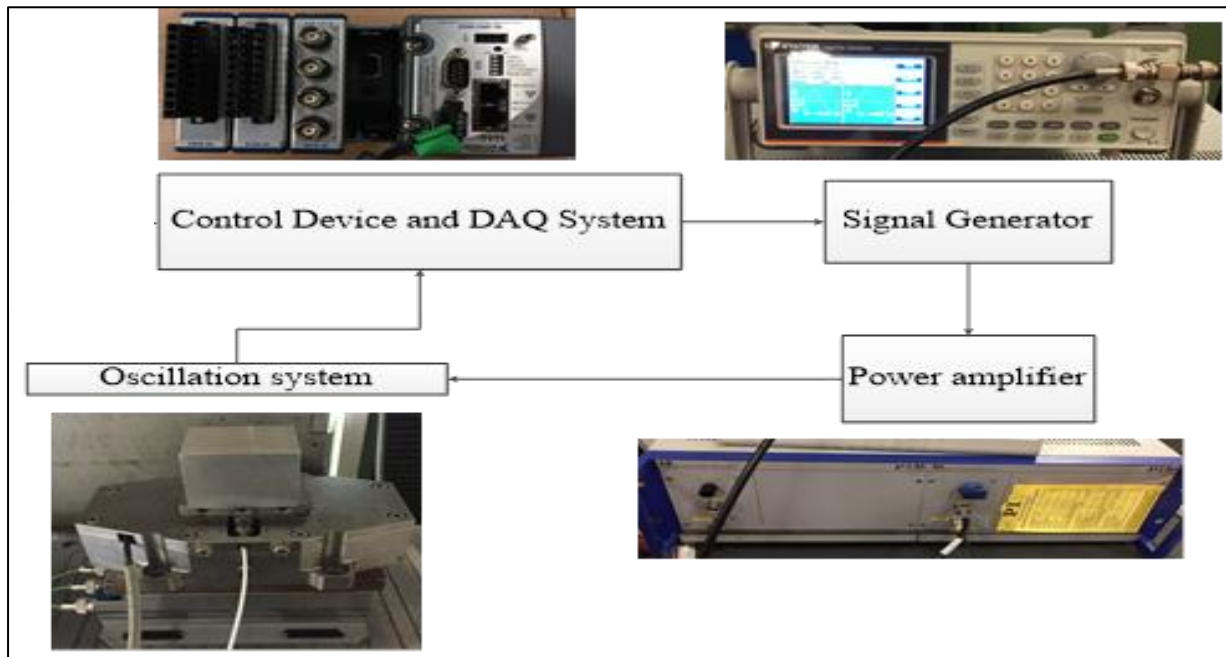


**Figure 7. 6: Experimental Configuration for Close Loop Control System.**

## 7.7 LabVIEW programming for the control system

LabVIEW software is used to interface experimental data and to control the displacement amplitude of oscillation during machining. The developed software can work with a PC and NI compact Rio device supported by real time and FPGA applications to keep DAQ and control the system response as fast as possible, because this project needed a faster controller response.

Figure 7.8 shows the developed code explorer with all LabVIEW codes and it can communicate between them during the milling process. In figure 7.9, the LabVIEW code ran in the CPU of the PC and it was used to display and record all experimental data that comes from the cRio device. Figure 7.10.a displays the code that runs independently in the cRio device for real time LabVIEW application. This code collected all measured experimental data from the FPGA application and then sent them to the code that runs on the PC. Also it can control the output signals that were sent to the oscillation jig via the signal generator as seen in figure 7.10.b.

The PID controller was set up on FPGA LabVIEW code shown in figure 7.11. Here, five output channels were designed in this code to measure all experimental data signals which are the sine wave signal, acceleration and three forces components X-Y-Z. The PID controller tried to minimise the error that was calculated from the difference between the magnitude of the force in X-axis and set point. Then the PID controller sent the correct signals to Real Time code to define the adjustment signal for the signal generator.

Figure 7.7 illustrates the front-end panel of the developed code.

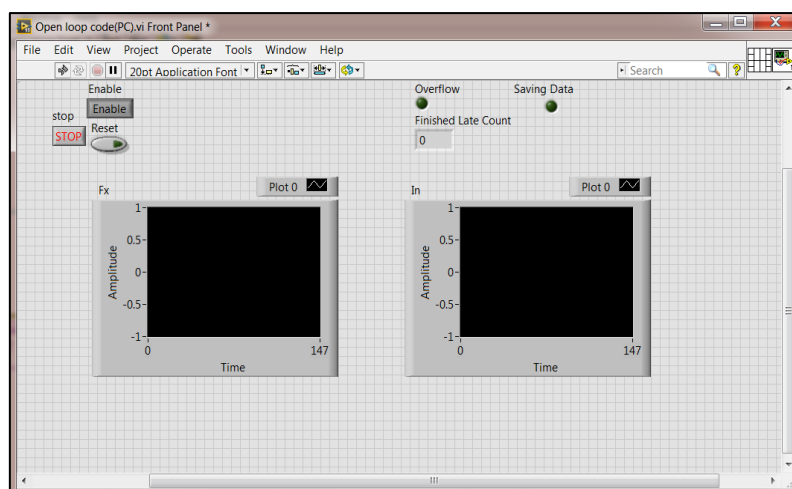


**Figure 7. 7: The front-end panel of the LabVIEW Code.**

Figure 7.8 shows the entire project in LabVIEW where all codes communicate between them during milling process.

The code in figure 7.9 runs continuously in the CPU of the PC and communicates with each function as follows:

- Part 1: The experimental data (signal generator outputs, acceleration and three forces are imported from the cRio device as highlighted with number 1 in figure 7.9.
- Part 2: This overflow function is used here to flag out if the system has lost some data during machining time.
- Part 3: The finish late function used to count how many times the system finished late.
- Part 4: is used to display and record the experimental data into the selected file.

The code in figure 7.10 runs independently and uninterrupted in real time cRio target PC, and it contains the following functions:

- Part 1: Start and finish functions of FPGA that is used for calling the FPGA code.
- Part 2: These three functions illustrated in figure 7.10a are designed to bring the experimental data from the FPGA system to real time LabVIEW code.
- Part 3: Send the experimental data to PC LabVIEW code as shown in figure 7.9.
- Part 4: This code is used to start the connection and apply the initial parameters of the signal generator.
- Part 5: this is a real time loop used to control and adjust the vibration amplitude via the signal generator.

The PID controller was set up in FPGA LabVIEW code shown in figure 7.11, and operates as follows:

- Part 1: Configure and run FPGA channels for import and export data or signals, and closed the FPGA system at the end.
- Part 2: RMS filter used to filter data before sending to the PID controller, more details are available in chapter 10, section 10.2.
- Part 3: PID controller used for controlling the oscillating stage. It works to minimise the error that is calculated from the difference between amplitude signals of force in X-axis and set point. Then the PID controller sent the correct signals to Real Time code (figure 7.10) to send it into the signals generator for adjustment.

## Chapter 7 Closed Loop Controller Development

- Part 4: Here, five output channels were designed in this part of LabVIEW code to record all experimental data that came from external channels Fx, Fy, Fz and acceleration.
- Part 5: is used for connection and sending the experimental data between real-Time code and FPGA LabVIEW code.

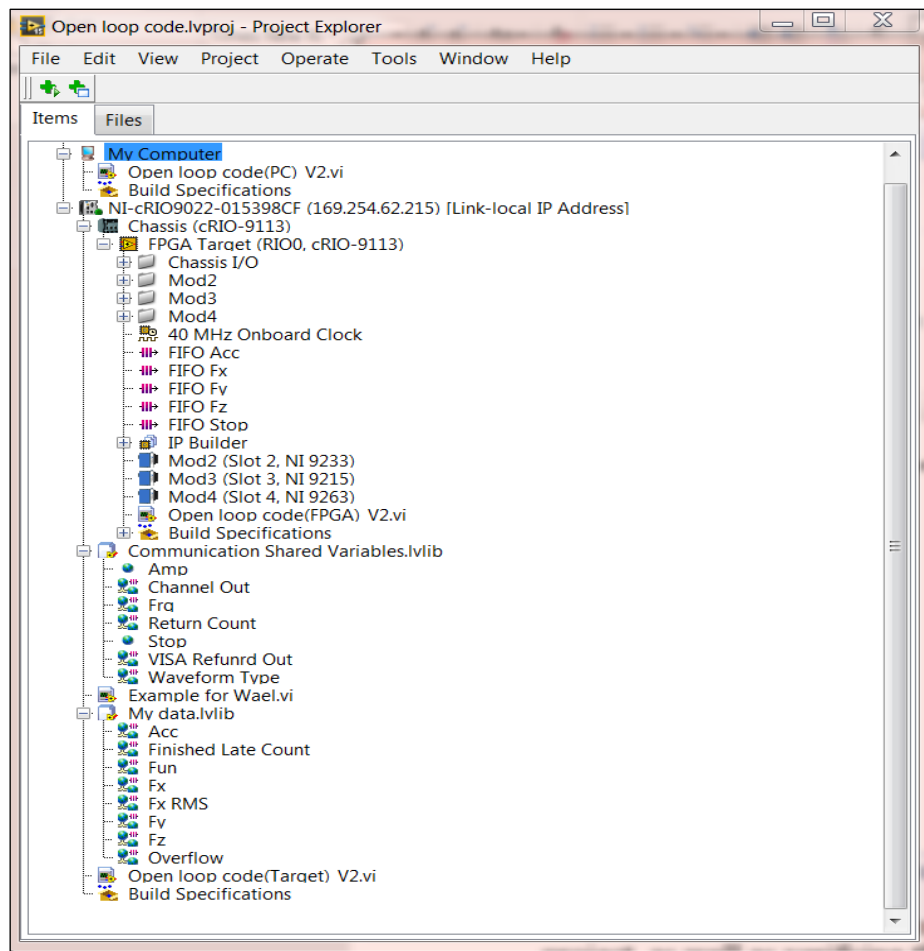


**Figure 7. 8: Project Explorer for LabVIEW codes.**

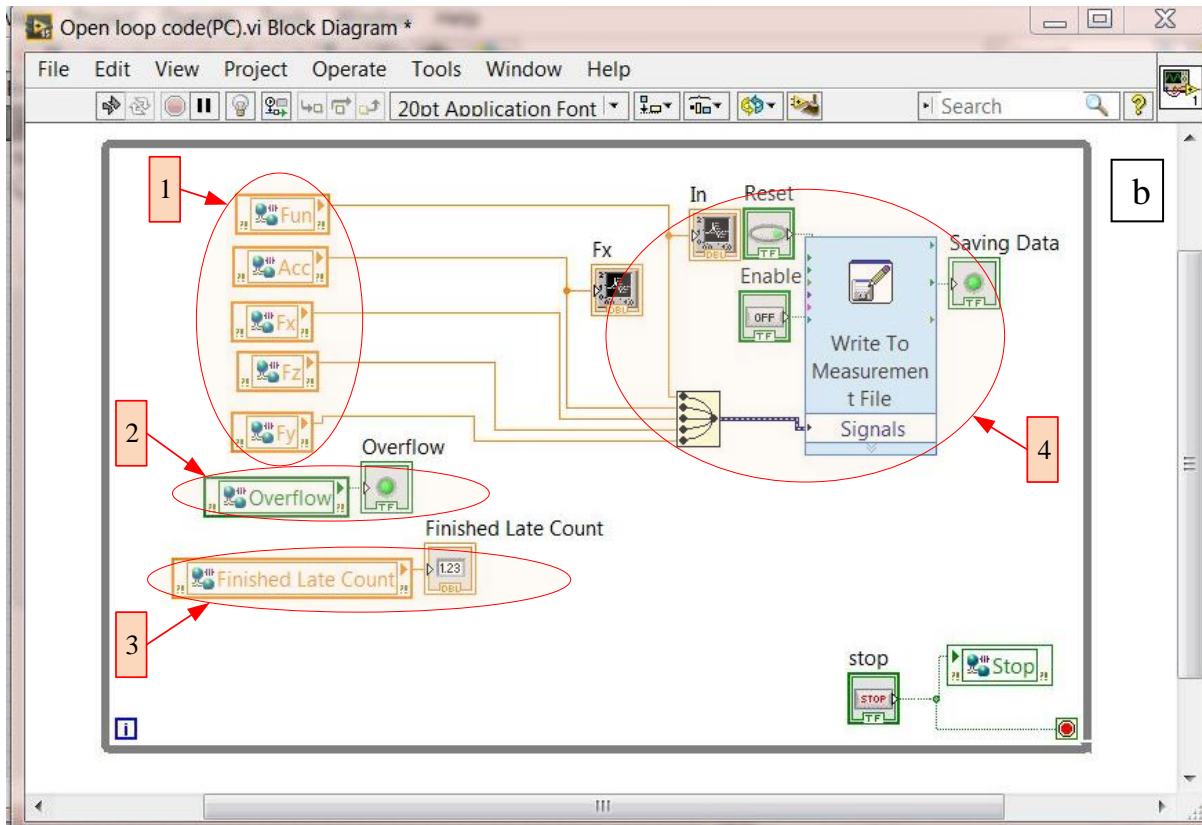
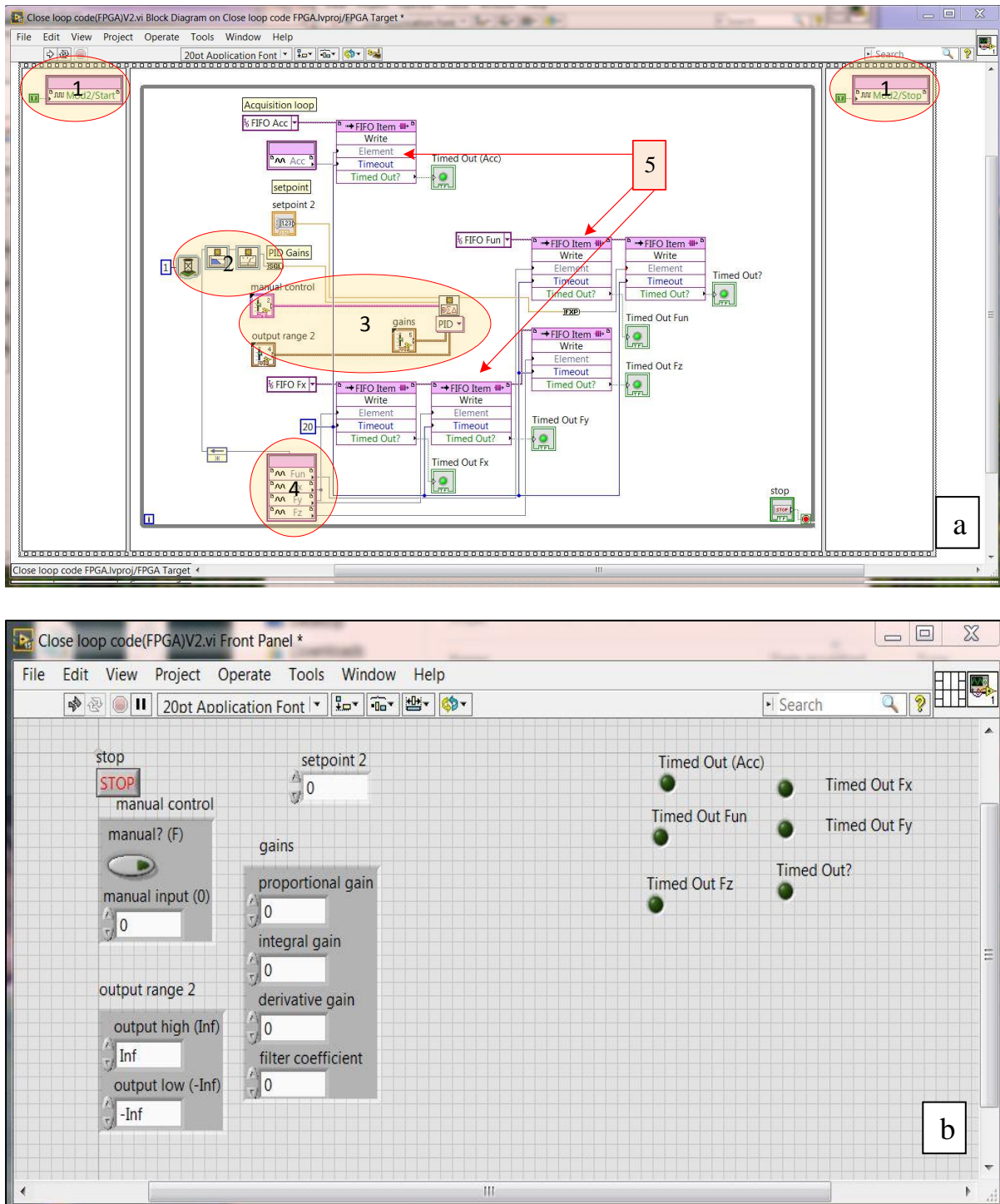


Figure 7. 9: LabVIEW code runs in PC (Block Diagram).



## Chapter 7 Closed Loop Controller Development



**Figure 7.11: code runs in FPGA device: a) FPGA Block diagram. b) FPGA Front Panel.**

## 7.8 Basic Design Consideration

The Design of the LabVIEW codes based on effective PID Controller is one of the key elements for this project, as well as verifying the performance of this PID controller in an actual vibratory milling process.

In the first stage of this work, the configuration of the open loop control system was used for identifying the initial parameters. Here, a number of experiments on vibratory milling were done and experimental data was collected and analysed in order to define set parameters for the PID closed loop controller. The developed PID controller can respond effectively to any persistent offset errors such as changing of set point and machining load disturbance in the actual milling process.

The PID controller may be improved to use in some industrial processes that require a control system or closed loop control system as noted from practical results of these experimental works.

## 7.9 Implementation of the Experiment

The essential part of the experimental design was evaluation of the PID controller's performance. The PID controller was designed and incorporated into a full set-up of the experiment that is displayed in figures 8.3 and 8.4 in Chapter 8 (preliminary studies) for substantiating the design and simulation results. The experiment set-up was based on initial and calibration results. The oscillation system was vibrated at a frequency of 125 Hz and sine wave amplitude was 3 Volts, this led to allowing the oscillation system to oscillate at 200  $\mu\text{m}$  in amplitude.

## 7.10 Model Identification from Experimental Data

System identification is the procedure of deriving a model from data however model estimation is the procedure of fitting a model with a specific model structure.

An actual experimental data test was undertaken as stated previously. The recorded input and output data were used to identify the model of the vibration system. For identification and

validation process, these input and output data were divided into two parts. For example, a set of 2,000 samples of data, was divided and then the first subset will contain the first 1,000 samples and second subset will contain the rest of the samples. The first part of input and output data samples will be used for identifying the plant model of the vibration system. Then, this plant model will be validated using the second part of input and output data. All these analyses and obtained processes were done using Matlab Identification Toolbox.

To identify the plant model from experimental data, the following procedure was used:

1. All input voltage signals, sampling time and output signals which are cutting forces in X- axis direction were loaded in MATLAB software.
2. The vectors of input and output signals were initialized in MATLAB work space.
3. After activation of the system identification toolbox was done, the data array of input and output signals were imported with zero start point and the value of 0.001 sec was set as the sampling rate.

In figure 7.12, the time domain representation of observed data, which are input signals and output cutting forces signals, was plotted with respect to the period of the sampling time.

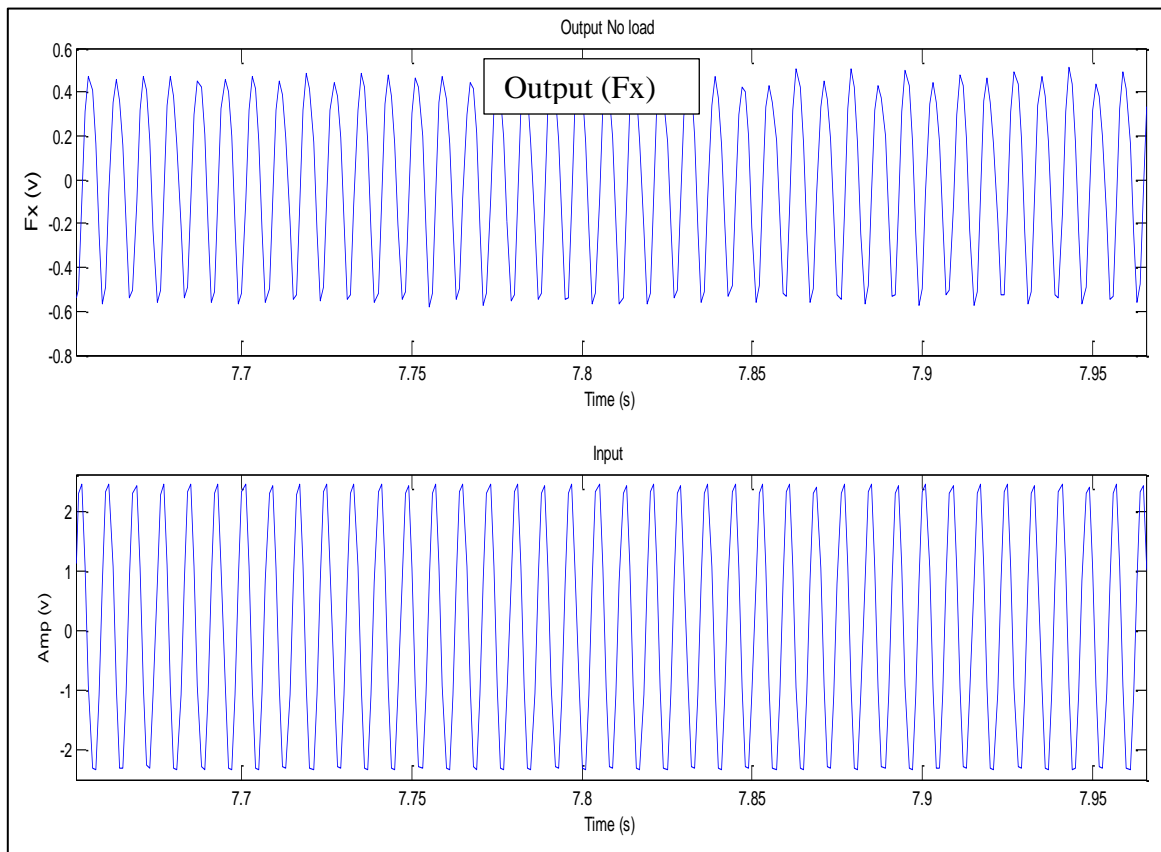


**Figure 7. 12: Time Domain Representation.**

## 7.11 Process Transfer Function

After loading examining experimental data, the model structure selection should be considered. The choice of model structure depends on the noise sequence, how well it is possible to estimate the noise. It is not essential to let the model have more parameters or more polynomials (freedom) for getting a better model estimation. The best model should be done by choosing a suitable structure in combination with several parameters (Andersson 1998).

Transfer function model can be estimated from experimental data using the MATLAB System Identification Toolbox. Here, a specific parametric model can estimate an input output relationship in the form of the transfer function. In addition, the estimate of transfer function can give hints to model complexity and model structure.

Three models of transfer function were estimated in the form of process models with transfer function. The best fit transfer function with validation data was chosen because it has lower loss function and FPE (Final Production Error) values equal to 0.0045 and 0.0047 respectively and best fit percentage when it was validated with validation data. This transfer function is represented below.

$$G(s) = \frac{12.166 e^{-0.011s}}{(0.064s+1)(0.001s+1)} \quad (7.3)$$

With Sampling interval (rate) = 0.001 sec

### 7.11.1 Step Response

To consider the dynamic response of the transfer function, the step input response was done in MATLAB software as illustrated in figure 7.13. Here, it notes that the behaviour of the second order transfer function is overdamped as the step response of the transfer function has an *S* shape with maximum slope at inflection point. This can confirm the system can easily reach the steady state position (Bequette, 2003).

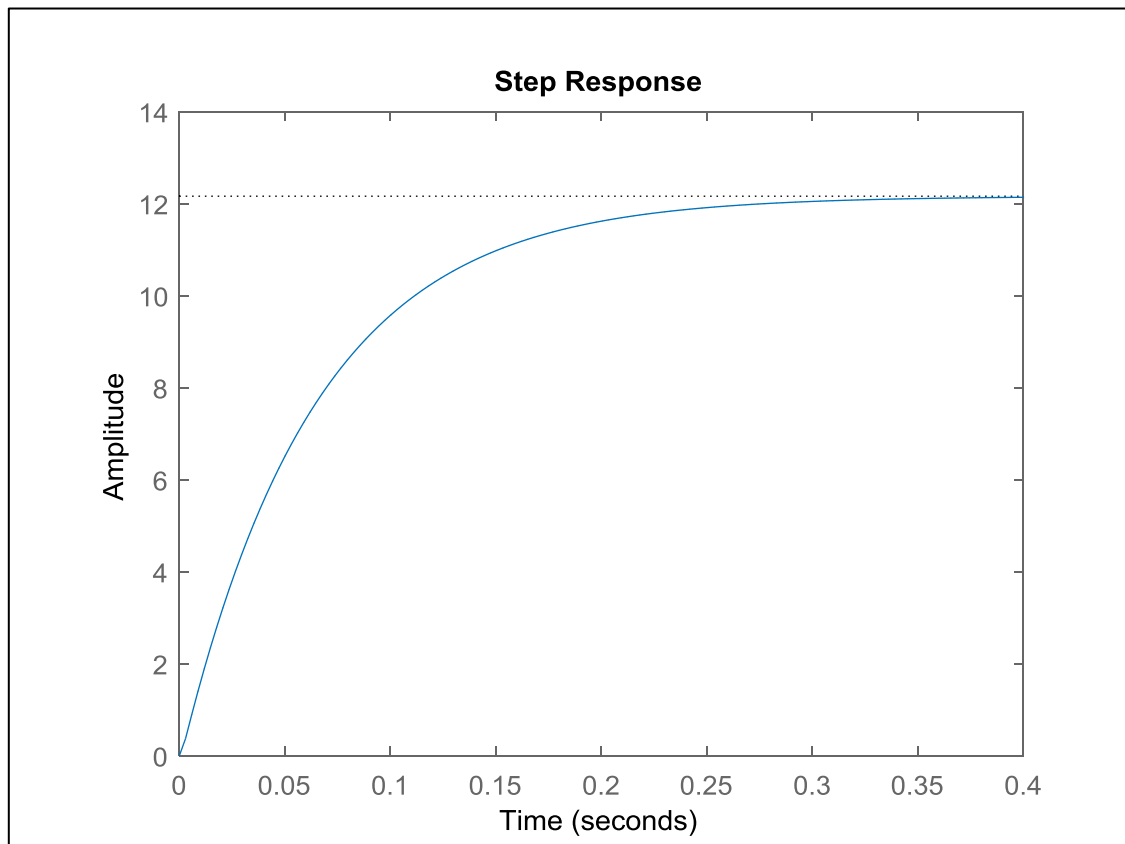


**Figure 7. 13: Process performance in Step-Response effect.**

### 7.11.2 Pole and Zero Plot

An approximate idea of pole-zero locations is obtained from a parametric model (transfer function) estimated in the previous section. Here, a pole-zeros plot is very useful to check for cancellation of poles or zeros. Also, a pole-zeros plot may indicate if the model order is too large. Then there will be poles and zeros located close together, in this case the model order should be reduced (Bequette, 2003).

Figure 7.14 below presents the Pole and Zero plot. In this figure, the poles are shown as “X” and there are no zeros “0” in the pole-zero map. The reason why this happens is that in the equation of process transfer function there is no value of zeros in the numerator, but there are two values of poles in the denominator.

The locations of poles in the pole-zeros map were in a position called a Left-Half-Plane (LHP), indicating a stable process. It also notes that the complex poles will yield an oscillatory response. For this system there is no imaginary component and both poles lay on the real axis. Here, as the poles move further to the left side of the Left-Half-Plane, they yield a faster response (Bequette, 2003).

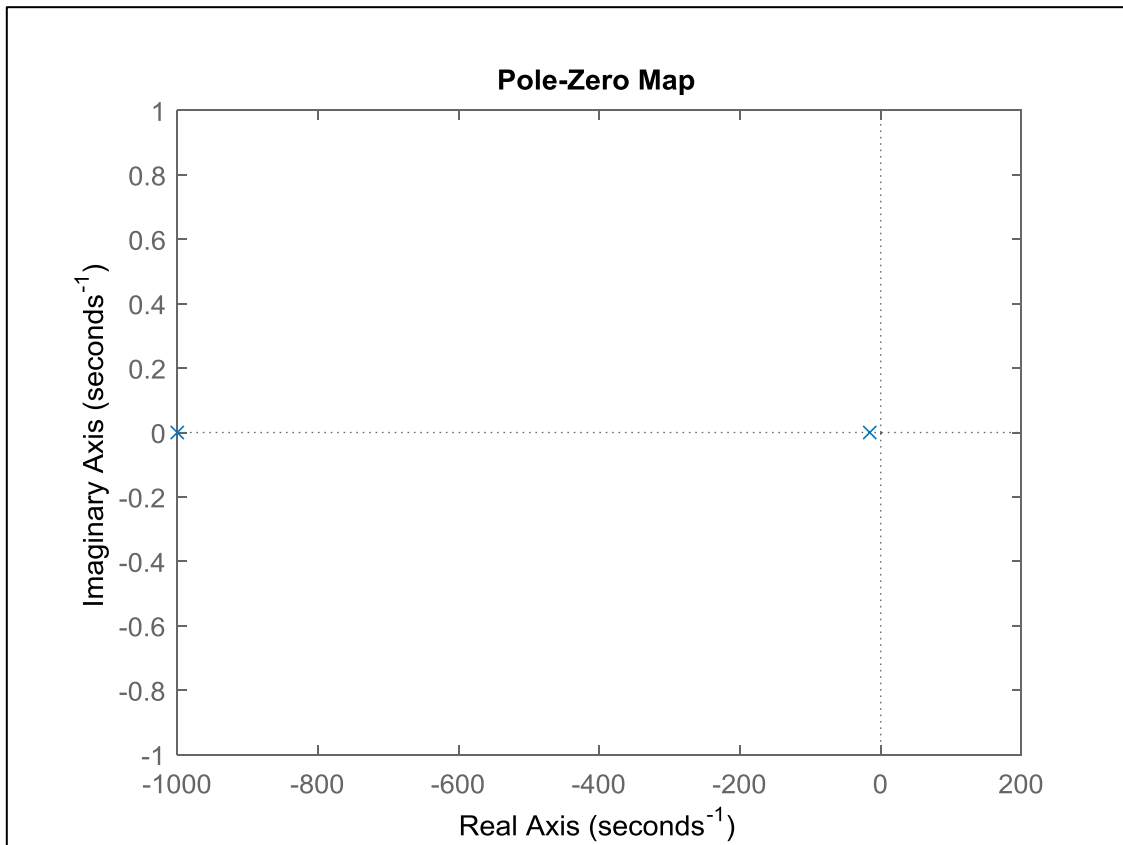


**Figure 7. 14: Pole and Zero representation.**

### 7.11.3 Validation Result

As mentioned in the previous section, the experimental data was divided into two parts; the first part was used for the identification process. However, here the second part was used to validate the correctness of the identified model (obtained transfer function).

In figure 7.15, the identified model was validated and for a given set of input data, the tool box calculates the outputs via the obtained transfer function (equation 7.3). In addition, the figure shows the comparisons between measured output data from the real system (in black) and simulated model outputs (in red). It also notes that the simulated model outputs, computed from obtained transfer function, can fit up to 83 % of the output data that was

measured from the real experiment. Here, the identified model was successfully validated for system identification procedures, then this identified model can be used for the control design process in the next section.

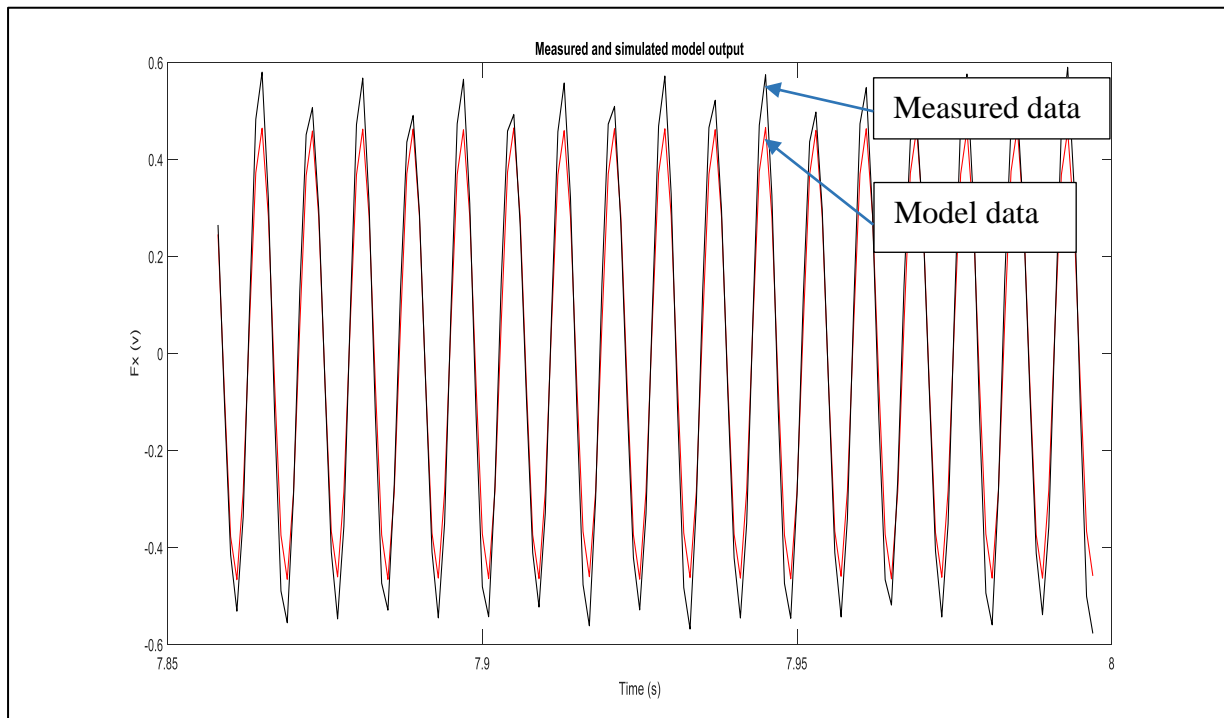


**Figure 7.15: Measured and Simulated model output representation.**

## 7.12 PID Controller Design

The aim of designing the PID controller in the vibration system is to reduce the error and eliminate the need for continuous operation of the system. In reality, the value of measurement desired is a set point and the error can be defined via calculating the difference between the output measurement and the set point.

$$\mathbf{Error = measurement - set\ point} \quad (7.4)$$

The PID controller has the following transfer function:

$$\mathbf{PID = K_p + \frac{K_i}{s} + sK_d} \quad (7.5)$$

The objective of the PID control design is to define the parameter of the controller ( $K_p, K_i$  &  $K_d$ ) to meet a given set point of the closed loop system performance requirements.

There are several methods to identify the PID controller's parameters, however in this project two methods were used; Classical Tuning method and Auto tuning method via MATLAB software. These are done to check that the observed parameters of the PID controller are in the acceptable range.

### 7.12.1 Classical Tuning Method

Initial parameters of the PID controller were defined using the classical tuning method called Cohen-Coon method and table 7.3 shows this approach which was adapted from Bequette, (2003). This allowed obtaining the actual parameters of the PID controller from the transfer function shown in equation 7.3.

**Table 7. 3, Cohen-Coon tuning parameters.**

Control Action	Kc	Ti	Td
P	$\frac{1}{K_p} \frac{T_p}{t_d} (1 + \frac{t_d}{3T_p})$		
P+I	$\frac{1}{K_p} \frac{T_p}{t_d} (0.9 + \frac{t_d}{12T_p})$	$t_d \frac{(30 + 3t_d/T_p)}{(9 + 20t_d/T_p)}$	
P+I+D	$\frac{1}{K_p} \frac{T_p}{t_d} (\frac{4}{3} + \frac{t_d}{4T_p})$	$t_d \frac{(32 + 6t_d/T_p)}{(13 + 8t_d/T_p)}$	$t_d \frac{4}{(11 + 2t_d/T_p)}$

From equation 7.3, it can be defined as:

$$G(s) = \frac{K e^{-T_d s}}{(1 + T_{p1} s)(1 + T_{p2} s)} = \frac{12.166 e^{-0.011s}}{(0.064s + 1)(0.001s + 1)} \quad (7.6)$$

Then:

$$K_p = 12.166$$

$$T_{p1} = 0.064$$

$$T_p = 0.001$$

$$T_d = 0.011465$$

$$K_c \text{ (Proportional gain)} = \frac{1}{K_p} \frac{T_p}{t_d} \left( \frac{4}{3} + \frac{t_d}{4T_p} \right) = \frac{1}{12.166} \frac{0.064}{0.0114} \left( \frac{4}{3} + \frac{0.0114}{4(0.064)} \right) = 0.62$$

$$T_i \text{ (Integral time)} = t_d \frac{(32 + 6t_d / T_p)}{(13 + 8t_d / T_p)} = 0.0115 \frac{32 + \frac{6(0.0115)}{0.064}}{(13 + \frac{8(0.0115)}{0.064})} = 0.0263$$

$$T_d \text{ (Derivative time)} = t_d \frac{4}{(11 + 2t_d / T_p)} = 0.0115 \frac{4}{11 + \frac{2(0.0115)}{0.064}} = 0.004$$

The parameters of the PID controller are obtained as:

$$K_p = K_c = 0.62$$

$$K_i = K_c / T_i = 23.57$$

$$K_d = K_c * T_d = 0.002$$

### 7.12.2 Auto Tuning Method

In this tuning method, the PID controller auto tuning toolbox in MATLAB has been used to identify the PID controller parameters that can let the PID controller successfully control the system at the desired level. The following procedures were used:

1. Using the system transfer function equation (7.3), a subsystem was designed in MATALB Simulink software to simulate the machining process as seen in figure 7.16.a.
2. For process control, the PID controller was set up into the designed subsystem with feedback closed loop signals, as shown in figure 7.16.b.
3. After the PID controller was fixed into the simulation system, the auto tuning toolbox for tuning the PID controller's parameters was run and the obtained parameters are as follows:

$$K_p = 0.31$$

$$K_i = 4.62$$

$$K_d = 0.00098$$

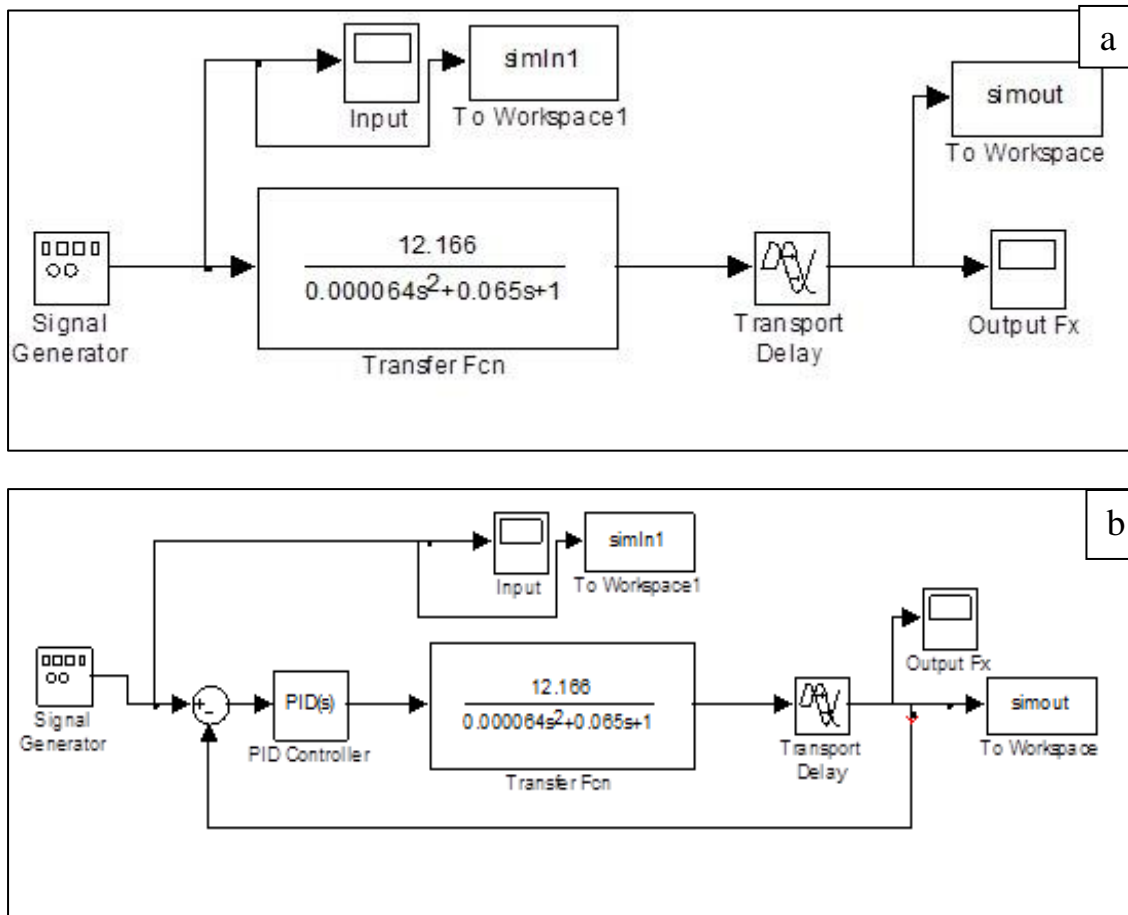


Figure 7. 16: Blocks design in Simulink: a) Process Subsystem. b) PID Closed Loop control.

Table 7. 4: The parameters of PID controller.

PID parameters	Classical Tuning Method	Auto Tuning Method
$K_p$	0.62	0.31
$K_i$	23.57	4.62
$K_d$	0.002	0.00098

Here, the parameters of the PID controller were obtained and it is observed that there is no big difference in the values of these parameters between the classical method and the auto tuning method. This led to a successful tuning process for the PID controller. However, for the actual machining process, there is some freedom or flexibility in the range between these

## Chapter 7 Closed Loop Controller Development

two methods to select the parameters of the PID controller depending on its stability performance. This flexibility range could be up to  $\pm 10\%$  of the obtained PID controller parameters.

# **Chapter 8**

## **Preliminary Studies**

## 8.1 Introduction

In this chapter, the preliminary experimental tests are presented. The purpose of these preliminary tests was to help acquire a first clear view of this process performance and identify any problem that affects the normal functioning of the system.

An open loop system of vibration was used in these experimental works. The LabVIEW software package was used along with a Data Acquisition system (DAQ) to realise a real-time position control of the piezo actuators. An accelerometer and three forces measurement device were used for measuring all signals during the milling process.

The full control system included a signal generator, a power amplifier for the piezo actuator, a charge amplifier, the data acquisition and NI Compact Rio data system. An aluminium work-piece was used for these experiments.

## 8.2 Experimental configuration

The system in figure 8.1 shows the open loop framework. First, a signal generator was used to generate sine wave signals that are fed to the power amplifier for a set up to 100 times, done to drive the piezo actuator to push-pull the displacement bridge which is inside the self-contained oscillating jig.



**Figure 8. 1: Experimental Configuration for Vibration system.**

Figure 8.2 shows the novel vibration system called the self-contained oscillating jig which was mounted on a three axis Kistler Dynamometer to measure three forces signals. An accelerometer was fit next to the work-piece's holder to measure the acceleration signals.

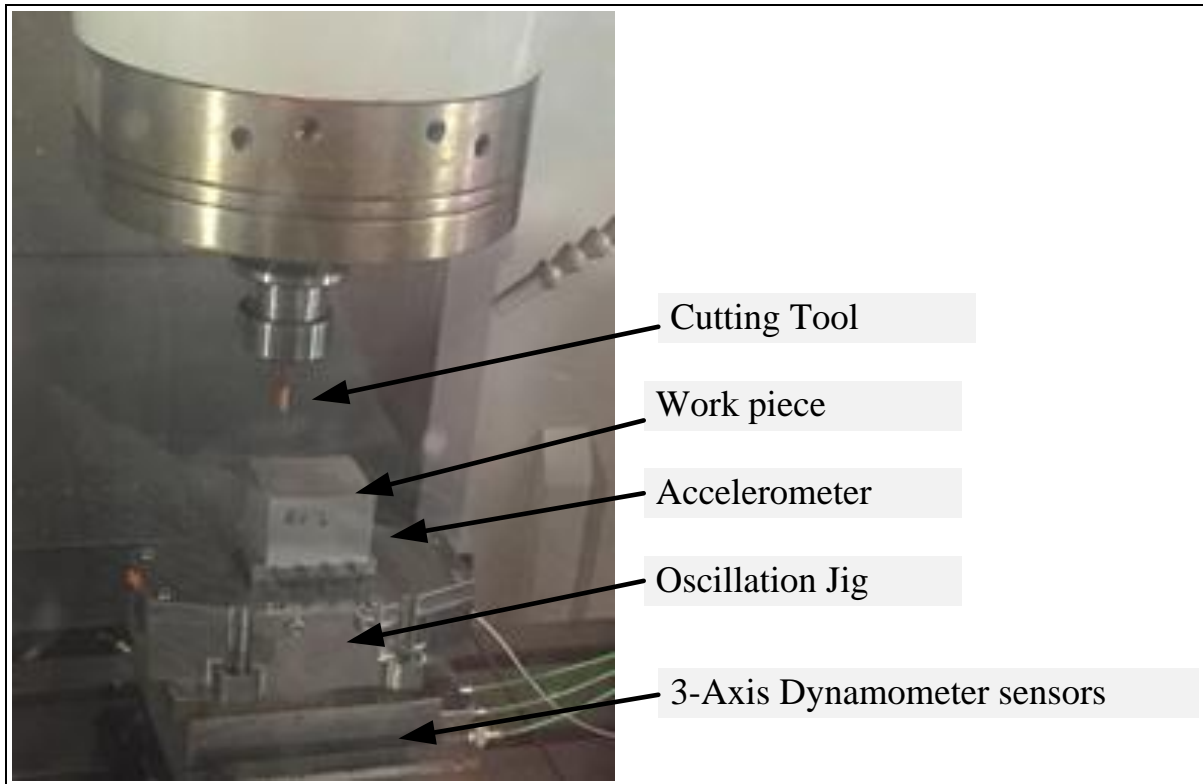


Figure 8. 2: Experimental setup on 5-Axis Milling Machine.

The flow chart of signal processing in these experimental tests is shown in figure 8.3. The accelerometer and dynamometer are recording the signals using cRio device and Labview software. Also, all data were stored on a Laptop for further analysis.

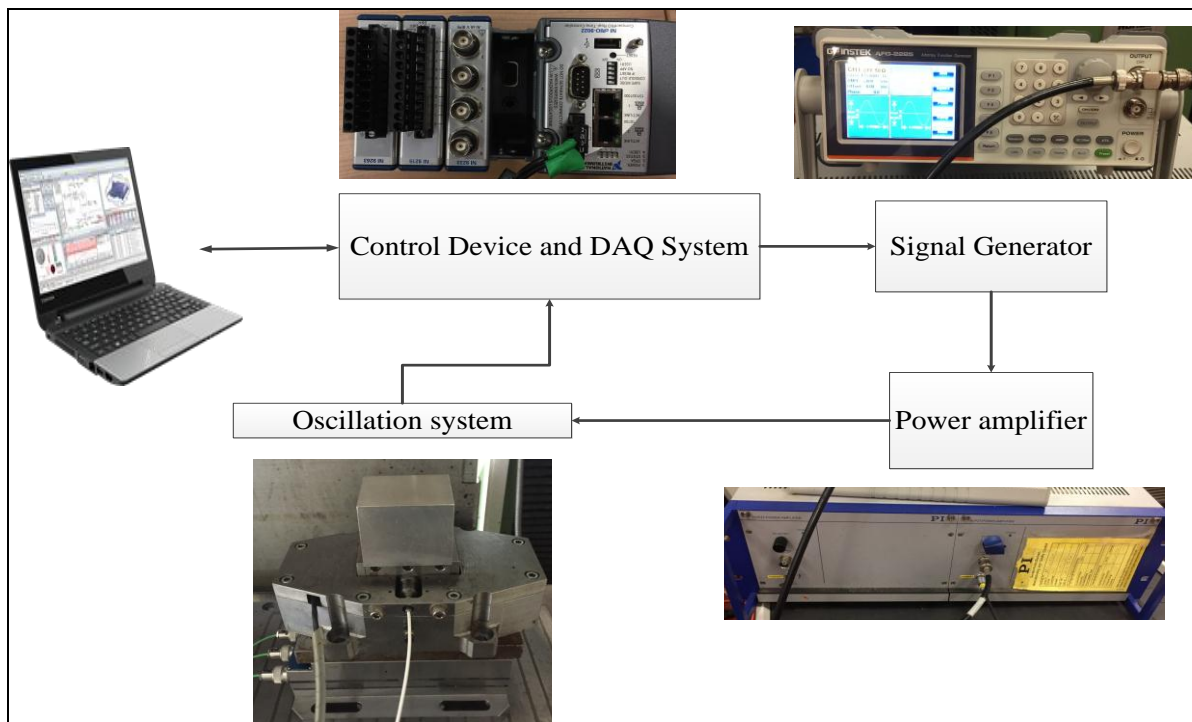
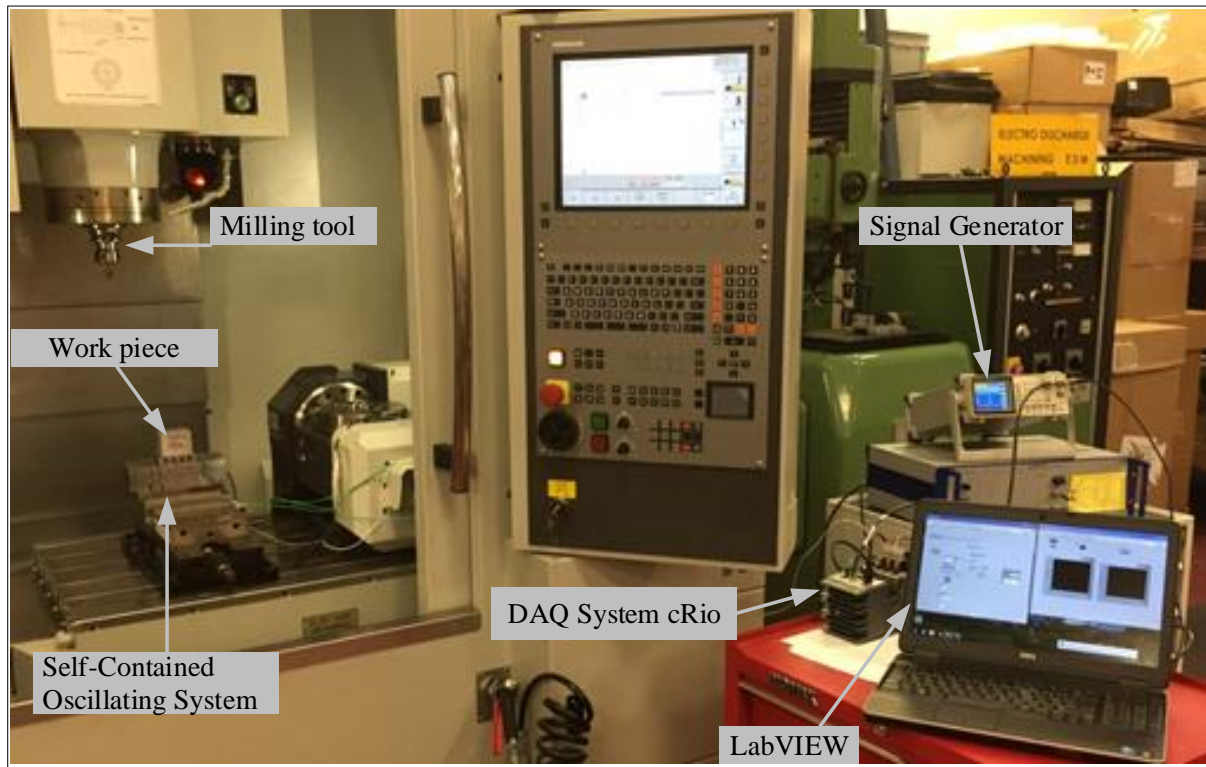


Figure 8. 3: Experiment Configuration for Control and DAQ system.

### 8.3 Experiment Setup

Figure 8.4 shows the facilities of experimental study, which includes Power Supply, Signal Generator, power amplifier, 5- axis milling Machine, Compact cRio Controller, Data Acquisition system (Labview), Self-contained oscillating system and Work-piece.



**Figure 8. 4: Actual setup For Vibratory Milling Experiment.**

The vibration of the work-piece is produced by the Self-Contained Oscillating system.

For high performance in the Data Acquisition system in recording and analysing all experiment data, the Real time LabVIEW-FPGA applications were used in this experimental work through a Compact cRio device that managed the entire data logging and real-time processing and closed-loop control.

In the actual experiment, the system was run as follows:

1. The signal generator sends the sine wave signals to the power amplifier then to the vibration system to start oscillating the work-piece.
2. The DAQ system starts collecting data from sensors (Accelerometer and Dynamometer).

3. The NI Compact cRio and LabVIEW Code were processing and recording experimental data.
4. The machine tool then starts cutting the work-piece with selected machining condition by running the CNC machine G-code as mentioned in chapter 4.

After the machining process, the work-piece surface roughness of each machining condition is measured by using a Surtronic Duo illustrated in appendix A-1. The work-piece finish surface was further examined visually using a microscope at different magnifications. Also, this microscope was used for the cutting tool wear validation by observing the wear mark on the tool cutting edge.

The configuration of the microscope is shown in figure 8.5.

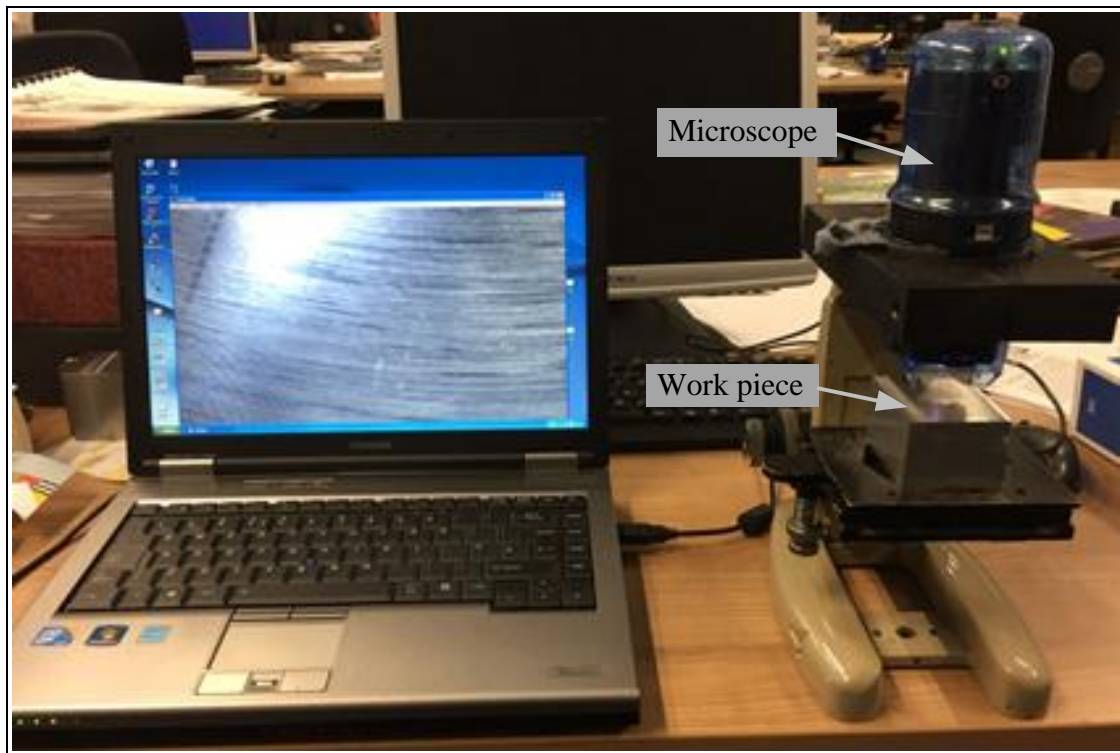


**Figure 8. 5: Microscope Device Configuration setup.**

## 8.4 Machining trials

This set of experimental work was conducted on a 5-axis milling machine in dry condition to investigate vibration amplitude, feed rate and spindle speed, tool wear, and surface roughness of the machined work-piece.

To avoid the resonant frequency of the machine spindle which is around 100 Hz, the oscillating stage was driven at 125 Hz and 3 volts with an amplitude about 200  $\mu\text{m}$  as determined in displacement calibration result in chapter 5, table 5.2.

In these preliminary experiments an open-loop control system is used. For the accuracy and readability of results, the surface roughness of samples was measured 3 times and the results were averaged.

### 8.4.1 Machining Process Parameters

The Linear Velocity of the tools was defined as:

$$v = r \times RPM \times 2 \pi \quad (8.1)$$

Where:

**v**: Linear velocity, in m/min

**r**: Milling tool radius, in metre

The tool feed rate was defined as:

$$V_f (m/min) = F_z * N * Z \quad (8.2)$$

Where  $F_z$  is feed per tooth,  $N$  is spindle speed in RPM and  $Z$  is the number of teeth on the tool

Therefore, for machining Aluminium the following spindle speed was selected from Machining handbook (PI: Total tooling; Quality and Service).

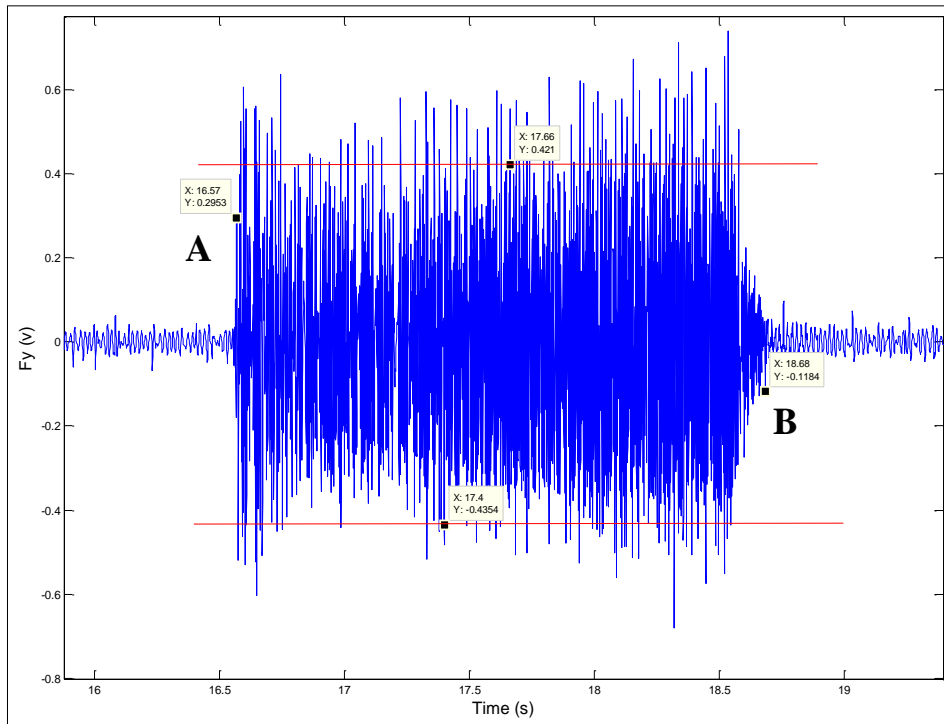
$N = 4500 - 6000$  RPM, which gives a cutting speed of 140-200 m/min for a tool diameter of 10 mm.

Table 8.1 shows the overall milling parameters for these preliminary tests where the examination of feed rate, spindle speed and depths of cut were obtained.

**Table 8. 1: Experimental machining parameters.**

<b>Milling parameters</b>	<b>Value</b>
Milling cutter type	Solid Carbide end mill (Coated: Ti 400)
Number of Teeth, $Z$	3
Diameter	10 mm
Helix angle	45°
Rake angle	15°
Spindle Speed, $N$	4500 – 6000 RPM
Feed per tooth, $F_z$	0.05-0.1 mm/tooth
Feed Rate	675 – 1800 mm/min
Cut type	Up Milling
Milling Condition	Dry
Workpiece	Aluminium
Depth of cut	0.5 & 1.0 mm
Vibration Frequency	125 Hz
Sine wave Amplitude	3 Volts (positive peak) or 6 Volts Peak to peak.
Vibration amplitude	About 200 $\mu\text{m}$ (positive peak) Or 400 $\mu\text{m}$ peak to peak.

Figure 8.6 shows cutting force signals recorded during machining. Here some data can be inferred such as forces and machining time. Also, it notes the start and finish time of contact zone between the tool and the work-piece (A and B). From these two values of time, the actual machining time can be determined. In this case the actual machining time is approximately 2 sec.



**Figure 8. 6: Typical actual cutting force signal in Y-direction.**

## 8.5 Results

This preliminary experimental work was divided in two sets. In the first set, work-pieces were machined in conventional mode (without Vibration), and in the second set work-pieces were machined in vibration assisted mode. For both machining modes the depth of cut was 0.5 and 1.0 mm. For each depth of cut, two sets for spindle speed (4500-6000 RPM) and feed rate, 0.05-0.1 mm/tooth were used. Machining programme codes were developed to run the 5 Axis CNC-Milling, some of these codes are given in appendix A-4.

### 8.5.1 Comparative Process Performance

Several tests were carried out to quantify the effect of machine parameters on process performance and the ability of the developed real-time closed loop controller operation. These parameters are presented in table 8.2

**Table 8. 2: Experimental Machining parameters.**

	Spindle Speed (RPM)	Feed Rate (mm/min)	Depth of Cut (mm)
Test 1	4500	675	1
Test 2	4500	1350	1
Test 3	4500	1350	0.5
Test 4	4500	675	0.5
Test 5	6000	900	1
Test 6	6000	1800	1
Test 7	6000	1800	0.5
Test 8	6000	900	0.5

### Cutting Forces

To illustrate the three main force components involved in milling their sketch is shown in figure 8.7 with a resultant cutting force  $F_c$  between two forces  $F_x$  and  $F_y$ . This resultant cutting force was calculated using the following formula or equation;

$$F_c = \sqrt{F_x^2 + F_y^2} \quad (8.1)$$

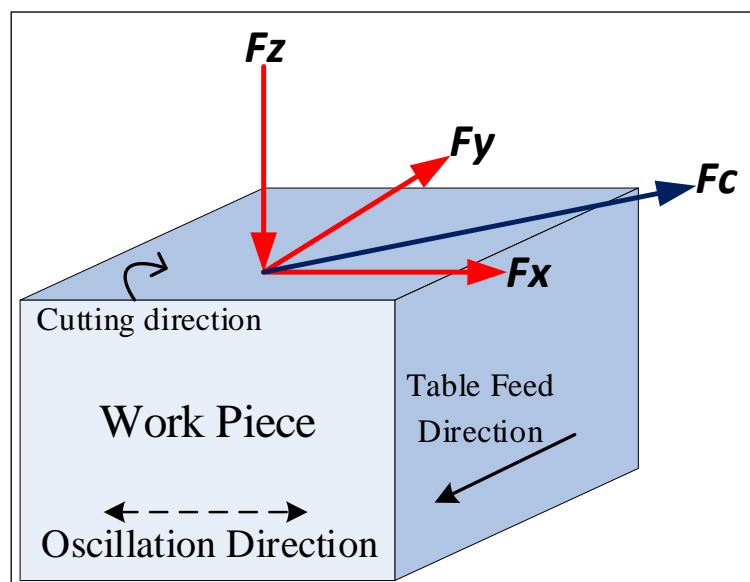


**Figure 8. 7: Cutting Forces Compounds.**

After repeating the experiment twice, the results were averaged over the milling process. In addition, figures 8.8 to 8.11 below depict the difference between forces in conventional mode and vibratory milling.

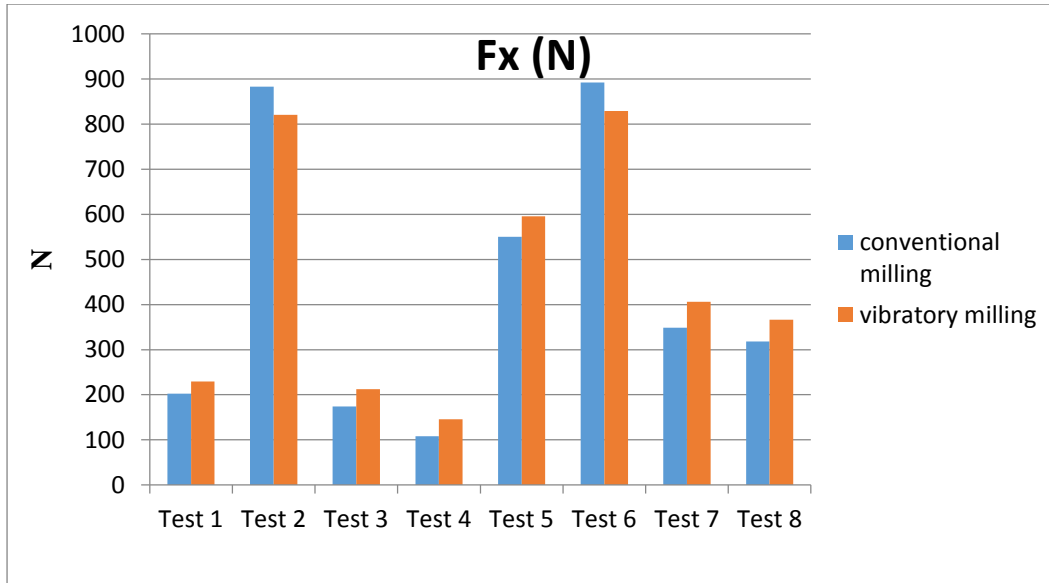


Figure 8. 8: Cutting Forces in X Axis Direction.

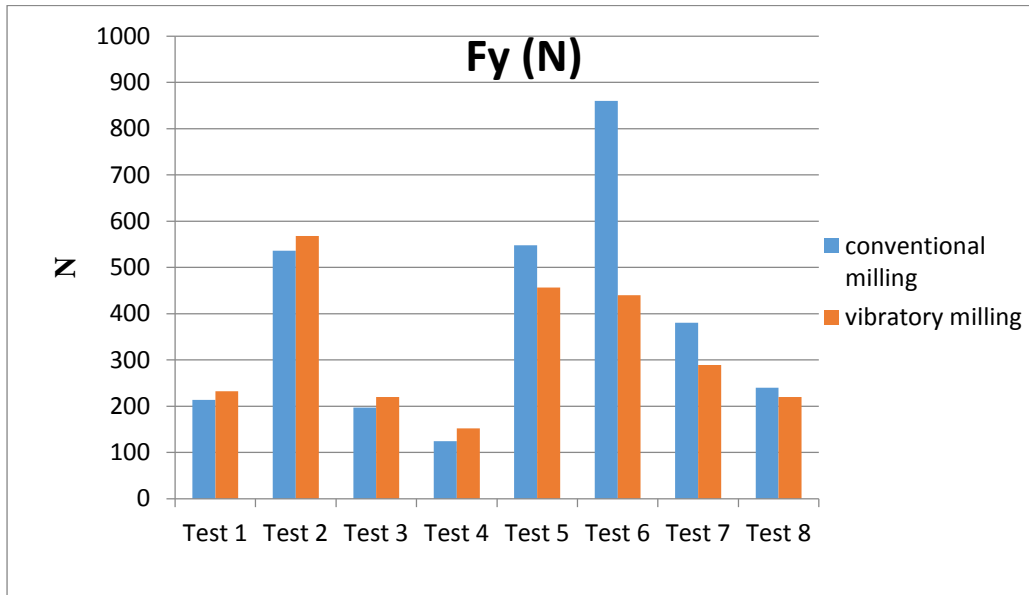
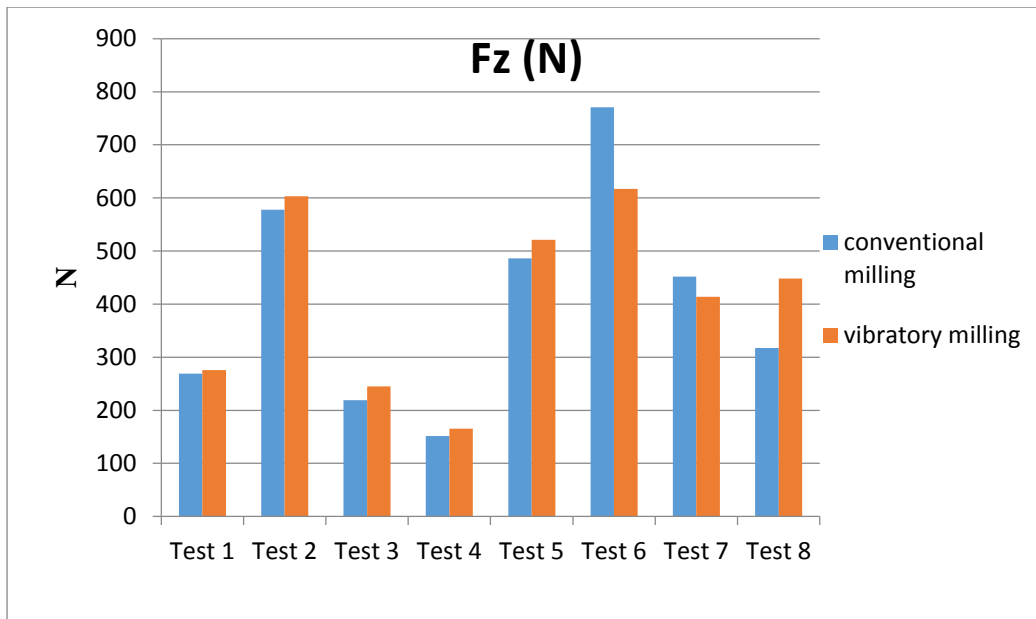
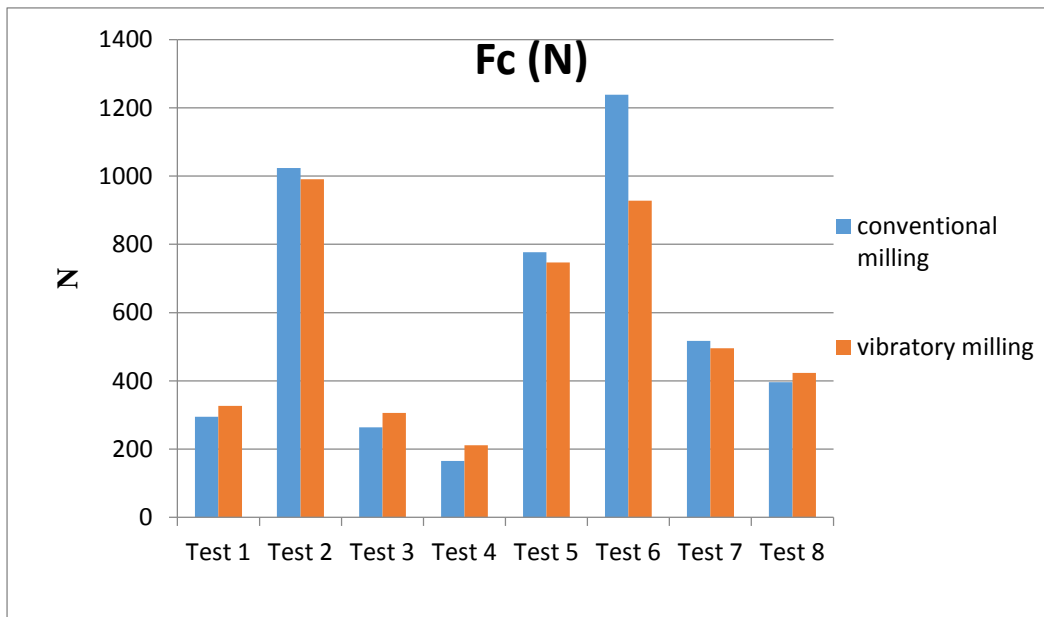


Figure 8. 9: Cutting Forces in Y Axis Direction.



**Figure 8.10: Cutting Forces in Z Axis Direction.**

The resultant forces between two directions X and Y are illustrated in following figure.



**Figure 8.11: Resultant Cutting Forces of X and Y Axis Directions.**

Referring to the results shown in figures 8.8, 8.9, 8.10 and 8.11, a difference in cutting forces was observed in milling or machining forces between two modes, conventional and vibratory milling. In some cases the cutting force in vibratory milling is higher than conventional milling.

Due to the high plasticity and softness of the aluminium material, the energy of the applied vibration was consumed by the damping in the work-piece material. Therefore, only in tests 5 to 8, the application of vibration reduced the cutting force up to 40 % as illustrated in Test 6 with machining parameters of 1,800 mm/min for feed rate, 6,000 RPM spindle speed and 1 mm depth of cut.

It was observed that with increasing depth of cut all forces in all directions were increased. However, as seen in Test 2 and 6, the resultant cutting forces can be reduced when high spindle speed is used.

### **Surface Roughness**

The Surface Roughness of all machines work-pieces was measured using a surface roughness measurement machine. Each sample's surface was measured at three different points and the results were averaged.

**R<sub>a</sub>** definition is the Arithmetical mean roughness (JIS B 0601(1994)) over a section of standard length that is sampled from the mean line on the roughness chart.

**R<sub>z</sub>** is Ten-point mean roughness over a section of standard length that is sampled from the mean line on the roughness chart. The distance between the peaks and valleys of the sampled line is measured in the y direction. Then, the average peak is obtained among the 5 tallest peaks (Y<sub>p</sub>), as is the average valley between the 5 lowest valleys (Y<sub>v</sub>). The sum of these two values is expressed in micrometres (µm) as illustrated in Figure 8.13.

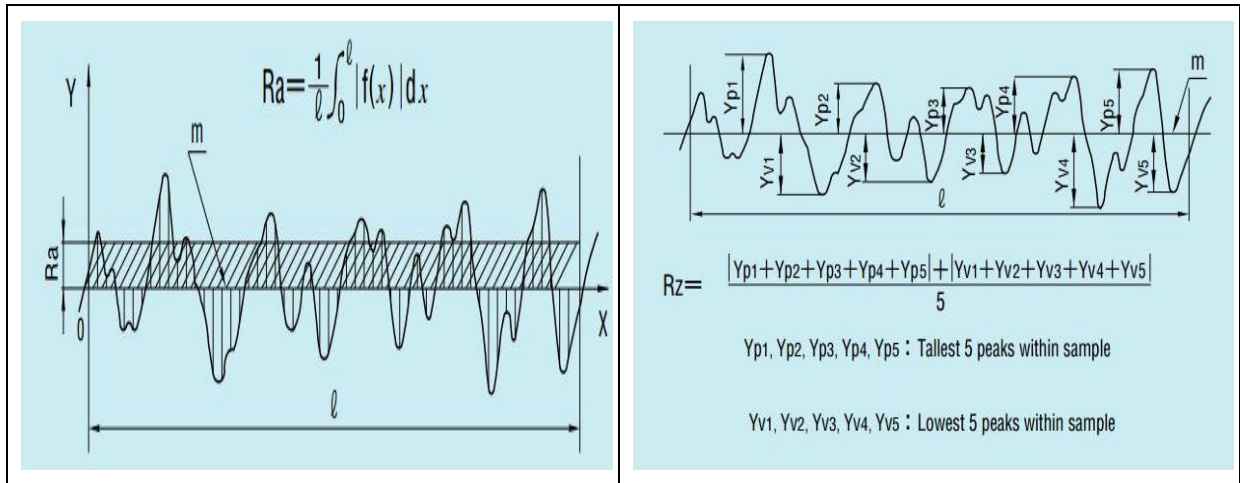


Figure 8. 12: the formula of Surface Roughness factors  $R_a$  and  $R_z$  (JIS B 0601, 1994).

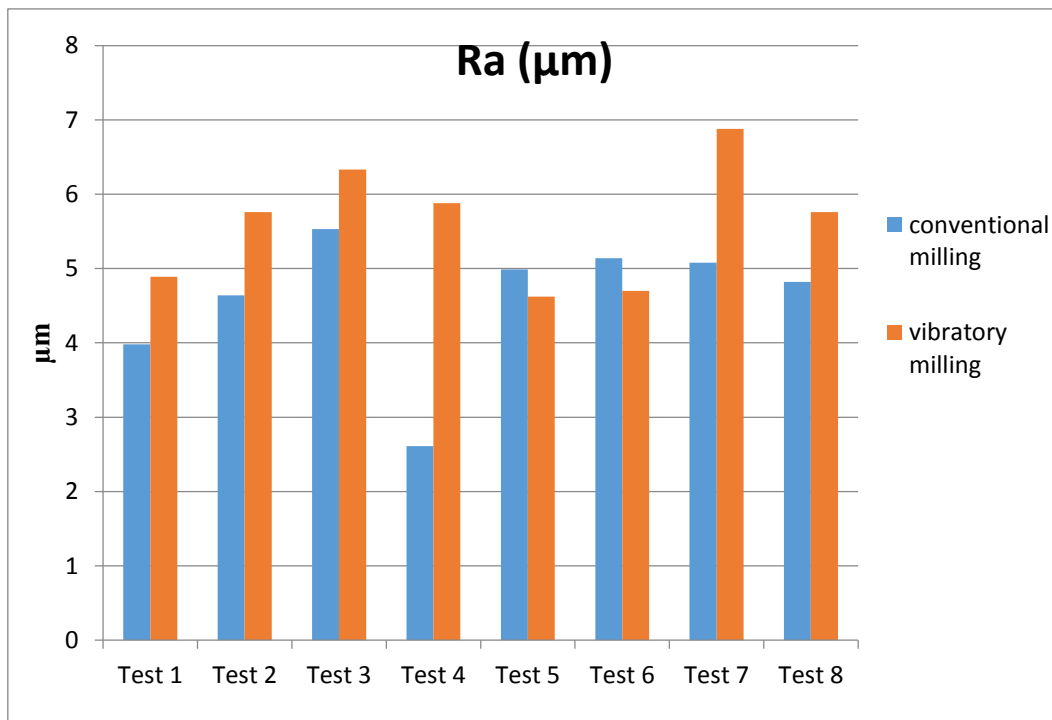
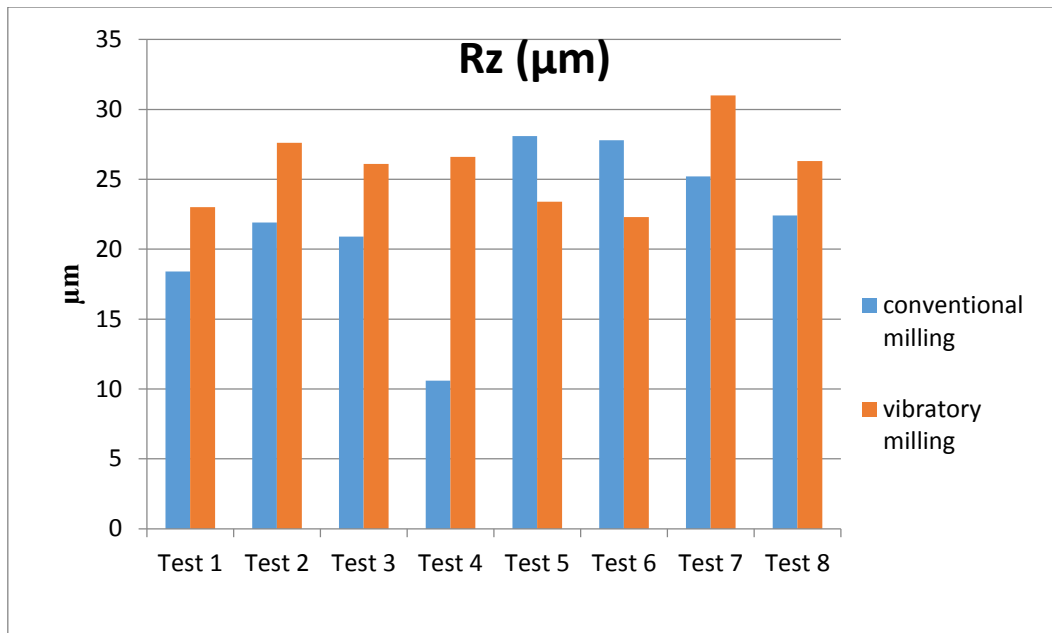


Figure 8. 13: Surface Roughness ( $R_a$ ).



**Figure 8. 14: Surface roughness (Rz).**

Figures 8.13 and 8.14 above show the results for surface roughness between conventional and vibratory milling for different machining conditions as stated in table 8.2.

It is seen in these experimental results for machining Aluminium that there are only two machining conditions (test 5 and test 6) showing the benefits of Vibration Assisted machining, where up to 20% reduction in  $R_a$  and  $R_z$  is observed with reference to conventional milling.

Here, the machining parameters were 1 mm depth of cut, high spindle speed (6,000 RPM).

One can deduct from this, that superimposed vibration can be effective in soft material, when deep cuts and high speed are used.

### Work-pieces imaging analysis

All work-pieces surface profiles were examined under the microscope, however, only two representatives are shown here for test runs No. 5 and 6 referring to table 8.2.

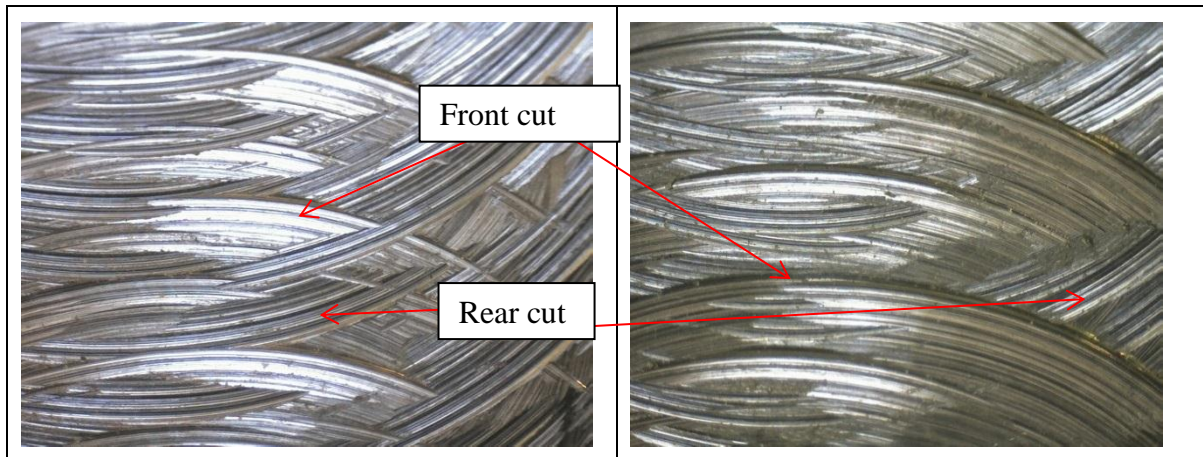


**Figure 8. 15: Work-piece surface finish image (a. Conventional milling and b. Vibratory milling) 60X.**

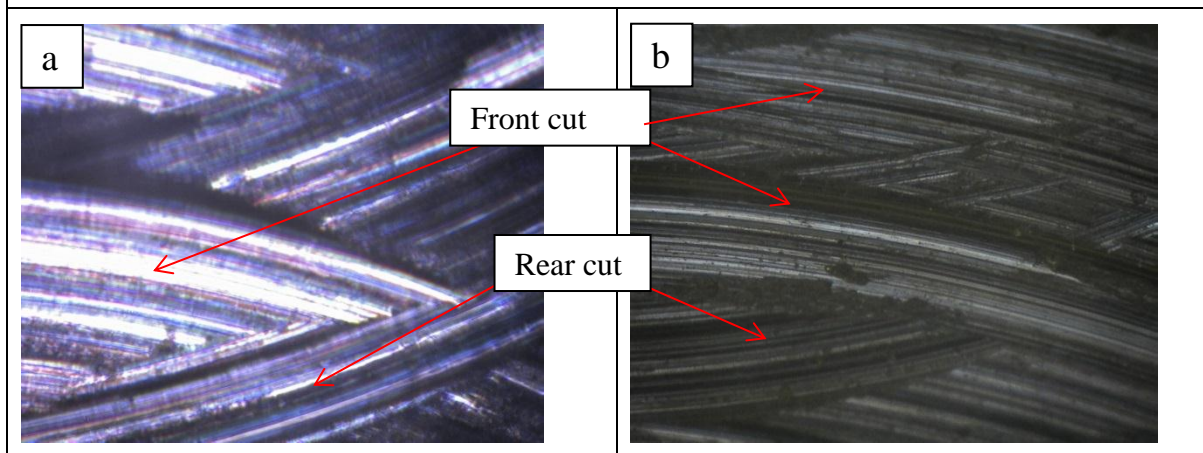


**Figure 8. 16: Work-piece surface finish image (a. Conventional milling and b. Vibratory milling) 200X.**

Figures 8.16 and 8.17 present imaging photos for work-piece surfaces after machining in condition of Test 5 with high spindle speed (6,000 RPM), feed rate of 900 mm/min and depth of cut equal to 1 mm. In addition, the cutting path seen in these figures notes that the milling tool can cut more material in the condition of vibratory milling better than in conventional milling.

Higher feed rate (up to 1,800 mm/min), shows the advantages of vibration assisted milling as tool cutting edges remove more materials from the work-piece as seen in figures 8.18 and 8.19.

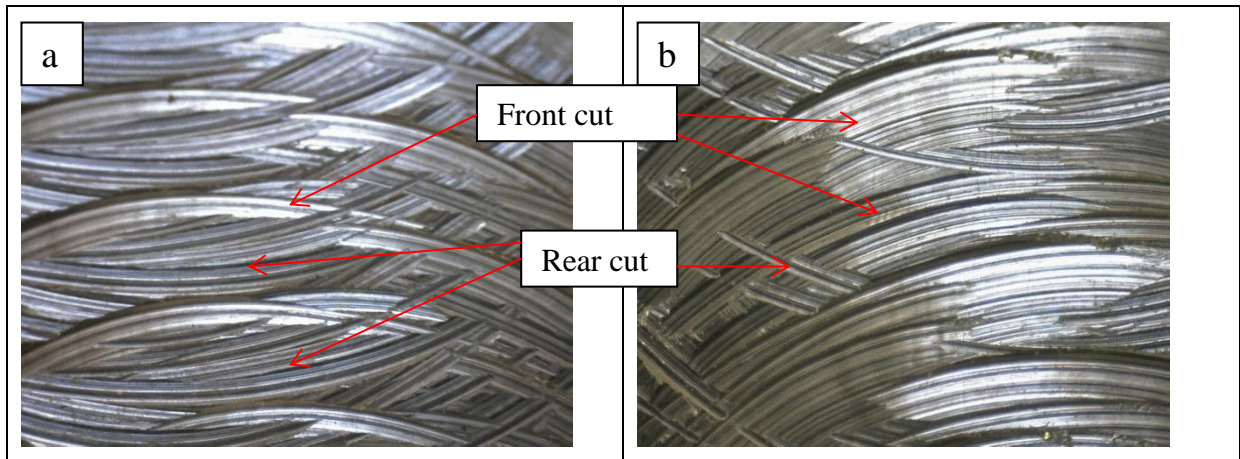


**Figure 8.17:** Work piece surface finish image (a. Conventional milling and b. Vibratory milling) 60X.

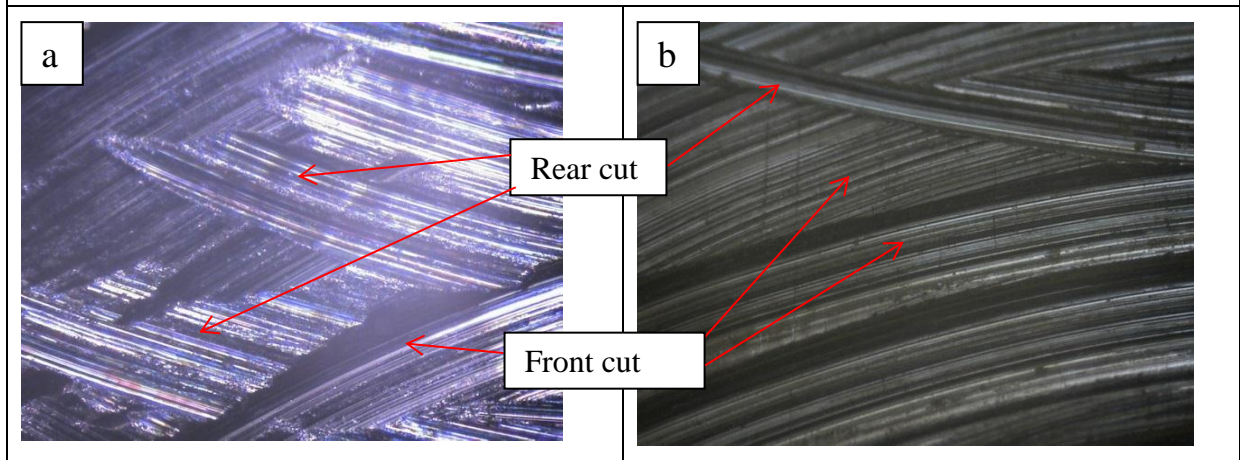


**Figure 8.18:** Work piece surface finish image (a. Conventional milling and b. Vibratory milling) 200X.

## 8.6 Remarks

The results of this preliminary study led to the following observations:

First, the vibration self-contained system was successfully employed for the five axis Milling Machine with all sensors and DAQ System to collect and record data in real machining. In addition, the surface roughness for each test was measured and averaged over three points.

Secondly, in high speed machining conditions such as Test 5 and Test 6, the superimposition of vibratory milling secured better process performance in the following terms;

- Average reduction in Cutting forces up to 40 %.
- Improve surface finish quality of the work piece by 20%.
- Allow cutting edges to remove more materials from work piece.

Finally, using these results of preliminary studies, further investigation and tests should be done with machining parameters ranging around parameters of Test 5 and Test 6 (6,000 RPM, 1,800 mm/min and 1 mm Depth of Cut).

# **Chapter 9**

## **Effect of Vibration on Milling Process**

## 9.1 Introduction

In the chapter of Preliminary studies, a set of experimental works in conventional and vibratory milling modes were carried out. However, for some machining parameters such as spindle speed and depth of cut, the application of vibratory milling did not perform as expected due to the elasticity of the work-piece material. Therefore, the effective or optimum machining parameters that secured a good performance will be taken as the baseline for the next experimental tests using Aluminium and mild Steel.

This chapter contains a comparative study which presents side by side the experimental results of Vibratory Milling and Conventional Milling. This set also presents cutting forces, milling power, torque, machining coefficient and surface roughness of the work-pieces. To observe the effect of machining parameters on Vibratory Milling such as feed rate, spindle speed and depth of cut, one of these parameters will be varied while keeping the other parameters constant.

The table 9.1 provides machining parameters for these experimental works while using Aluminium and steel. The Spindle speed was constant, but Feed rate and depth of cut were varied. All these machining parameters were selected as recommended in the tooling specifications book (Total Tooling, 2014). The vibration amplitude and frequency were chosen to avoid the resonant frequency of the machine spindle unit and oscillation system.

**Table 9. 1: Experimental machining parameters.**

<b>Milling parameters</b>	<b>Value</b>
Milling cutter type	Solid Carbide end mill (Coated: Ti 400)
Number of Teeth	3
Diameter	10 mm
Helix angle	45°
Rake angle	15°
Spindle Speed For Aluminium	6000 RPM
Spindle Speed For Steel	2300 RPM
Feed Rate For Aluminium	750 – 2000 mm/min
Feed Rate For Steel	50 mm/min
Cut type	Up Milling
Milling Condition	Dry and only air for Steel
Work-piece	Aluminium and Steel
Depth of cut for Aluminium	0.75, 1, 1.25 and 1.5 mm
Depth of cut for Steel	0.25, 0.5, 0.75 and 1.00 mm
Vibration Frequency	125 Hz
Sine wave Amplitude	3 Volts (positive peak)
Vibration amplitude	About 200 µm (positive peak)

## 9.2 Cutting Forces in Milling process

During milling, the forces were measured in three directions X, Y and Z axis with the normal cutting force in Z axis being ( $F_z$ ), however the full cutting force ( $F_c$ ) is the result between two forces in direction of X and Y axis.

### 9.2.1 Effect of depth of cut

Figures 9.1 and 9.2 depict the cutting forces for machining two types of work-pieces with different values of depth of cut. The machining parameters for the aluminium work-piece were 6,000 RPM for Spindle Speed and 1,800 mm/min for feed rate, however for machining the steel work-piece, they were 2,300 RPM and 50 mm/min for spindle speed and feed rate respectively. In figure 9.1, milling forces for machining aluminium in dry condition were presented in two machining modes; without vibration (figure 9.1.a) and with vibration (figure 9.1.b). It is observed that when the depth of cut was increased all cutting forces components were increasing rapidly.

In addition, figure 9.2 gives the results of machining mild steel. For coolant application, only pressurized air was applied to the cutting zone. The measured milling forces displayed in graphs show the relationship between depth of cut and cutting forces in all directions as in the case of machining aluminium.

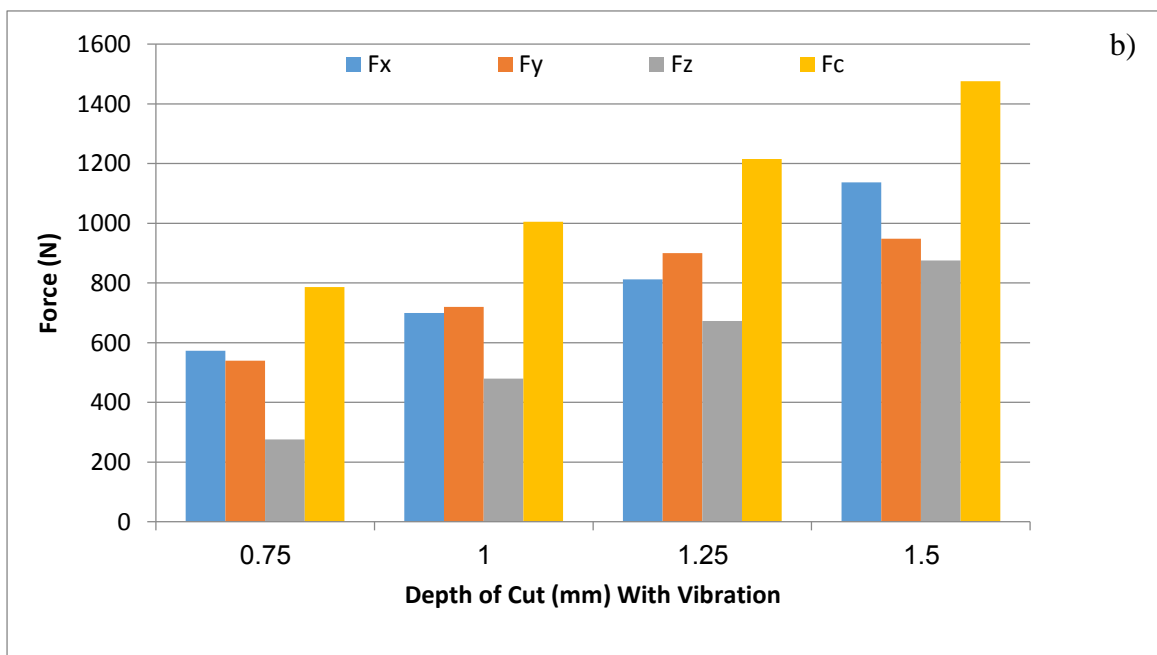
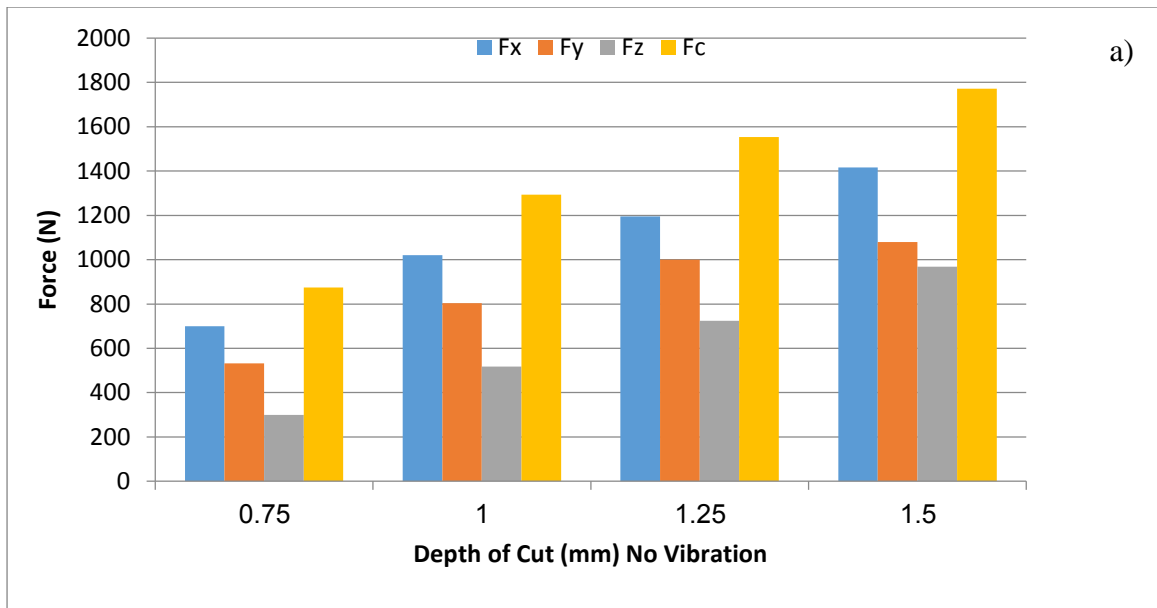


Figure 9. 1: Milling Forces for Aluminium: a) Conventional milling. b) Vibratory Milling.

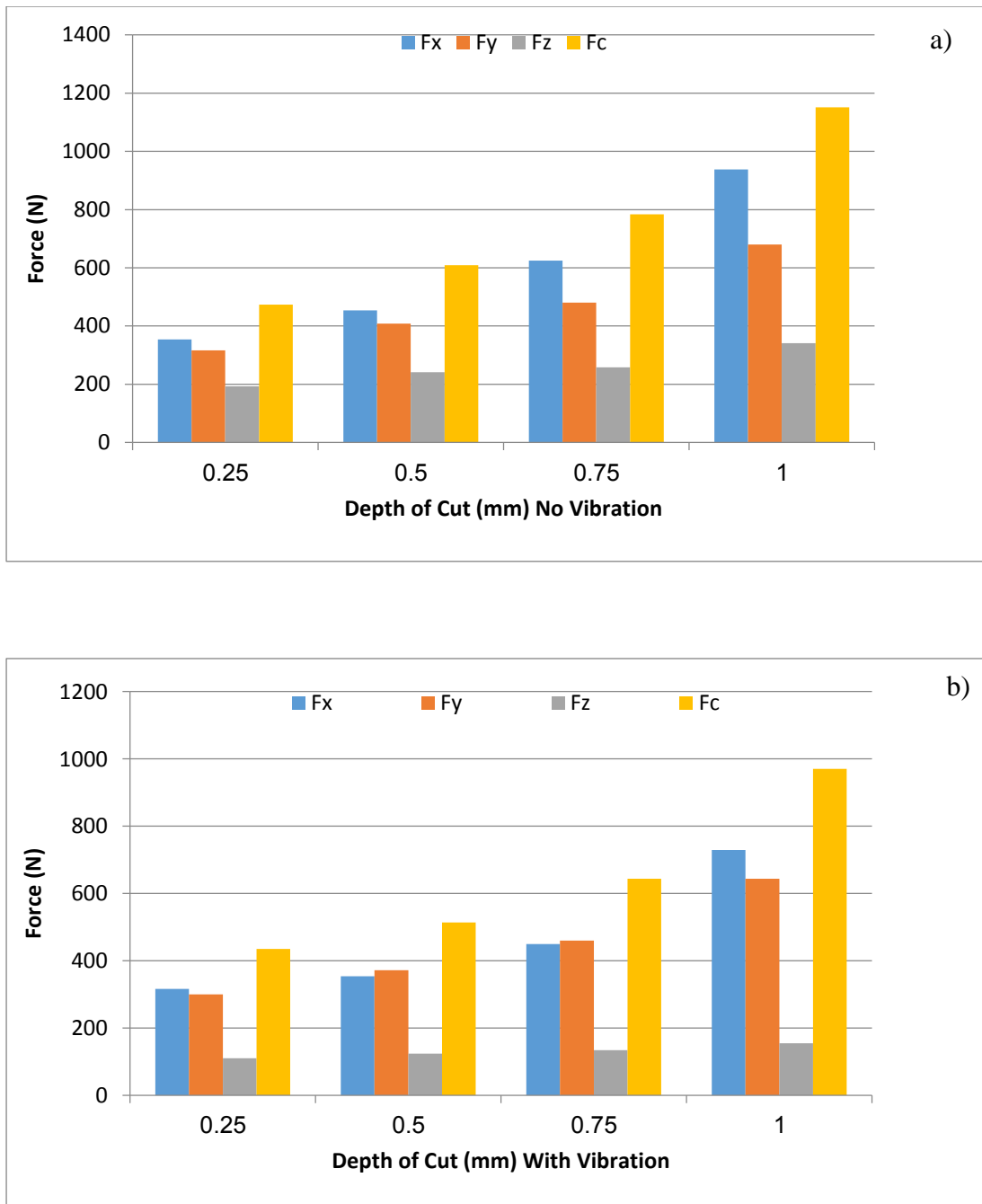


Figure 9. 2: Milling Forces for Steel: a) Conventional milling. b) Vibratory Milling.

### 9.2.2 Effect of vibratory milling

#### **Vibratory milling effect in Normal force ( $F_z$ ):**

In machining, the force that is applied vertically to the work-piece defined as Normal force. Figures 9.3 and 9.4 display the performance of the milling process in terms of Normal force ( $F_z$ ), in figure 9.3.a, the depth of cut was constant (1 mm) but the feed rate was variable from 750 to 2,000 mm/min. However, in figure 9.3.b. the feed rate was fixed at 1,800 mm/min and the depth of cut varied. In addition, these two figures show some benefits of vibratory milling by reducing normal force up to 10 % compared to conventional milling.

Figure 9.4 shows normal forces for machining a steel work-piece with different values of depth of cut. Here the application of vibration to milling decreased the normal forces up to 50 % compared to conventional milling. It also shows that changing the work-piece material from Aluminium to harder material such as mild Steel provided higher benefits of vibration assisted machining.

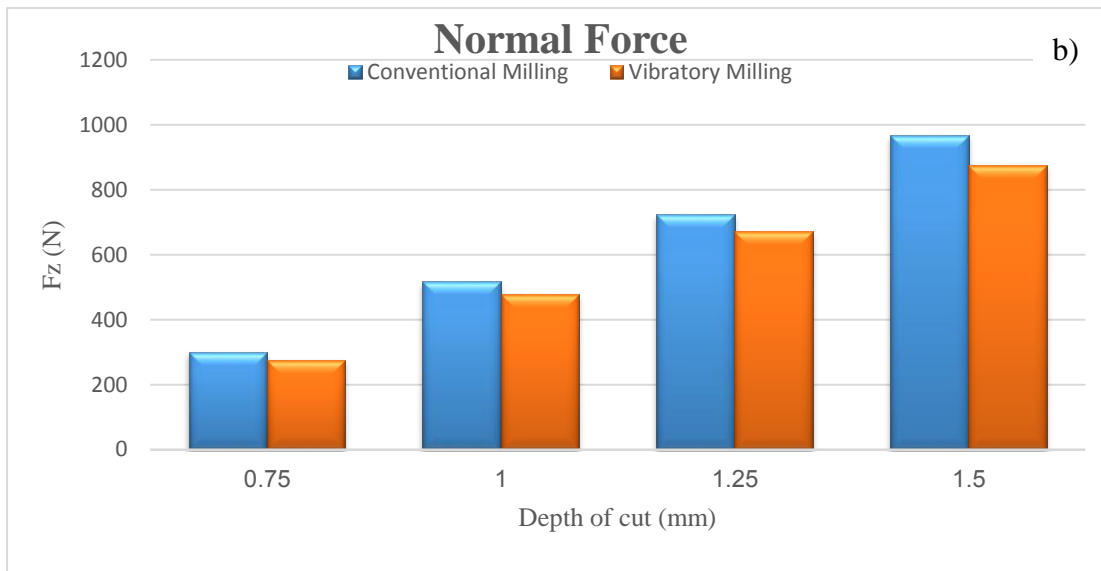
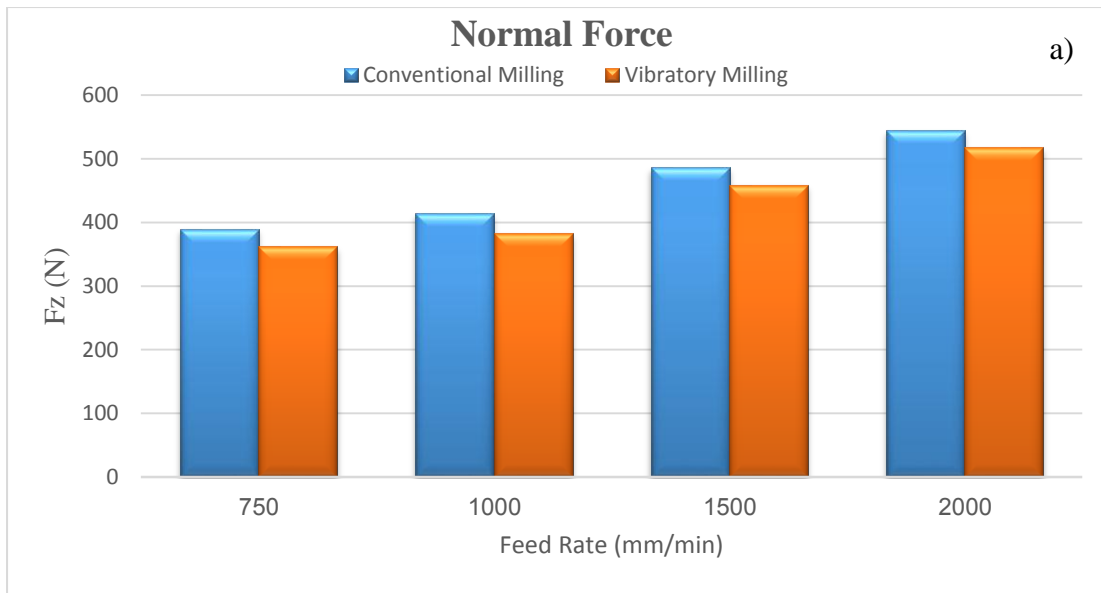
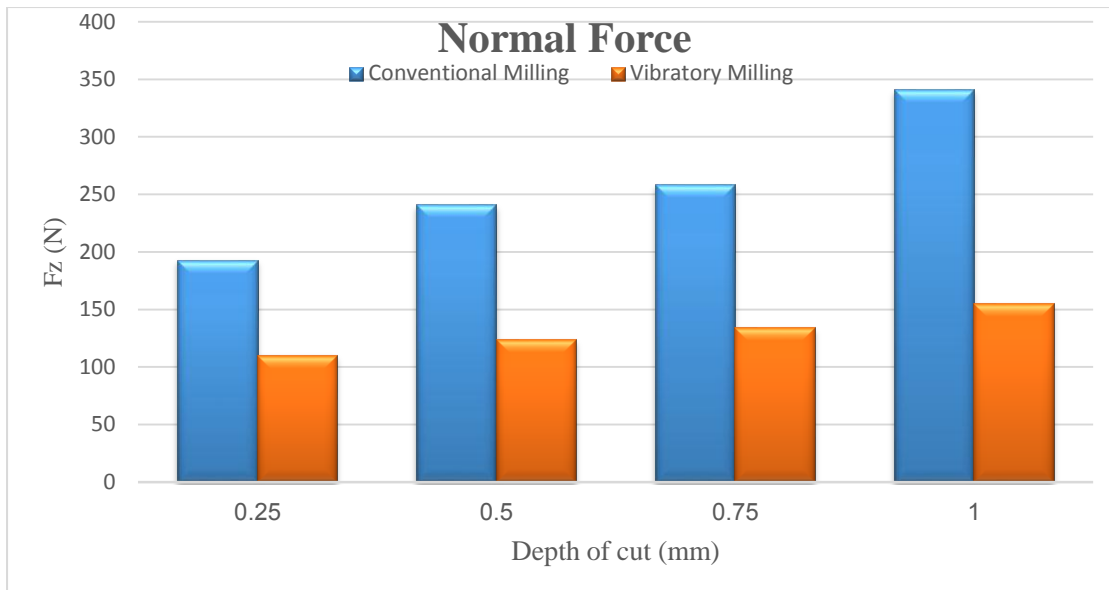


Figure 9. 3: Normal Force for milling Aluminium: a) Varying feed rate. b) Varying depth of cut.



**Figure 9. 4: Normal Force for milling Steel.**

**Vibratory milling effect on Resultant Forces ( $F_c$ ):**

Figure 9.5 shows the experimental results of machining an aluminium work-piece with different set values of depth of cut and feed rate, using the same machining parameters that were illustrated in the previous section. Here the resultant cutting forces show that there is an average decrease of 25 % in vibratory milling compared to conventional milling, including mild steel as seen in figure 9.6.

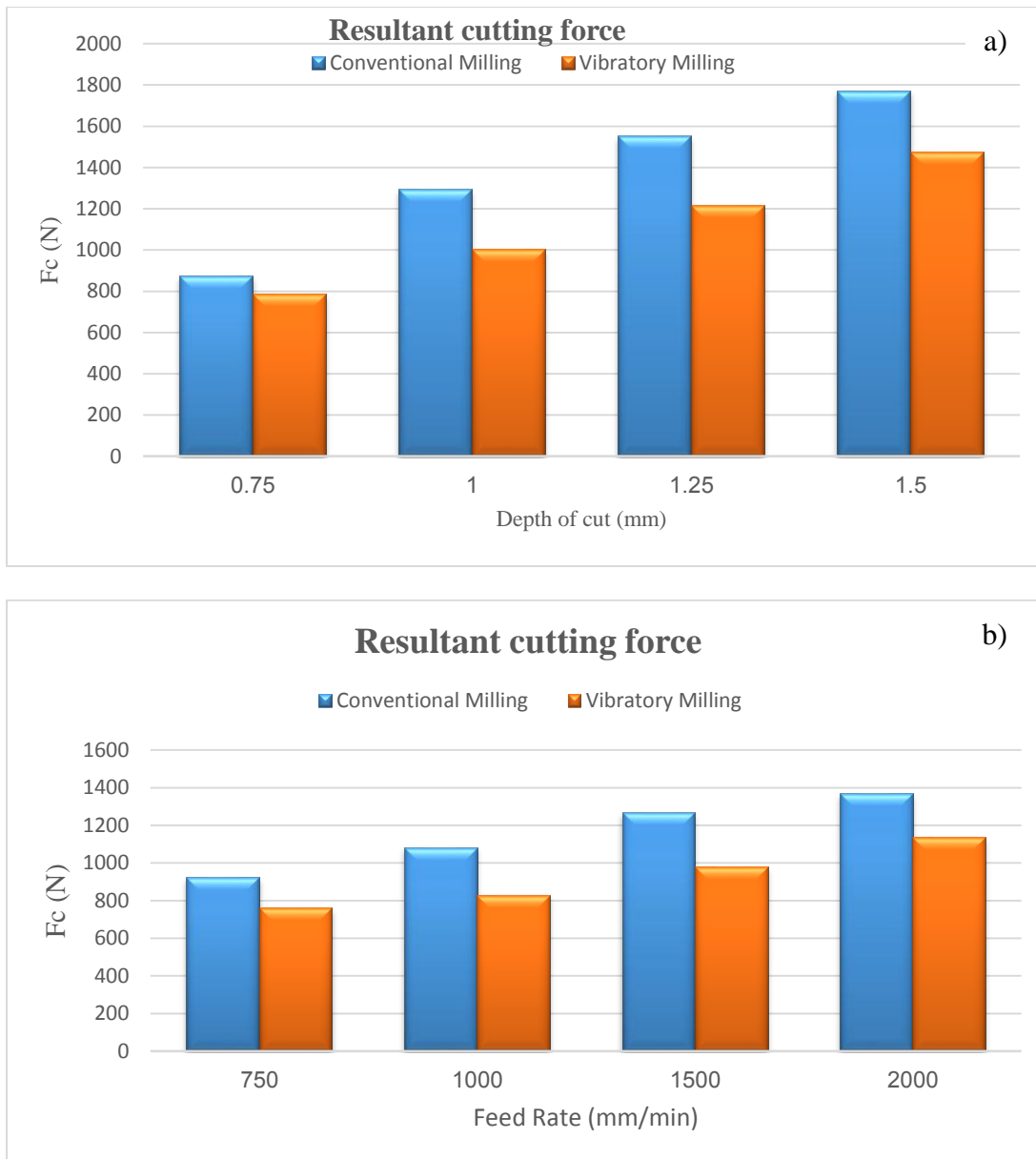


Figure 9. 5: Resultant cutting Force for Aluminium: a) Varying feed rate. b) Varying depth of cut.

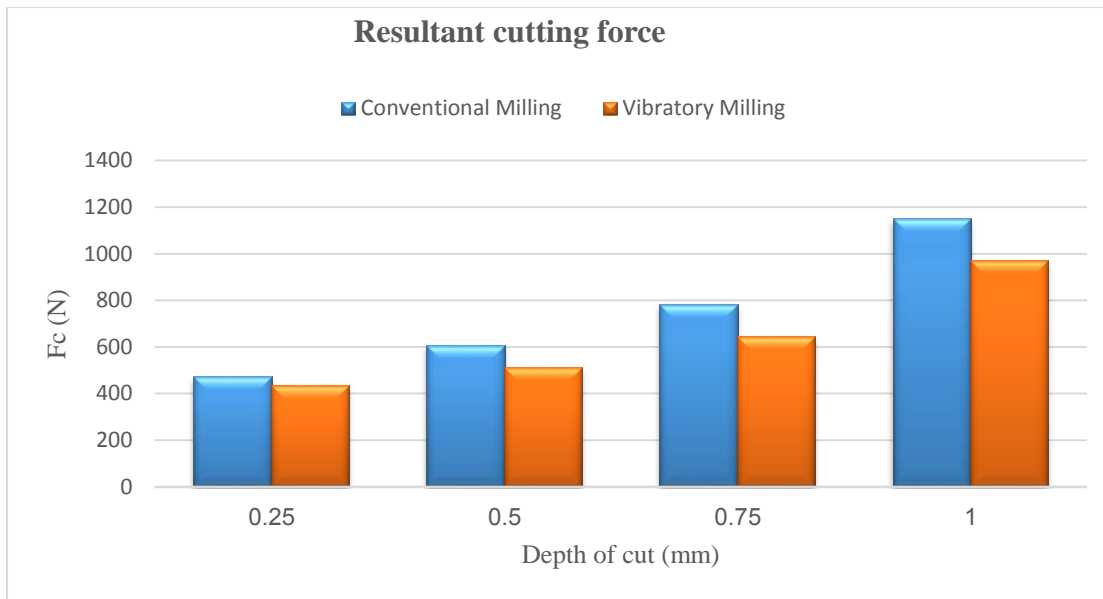


Figure 9. 6: Resultant Cutting Force for Steel.

### 9.3 Milling Power and Torque

Milling power was calculated using equation 9.1, the resultant cutting force (FR) for  $F_x$ ,  $F_y$  and  $F_z$  forces was defined by equation 9. 2. As referee to chapter 2, section 2.5.

$$Power (W) = \frac{Cutting\ Force\ (FR) * Feed\ Rate\ (\frac{mm}{min})}{60 * 1000} \quad (9.1)$$

$$FR (x, y \& z) = \sqrt{Fx^2 + Fy^2 + Fz^2} \quad (9.2)$$

To calculate milling torque, equation 9.3 was used (Kalpakjian and Schmid, 2010).

$$Mc (Nm) = \frac{power(w)}{\omega} = \frac{power(w)}{2 * \pi * \frac{RPM}{60}} \quad \text{then;}$$

$$Mc (Nm) = \frac{30 * power(w)}{\pi * RPM} \quad (9.3)$$

The graphs in figures 9.7 and 9.8 show the milling Power and Torque for machining two materials (aluminium and steel).

From figure 9.7, it can be observed that the decreases of cutting forces in vibratory milling led to a proportional reduction in power consumption by the process.

Figure 9.8 shows the torque as a function of depth of cut. It is observed that in vibratory mode, the process had low torque compared to conventional milling. An average reduction of 20 % was achieved in machining both materials (Aluminium and steel) using vibration.

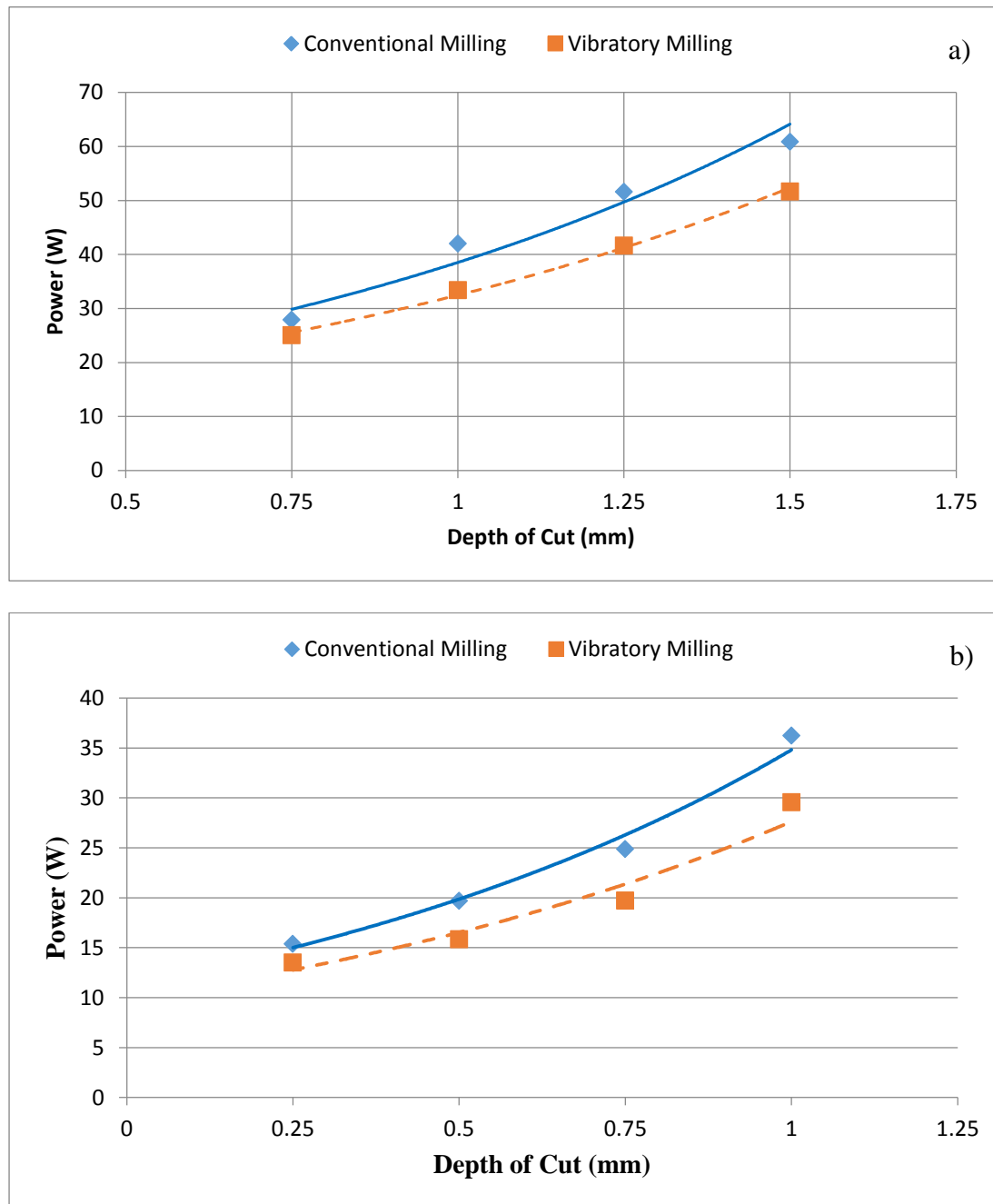


Figure 9. 7: Milling Power Consumption: a) Aluminium. b) Steel.

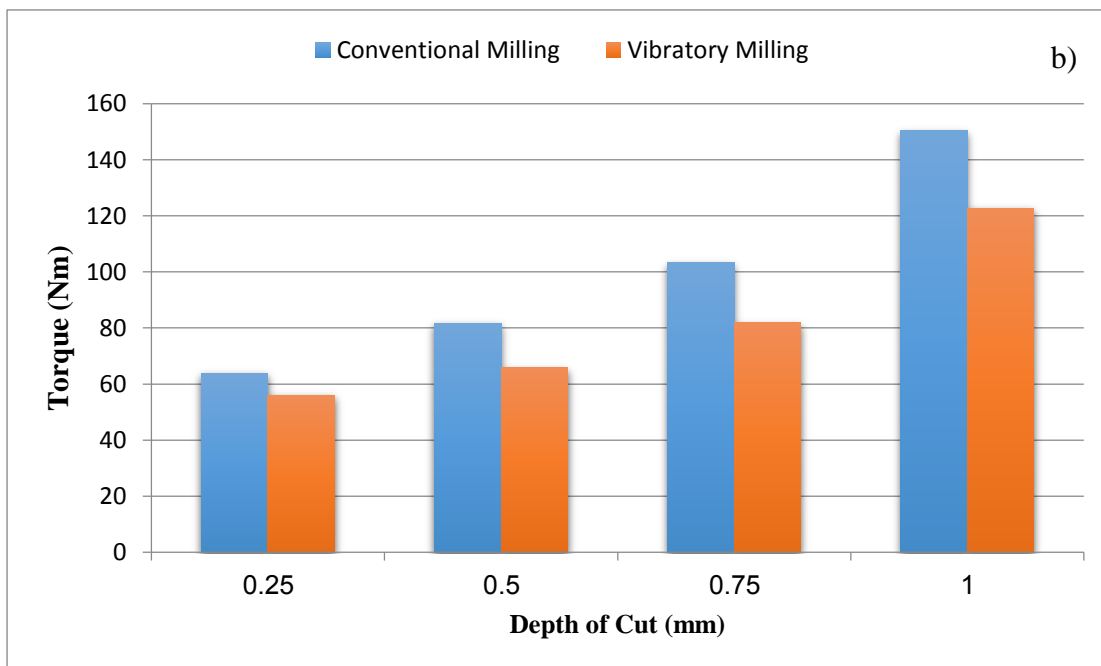
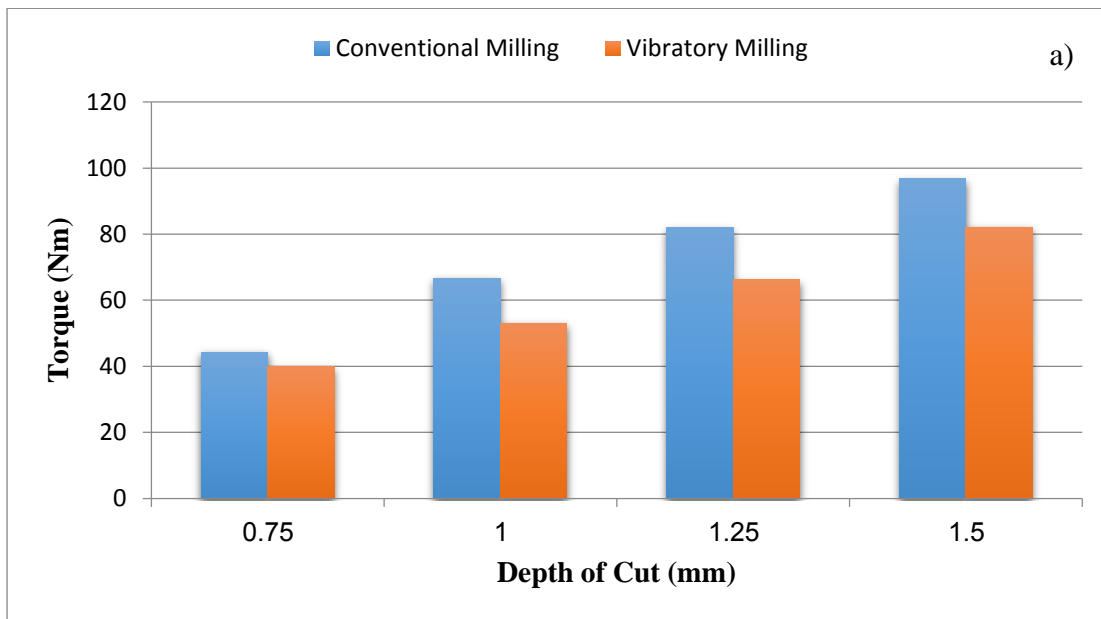


Figure 9. 8: Milling Torque: a) Aluminium. b) Steel.

## 9.4 Milling Coefficient

Milling force ratio or milling coefficient is defined as

$$\mu = F_c/F_z \quad (9.4)$$

It is an important parameter that gives the indirect information about the efficiency of machining (Rowe, 2013).

The Milling Coefficient for machining aluminium and steel using conventional and vibratory modes is shown in figure 9.9, where in figure 9.9.a, for aluminium, the milling coefficient is lower with the increasing of depth of cut, even when using the vibratory milling application. This is due to the characteristic plasticity and gumminess of aluminium. However, in hard materials such as steel, the machining coefficient increased when a greater depth of cut was applied, as seen in figure 9.9.b. It shows that there is an improvement in Milling Coefficient up to 46 % with machining under vibratory milling. Finally, the rising values of the Milling Coefficient led to enhanced material removal.

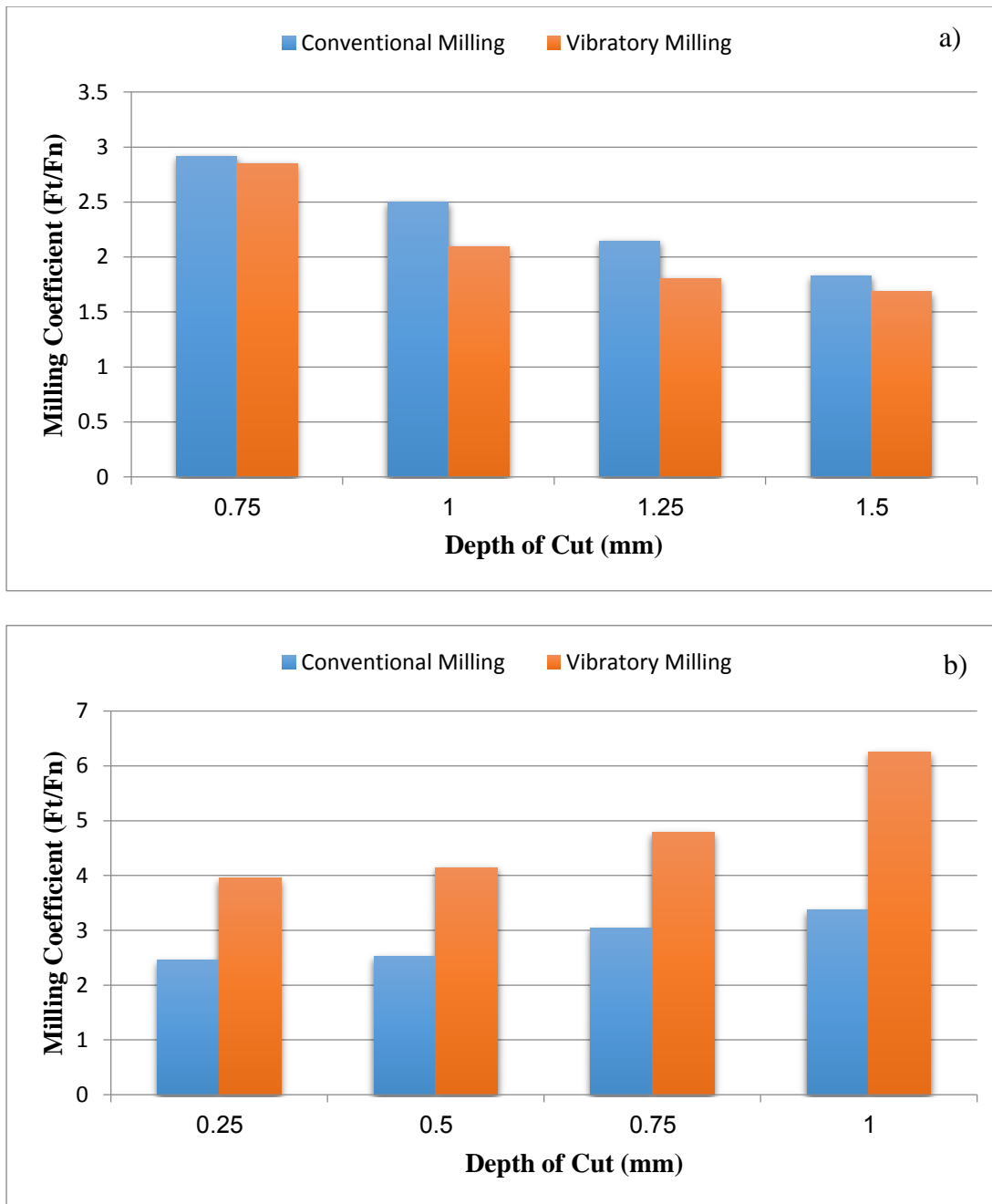


Figure 9. 9: Milling Force Ratio: a) Aluminium. b) mild Steel.

## 9.5 Surface Roughness

Results in figures 9.10 to 9.14 depict the measured surface roughness  $R_a$  and  $R_z$  for the two machining modes, conventional and vibratory milling.

Figure 9.10 shows an example of work-piece surface finish profile which was measured using a contact surface roughness device called TAYLOR HOBSON.

Figure 9.11 shows the effect of feed rate on the surface finish. In this test, the depth of cut and spindle speed were fixed at 1 mm and 6,000 RPM respectively but the feed rate was varied. It is seen that the surface roughness decreases with the increase of feed rate value, so the increase of feed rate gives a good surface finish. For example, in feed rate of 2,000 mm/min,  $R_z$  value is 2.99  $\mu\text{m}$  but in 1500 mm/min feed rate was 3.6  $\mu\text{m}$ . In general, an overall reduction of 25 % was achieved in vibratory milling mode.

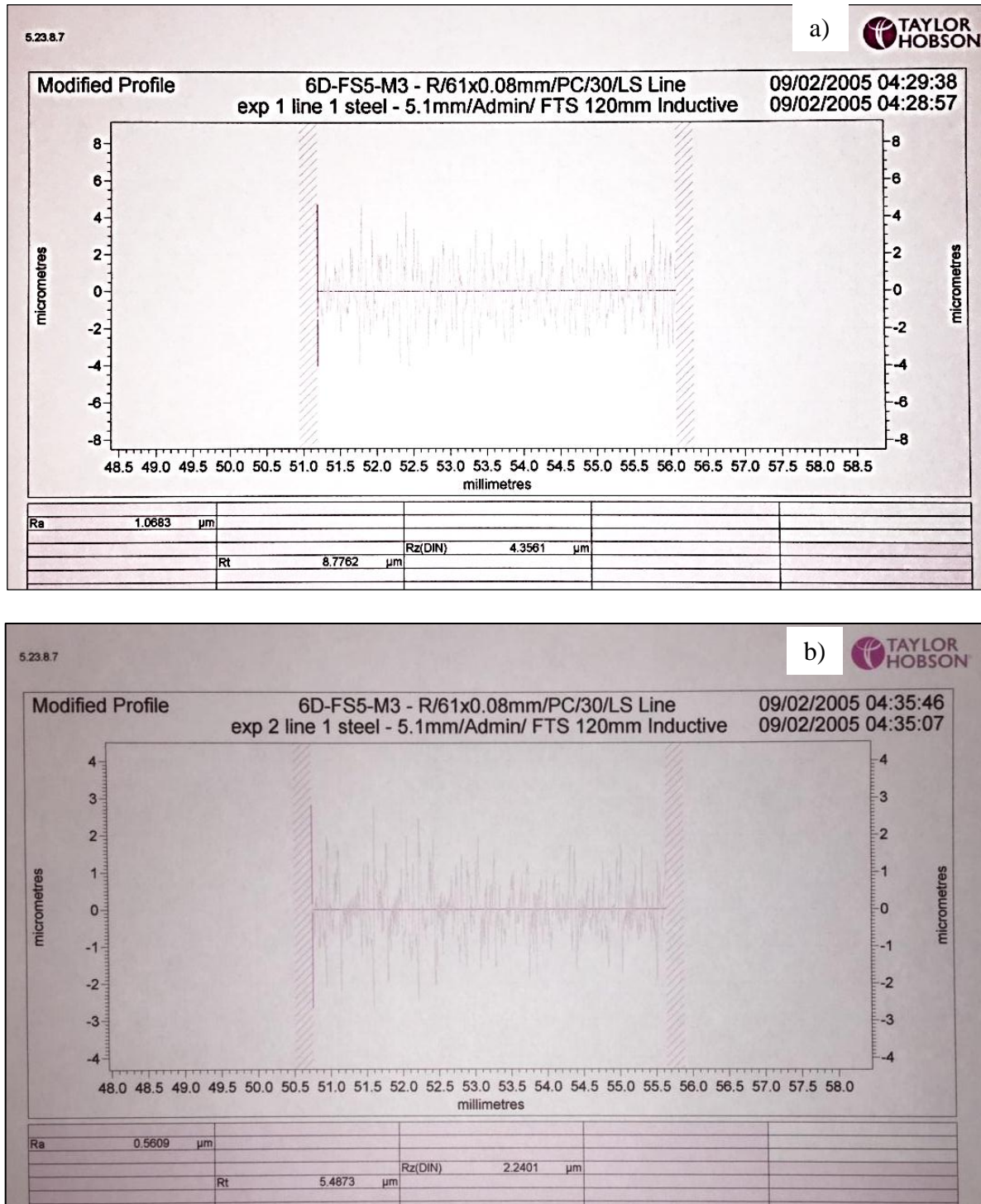


Figure 9. 10: Surface Finish Profile for Steel Work Piece: a) Conventional Milling. b) Vibratory Milling.

Figures 9.12 and 9.13 show the effect of depth of cut on surface finish quality. It is observed that for both types of material at high depth of cut, the Surface Roughness  $R_a$  and  $R_z$  become small, so the surface finish quality is relatively good. For the vibratory milling application, the surface finish quality in the hard material (Steel) is much better than soft material (Aluminium), on average, due to its plastic properties. In addition, a better surface finish quality was achieved when the application of vibratory milling is taken into account. Here, on average, the improvement in surface finish achieved with vibration, was 50% for the steel work-piece and 25% for the aluminium work-piece. However, for the aluminium material the surface finish becomes rougher when depth of cut is more than 1 mm in vibration mode.

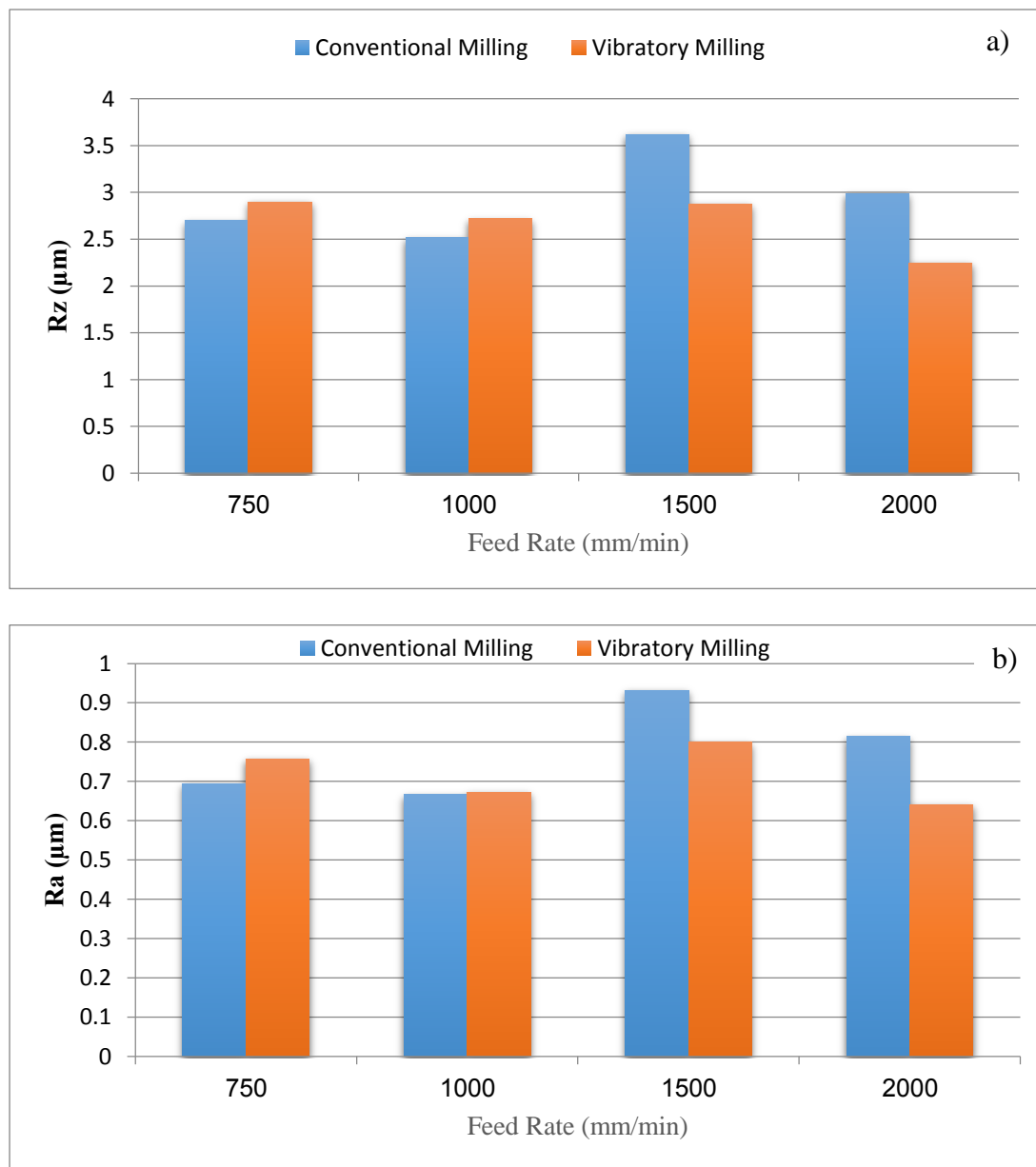
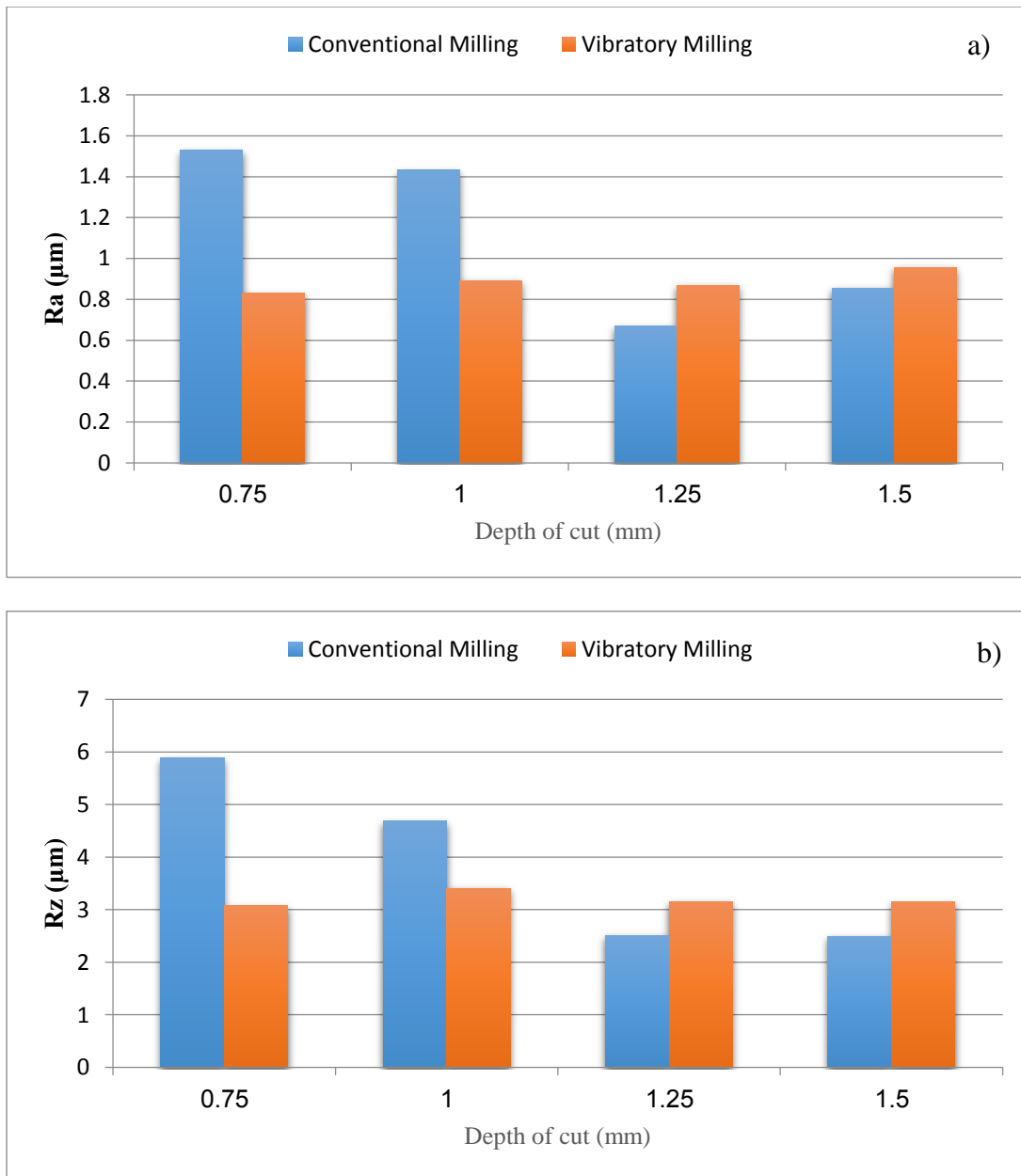
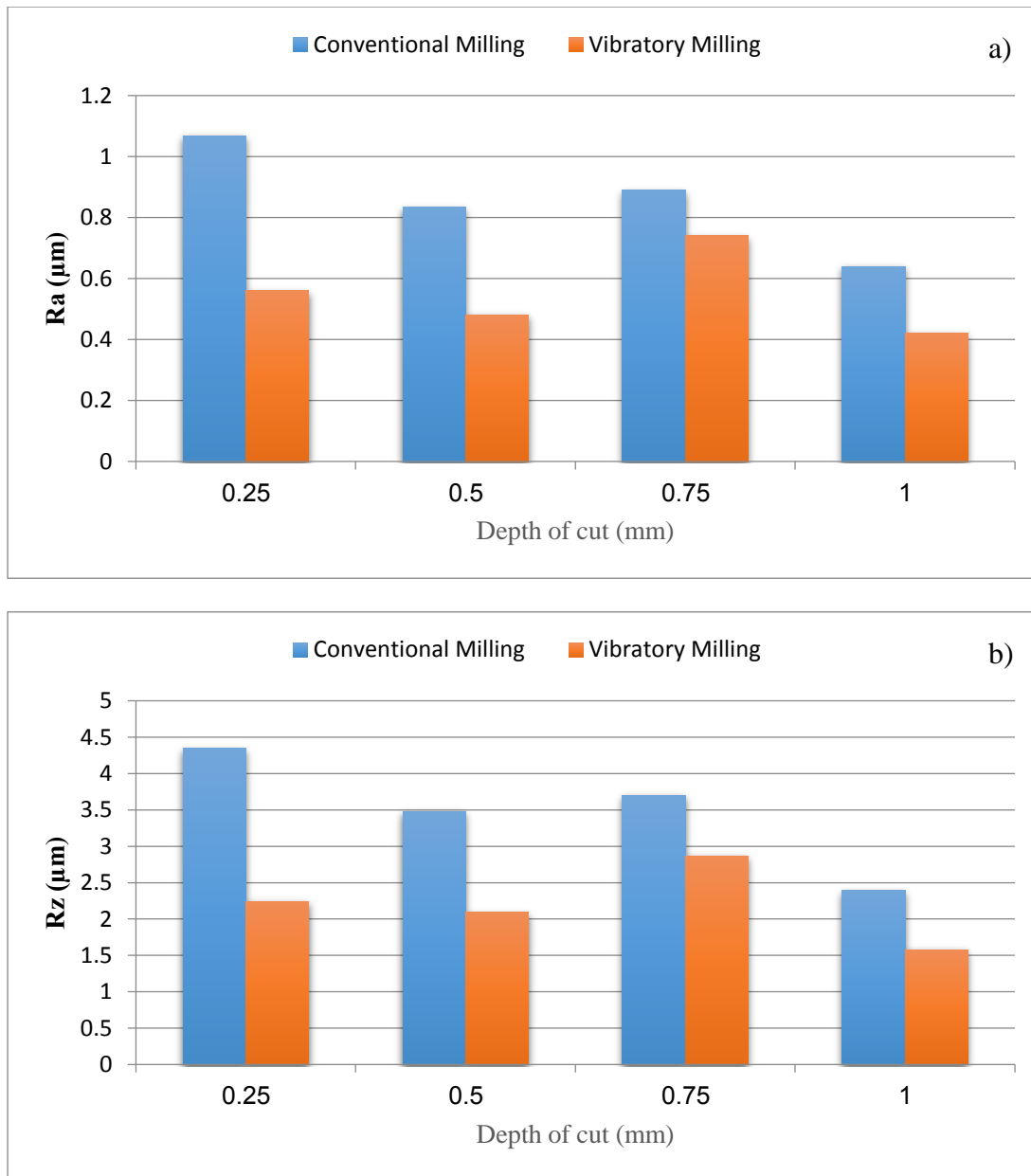


Figure 9. 11: Effect of Feed Rate on Surface Roughness (Aluminium): a) Rz Value. b) Ra Value.



**Figure 9. 12: Effect of Depth of Cut on Surface Roughness (Aluminium): a) Rz Values. b) Ra Values.**



**Figure 9.13: Effect of Depth of Cut on Surface Roughness (Steel): a) Rz Value. b) Ra Value.**

Figure 9.14 shows a 3-D surface profile measured by GFM 3D. Here, 3-D profile photos were taken after machining a Steel work-piece in both modes, conventional and vibratory milling. The machining parameters were spindle speed 2,300 RPM, 0.5 mm depth of cut and 50 mm/min feed rate. Figure 9.14.a displays the surface finish profile for conventional milling, but the case of vibratory milling is shown in figure 9.14.b.

The surface finish profile in conventional milling was uneven and random with  $Ra$  value of  $0.83 \mu\text{m}$ , but with vibratory milling, the surface finish profile was more uniform with surface roughness value  $Ra$  equals  $0.48 \mu\text{m}$ .

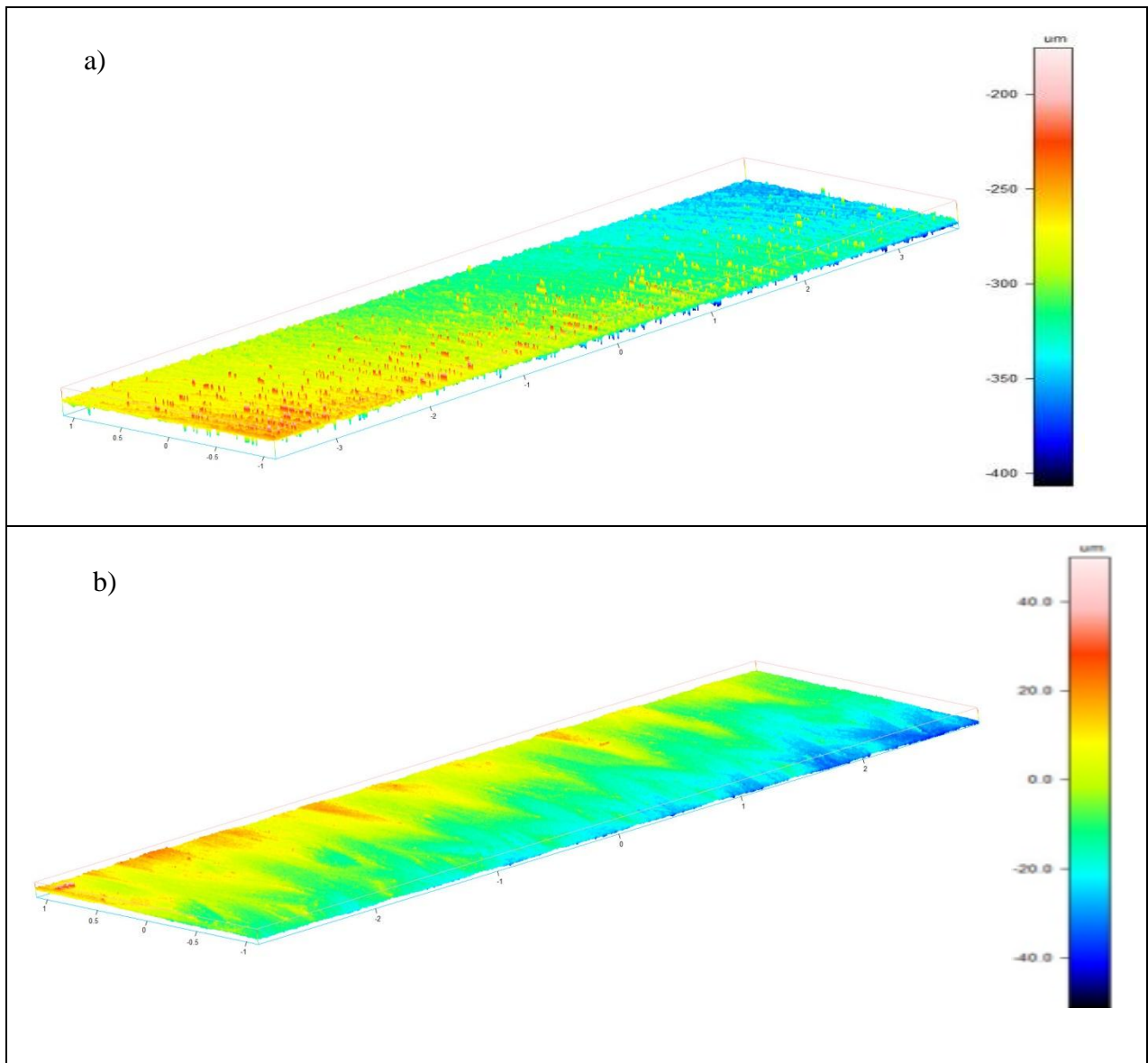


**Figure 9. 14: 3D surface finish profile: a) Conventional Milling. b) Vibratory Milling.**

## 9.6 Chips formation

The application of Vibratory milling produced much smaller and shorter chips, instead of a large and continuous chip as in conventional milling. Figures 9.15 and 9.16 show the types of chips–produced by conventional and vibratory milling. In figure 9.15, the aluminium work-piece was machined at 6,000 RPM spindle speed and 1,800 mm/min feed rate with 1 mm depth of cut. However, the steel work piece was machined with 0.75 mm depth of cut, 2,300 RPM and 50 mm/min feed rate, and the chips are shown in figure 9.16. Both materials are machined using two modes, with vibration and without vibration. Chips in figures 9.15.a and 9.16.a are bigger, longer and thicker than the chips shown in figures 9.15.b and 9.16.b. It is because the introduction of the vibration led to discontinuous chip, consequently the chips in vibratory cutting are thinner and smaller. The important role to get this type of chip is the intermittent motion of the work-piece. This means that one could avoid using a “chip breaker”, that is a common tool used in industries to produce a smaller and discontinuous chip.

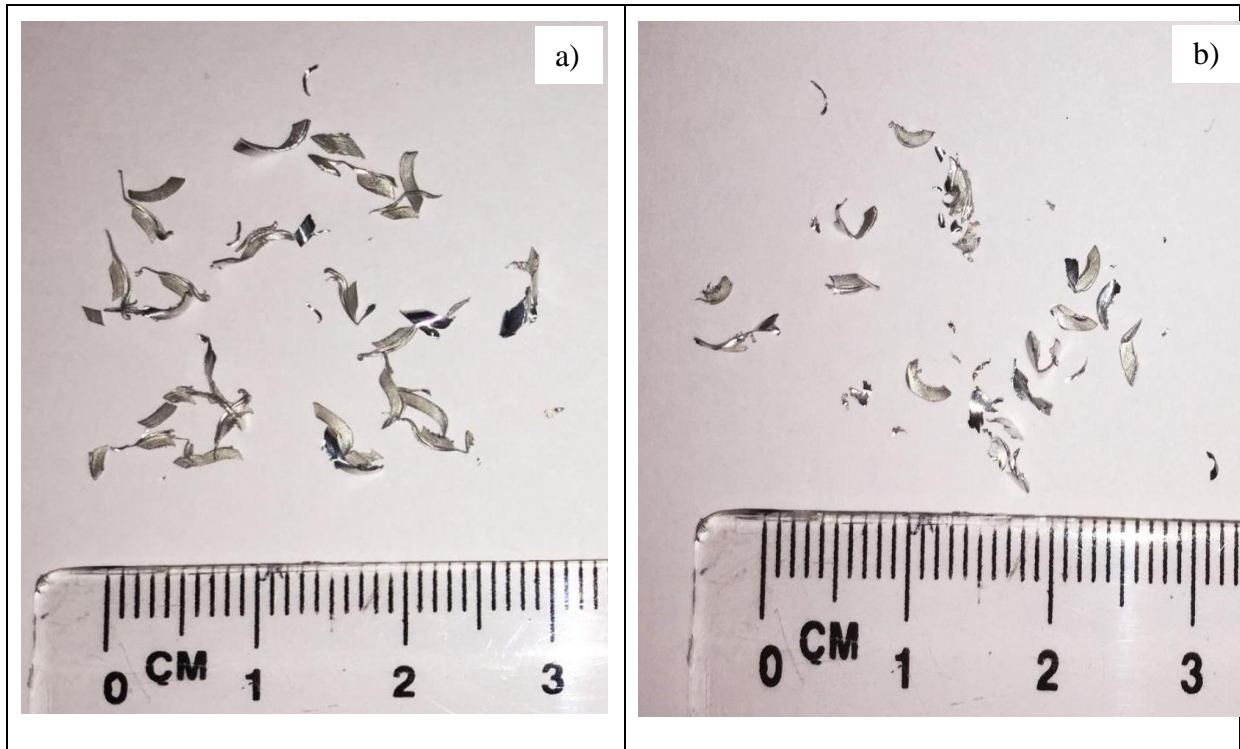


Figure 9. 15: Chips performs after machining Aluminium: a) Conventional Milling. b) Vibratory Milling.

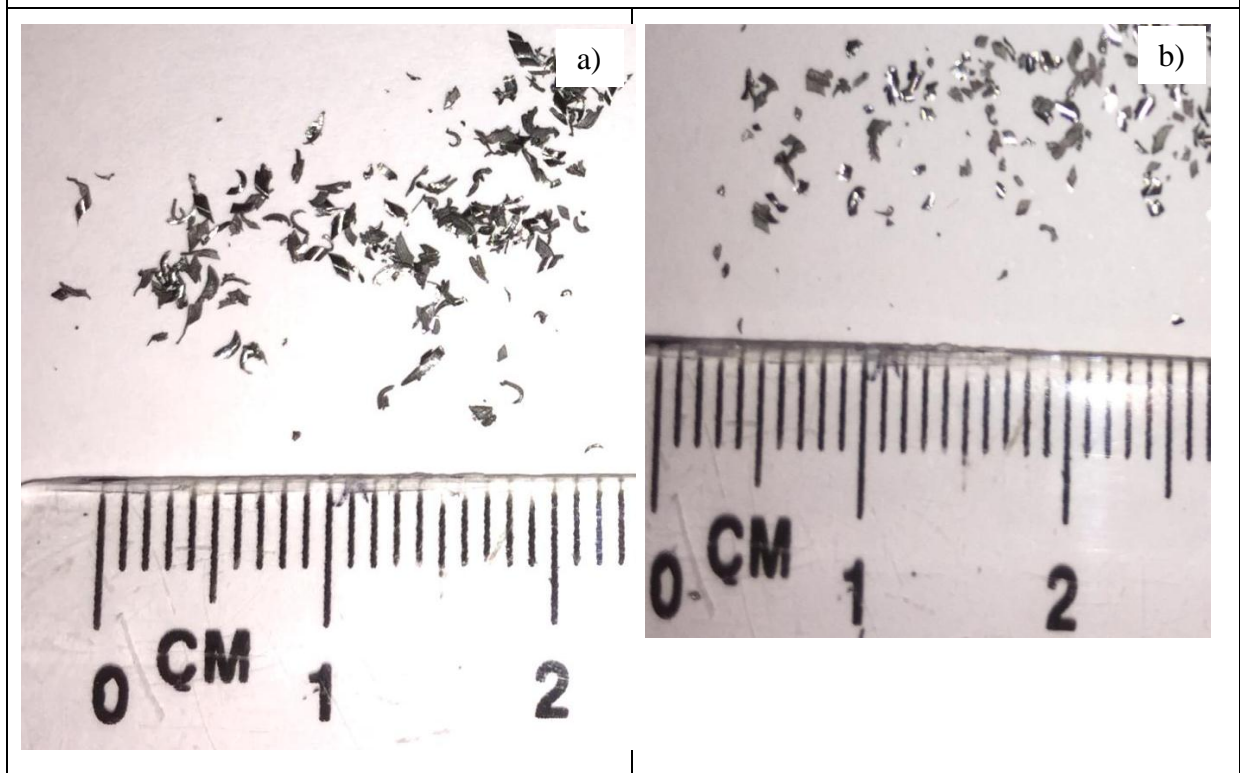


Figure 9. 16: Chips performs after machining steel: a) Conventional Milling. b) Vibratory Milling.

With the same machining conditions, vibratory milling is more consistent than conventional milling. Table 9.2 below shows an observation from this investigation through experimental works.

**Table 9. 2: Comparison in chip’s performance between conventional and vibratory milling.**

	Vibratory Milling	Conventional Milling
Chip length	Thinner thickness and short.  Depending on amplitude, spindle speed and feed rate.	Always long.  Depending on feed rate and spindle speed.
Chip Formation	Shorter and discontinuous chip.  Depending on frequency, amplitude and spindle speed.	Always continues.  Depending on feed rate and spindle speed.

Depending on the frequency and amplitude, vibro milling produced much smaller chips which are easy to clear from workspace, as opposed to conventional cutting that generates long chips, which is a problem in industrial environments.

## 9.7 Tool Wear

In this investigation, two new tools were used for conventional and vibratory milling with the same machining time. The cutting tool tip wear was examined in this study using visual observation under microscope focusing on the cutting edge and Rake face of each tool. Figure 9.17 shows the microscope picture of the tool edge.

In conventional milling, the built-up edges start appearing in the tool face as shown in figure 9.17.a. However, as displayed in figure 9.17.b with the application of vibratory milling, the effectiveness of built-up edges is reduced. The built up edges normally appear in the milling process because the operation is intermittent where the cutter edge alternately engages and disengages with the work-piece. When the tool suddenly disengages from the work-piece, the built up edges will be welded on the tool face during the cutting to be torn off (Zahoor et al. 2016). In vibratory milling, the work-piece is oscillated and this oscillation leads to a very short contact time between the edge and the work-piece and reduces friction. The two figures below show that the tool stays clean with no sign of adhesion or wear on vibratory milling. The built-up edge can protect the tool during cutting but it leads to increase the cutting forces and poor surface finish.

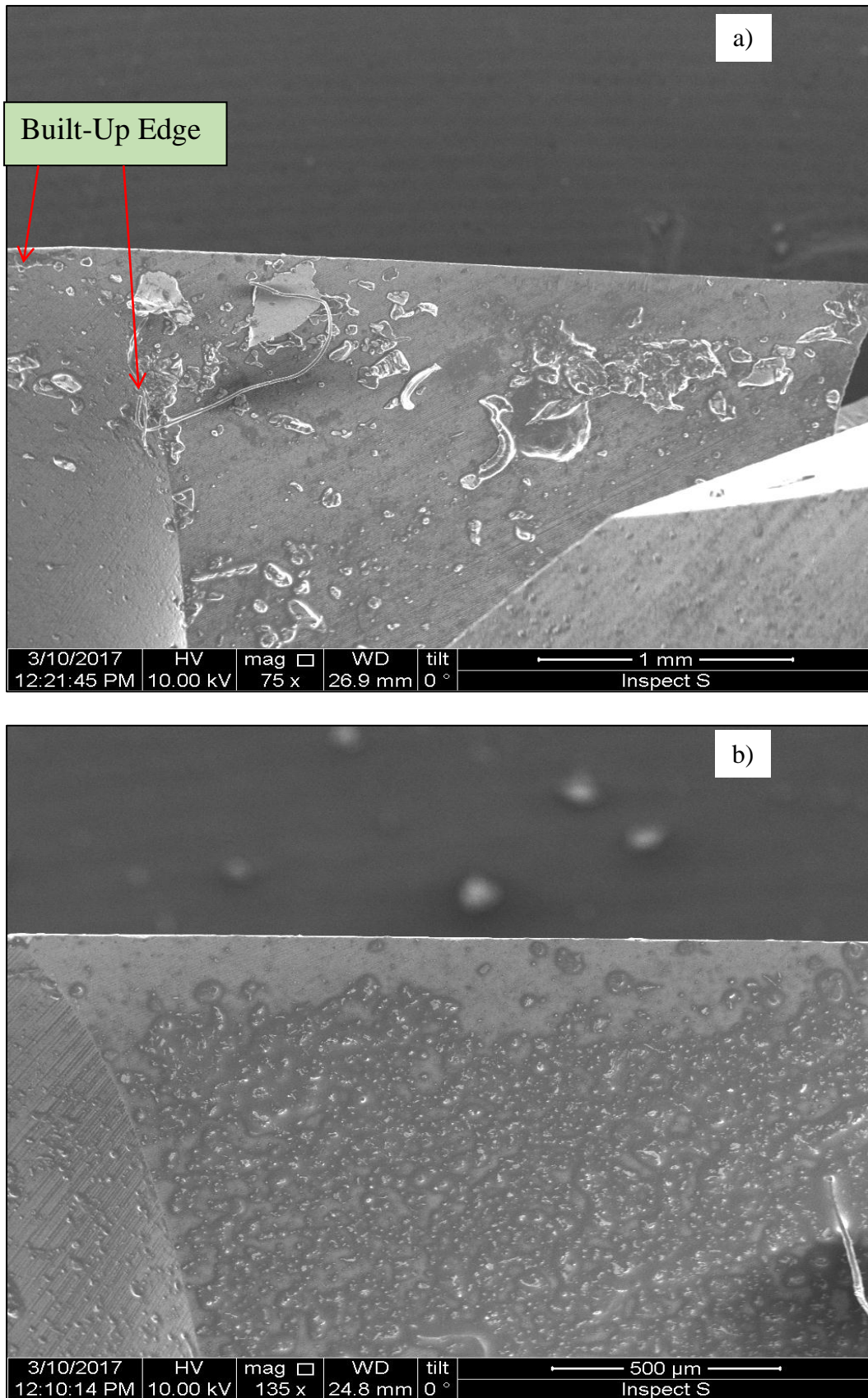


Figure 9. 17: End mill cutter tool: a) Conventional Milling. b) Vibratory Milling.

## 9.8 Effect of Machining Time

Figure 9.18 below shows the actual machining time for conventional and Vibratory milling. The signals show when the cutting tool starts and finishes cutting the work piece. Here, it is observed that the machining time (cutting time) using the vibratory milling application is less than in conventional mode. The machining time for conventional milling was nearly 72 seconds but 69 seconds for vibratory milling. Therefore, three seconds were reduced in about 70 seconds machining time using the application of vibratory milling.

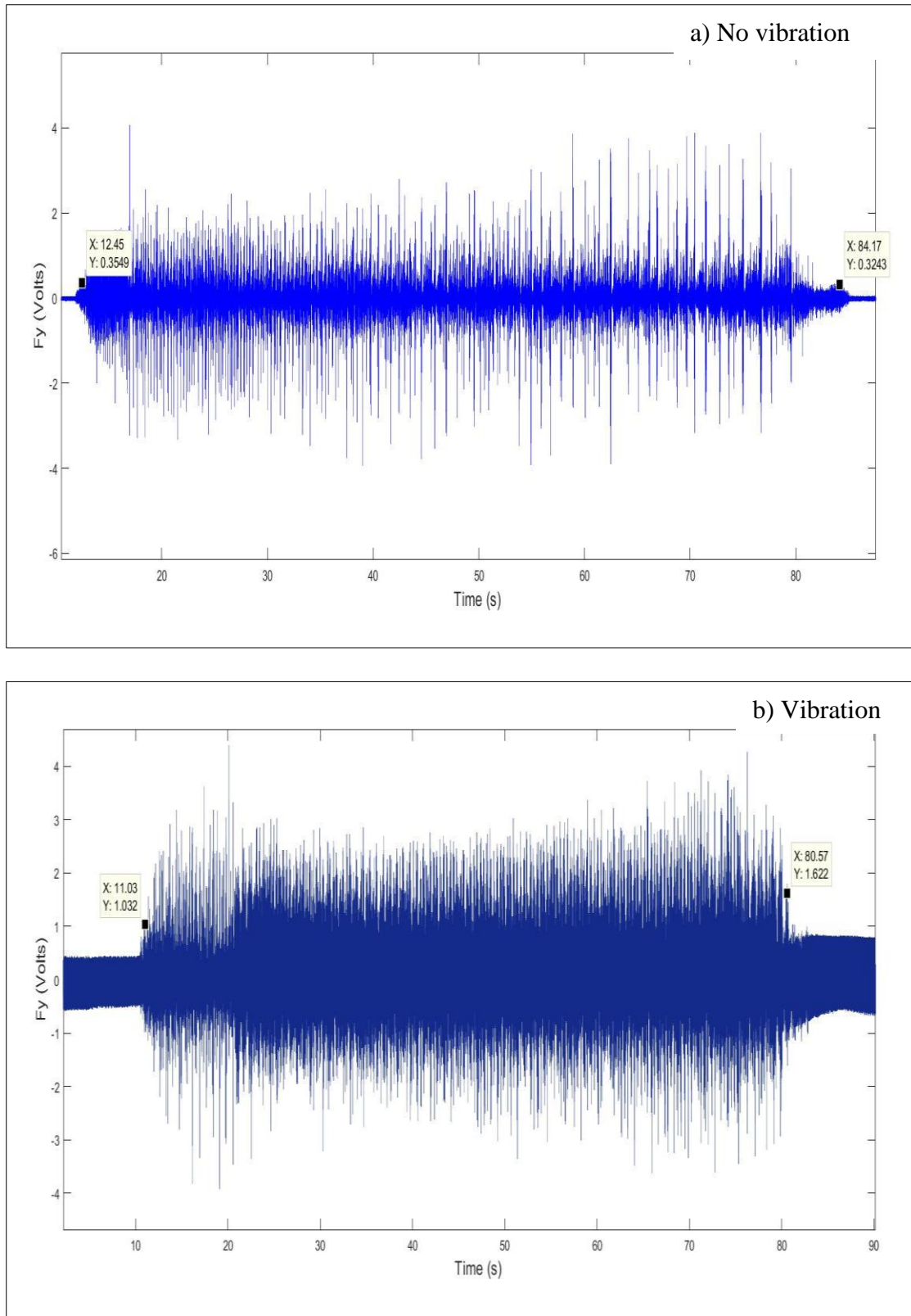


Figure 9. 18: Sample signals of Actual Machining: a) Conventional Milling. b) Vibratory Milling.

## 9.9 Remarks

From the results presented here, the following advantages of vibratory machining can be put forward:

- The application of vibratory milling decreased cutting forces, power, torque and improved the surface finish quality of the work-piece.
- The chips are, shorter and discontinuous.
- With vibration, the built up edge and tool wear has reduced, thus extending the tool life.
- In vibration assisted milling the values of the Machining Coefficient could be higher than in conventional milling especially with hard materials (steel). Thus, more material will be removed from the work-piece.
- Due to the vibratory milling, the tool edge removes or cuts more material from work piece than the conventional milling. Therefore, the time of the machining process can be shorter.

## Chapter 10

# Performance of the Closed Loop control System

## 10.1 Introduction

In this chapter, the experimental works deal with the control of vibration parameters during the vibratory milling process and the effect of the developed controller performance on the milling process is presented. In the previous chapter, the oscillation parameters such as frequency and amplitude were set before starting the vibratory milling process. However, it was not clear during machining or milling time whether the vibration parameters especially the vibration amplitude was affected by milling or cutting forces. In addition, this is the reason why the PID Closed Loop control procedure was used in this project.

Here, the vibration system or oscillation jig is driven at the desired frequency while the PID controller is controlling the amplitude of chosen force signals that is described in the next section. Moreover, this chapter gives a comparative study of conventional and vibratory modes with open loop and closed loop controllers. Here, the PID controller was designed and implemented in the closed loop condition. The performance of the PID controller is emphasised via putting side by side the results of open loop and closed loop control procedures.

In the experimental works of this chapter, the normal force  $F_z$ , cutting forces  $F_x$  and  $F_y$  that were used to calculate  $F_c$  (the resultant force in both directions X-axis and Y-axis) and surface roughness were measured for machining two materials, aluminium and mild steel. These measurement data allow calculating the power and torque of the milling process.

## 10.2 Experimental Approach

The PID closed loop control system was explained previously in chapter 7. After investigating all output signals from sensors such as the accelerometer and dynamometer, it was observed that the suitable output signal that can be used as a feedback signal is the measured force signal in X- axis direction ( $F_x$ ) as it has less noise than the accelerometer signals and it is measured in the same direction of oscillation. Therefore, the measured force signals, from Kistler dynamometer sensors, provided the feedback to the control loop. In the closed loop control experiment, the feedback signals were filtered with cut-off filter frequency of 100Hz. The Root Mean Square (RMS) values are calculated from filtered feedback signals. In chapter 5, the calibration results showed that at oscillation amplitude 200  $\mu\text{m}$  the RMS value of measured X-axis direction cutting force ( $F_x$ ) equals 0.35 Volt. Here, this RMS value of  $F_x$  cutting force feedback signals is used as a set point of the closed loop PID controller. Therefore, the PID controller will adjust the amplitude or the RMS values of the excitation signals to the signals generator in order to keep the set point value (0.35 Volt) constant during machining time regardless of milling forces applied to the work-piece.

Several experiments were performed using this closed loop control approach with the two materials. The experimental results were compared with those of the open loop control system and conventional milling.

Figure 10.1 shows the diagram of the closed loop control system developed and designed for this experimental work.

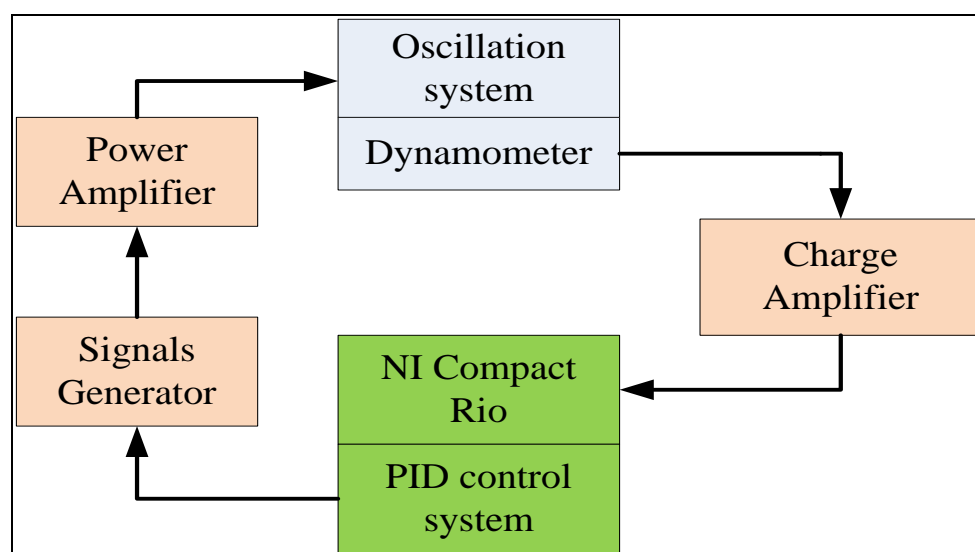


Figure 10. 1: Closed Loop Control System Configuration.

Table 10.1 represents the experiment parameters and machining conditions for the experimental works for this chapter.

**Table 10. 1: Experimental parameters for Vibratory Milling.**

<b>Milling parameters</b>	<b>Value</b>
Milling cutter type	Solid Carbide end mill (Coated: Ti 400)
Number of Teeth	3
Diameter	10 mm
Helix angle	45°
Rake angle	15°
Spindle Speed For Aluminium	6000 RPM
Spindle Speed For Steel	2300 RPM
Feed Rate For Aluminium	900 and 1800 mm/min
Feed Rate For Steel	50 mm/min
Cut type	Up Milling
Milling Condition	Dry and only air for Steel
Work-piece	Aluminium and mild Steel
Depth of cut for Aluminium	1 mm
Depth of cut for Steel	0.25, 0.5, 0.75 and 1.00 mm
Vibration Frequency	125 Hz
Sine wave Amplitude	3 Volts (positive peak)
Vibration amplitude	About 200 µm (positive peak)
PID Controller set point	0.35 Volt
PID Controller Parameters	P =0.31 , I = 4.62 & D =0.001

### 10.3 Performance of the closed loop PID Controller

In chapter 7, the design and implementation of the PID controller in closed loop mode was presented. Here, the PID controller used the feedback signals that come from the X-axis dynamometer forces sensor (value of  $F_x$ ) to control the amplitude of the oscillation and tried to keep it within set-point for the PID controller. In this chapter the PID controller worked in actual real machining time to quantify its effect on process performance.

Figures 10.2 and 10.3 show the output signals for measured forces in X- direction ( $F_x$ ) during machining time in open loop control as displayed in figure 10.2. Some errors in the stability of the system are seen in the signals where the amplitude is not stable. However, the Closed Loop PID controller was implemented to control with unity feedback thus it can fix the errors that happen during actual milling and under cutting forces disturbance. Then, it led to optimizing the system stability by keeping  $F_x$  force signal's amplitude within set-point value as seen in figure 10.3.

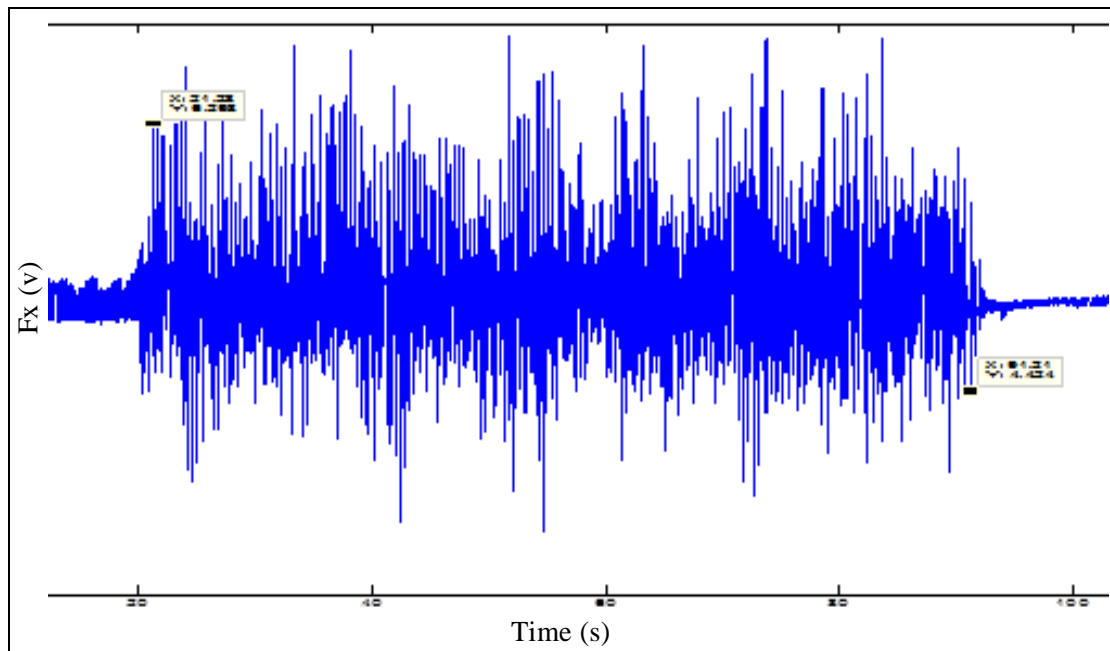


Figure 10. 2: Actual  $F_x$  Signals in Open Loop control mode.

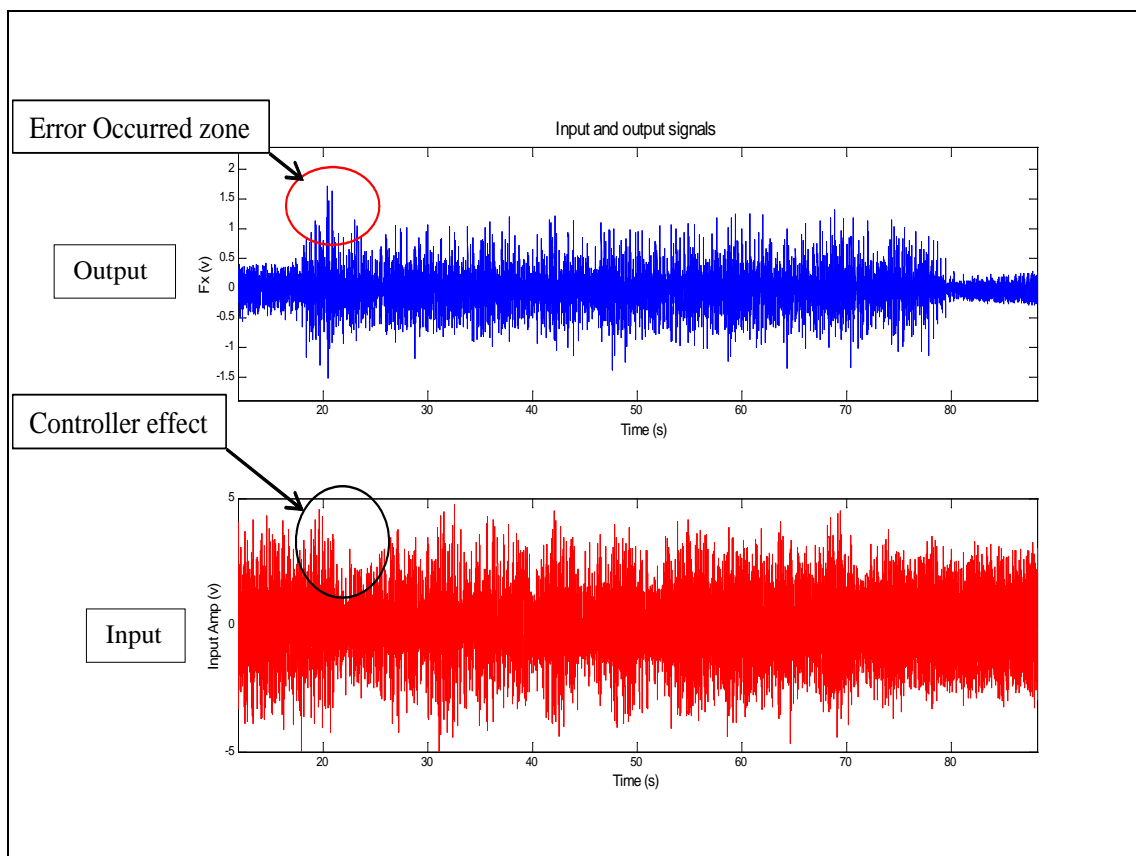


Figure 10. 3: Actual Input and Output Signals in Closed Loop Control Mode.

## 10.4 Milling Forces

Figures 10.4 and 10.5 show the variation of normal cutting force ( $F_z$ ) and Resultant cutting force ( $F_c$ ) during machining aluminium and mild steel. Here three sets of tests were used; Conventional Milling and Vibratory Milling with two modes, open loop and closed loop control.

In machining aluminium, the Normal cutting force in figure 10.4.a has been reduced by 23 % using vibratory milling with open loop control procedure. However, a further reduction of 13 % has been reached with the effects of closed loop PID controller giving a total improvement of 36%. The same reduction in Resultant cutting force ( $F_c$ ) has been reached in both control procedures; open loop control and PID closed loop control as seen in figure 10.4.b.

Figure 10.5 shows cutting forces after machining mild steel in terms of depth of cut using the machining parameters presented in table 10.1. Taking notice of the normal force results graph in figure 10.5.a, an obvious reduction is detected. This reduction reached the percentage of 49 % for normal cutting forces compared to conventional milling and 15 % compared to open loop control. However, the effect of the closed loop PID controller on resultant cutting forces resulted in 48 % reduction compared to conventional milling and 38 % compared to open loop control system as seen in figure 10.5.b. The reason behind this is that the PID control action was using feedback signals for one direction force value ( $F_x$ ) of resultant cutting forces as tracking point.

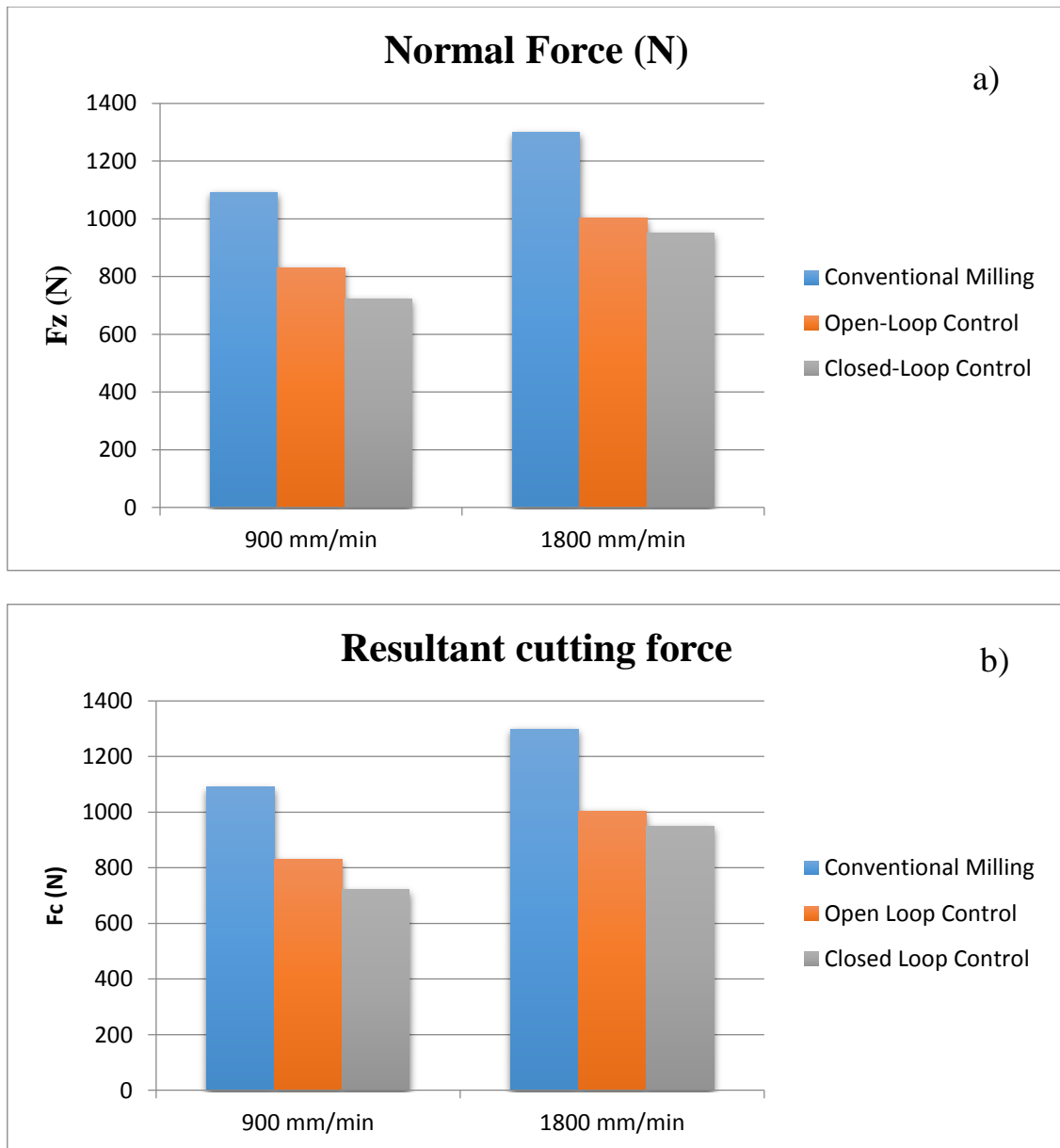
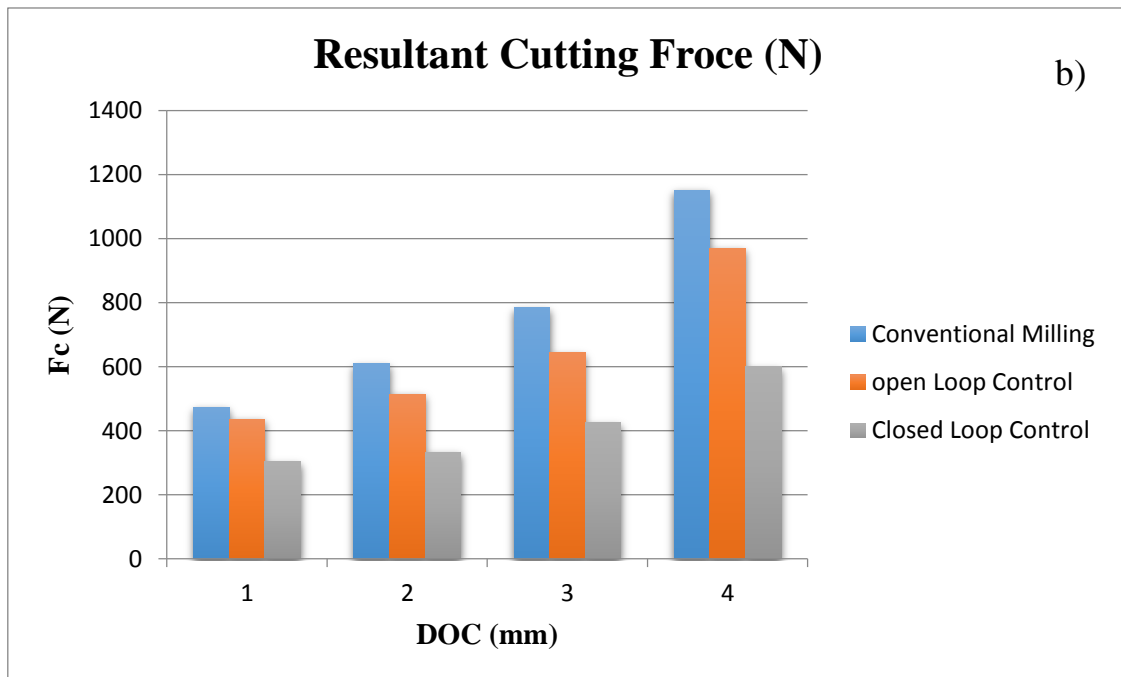
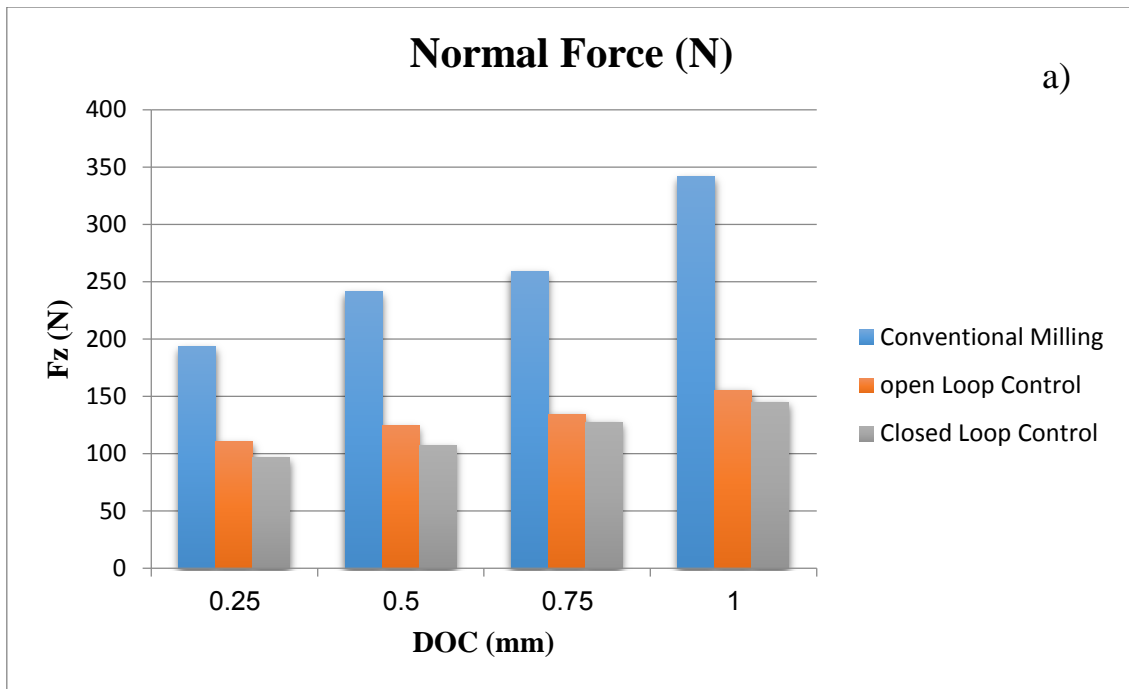


Figure 10. 4: Machining Aluminium Cutting Forces; a) Normal Force. b) Resultant force.



**Figure 10. 5: Machining Mild Steel Cutting Forces; a) Normal Force. b) Resultant Force.**

## 10.5 Milling Power and Torque

The Power and Torque have been calculated using equations 9.1 and 9.3 in chapter 9.

The results in figures 10.6 and 10.7 present the system performance in terms of Power and Torque for machining two kinds of material. As mentioned in table 10.1, for machining aluminium, only the feed rate was varied from 900 mm/min to 1,800 mm/min. However, the depth of cut has been changed in four steps from 0.25 mm to 1 mm when machining the mild steel work-piece.

Figure 10.6 presents the milling power for the aluminium work-piece (figure 10.6.a) and mild steel (figure 10.6.b) by putting side by side conventional milling, vibratory milling in open and closed loop control. Figure 10.6.a shows the reduction of milling power achieved by vibratory milling, there is a further 6 % reduction with the effect of closed loop PID controller. Moreover, in machining mild steel, the milling power has been reduced up to 21 % with the open loop control and up to 46 % with the closed loop PID control as seen in figure 10.6.b. Thus, more reduction in milling power up to 25 % was achieved using the closed loop control system.

The same results were achieved with milling torque in figures 10.7.a and 10.7.b. So, the PID controller keeps the cutting force in the average point. Here, the controller outcomes over the errors can lead to reduce milling torque and power.

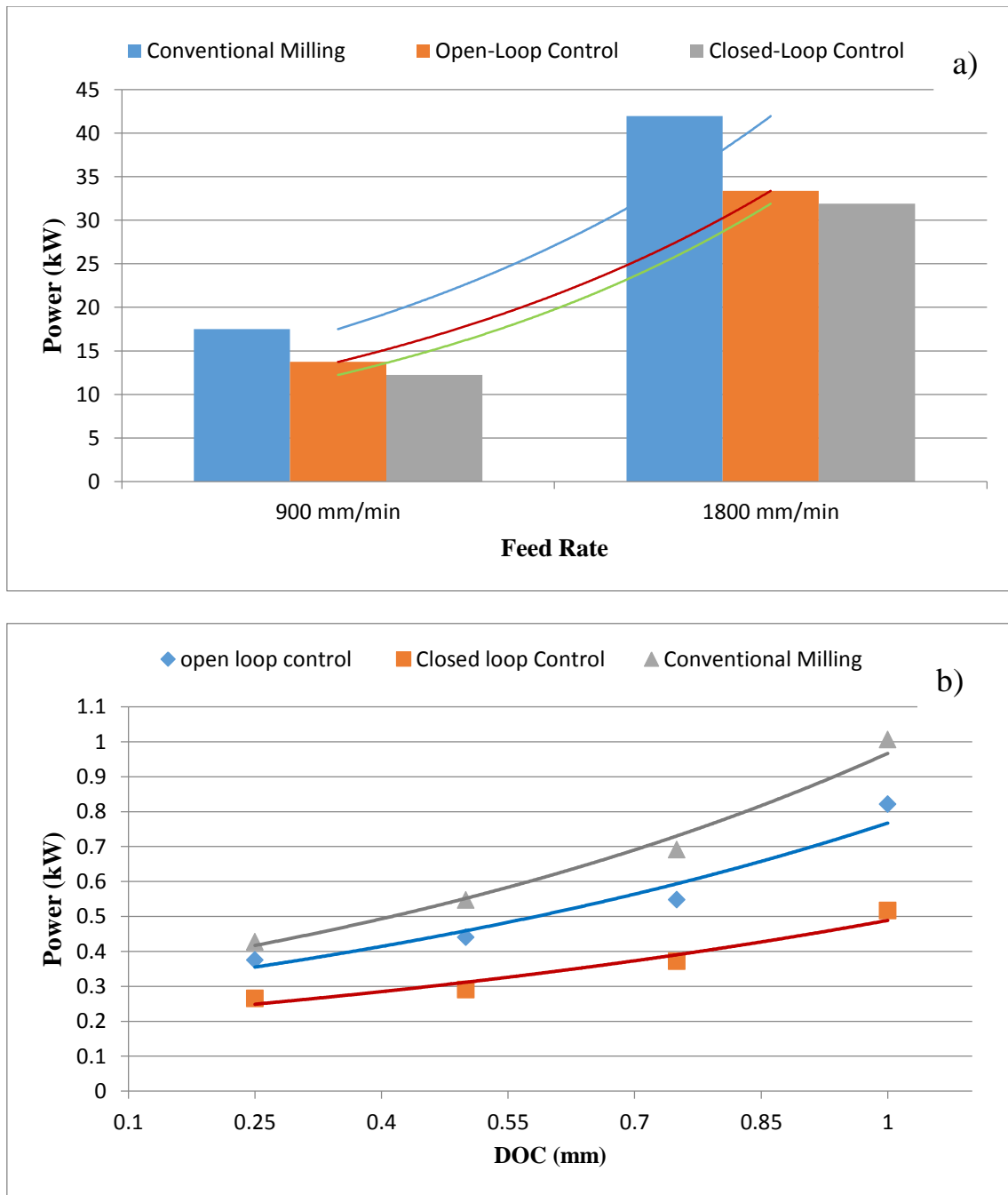


Figure 10. 6: Milling Power Consumption in Closed Loop Control mode, a) Aluminium. b) Steel.

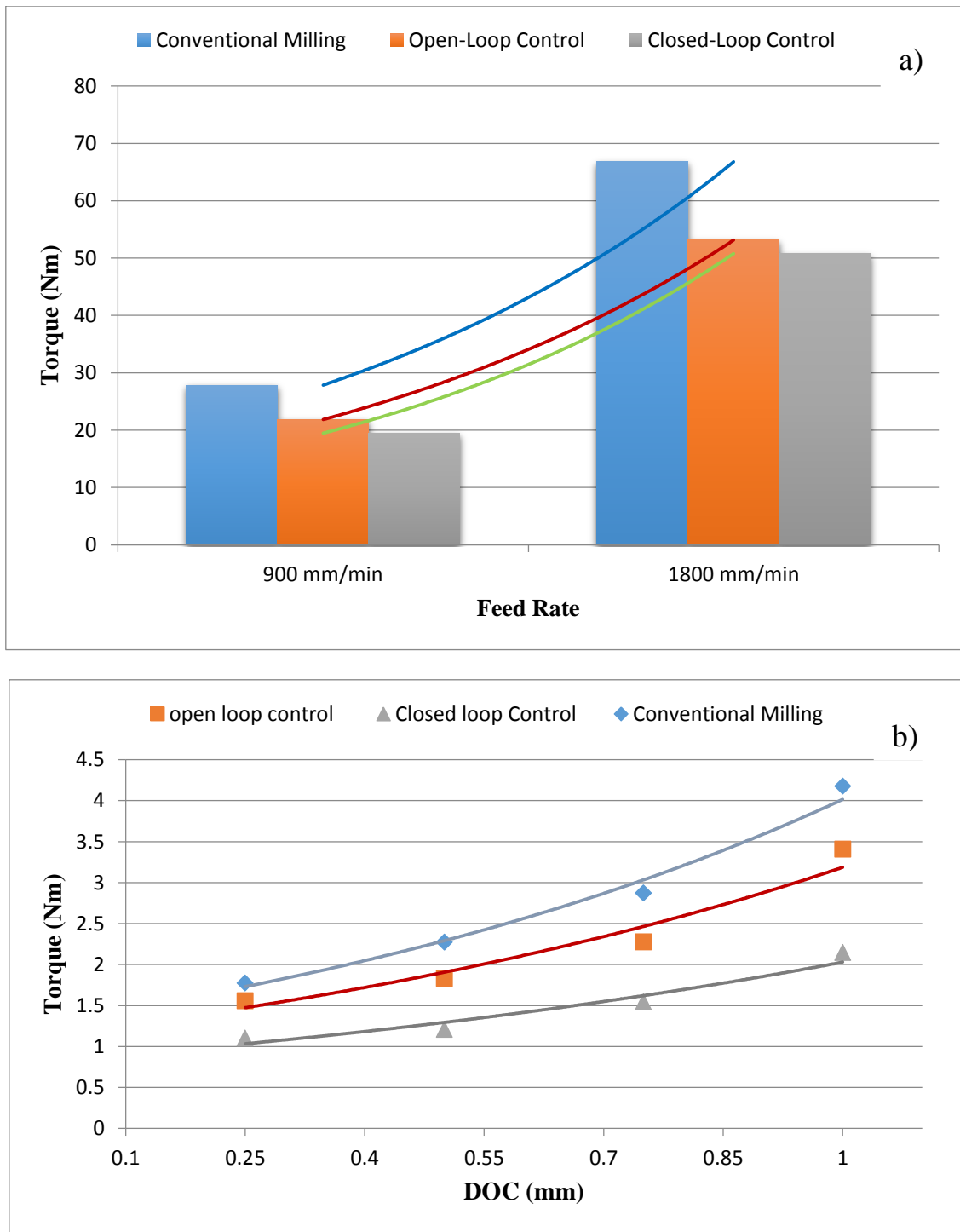


Figure 10. 7: Milling Torque in Closed Loop Control Mode: a) Aluminium. b) Mild Steel.

## 10.6 Surface Roughness

Figures 10.8 and 10.9 illustrate the surface roughness  $Ra$  and  $Rz$  during each milling trial for Aluminium (figure 10.8) and mild Steel (figure 10.9) for three machining conditions; conventional milling, open loop and closed loop control vibratory milling.

In figure 10.8, for Aluminium work-pieces, the surface roughness is better with high feed rate up to 1,800 mm/min as seen in this bar chart. The reason behind this point is that due to the nature of the work-piece, in soft material like Aluminium the modulus of elasticity is lower than in hard materials such as mild steel, so it needs faster cutting speed to cut properly as mentioned previously in chapter 9. The improvement was 37% compared to conventional milling. In addition, it was observed that there is further reduction in surface roughness values up to 6% over open loop control when the PID closed loop controller is used. Therefore, a better surface finish was obtained when application of closed loop control procedure applies to Vibratory milling.

An improvement of surface quality for the machined mild steel work-piece during vibratory milling with unity feedback PID control system was achieved and tended to be better with the increasing depth of cut as seen in figure 10.9. Here, the results indicate that the application of vibratory milling in both open loop and closed loop control techniques produced better surface finish than conventional milling. It can improve the surface roughness of the work-piece up to 52% and 24% in vibratory milling with open loop control technique.

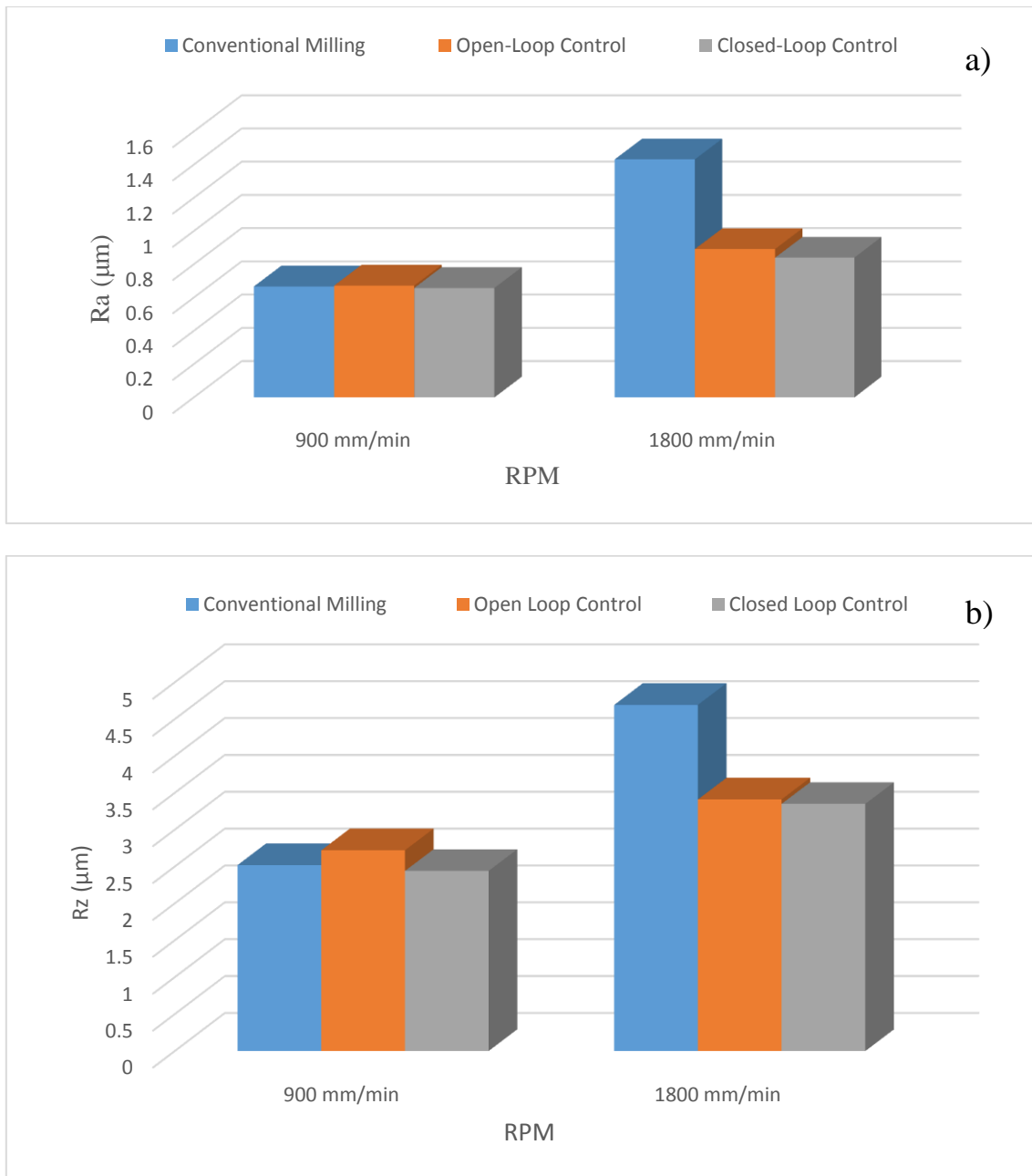


**Figure 10. 8: Surface Roughness for Machining Aluminium: a) Rz Value. b) Ra Value.**

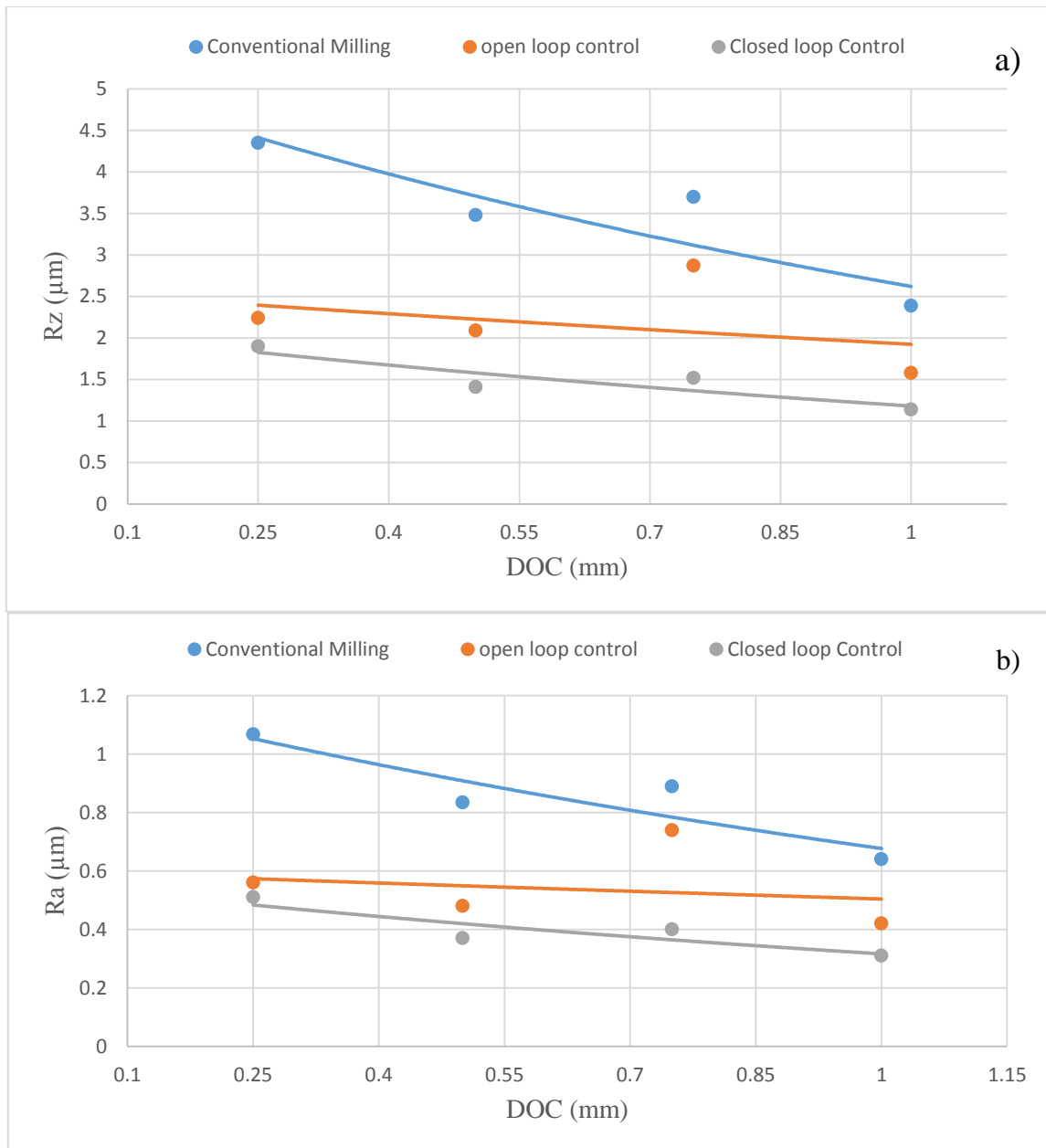
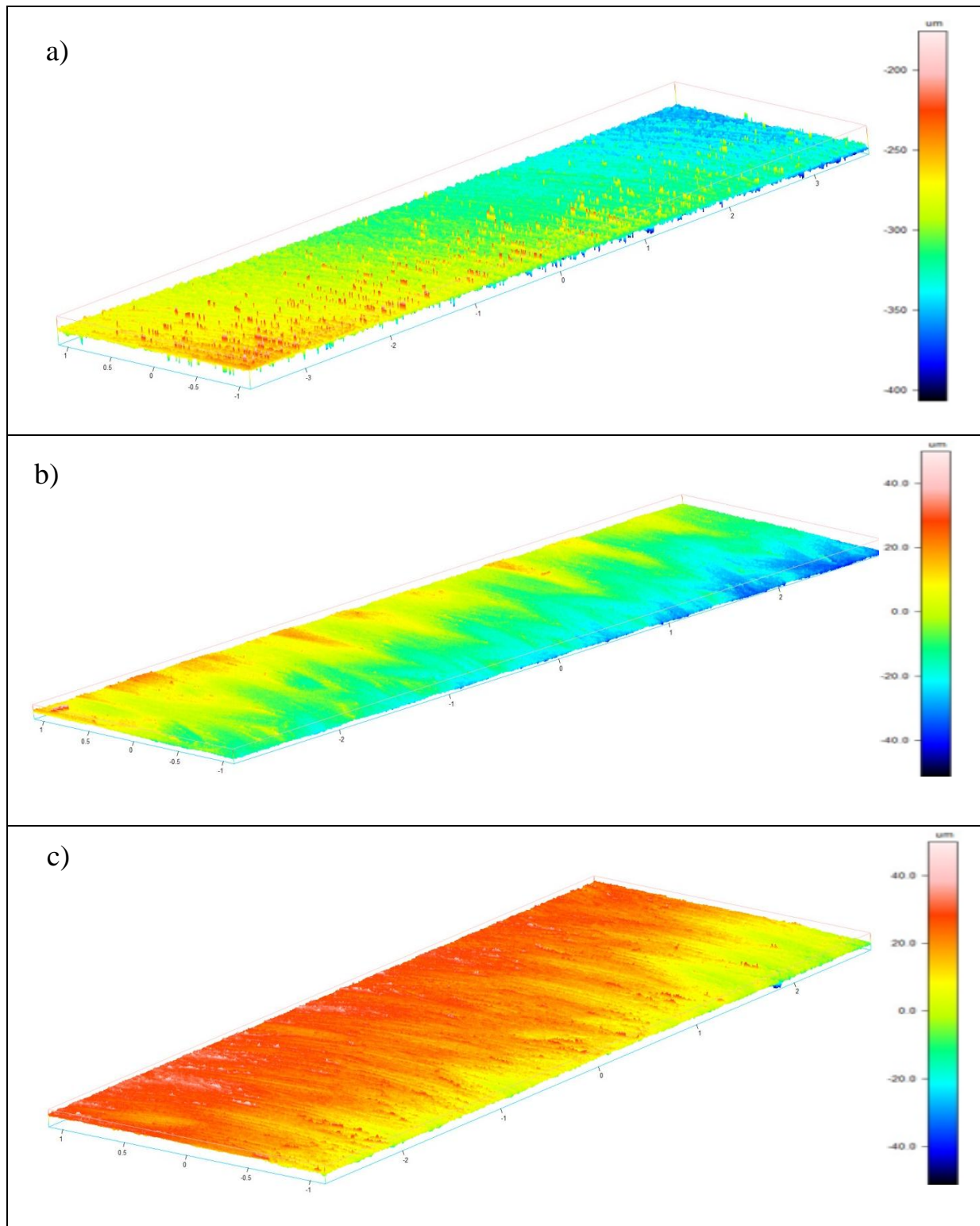


**Figure 10. 9: Surface Roughness for Machining Mild Steel: a) *Rz* Value. b) *Ra* Value.**

In Figure 10.10, the images show the machining surface measured by GFM 3D surface profile. Here, 3-D profile photos were taken after machining a Steel work-piece in three modes conventional, closed loop and open loop control vibratory milling. The machining parameters were spindle speed 2,300 RPM, 0.5 mm depth of cut and 50 mm/min feed rate. Figure 10.10.a displays the surface finish profile after conventional milling, but the cases of vibratory milling with open loop control and closed loop control are shown in figures 10.10.b and 10.10.c.

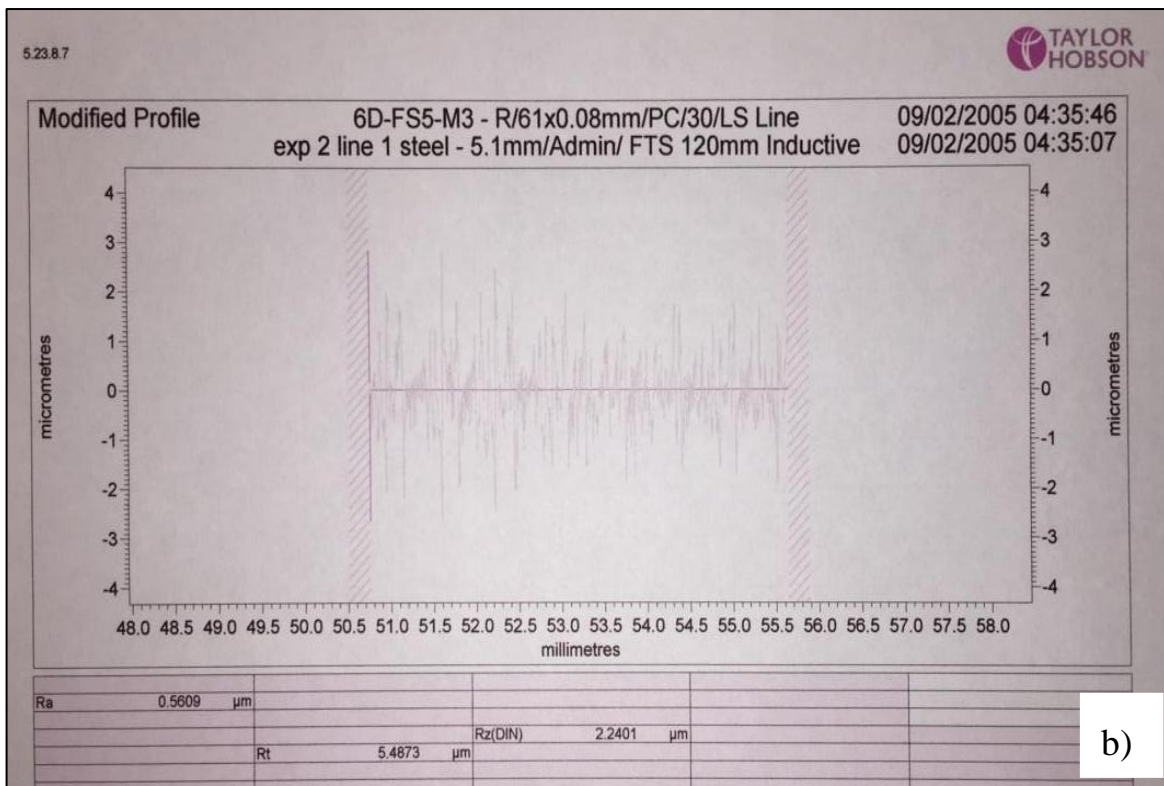
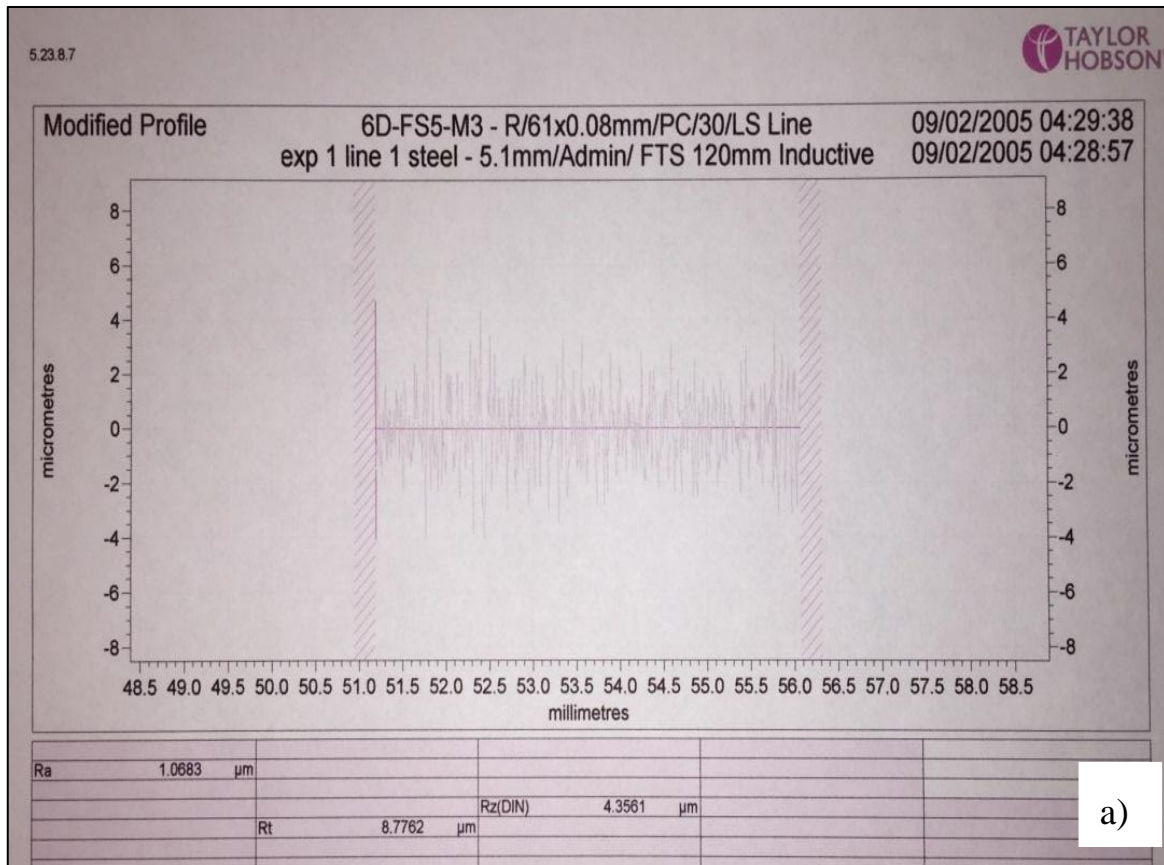
The surface finish profile in conventional milling was uneven and random with  $Ra$  value of  $0.83\ \mu\text{m}$ , but with vibratory milling, the surface finish profile was more uniform with surface roughness value  $Ra$  equals  $0.48\ \mu\text{m}$ . A better uniform surface with the closed loop PID controller effect gave  $Ra$  value equals  $0.37\ \mu\text{m}$  as seen in figure 10.10.c.

Figure 10.11 shows another example of work-piece surface finish profile which was measured using the Taylor Hobson device. The material of the work-piece was mild steel. The machining parameters were 0.25 mm for depth of cut, 2,300 RPM for spindle speed and 50 mm/min for feed rate. The reports in figure 10.11.c prove physically that there is improvement in finish surface quality with the application of vibratory milling. The best improvement was achieved by using the PID closed loop control procedure with surface roughness  $Rz$  value equals  $1.9\ \mu\text{m}$ . However, for open loop control procedure and conventional milling it was equal 2.24 and  $4.35\ \mu\text{m}$  respectively as seen in figures 10.11.a and 10.11.b.



**Figure 10. 10: 3D surface finish profile: a) Conventional Milling. b) Open Loop Control Vibratory Milling. c) Closed Loop Vibratory Milling.**

Chapter 10 Performance of the Closed Loop control System



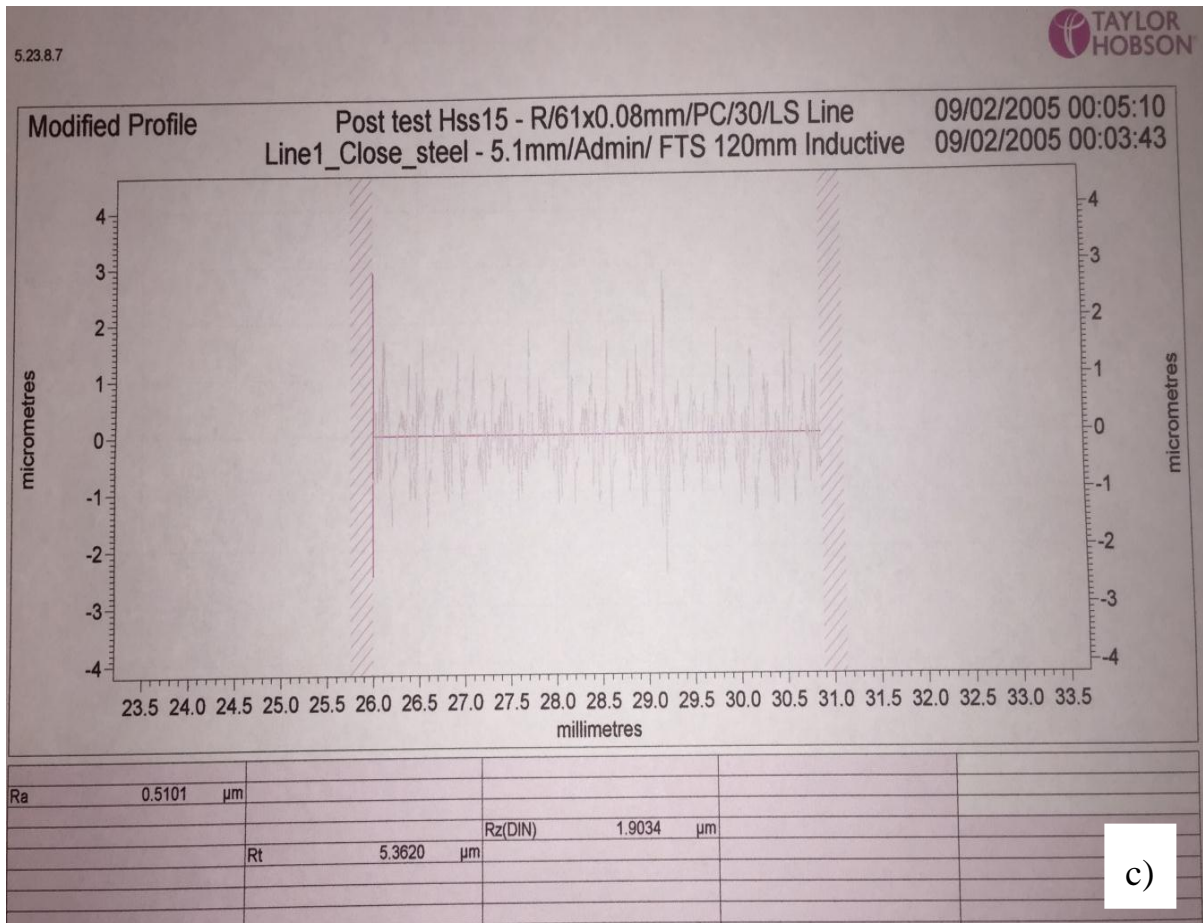


Figure 10. 11: Surface Finish Profile for mild Steel Work Piece: a) Conventional Milling. b) Open Loop Control Vibratory Milling. c) Closed Loop Vibratory Milling.

## 10.7 Remarks

In this study, the PID closed loop controller has been successfully designed and implemented to the application of vibratory milling. For faster feedback control response, the FPGA and Real time LabVIEW application were designed and used to control the vibration stage. In this experimental work the cutting force  $F_x$  was used as feedback tracking signals for the PID controller. One main advantage of using PID closed loop control is that the controller can control vibration amplitude regardless of any externally applied force or disturbance.

The following advantages were observed:

1. The experimental set of PID closed loop controller showed a clear benefit of this system over the open loop control procedure.
2. The PID closed loop controller can reduce cutting force up to 38 % over the open loop and up to 48 % over conventional milling.
3. A successful reduction of milling power has been reached with the closed loop PID control system up to 46 % comparing to conventional milling.
4. An improvement in surface roughness has been observed in vibratory milling when using the closed loop control system more than using the open loop control system in both materials Aluminium (6%) and mild Steel (24%).

# **Chapter 11**

## **Conclusions and Recommended Further Works**

## 11.1 Conclusions

The main aims of this project were to design a controller to gauge the vibration amplitude of vibratory milling process during machining and to investigate the effect of low frequency superimposed vibration of the work-piece.

Amplitude or displacement calibration was obtained for vibration system to identify the relationship between the applied voltage with frequency and displacement. An Eddy current sensor was used for displacement calibration tests for its high accuracy, less noise and small size.

The experimental works of calibration process revealed that the optimum driving voltage was 3 volts with optimum driving frequency equals 125 Hz.

Process Identification was carried out for the characteristics of the static and dynamics for the spindle unit of the CNC machining. Here, the stiffness and natural frequency of the spindle unit were obtained using experimental works which include an impact hammer test and harmonic excitation force test using piezoelectric actuator. In addition, the natural frequency of the milling machine's spindle unit was identified at frequency about 100 Hz and this frequency value should not be applied into vibration system during vibratory milling process.

The static stiffness and compliance of the milling machine's spindle unit were obtained using external force that was applied into the spindle nose. The results of the force deflection show the relationship between the external force and deflection of spindle unit. Also, these results observed a linear relationship with average value of stiffness about  $K= 24.68 \text{ N}/\mu\text{m}$  and compliance value about  $C_s= 0.04 \mu\text{m}/\text{N}$ .

Moreover, as excitation frequency approaches with the resonant frequency of the spindle unit (100 Hz), the spindle unit has the lowest stiffness and highest compliance value. Therefore, this resonant frequency should be avoided during vibratory milling process.

The vibration system was identified using observed data. The PID controller was designed and simulated successfully for controlling vibration amplitude of oscillation system. the set point of the controller was the recommend value of displacement amplitude (200  $\mu\text{m}$ ).

In addition, the simulation results show a good performance for PID controller with the best characteristics of step response performance such as rise time and overshoot.

The PID controller has been tuned successfully and its parameters were obtained using Matlab software and satisfied the requirements of the vibration system.

For experimental works, the faster real-time response system was used for data acquisition system and controlling the vibration system during vibratory milling process. This includes FPGA and Real-time applications that allowed embedding PID controller into vibration system to control the vibration amplitude during actual machining time. This is fundamentally a new development to control the oscillation amplitude by tracking the errors inside the cutting zone during machining process and this has never been done before.

During experimental works of machining work-pieces of aluminium and soft steel in open loop control system, the following points were observed:

- In the application of vibratory milling there was an average decreasing about 25% in cutting forces comparing to conventional milling.
- There is an improvement in milling coefficient up to 46% when using vibratory milling application rather than conventional milling with improved the material removal.
- In surface finish quality, there is an overall improvement for both materials aluminum and mild steel up to 25% compare to conventional milling.
- The chip in vibratory milling application are smaller, shorter and thinner than using conventional milling.
- The build-up edges increased the cutting forces but protect the tool edge in conventional milling. However, vibratory milling does not load the tool continuously, as intermittent cutting releases cutting edge, thus it extends tool life.
- Vibratory milling mode reduces the machining time comparing to conventional milling. This is one key element that is not mentioned elsewhere in literature. The reason behind that is the vibratory milling allow cutting edge removes more materials than conventional milling.

The PID closed loop control system was successfully implemented into vibratory milling process. Here, the PID controller use the feedback signals that come from forces sensor during machining process. The PID control action with unity feedback was successful in tracking and fixing the errors on the vibration amplitude. The PID control action helps to retain the stability of the cutting forces and control the actual vibration amplitude. For the first time in vibratory milling, a closed loop control is used control inside the cutting zone.

The PID closed loop control system secured a further reduction in milling cutting forces than open loop control system. This reduction was 35% less than vibratory milling with open loop control system. Here, the PID controller with unity feedback signals kept the cutting force around the average point.

The PID control action to kept the cutting forces stable, leading to an improvement in finish surface quality of the work-pieces more than using the open loop control system. The surface roughness of work-piece was improved up to 52% referring to conventional milling and up to 24% of vibratory milling with reference to open loop control system.

The application of vibratory milling reduces forces by a reduction in chip thickness and in vibratory milling the chips are smaller so the machining time and cutting forces required in vibratory milling are only that necessary to remove the smaller volume of chip compared to conventional milling.

## 11.2 Recommendations for future work

Some recommendations for further work are listed as follow:

- Further investigation on vibratory milling with a range of vibration frequency and amplitude to obtain the optimum point for vibratory milling process.
- Design and manufacturing a 2-D vibration system in order to produce elliptical motion in vibratory milling.
- Design, develop and implement 2-D PID controller with closed loop system which can allow controlling vibration amplitude in elliptical motion.
- Investigate a full study of oriented elliptical amplitude for vibratory milling to characterise the 2-D vibration system.
- Investigation into various work materials, along with a wide range of cutting tool..

# References

## Reference

- Astashev, V.K. and Babitsky, V.I., 2007. Processes in ultrasonic systems. *Foundations in Engineering Mechanics*, pp.131–194.
- Abuthakeer, S.S., Mohanram, P. V. and Mohankumar, G., 2011. Static and dynamic performance improvement of conventional computer numerical control machine tool bed with hybrid welded steel. *American Journal of Applied Sciences*, 8(6), pp.610–616.
- Altintas, Y. and Weck, M., 2004. Chatter Stability of Metal Cutting and Grinding. *CIRP Annals - Manufacturing Technology*, 53(2), pp.619–642. Available at: <http://www.sciencedirect.com/science/article/pii/S0007850607600328>.
- Andersson, L., 1998. A manual for system identification. ... *Identification. KF ...*, pp.1–8. Available at: [http://automatica.dei.unipd.it/public/Schenato/PSC/2010\\_2011/gruppo4-Building\\_termo\\_identification/IdentificazioneTermodinamica20072008/Biblio/Articoli/a manual for system identification.pdf](http://automatica.dei.unipd.it/public/Schenato/PSC/2010_2011/gruppo4-Building_termo_identification/IdentificazioneTermodinamica20072008/Biblio/Articoli/a manual for system identification.pdf).
- Archenti, A. et al., 2012. A new method for circular testing of machine tools under loaded condition. *Procedia CIRP*, 1(1), pp.575–580. Available at: <http://dx.doi.org/10.1016/j.procir.2012.05.002>.
- Astashev, V.K. and Babitsky, V.I., 2007. Processes in ultrasonic systems. *Foundations in Engineering Mechanics*, pp.131–194.
- Astrom, Karl J. and Hagglund, T., 1994. *PID controllers : Theory, Design and Tuning* Second edition., Research Triangle Park: Instrument society of America.
- B. Wayne Bequette, 2003. *Process Control: Modeling, Design, and Simulation* M. V. Argosy, ed., Upper Saddle River, New Jersey 07458: Bernard Goodwin.
- Babitsky, V.I., Mitrofanov, A. V. & Silberschmidt, V. V., 2004. Ultrasonically assisted turning of aviation materials: Simulations and experimental study. In *Ultrasonics*. pp. 81–86.
- Boisson, J. et al., 2014. Analytical approach for mechanical resonance frequencies of high-speed machines. *IEEE Transactions on Industrial Electronics*, 61(6), pp.3081–3088.
- Bonifacio, M.E.R. & Diniz, A.E., 1994. Correlating tool wear, tool life, surface roughness and tool vibration in finish turning with coated carbide tools. *Wear*, 173(1–2), pp.137–

## References

144.

- Brehl, D.E. and Dow, T.A., 2008. Review of vibration-assisted machining. *Precision Engineering*, 32(3), pp.153–172.
- Campa, F.J., Lopez De Lacalle, L.N. & Celaya, A., 2011. Chatter avoidance in the milling of thin floors with bull-nose end mills: Model and stability diagrams. *International Journal of Machine Tools and Manufacture*, 51(1), pp.43–53. Available at: <http://dx.doi.org/10.1016/j.ijmachtools.2010.09.008>.
- Chern, G.L. and Chuang, Y., 2006. Study on vibration-EDM and mass punching of micro-holes. *Journal of Materials Processing Technology*, 180(1–3), pp.151–160.
- D’Azzo, J. and Houpis, H., 1966. *Feedback Control System Analysis and Synthesis* second edition., McGraw-Hill College.
- Denkena, B., Litwinski, K.M. and Boujnah, H., 2016. Detection of tool deflection in milling by a sensory axis slide for machine tools. *Mechatronics*, 34, pp.95–99. Available at: <http://dx.doi.org/10.1016/j.mechatronics.2015.09.008>.
- Endo, T., Tsujimoto, T. and Mitsui, K., 2008. Study of vibration-assisted micro-EDM-The effect of vibration on machining time and stability of discharge. *Precision Engineering*, 32(4), pp.269–277.
- EWAD, H., 2015. *Development of A closed Loop Control System for Vibration Assisted Grinding*. Liverpool John Moores University.
- Frankowski, G. and Hainich, R., 2009. DLP-Based 3D Metrology by Structured Light or Projected Fringe Technology for Life Sciences and Industrial Metrology. *Emerging Digital Micromirror Device Based Systems and Applications*, 7210, p.72100C–72100C–12. Available at: <http://proceedings.spiedigitallibrary.org/proceeding.aspx?articleid=809222>.
- GFM\_3D, 2012. Optical 3D surface analysis GFM. Available at: <http://www.gfm3d.com>.
- Ikawa, N. et al., 1991. An Atomistic Analysis of Nanometric Chip Removal as Affected by Tool-Work Interaction in Diamond Turning. *CIRP Annals - Manufacturing Technology*, 40(1), pp.551–554.

## References

- Kalpakjian, S. and Schmid, S.R., 2010. *Manufacturing Engineering and Technology*,
- King, R. I., Hahn, R.S., 1986. *Modern Grinding Technology*, New York, USA: Chapman and Hall.
- Kistler Instrument Croup, 2017. 3-Component Dynamometer with integrated electronics Type 9257BA. Available at: <https://www.kistler.com/us/en/>.
- Koura, M.M.F., Zamzam, M.L. and Shaaban, A.A.S., 2014. Simulation approach to study the behavior of a milling machine's structure during end milling operation. *Turkish Journal of Engineering and Environmental Sciences*, 38(2), pp.167–183.
- Liu, X. and Cheng, K., 2005. Modelling the machining dynamics of peripheral milling. *International Journal of Machine Tools and Manufacture*, 45(11), pp.1301–1320.
- Mao, K. et al., 2010. Stiffness influential factors-based dynamic modeling and its parameter identification method of fixed joints in machine tools. *International Journal of Machine Tools and Manufacture*, 50(2), pp.156–164.
- Matsumura, T. and Ono, T., 2008. Cutting process of glass with inclined ball end mill. *Journal of Materials Processing Technology*, 200(1–3), pp.356–363.
- micro-epsilon, 2016. The Eddy NCDT 3010 S2 Current Sensor. Available at: [www.micro-epsilon.co.uk](http://www.micro-epsilon.co.uk).
- Mitrofanov, A. V., Babitsky, V.I. and Silberschmidt, V. V., 2004. Finite element analysis of ultrasonically assisted turning of Inconel 718. *Journal of Materials Processing Technology*, 153–154(1–3), pp.233–239.
- Moriwaki, T., Shamoto, E. and Inoue, K., 1991. Ultra-Precision Diamond Turning of Stainless Steel by Applying Ultrasonic Vibration. *Journal of the Japan Society for Precision Engineering*, 57(11), pp.1983–1988.
- National Instruments UK, 2011. Introduction to LabVIEW Real -Time and FPGA. Available at: <ftp://ftp.ni.com/pub/events/nits/presentations/2010/IntrotoLabVIEWandRTFPGA.pdf>.
- National Instruments UK, 2017. What Is the CompactRIO Platform. Available at: <http://www.ni.com/compactrio/whatis/>.
- Ogata K., 2010. *Modern Control Engineering* Fifth Edition. Marcia J. Horton, ed., United States of America: Prentice Hall.

## References

- Phillips C. L., 2000. *Feedback Control Systems* 4th Edition. Royce D. Harbor, ed., University of West Florida: Emeritus, Auburn University. Available at: 9780139490903.
- Physik Instrumente (PI) GmbH & Co. KG, 2017. P-212 PICA Power Piezo Actuator. Available at: <https://www.physikinstrumente.com/en/products/piezoceramic-actuators/stack-actuators/p-212-pica-power-piezo-actuator-101550/>.
- Prakosa, T., Wibowo, A. and Ilhamsyah, R., 2013. Optimizing Static and Dynamic Stiffness of Machine Tools Spindle Shaft ,. , 20(4), pp.0–7.
- The WNT Group, 2014. *Total Tooling = Quality and Service*, Available at: <https://www.wnt.com/uk.html>.
- W. Brian Rowe, 2013. *Principles of Modern Grinding Technology*,
- Xin-hong, Y. et al., 2006. Research on Ultrasonic Vibration Grinding of the Hard and Brittle Materials. *Chinese Journal of Aeronautics*, 19, pp.9–13.
- Zahoor, S. et al., 2016. Effect of machine tool ' s spindle forced vibrations on surface roughness , dimensional accuracy , and tool wear in vertical milling of AISI P20. *The International Journal of Advanced Manufacturing Technology*. Available at: <http://dx.doi.org/10.1007/s00170-016-9346-1>.

# Appendix

## Appendix

### A-1 Equipment

#### Milling Tool

For experimental works the End milling cutter tools were used to cut the work-pieces. These tools are coated by Titanium (Ti 400) with 10 mm diameter. It is also named as High Speed Coated Ti 100. For comparison purposes, two cutting tools were used for conventional and vibratory milling with the same Rake angle, Helix angle, Diameter and number of cutting teeth.

Figure A.1 shows the actual image of End milling cutter, also its specifications and geometrics is listed in table A.1.



**Figure A. 1: The End Milling Cutter Tool.**

**Table A. 1: End-Milling Cutting tool Specifications (The WNT Group 2014).**

Parameters	Value
Tool Name	Solid Carbide End Milling Cutter High Speed Steel (HSS)
Coated	Titanium (Ti 100)
Application Temperature	800° C
Number of teeth	3
Helix Angle	45°
Rake angle	15°

Tool Diameter	10 mm
---------------	-------

**Machining tool specifications**

Tool name: Solid Carbide end milling cutter

Coated tool: Ti 400.

Number of teeth: 3

Helix angle ( $\lambda_s$ ) = 45°      Rake angle = 15°      Diameter = 10 mm.

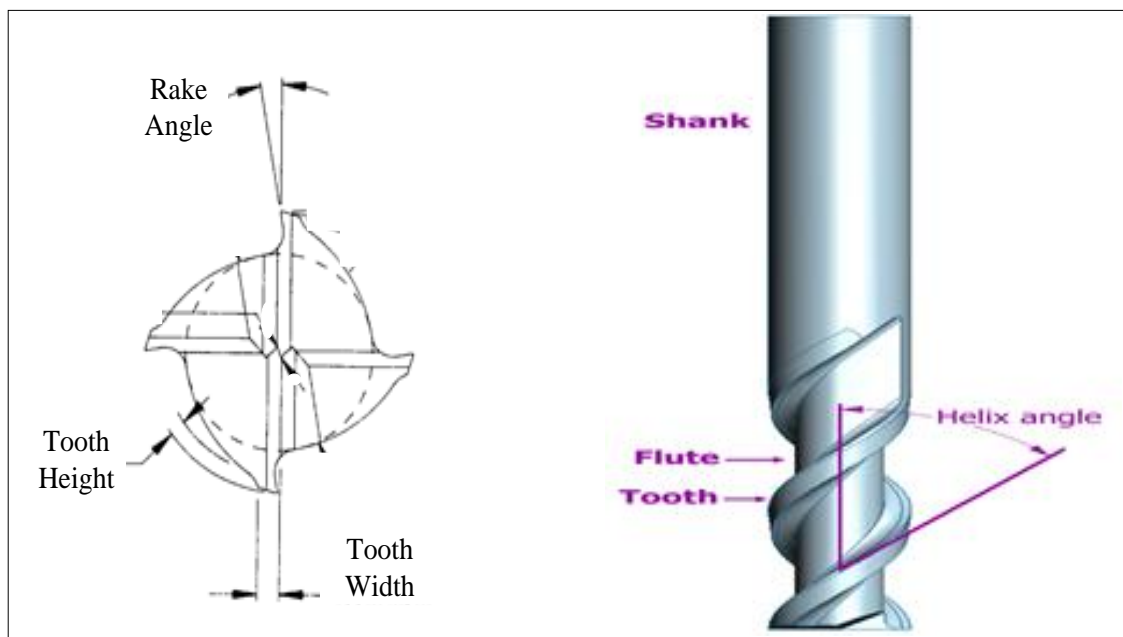


**Figure A. 2: Milling tool geometry (Rocketmagnet, 2007)**

**Accelerometer**

The most commonly used sensors for measuring vibration responses of structures is the accelerometer. The accelerometer used for the experimental works was a Kistler 8704B100 (figure A.3) and this sensor has low base strain, low thermal transient response, voltage mode, low impedance and is lightweight.

The signal of the accelerometer was recorded using the NI 9233 dynamic signal acquisition module that was mounted into an NI Compact Rio 9022 chassis.

Table A.2 shows the specifications of the accelerometer sensor.



**Figure A. 3: The accelerometer Kistler 8704B100**

**Table A. 2: Kistler Accelerometer Specifications**

Parameters	Value
Measurement Range	$\pm 100$ g
Frequency Response $\pm 5\%$	0.5 kHz – 10 kHz
Sensitivity $\pm 5\%$	50 mV/g
Operating Temperature	$-54^{\circ}$ C – $100^{\circ}$ C
Housing Base	Titanium
Weight	8.6 Grams

## Displacement Sensor

The Eddy NCDT 3010 S2 current sensor was used in this project to measure the actual displacement or amplitude of oscillation when the work-piece holder system is vibrated. This sensor is a non-contacting displacement measuring system based on the eddy current principle. It can only measure displacement from the targets that are made of electrical conductive materials such as aluminium and steel which may be either ferromagnetic or non-ferromagnetic.

The eddy current can be operated in an environment with a temperature range between  $-50^{\circ}$  C and  $150^{\circ}$  C. This sensor also can measure a displacement range up to 2 mm with resolution of

## Appendix

0.1  $\mu\text{m}$ . Table A.3 displays more specifications and technical data for the Eddy NCDT 3010 S2 current sensor (micro-epsilon 2016).

The system structure of the eddy current displacement sensor is a compact, single channel system consisting of an eddy current sensor, a sensor connecting cable and a charge amplifier as seen in figure A.4.

**Table A. 3: The specifications of Eddy NCDT 3010 S2 current sensor.**

<b>Technical Data</b>	<b>Value</b>
Measuring Range	2 mm
Offset Distance	0.2 mm
Linearity	$< \pm 0.25\% \text{ FSO}$
Resolution	0.1 $\mu\text{m}$
Frequency Response	25 kHz
Temperature Range	-50 to 150 °C
Temperature Stability ( $\leq$ midrange)	$< 0.05\% \text{ FSO}$
Signal Voltage Output	From 0 to 10 Volts
Signal Current Output	From 0 to 10 mA
Power Supply	24 VDC
Sensor Weight	9 grams



**Figure A. 4: System structures of the Eddy current sensor. a) Eddy Sensor. b) Amplifier.**

## Oscilloscope

In applications of science and engineering, the Oscilloscope is used as diagnostic equipment and it can be classified as one of the most important pieces of equipment for many experimental works. In this device the electrical voltage can be displayed as a function of time, also the Oscilloscope can obtain voltage versus time and the picture of electrical signals.

Some points can be evaluated using the Oscilloscope such as:

1. Display the signals of voltage with varied time.
2. Evaluate the noise extant into the measured signals and the noise value changes.
3. The frequency signals calculations.

In this project, the Oscilloscope was used to obtain and validate the output signals from the controller and sensors during conventional and vibratory milling. Figure A.5 displays the image of Tektronix oscilloscope that carried model number TDS 3054 which was used in the experimental works of this project. It has four input channels with four different display colours.



Figure A. 5: Tektronix Oscilloscope

## Surface Roughness Measurement Device

In this project, three measurement devices were used to measure the surface roughness and give the image profile of the finished work-piece surface.

### Taylor-Hobson Measurement Device

Figure A.6 shows the Subtonic Couple of Taylor-Hobson surface roughness measurement device. It was used to measure the surface roughness of the work-pieces after milling experiments. It was only used on the experimental works of preliminary studies. The main parameters of surface roughness such as Ra, Rz and Rt can be measured using this measurement device.

The Taylor-Hobson measurement device contained two parts; top and bottom. In the upper part, there is a controller and display screen which can calculate and display the key parameters of the surface roughness. However, the bottom part of the device has a diamond stylus that could draw across the work-piece. To ensure that the required horizontal distance was travelled for passable measurement, the traverse mechanism should be well driven.



Figure A. 6: The Taylor-Hobson surface roughness measurement device

### **Surface Texture Analysis Device**

In this project, another contact measurement device called the Form Talysurf Series 120 surface analysis was used in the main sections of the experimental works. Here, this device can provide a wide range of functionality and more accurate results. It is also used to measure the surface roughness for machined work-pieces in further experimental works after the experimental works of preliminary studies.

The Form Talysurf Series 120 consists of the following structures:

- A column which provides a stable mounting for the traverse unit and also allows for precise height and angle adjustment.
- An epoxy granite base to ensure a firm support of the column and work-piece.
- A control module which all the moving parts are connected to. So, the units could be controlled manually.

Figure A.7 shows the whole configuration of the Form Talysurf Series 120 device.

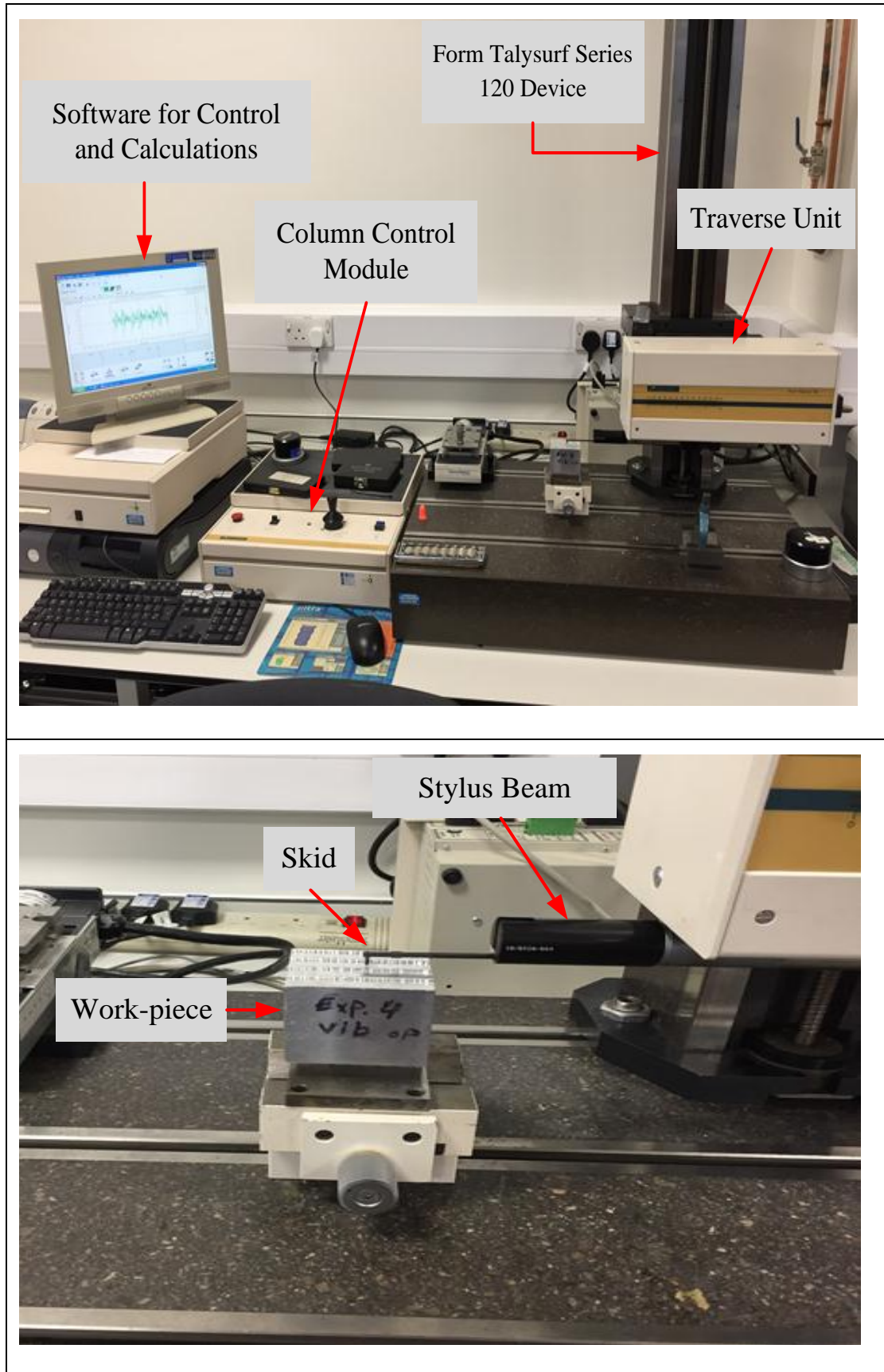


Figure A. 7: The Form Talysurf Series 120 Surface Analysis Instrument

### **3D GFM Surface Profiler**

The surfaces of the machined work-pieces were also measured using 3D GFM Surface Profiler to provide a 3D surface finish imaging. This device is a contactless device as seen in figure A.8.

The 3D GFM Mikro CAD device is widely used in surface profile tests. In addition, this device used a high speed camera to capture the distorted fringes, and it can measure the phase shift of fringes at each pixel level (Frankowski & Hainich 2009).

The 3D GFM Mikro CAD instrument has a single camera which can provide a fixed view field. Here are some technical specifications for this device (GFM\_3D 2012):

- 100 mm Stand-off distance
- 13 mm X 8 mm Field of View
- 1  $\mu\text{m}$  Vertical Resolution
- 17.3  $\mu\text{m}$  Lateral Resolution

The whole configuration of the 3D GFM Mikro CAD instrument is presented in figure 4.15.

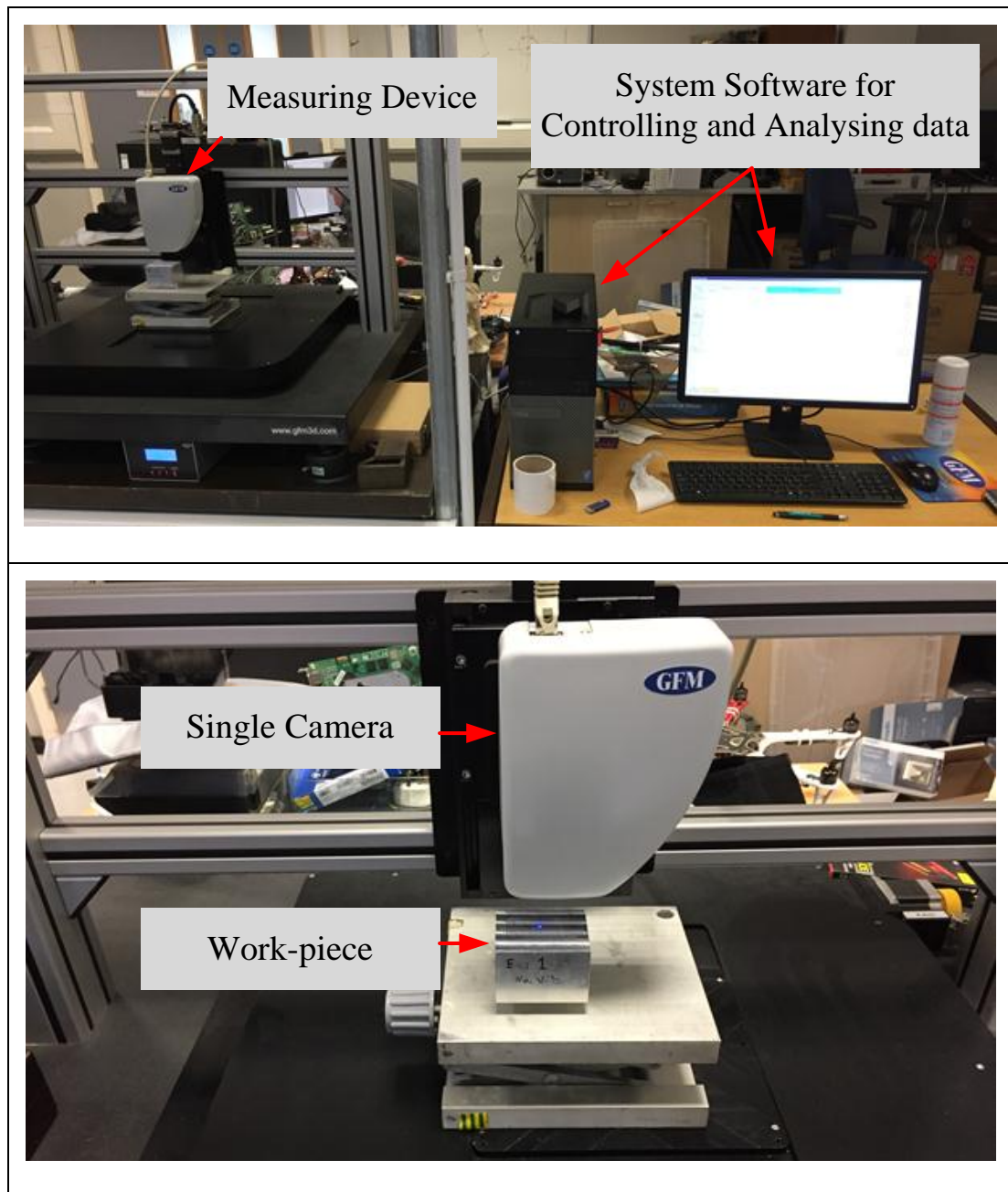
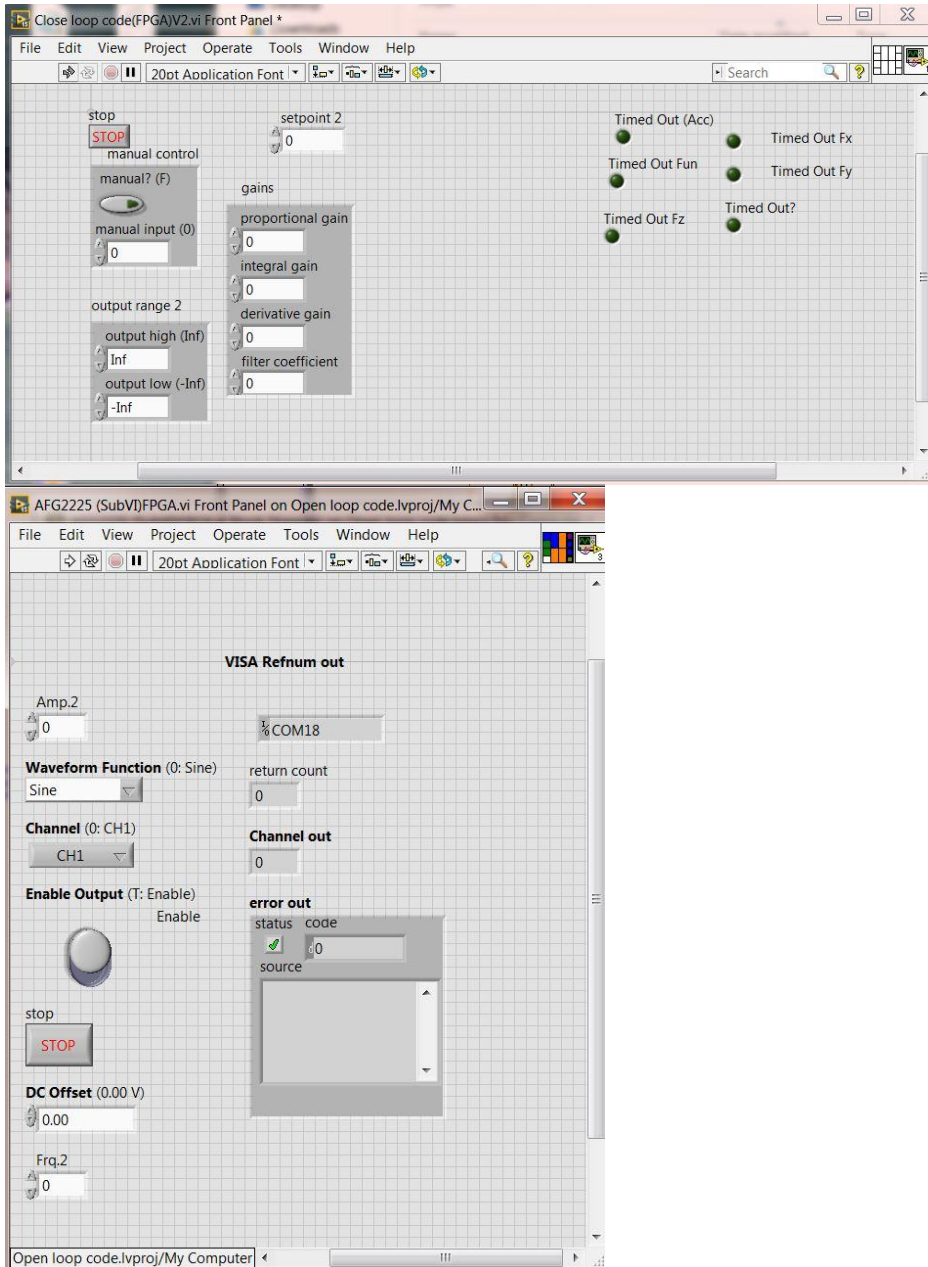


Figure A. 8: The 3D GFM Mikro CAD instrument

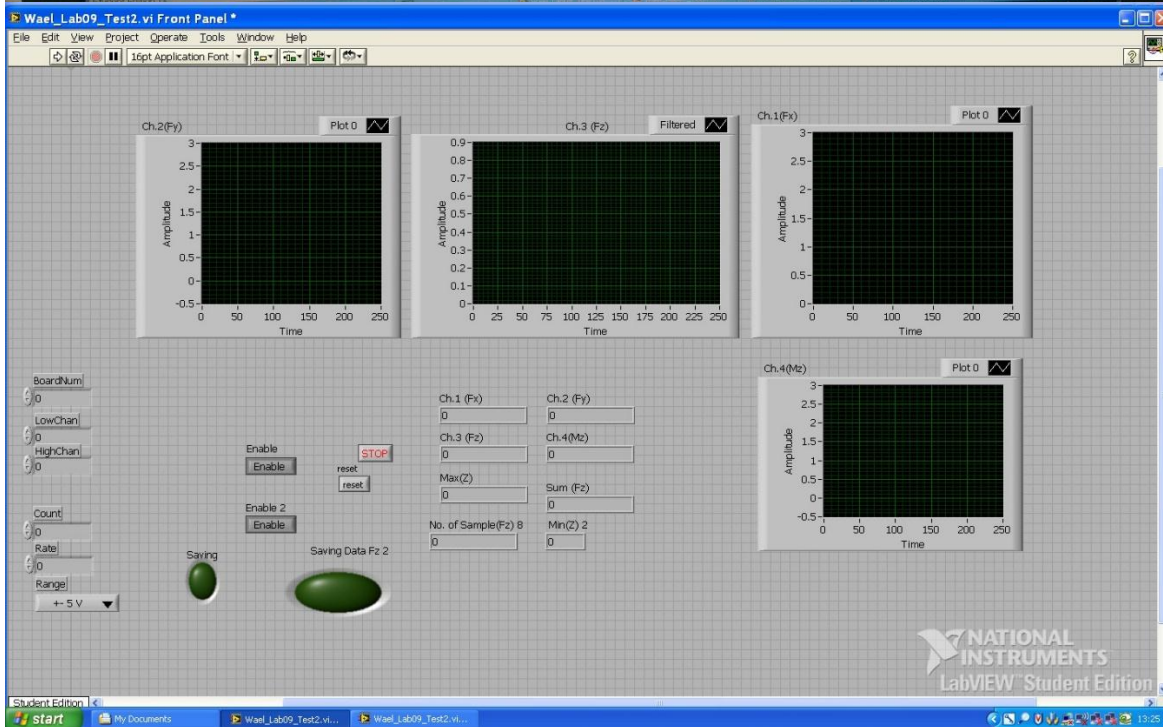
## Appendix

In this study, three programs were used for designing, simulations, investigations and system control. The programs are Solid-works, Matlab with Simulink and LabVIEW.

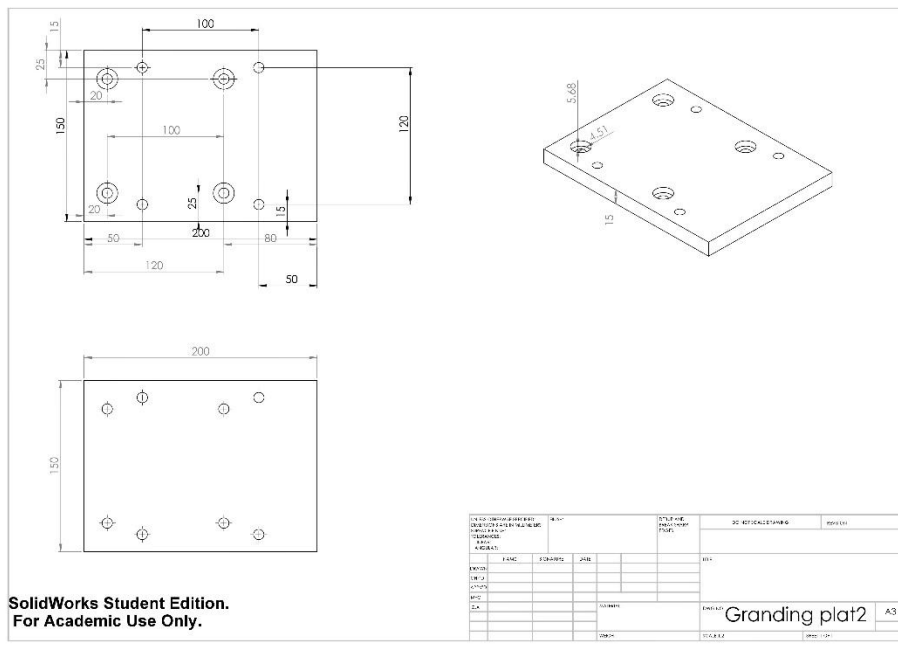
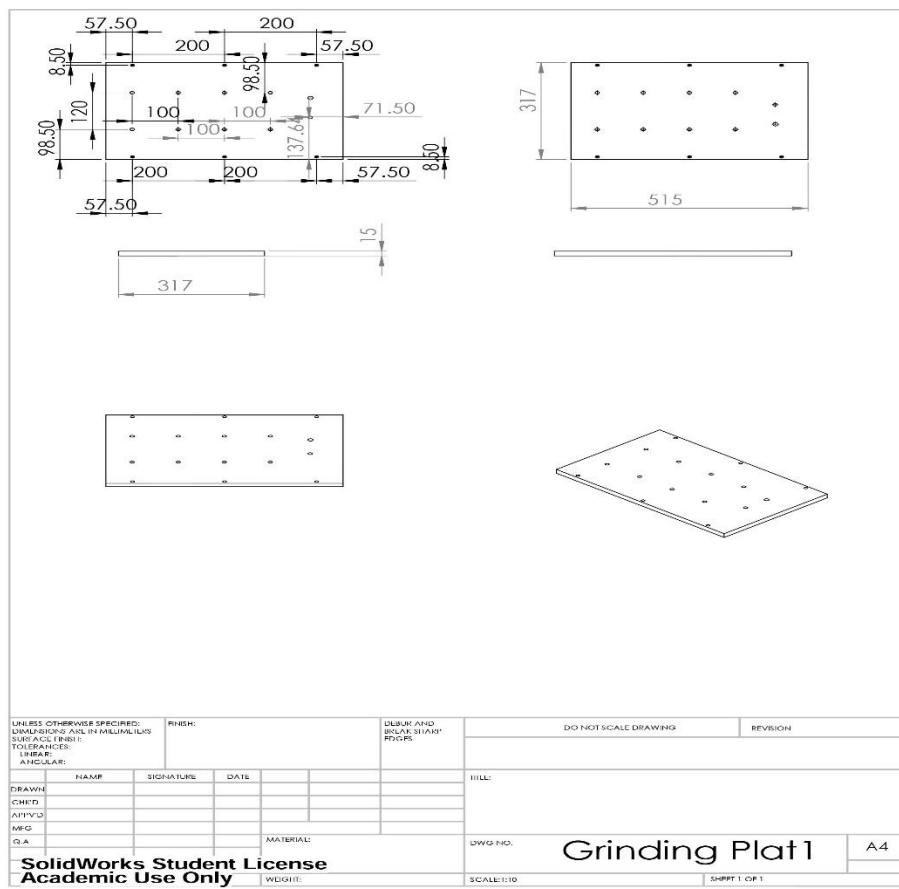
### A-2 LabVIEW Code



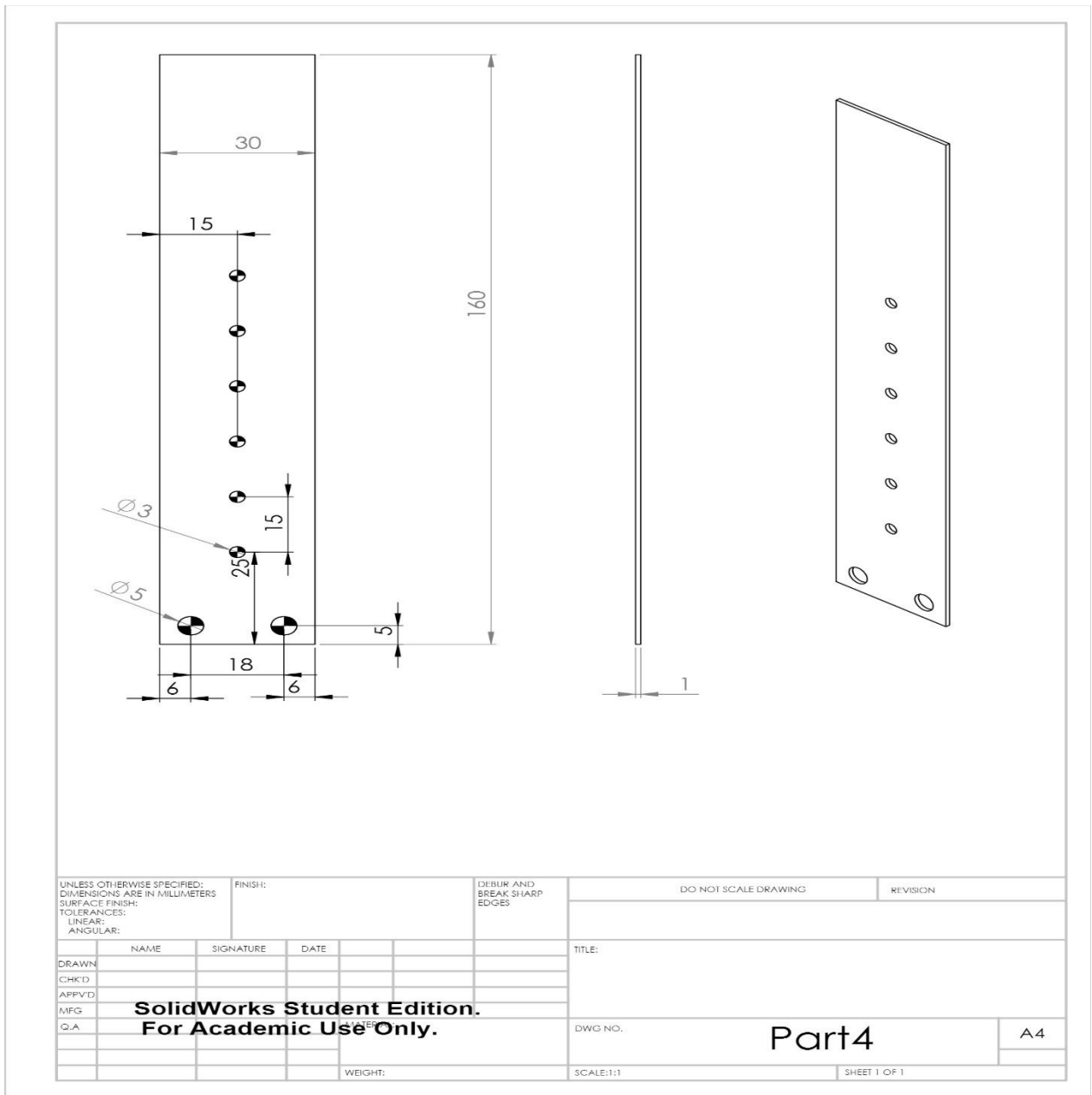
# Appendix



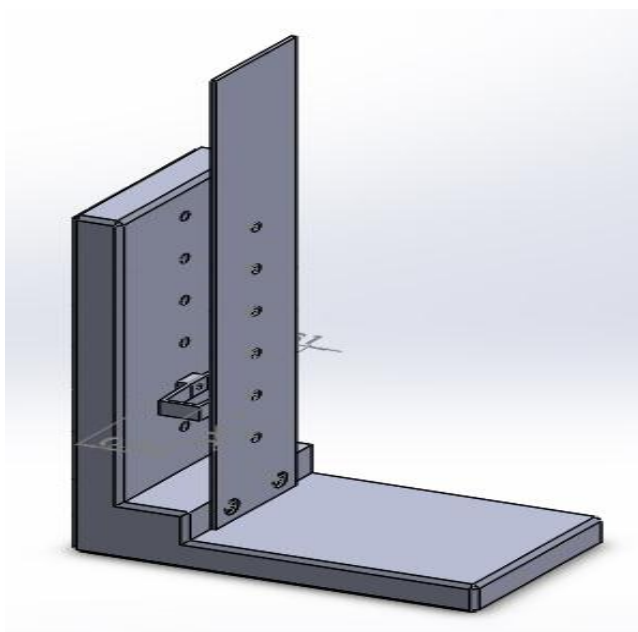
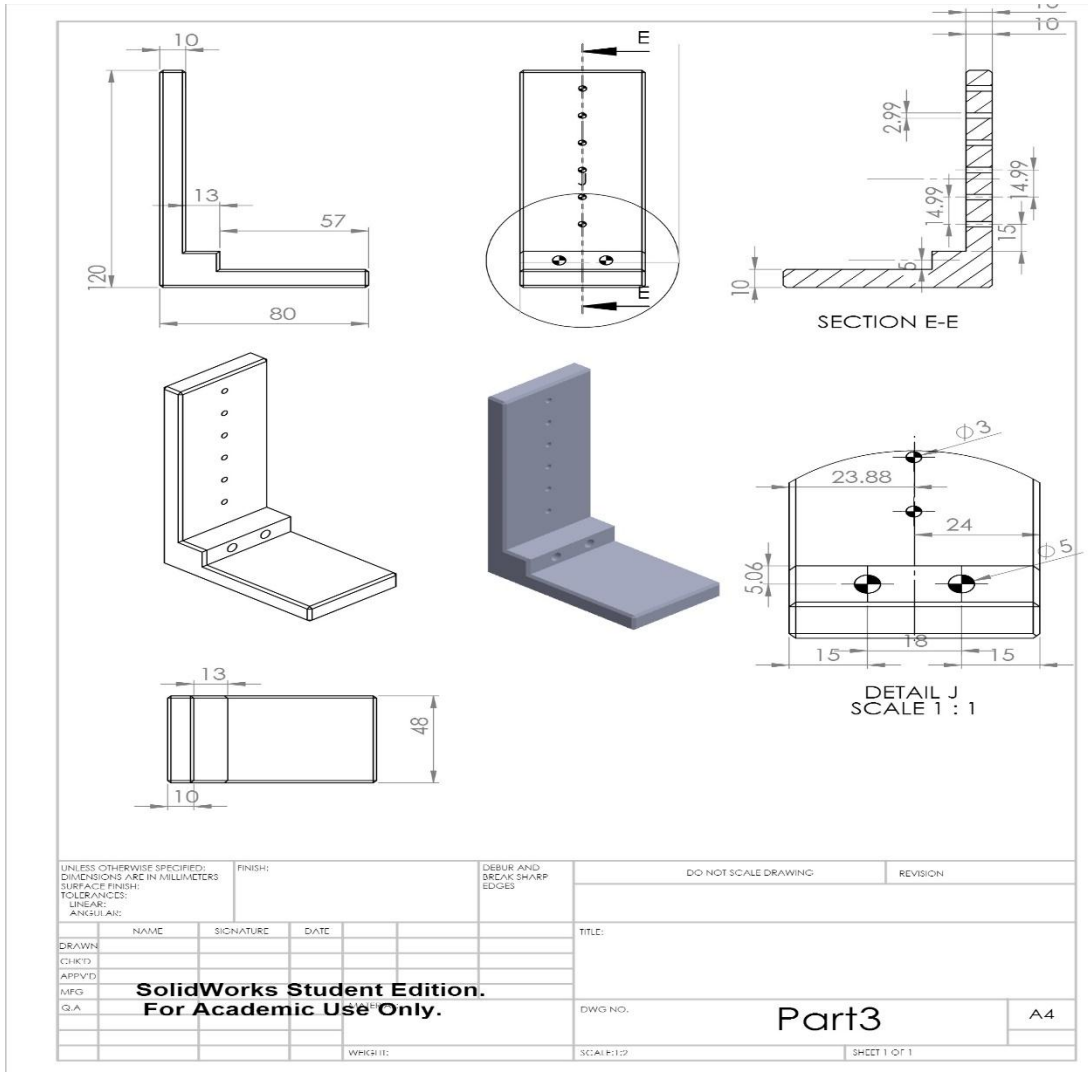
A-3 SolidWorks design sheets



**Design Initial Vibration System:**



# Appendix



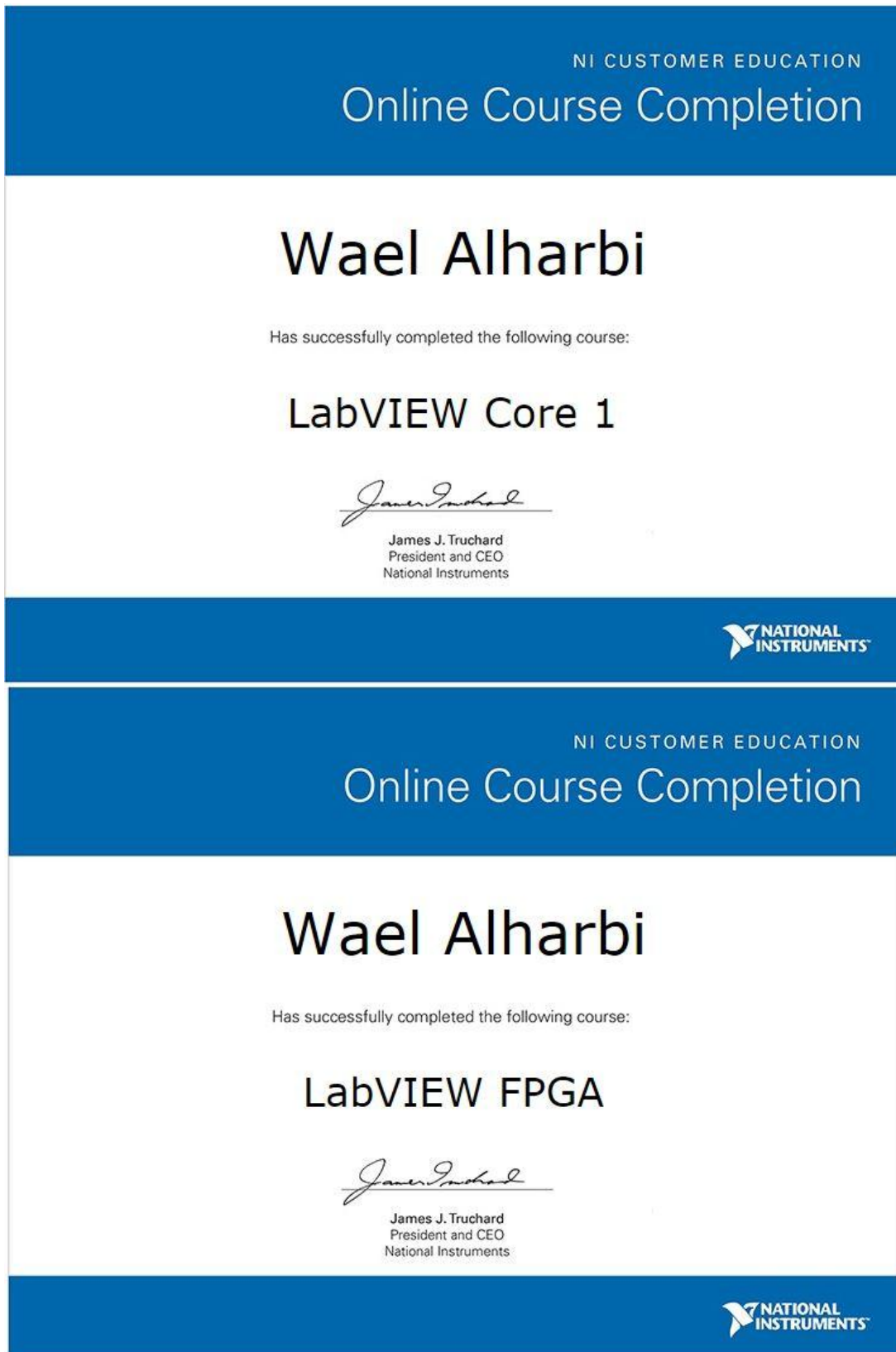
**Work-piece design:**

The drawing shows a milling workpiece with the following dimensions and features:

- Isometric Views:** Three views showing the 3D shape of the part, which is a rectangular block with a stepped top surface and a small notch on one side.
- Orthographic Views:**
  - Top View:** Shows a width of 59 mm and a depth of 50 mm.
  - Front View:** Shows a total height of 60 mm. The top surface is stepped, with a top section of 19 mm height and a bottom section of 1.50 mm height. The total width is 60 mm.
  - Side View:** Shows a depth of 50 mm and a notch width of 10 mm.
  - Bottom View:** Shows a width of 59 mm and a depth of 60 mm.

UNLESS OTHERWISE SPECIFIED: DIMENSIONS ARE IN MILLIMETERS				FINISH:		DEBUR AND BREAK SHARP EDGES		DO NOT SCALE DRAWING		REVISION	
SURFACE FINISH:											
TOLERANCES:											
LINEAR:											
ANGULAR:											
NAME		SIGNATURE		DATE				TITLE:			
DRAWN											
CHK'D											
APPV'D											
MFG											
Q.A											
								DWG NO. Milling workpieces V2		24	
								SCALE:1:2		SHEET 1 OF 1	

**A-4 LabVIEW training certificates**



NI CUSTOMER EDUCATION  
Online Course Completion

# Wael Alharbi

Has successfully completed the following course:

## LabVIEW Real-Time 1



James J. Truchard  
President and CEO  
National Instruments



## A-5 G-code of CNC-Machining Center

Sample machining code for the 5-axis CNC milling centre.

Manual operation	Programmin
Error	
0	BEGIN PGM mill-lines-w1 MM
1	BLK FORM 0.1 Z X+0 Y+0 Z-40
2	BLK FORM 0.2 X+50 Y+50 Z+0
3	TOOL CALL 4 Z S4500
4	M6
5	L X+0 Y+0 Z+50 R0 FMAX M3
6	L X-10 Y+7 R0 FMAX
7	L Z-0.5 FMAX
8	L X+70 R0 FZ0.05
9	L Z+5 FMAX
10	L X-10 Y+19 R0 FMAX
11	L Z-1.5 R0 FMAX
12	L X+70 R0 FZ0.05
13	L Z+5 FMAX
14	L X-10 Y+31 R0 FMAX
15	L Z-0.5 FMAX
16	L X+70 R0 FZ0.1
17	L Z+5 FMAX
18	L X-10 Y+43 R0 FMAX
19	L Z-1.5 FMAX
20	L X+70 R0 FZ0.1
21	L Z+2
22	L Z+50 FMAX
23	M76
24	CALL PGM endprogram
25	M30
26	END PGM mill-lines-w1 MM

Manual operation	Programmin
Error	
0	BEGIN PGM mill-line4 MM
1	BLK FORM 0.1 Z X+0 Y+0 Z-40
2	BLK FORM 0.2 X+50 Y+50 Z+0
3	TOOL CALL 4 Z S6000
4	M6
5	L X+0 Y+0 Z+50 R0 F1500 M3
6	L X-10 Y+43 R0 F1500
7	L Z+5
8	L Z-0.5 F1500
9	L X+70 R0 FZ0.05
10	L Z+2 F1500
11	L Z+50
12	M76
13	CALL PGM endprogram
14	M30
15	END PGM mill-line4 MM

Manual operation	Programmin	Manual operation	Programmin
Error		Error	
0	BEGIN PGM mill-line2 MM	0	BEGIN PGM mill-line1 MM
1	BLK FORM 0.1 Z X+0 Y+0 Z-40	1	BLK FORM 0.1 Z X+0 Y+0 Z-40
2	BLK FORM 0.2 X+50 Y+50 Z+0	2	BLK FORM 0.2 X+50 Y+50 Z+0
3	TOOL CALL 4 Z S6000	3	TOOL CALL 4 Z S6000
4	M6	4	M6
5	L X+0 Y+0 Z+50 R0 F1500 M3	5	L X+0 Y+0 Z+50 R0 F1500 M3
6	L Z+5 F1500	6	L X-10 Y+7 R0 F1500
7	L X-10 Y+19 R0 F1500	7	L Z-1 F1500
8	L Z-1 R0 F1500	8	L X+70 R0 FZ0.05
9	L X+70 R0 FZ0.1	9	L Z+5
10	L Z+2	10	L Z+50 F1500
11	L Z+50 F1500	11	M76
12	M76	12	CALL PGM endprogram
13	CALL PGM endprogram	13	M30
14	M30	14	END PGM mill-line1 MM
15	END PGM mill-line2 MM		

A training certificate.

**Engineering**  
Technology Group

This is to certify that

---

**Wael Naji Alharbi**

---

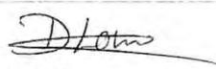
Has completed the

**ENGINEERING TECHNOLOGY GROUP  
PRODUCT SERVICE TRAINING  
MILLING COURSE  
Heidenhain iTNC 530**

---

DATE **26th May, 2016**

---

<b>ANDY BELCHER</b> Technical Engineer	
<b>DAVID LOWE</b> Technical Manager	
<b>CHLOE REEVE</b> Training School Co-ordinator	

## A-6 Publishing Papers

Eward H, Alharbi Wael Naji and Batako A., (2015) “*Development of a control system for Vibration Assisted Grinding*”, Proceeding of the 9<sup>th</sup> Saudi Student Conference in London, United Kingdom, July 2015.

Alharbi W, Eward H, Abass M, Chen X and Batako ADL. “*Development of a control system for Vibration Assisted Grinding*”, the 23rd Mediterranean Conference on Control and Automation, United Kingdom, February 2015.

Alharbi Wael Naji, Ewad Heisum and Batako ADL., “*Development of a control system for Vibration Assisted Machining*”, The Annual International Conference on Aeronautical, Automotive and Manufacturing Engineering (ICAAME'2016), London (UK), March 2016.

Alharbi, Wael. Batako, A. Gomm, J. B., “*Development of PID Controller for Vibratory Milling*”, the 14th International Conference on Manufacturing Research (ICMR 2016), Loughborough University, Leicestershire, UK, September 2016.

Alharbi, Wael. Batako, A. and Gomm, B., “*PID Controller Design for Vibratory Milling*”, ISER - 196th International Conference on Science, Technology, Engineering and Management (ICSTEM), Marrakech, Morocco. July 2017.

Alharbi, W. & Gomm, B., 2017. Genetic Algorithm Optimisation of PID Controllers for a Multivariable Process Introduction: Design methodology: iJES, 5(1), pp.77–96. Available at: <https://doi.org/10.3991/ijes.v5i1.6692>.